University "Ss. Cyril and Methodius"
Faculty of Civil Engineering-Skopje
Chair of Structural Analysis

EXPERIMENTAL AND ANALYTICAL RESEARCH OF STRENGTHENED MASONRY

SERGEY CHURILOV

A doctoral dissertation submitted to the Chair of Structural Analysis,
Faculty of Civil Engineering-Skopje, University "Ss. Cyril and Methodius",
for the academic degree of Doctor of Technical Sciences.

June, 2012

Sergey Churilov
Experimental and Analytical Research of Strengthened Masonry
Doctoral dissertation

University "Ss. Cyril and Methodius"
Faculty of Civil Engineering-Skopje
Chair of Structural Analysis

Experimental and Analytical Research of Strengthened Masonry

Sergey Churilov

Doctoral dissertation

Mentor:

Prof. Elena Dumova-Jovanoska, PhD
University "Ss. Cyril and Methodius", Faculty of Civil Engineering-Skopje

Evaluation committee:

Prof. Elena Dumova-Jovanoska, PhD
University "Ss. Cyril and Methodius", Faculty of Civil Engineering, Skopje, Macedonia

Dr.-Ing. Christoph Butenweg, PhD
RWTH, Lehrstuhl für Baustatik und Baudynamik, Aachen, Germany

Prof. Gjorgi Kokalanov, PhD
University "Ss. Cyril and Methodius", Faculty of Civil Engineering, Skopje, Macedonia

Prof. Kiril Gramatikov, PhD
University "Ss. Cyril and Methodius", Faculty of Civil Engineering, Skopje, Macedonia

Prof. Lidija Krstevska, PhD
University "Ss. Cyril and Methodius", Institute of earthquake engineering and engineering seismology, Skopje, Macedonia

A review from evaluation of the dissertation was published in University bulletin No. 1029, April 17, 2012.

Public presentation: Skopje, June 8, 2012.

To Oleg and Sanja.
For your inspiration and unconditional support.

233. If a builder builds a house for someone,
even though he has not yet completed it;
if then the walls seem toppling,
the builder must make the walls solid from his own means.

— Hammurabi 1700 BCE [King, 2011]

ACKNOWLEDGMENTS

It would have been next to impossible to write this thesis without the help of Prof. Elena Dumova-Jovanoska, who not only served as my mentor, but also encouraged and challenged me throughout my academic program. I sincerely thank her for the help, guidance, suggestions, careful advices and fruitful discussions.

I am heartily thankful to my co-mentor, Dr.-Ing. Christoph Butenweg, for his exceptional ideas and useful comments without whose knowledge and assistance this study would not have been successful.

I would like to thank also Prof. Lidija Krstevska for her discussions, careful reading and valuable suggestions and Prof. Gjorgi Kokalanov for his discussion and ideas for future work in numerical analysis.

Many thanks to Prof. Petar Cvetanovski for his support and management in preparation of the experimental tests. This work would not be possible without the hard work and endless efforts of the lab staff at the Faculty of Civil Engineering, Milorad Jovanovski, Borivoje Jovik and Velimir Zlateski.

I would like to express my sincerest gratitude to South Eastern European Graduate School for Master and PhD formation in Engineering (SEEFORM), supported by German Academic Exchange Service (DAAD) and coordinated by Prof. Dr.-Ing. Rüdiger Höffer for participation and support in the doctoral program.

I am really grateful to Assoc. Prof. Viktor Gavrilovski for contribution in data acquisition during the experimental tests.

The major experiment materials for this study, clay bricks, reinforced concrete elements, test set-up admixtures were provided by factories "Elenica" from Strumica, "Karpos" from Skopje and "ADING" AD from Skopje. The set-ups for the measuring devices as well as the hydraulic control system was developed by "Ivotehna" from Skopje. I really appreciate their support.

In the end, I wish to acknowledge my family, all my friends and colleagues who supported me and contributed in development of this study.

ABSTRACT

The main structural elements in masonry buildings are the masonry walls. They are responsible for the load transfer and the global stability of the building when subjected to vertical and horizontal forces. The combination of the gravity and horizontal loads, such as seismic actions, attracts axial forces, bending moments and shear forces. All these contribute to the imbalance of the building and may lead to damage or collapse of the building. A large number of existing unreinforced masonry buildings are still present and operational throughout the world. Their presence in the building stock within area with high seismic activity requires careful assessment of their seismic behaviour and retrofitting. Moreover, the existing unreinforced masonry buildings are composed of inhomogeneous material, not capable to carry tension forces. Additionally, many masonry building do not satisfy the latest seismic design provisions.

The seismic behaviour and resistance of unreinforced masonry buildings can be improved by strengthening or retrofitting in cases of seriously damaged walls. Usually, traditional strengthening methods are applied, with the common use of reinforced concrete jackets. However, there is insufficient knowledge about the seismic behaviour of jacketed masonry, due to lack of experimental and analytical investigations. The design of those walls is usually based on empirical relations which may result in over- or under-design. Therefore, this thesis focuses on two issues: (1) to compare the behaviour of the unreinforced and strengthened masonry with RC jackets subjected to lateral in-plane cyclic loads, and (2) to suggest a reliable analytical method for evaluation of the seismic resistance and performance of the jacketed masonry buildings.

Based on the extensive literature review, an experimental test programme was established, aiming to identify the mechanical properties of masonry and its components. Based on the obtained results, the effects of variable wall geometry and precompression level were considered on the performance of the unreinforced and jacketed masonry walls, tested in real scale and subjected to alternating cyclic in-plane forces. The analytical models for reinforced masonry were used to investigate the capacity of the jacketed masonry due to the similarity of both structural materials and the similar behaviour when exposed to horizontal actions. The effectiveness of the strengthening method was verified experimentally and an increase in the seismic resistance of the strengthened masonry walls was obtained when compared to the resistance of the reference unreinforced walls. However, the ductility performance was not improved. An analytical model for evaluation of

RC jacketed masonry walls was proposed, based on the contribution of the masonry and the horizontal reinforcement. The contribution of the vertical reinforcement to the resistance of the walls was ignored, because the tests were performed without anchorage of the vertical reinforcement in the top and bottom beams. This approach was used in order to study the behaviour of the strengthening structural material, rather than to investigate the behaviour of a strengthened structural element - wall. Based on the obtained results, the proposed method for evaluation of the seismic performance of jacketed masonry walls was used to study the strengthening effects on an existing building. The elasto-plastic force-deformation relations for unreinforced and strengthened masonry walls, based on the experimental results, were implemented in a displacement-based analysis software, through a newly developed analysis module. The capacity spectrum method was applied to validate the efficiency of the strengthened material and to assess the seismic resistance of the building.

The research presented in the thesis follows the concept of the new generation of design codes for masonry buildings. The obtained results enable application of the analytical approach for design of masonry buildings in cases of strengthened masonry buildings.

Keywords: masonry, earthquake, strengthening, RC jacket, experiment, analytical, cyclic load, in-plane, shear, seismic resistance.

CONTENTS

LIST OF FIGURES

LIST OF TABLES

ACRONYMS

URM unreinforced masonry

RC reinforced concrete

UMW unreinforced masonry wall

UMWs unreinforced masonry walls

SMW strengthened masonry wall with RC jackets

SMWs strengthened masonry walls with RC jackets

DT displacement transducer

CEVD coefficient of equivalent viscous damping

CSM Capacity Spectrum Method

FEM Finite Element Method

OMA Operational Modal Analysis

AVT Ambient vibration tests

AV Ambient vibration

FE Finite element

LIST OF SYMBOLS

Abbreviations

A	gross area
CR	corner roundness
Cr	presence of cracks
Md	mass (dry)
Mf	mass after freezing
Ms	mass (saturated)
SS	surface smoothness on brick plane
WA	water absorption

Greek Letters

α	boundary conditions of a wall
α'	bending moment inflection point coefficient
α_1, β	stiffness degradation parameters
χ	factor for direction of compressive stress
δ	shape factor
ϵ, ϵ_m	masonry strain
γ_c	partial safety factor for concrete
γ_d	dry density of masonry unit (or masory)
γ_g	masonry grout factor
γ_M	partial safety factor for masonry
γ_m	partial safety factor for mortar
γ_s	partial safety factor for steel
κ	shear coefficient
μ_c	friction coefficient of the unit-mortar interface
μ_u	ductility
ν	Poisson's ratio

ν_m	shear strength of masonry
ω_n	natural frequency of vibration
Φ	horizontal reinforcement capacity reduction factor
ϕ_c	angle orientation of the principal compressive stress
ϕ_m	material resistance factor for masonry
ϕ_s	material resistance factor for reinforcing bars
ϕ_t	angle orientation of the principal tensile stress
ψ_2	combination factor for quasi-permanent value of a variable action
σ_0	average normal stress in the wall
σ_{allow}	allowable stress in the wall
σ_d	design compressive stress perpendicular to the shear
σ_m	masonry stress
$\sigma_{n,ult}$	principal tensile stress in the wall at ultimate load
σ_p	principal stress in the middle section of a wall
τ	average shear stress in horizontal section of the wall
τ_0	average shear stress in the wall
τ_{max}	average shear stress in horizontal section of the wall
$\tau_{n,ult}$	ultimate average shear stress in the wall at ultimate load
θ	drift ratio (rotation of a wall)
ξ	damping ratio
ξ_0	initial viscous damping in the elastic range
ξ_{eff}	effective damping
ξ_{eq}	coefficient of equivalent viscous damping
ξ_{hyst}	equivalent viscous damping ratio due to hysteretic behaviour
Ø	bar diameter

Latin lower case letters

$\epsilon_m^{'}$	masonry strain at maximum stress level
b	shear stress distribution factor

b_w	thickness of a wall without flanges
c	damping coefficient
c	depth of neutral axis
d	effective depth of the section
d_{cr}	horizontal displacement at crack limit state
d_{Hmax}	horizontal displacement at maximum resistance
d_{max}	horizontal displacement at ultimate limit state
e	eccentricity of the vertical load
$f_{bt,cal}$	calculation tensile strength of masonry units
$f_{bt,flex}$	tensile flexural strength of a brick
f_b	normalized compressive strength of the masonry unit
f_{ck}	compressive strength of concrete
f_k	characteristic compressive strength of masonry
$f_{m,comp}$	compressive strength of mortar
$f_{m,test}$	compressive strength of masonry obtained in test
$f_{mt,flex}$	tensile flexural strength of mortar
f_m	compressive strength of mortar
f'_m	compressive strength of masonry normal to the bed joint
f_{rd}	shear strength of concrete
f_{st}	average compressive strength of masonry units
f_t	tensile strength of masonry
f_{vk0}	characteristic shear strength of masonry under zero compressive stress
f_{vk}	characteristic shear strength of masonry
f_{wv}	shear strength of masonry
f_{yh}	yield strength of horizontal reinforcement
f_{yv}	yield strength of vertical reinforcement
f_y	yield stress of reinforcement steel
h, h_w	height of a wall

l' distance of wall edges to reinforcement bars

l, l_w length of a wall

l_c length of the compressed part of the wall, ignoring the part of the wall that is in tension

m mass

n number of vertical bars

p_k correction factor

p_v reduction factor for ultimate bending moment

r modulus of elasticity ratio

s horizontal distance between vertical reinforcement bars

t, t_w thickness of a wall

t_c thickness of a concrete jacket

T_w thickness of a jacketed wall

u_0 horizontal displacement at maximum force for a cycle

z lever arm between the compressive and tensile force

Latin upper case letters

$\frac{M_f}{V_f d_s}$ shear span ratio

A_{env} area below the experimental envelope curve

A_e effective cross-sectional area of the wall

A_g gross cross-sectional area of the wall

A_{hyst} area of hysteresis cycle

A_{sh} area of horizontal reinforcement

A_{sv} area of vertical reinforcement

A_{uc} uncracked portion of the effective cross-sectional area of a wall

A_{vt} total area of distributed vertical reinforcement

A_w area of the horizontal cross-section of the wall

C_{rh} horizontal reinforcement capacity reduction factor

C_{rv} vertical reinforcement capacity reduction factor

E_c modulus of elasticity of concrete

E_{Diss} dissipated energy

E_m, E modulus of elasticity of masonry

E_{SMW} modulus of elasticity for strengthened masonry

E_{Sto} stored energy

E_{UMW} modulus of elasticity for unreinforced masonry

F_{max} ultimate compressive load

G shear modulus of masonry

G_{test} shear modulus of tested masonry walls

H horizontal load

H_0 maximum horizontal force of a cycle

H_{cr} horizontal force at crack limit state

H_{dmax} horizontal force at ultimate limit state

H_{max} maximum horizontal load

$H_{sd,eq}$ design shear resistance of equivalent wall

$H_{str,f}$ flexural resistance of reinforced masonry wall

$H_{str,sl}$ sliding shear resistance of reinforced masonry wall

$H_{str,s}$ shear resistance of reinforced masonry wall

$H_{u,f}$ flexural resistance of unreinforced masonry wall

$H_{u,sl}$ sliding shear resistance of unreinforced masonry wall

$H_{u,s}$ shear resistance of unreinforced masonry wall

I moment of inertia of a cross-section

I_E reduced moment of inertia of a cross-section

$K_{e,eq}$ lateral stiffness of equivalent wall

$K_{e,jack}$ lateral stiffness of RC jacket

$K_{e,w}$ lateral stiffness of original masonry wall

K_e lateral effective stiffness

$K_{s,i}$ secant stiffness at i cycle

K_s secant stiffness at elastic limit

L length of a wall

M_{Ru} ultimate bending moment

N vertical load

P_d axial compression load

P_f factored axial load

T_y factored tensile force at yield of the vertical reinforcement

Part I

INTRODUCTION

This part gives introductory information on the objectives, motivation and the methodology used throughout the thesis and a concise literature review.

Historical overview of masonry structures together with an overview of typical masonry buildings in Macedonia is given first. Building materials applied in Macedonian traditional buildings are presented also. A summary of the most important aspects of in-plane behaviour of masonry structural elements are explained later. Different test set-ups for in-plane shear behaviour of walls subjected to cyclic loads are outlined.

Next, strengthening techniques and materials with special attention to reinforced concrete jacketing are presented.

After that, design procedures for estimation of shear capacity of masonry walls by various analytical models and code provisions are summarized.

In the end, a review of the local experience in strengthening masonry is given. It includes experimental, analytical and numerical investigations performed so far.

1 INTRODUCTION

Masonry together with wood is considered as one of the most important building materials in the history of mankind. It consists of individual units laid together and bonded by mortar. The units can be brick, stone, marble, granite, travertine, limestone, concrete blocks, glass blocks, stucco, and tile. The mortar can be made from lime, cement or their combination in appropriate ratios. Masonry has been used as construction material for several thousand of years. The first masonry structures appear in the Neolithic age that began approximately 10,000 years ago. During this time, the process of using fire to craft mortar or plaster was discovered. The mortar was combined with stone, mud or straw to build the world's first permanent man-made structures. From this time onward, masonry became the building method of choice for the civilization. From the Tower of Babylon, pyramids of Egypt, Great China Wall, to the Greek Parthenon, masonry has helped build some of the world's most iconic structures.

In the last decades other materials like steel and concrete have been used frequently and thus replacing masonry as a structural material. This situation is present and particularly remarkable in Macedonia, where almost all new buildings are constructed using reinforced concrete. This material appears to be particularly practical and economical. In the recent past, masonry has been mostly used as a non-structural material, as an infill of reinforced concrete and steel frames. The research and the development of design rules for reinforced concrete structures increased and caused insufficient knowledge about masonry. Although there is national masonry code adopted from the regulations valid in the previous mother state of Yugoslavia, masonry was forgotten as load bearing material. This situation got worse after the catastrophic, 1963 Skopje earthquake that caused collapse to about 10% of the buildings, while other 65% were damaged beyond economical repair.

Many urban and suburban settlements in Macedonia are located in regions with high seismicity. As proven by historical data, many ancient settlements and towns were destroyed by earthquakes. The town of Scupi, capital of ancient state of Dardania, was first destroyed by devastating earthquake in 518. It is assumed that the intensity level of the shaking was 10-11. The town of Skopje was build nearby, but it will suffer another great destruction in 1555 by earthquake with intensity level 10. It led to a destruction of about 70-80% of the buildings.

Scupi was founded in the 2nd century BC as a Roman military camp.

Stobi was ancient town of Paeonia.

Historical data and archaeological excavations in the ruins of another ancient town, Stobi, presume that the town was destroyed by an earthquake in the second half of the III century. They confirm that after it was completely deserted in the VI century from economical and safety reasons, the town of Stobi collapsed after another great earthquake.

During the time, people invented some specific measures to improve the seismic behaviour of masonry structures. These include connecting stones, tying of walls, strengthening of wall corners and zones of wall connections. Nevertheless, masonry structures represent the most vulnerable type of structures in the existing building stock.

Earthquake ground motion causes development of seismic, inertial forces acting on the buildings. These forces cause additional shear and bending stresses which usually exceed the material strength. This leads to a damage in the masonry structural elements. Since masonry can be stressed high in compression and relatively low in shear and bending, the resulting damage can be extremely high and in the end, it can lead to a full collapse of the building. Masonry walls are considered as primary structural elements which support other structural elements, like floors, domes, arches and vaults. If designed, constructed and connected properly, they could be able to resist in-plane actions from wind and earthquake. Many recent seismic actions caused severe damage to unreinforced masonry, which led to the idea that the plain masonry is not able to resist the seismic forces and should be strengthened or retrofitted.

In the last decades, many countries performed extensive studies of the behaviour of masonry structures subjected to seismic actions. Their behaviour during earthquakes has been analysed, while many experiments to specify basic seismic parameters have been carried out. Considerable experimental research has been also accomplished to investigate the causes of damage and to develop methods suitable for seismic retrofit and rehabilitation of existing masonry buildings. As a result, many technical solutions which improve masonry structural and material imperfections became available. As experimental tests and recent earthquakes proved, application of these methods to existing masonry buildings can provide the same level of earthquake resistance as in the case of buildings designed and constructed according to the latest building codes.

1.1 MOTIVATION

The fundamental disadvantage of existing masonry buildings located in active seismic regions is the fact that usually they are old buildings, constructed from inhomogeneous material and mainly designed to support vertical loads only. Moreover, masonry properties are important parameters that govern its seismic behaviour. Although masonry has relatively high compressive strength, its tensile strength is very low. Therefore, masonry is not able to carry tension forces and those buildings are particularly vulnerable to seismic actions and susceptible to extreme damage. This situation stimulates profound knowledge for seismic behaviour and reliability analysis of these structural systems. In addition, many existing masonry buildings do not satisfy the latest seismic design and construction recommendations. To increase their bearing capacity, often they are strengthened and different strengthening techniques are available. Even though some scientific experimental and analytical level of research exists, the process of masonry strengthening, particularly in Macedonia, is primarily based on engineer's and workmen experience. Until today, many masonry buildings have been strengthened and almost exclusively traditional strengthening techniques, such as repair of cracks, grouting and jacketing, have been used. Some of them are based on the analysis of earthquake damage observation and engineering judgement, and have not been actually verified, but some of them were verified by laboratory tests. Strengthening with RC jackets was the technical measure selected to be studied in this thesis. This measure was experimentally verified only in a handful of cases. To be able to determine recommendations for application of the strengthening method, as well as to obtain suitable knowledge for the behaviour of strengthened masonry buildings subjected to seismic actions, a need for experimental and analytical research emerges. This dissertation is motivated by two research questions: (1) how unreinforced and strengthened masonry walls behave under in-plane cyclic loads? (2) how and which analytical method could be applied to obtain the response of the masonry wall when subjected to seismic forces? To examine these questions, the current study elaborates a traditional strengthening method by comparing experimentally and analytically its efficiency in relation to the unreinforced masonry.

1.2 OBJECTIVES

Even today there are many masonry buildings constructed from stone, brick or their combination which are still in operation. This is more evident in rural areas in Macedonia, while the number of existing masonry buildings in urban areas should not to be neglected. These buildings were usually constructed from brick units and lime/cement or cement mortar. Most of them were made from unreinforced masonry and only small number were constructed from confined masonry. Being composite material, its behaviour strongly depends on the mechanical properties of the components, the workmanship and the details of connections to other structural elements. However, when exposed to seismic loads these buildings suffer great damage and experience out-of-plane or in-plane failures.

On the other hand, when decision to strengthen a building is made, usually it implies application of traditional methods. The idea is to improve the seismic resistance of the structure by increasing its strength and ductility. Beside technical aspects, there are some general criteria for selecting a method for strengthening, regarding costs of intervention, importance of the building, availability of the selected technology and qualified technical workforce, time needed to apply the intervention and etc. However, the main issue with this solution is the need to fully understand the implications induced by application of such measures. The latter is of much relevance, as the basic criteria for strengthening is correlated with the expected seismic loads and the seismic capacity of the structure, namely to control the seismic resistance of a building. To fulfil this, experimental tests are necessary to determine the general parameters that define the rigidity of the structure as well as its strength and deformation properties, modal parameters and capability of the masonry structural elements to dissipate seismic energy.

Thus, the main objective of this research is to evaluate the behaviour of unreinforced and strengthened masonry walls under in-plane cyclic loading. This research studies masonry strengthening with RC jackets applied on both sides of the masonry walls. The evaluation of the behaviour of the masonry walls aims at performing: (a) an experimental assessment of the effects of variable geometry ratio and level of pre-compression load to analyse the effectiveness of the strengthening intervention; (b) validation of design models for unreinforced and reinforced masonry available in the literature; (c) selection and proposal of an analytical model for design of RC jacketed walls based on the resemblance of the jacketed walls with reinforced masonry walls; and (d) application of the proposed model for seismic verification of an existing building based on experimental results.

1.3 METHODOLOGY

Firstly, literature review was carried out aiming to better understand the behaviour of the masonry walls and to collect the information related to the past and recent experimental, numerical and design procedures for unreinforced and strengthened masonry walls.

Secondly, experimental analysis was performed after determination of the needed parameters. According to the developed test matrix, it was decided to analyse the masonry walls by recreation of the circumstances in which the walls are present on a site. It determines the necessary number of walls to be tested, the wall length to height ratio, pre-compression loads and boundary conditions to be applied. Clay brick units, lime mortar, steel mesh and concrete were selected as the main building materials to be tested. The experimental work was divided in two parts: (1) mechanical identification and evaluation of the mechanical properties of masonry and its components; (2) evaluation of the behaviour of unreinforced and strengthened masonry walls subjected to cyclic lateral loads and associated failure mechanisms, lateral capacity, force-displacements hysteresis diagrams, stiffness degradation and capacity for energy dissipation.

Thirdly, validation of the available design methods and analytical models with the obtained experimental results was carried out. Since no analytical model for design of RC jacketed walls was given in the literature, the goal was to test and suggest a design model for reinforced masonry walls to be used for RC jacketed masonry walls. The small amount of test result does not allow development of a design model nor could give reliable data for improvement of the existing models. Therefore, a model for reinforced masonry was proposed to analytically calculate the bearing capacity of masonry walls.

In the end, the effectiveness of the design method was illustrated on a school masonry building, by application of displacement-based approach.

1.4 OUTLINE OF THE THESIS

The thesis is divided in seven chapters: (1) introduction, (2) literature review, (3) experimental research on the behaviour of masonry components, (4) experimental behaviour of masonry walls, (5) analytical evaluation of seismic behaviour of masonry walls, (6) application of analytical model for analysis of masonry buildings and (7) conclusions and final remarks.

Chapter 2 presents a historical overview of masonry structures throughout the world. A review of the common structural systems found in traditional masonry buildings in Macedonia, the disposition of walls in plan and along the height of the building, floor types, as well as building materials are also reported. This review helps in determination of usual vertical load levels present in masonry buildings in the country. In the following parts of this Chapter, in-plane behaviour of masonry walls is given and a brief review of the most commonly used test set-ups for investigating shear behaviour are outlined. The correlation with the main topic of this research is established with an overview of the strengthening techniques and materials for masonry. Finally, analytical design procedures for unreinforced and reinforced masonry suggested by researchers and given by design codes are presented. These are later used to compare the test results with the theoretical models available in the literature.

Chapter 3 deals with experimental research of the behaviour of masonry components and structural masonry. Results from experimental tests on clay bricks, lime mortar, concrete and reinforcement bars are presented. Compressive strength and initial shear strength of masonry was tested and the results are shown in the end of this Chapter. The identified mechanical properties of masonry and the components were used for analysis in the following chapters.

Chapter 4 explores the in-plane behaviour of unreinforced and strengthened masonry walls subjected to constant vertical load and cyclic horizontal load reversals. Details of the experimental program, materials and geometry of the masonry specimens, the process of building the specimens, the description of the test set-up and testing procedures is presented in the beginning. The obtained test results for unreinforced and strengthened walls are summarized in separate sub-chapters. The test results are systematized and deal with identification of the failure modes, description of the behaviour in form of force-displacement diagrams, determination of stiffness degradation and the capacity for energy dissipation. For simplification of the behaviour, the experimental seismic performance of both masonry materials is presented as bilinear idealized force-displacement diagrams. In the end, a comparison of the behaviour of strengthened and unreinforced masonry walls is given.

Chapter 5 investigates the ability of the analytical models available in the literature to predict the lateral capacity of the tested walls. Four approaches describing shear, bending and sliding shear failure mechanisms have been used. A correlation between the test results and the calculated maximum capacity has been made.

Chapter 6 shows application of a displacement-based approach, based on the capacity spectrum method. It is used to capture the behaviour of unreinforced and strengthened masonry under in-plane loads. This chapter provides an overview of a software program for static non-linear analysis of masonry buildings based on design provisions and failure mechanisms for masonry. The non-linear effects of masonry are introduced as bilinear curves and the capacity curve of a building is created following an iterative procedure. The capacity spectrum method is used to verify the safety of a building and to detect the possible damage levels.

Finally, chapter 7 gives summary of the present work together with the main conclusions that resulted from the research. A significance of the findings in this research are summarized together with a research contribution. Moreover, advantages and limitations of the current research, as well as recommendations and suggestions for further work are given.

2 LITERATURE REVIEW

2.1 HISTORICAL OVERVIEW OF MASONRY STRUCTURES

Two major structural problems are related to building masonry structures: how to achieve certain height and how to span openings or horizontal and vertical spaces [Drysdale et al., 1999]. In vertical direction columns and walls are generally used, while in horizontal direction main structural elements are connecting beams, girders and arches. Beside them, some structural elements, like domes and vaults span the space vertically and horizontally in the same time.

Together with wood, masonry is the oldest building material still in use in civil engineering. The technique for laying stone or brick units with or without mortar turn out to be very successful which is justified with its simplicity and durability. Most probably, the first masonry structure was a pile of natural stones connected with earth mud. As different tools were discovered, people started to modify the stones in regular shapes. The first bricks were made from mud or clay, shaped in desired form, usually rectangular and dried in the sun. These bricks were laid to create walls by using mud as bounding material. This simple process in building construction was used to erect shelters, particularly along the valley of river Nile and in Mesopotamia [Croci, 1988]. The tradition to dry the bricks presents natural evolution and first prefabricated building component. This process increased the strength and durability of the bricks, but in the same time required certain amounts of fuel, which was not available at all times.

Mesopotamia largely corresponds to modern-day Iraq, north-eastern Syria, south-eastern Turkey and south-western Iran.

One of the first masonry buildings discovered near the lake Hullen in Israel (9000-8000 BC) are considered as the first permanent

Figure 1: Great pyramid of Giza (2570 BC).

Figure 2: Rome Colosseum (72-80 AD).

Figure 3: Hagia Sophia (532-537), made from ashlar stone and bricks.

stone masonry houses constructed in dry stone with circular shape [Lourenço, 1996]. Other legacies of stone masonry survived until present time. They serve as testimonies of ancient and medieval cultures, the Egyptian architecture with its pyramids (2800-2000 BC), Figure 1, the Roman and Romanesque architecture (0-1200) with its temples, palaces, arches, columns, churches, bridges and aqueducts, Figure 2.

The Romans were great builders and there are examples of their buildings and structures for almost any purpose. Their greatest invention was pozzolanic cement made by mixing sandy volcanic ash and lime mortar. This material was used for concrete and mortar and owing to its great strength, masonry construction was extended to domes, bridges and aqueducts. Romans continued building in the Eastern Empire, especially by building churches, some of them on large scale as Hagia Sophia in today's Istanbul, built in 532-537, see Figure 3.

Figure 4: Aachen Cathedral 'Kaiserdom' (805 AD).

The Gothic architecture (1200-1600) flourished during the high and late medieval period. It evolved from Romanesque architecture and was succeeded by Renaissance architecture. It is most familiar as the architecture of many of the great cathedrals, see Figure 4, abbeys and churches of Europe. It is also known as the architecture of many magnificent castles, palaces, town halls, universities and to a less prominent extent, private dwellings.

There were three most important phases in Gothic architecture that changed massive Roman structures into characteristic light Gothic structures with large openings [Oliveira, 2003]. The first one was application of arch ribs connected to roof structures that enabled decrease of the thickness of masonry between ribs. The second phase allowed additional reduction of weight by replacement of semicircular arches with parabolic arches. They permitted architectonic flexibility and solution of the complicated geometrical problems. The third benefit was obtained by replacing heavy supporting walls around building perimeter with flying buttresses and towers which were better aligned with the thrust lines of the loads. These key phases led to development of masonry framing elements that support compression loads only.

The Gothic architecture was followed by Renaissance. It first appeared in Florence with new concepts of forms and proportions never seen before. The structures from that period are characterized by regular shapes and symmetry in plan layout and along the height. One of the most impressive structural achievements from Renaissance architecture are churches and in particular domes. Among them, without doubt, the most interesting structures are the church of St. Maria del Fiore in Florence (1296-1436) and the basilica of St. Peter in Rome (1506-1626), Figure 5.

As Hendry and Khalaf [2000] point out, during the period of Industrial revolution in Europe in 18th and 19th century, the population

(a) St. Maria del Fiore church, Florence. (b) St. Peter basilica, Rome.

Figure 5: Impressive Renaissance domes in architectural masterpieces.

expanded and towns and cities grew proportionally. This led to building on large scale, but with exception of some industrial buildings, this was entirely of masonry and timber until the end of 19th century. The new industrial development required great deal of construction and beside masonry, cast iron and concrete contributed in radical evolution of building techniques. The most representative structures from that time are big iron and steel bridges, like the Firth of Forth Bridge in Scotland. Later, masonry was displaced by steel and concrete, but it retained a predominant position in building low- and medium-rise houses and as non-structural infill material in steel and concrete structures.

Presently, on the market masonry units can be found in different shapes and materials. There are different types of mortar and different techniques for building. Some manufacturers offer complete masonry systems for building walls and floors, usually utilizing modern units of lightweight concrete, aerated concrete or calcium silicate units. Traditional clay units are still produced, but modern clay blocks with excellent thermal insulation, sound insulation, fire protection and living comfort are slowly taking their place in the building industry. Moreover, modern masonry units with high mechanical strengths and in combination with very good bond with the masonry mortar improve their usefulness for earthquake-safe buildings. Recently, there has been an increasing interest in reinforced masonry, prestressed masonry and mortarless masonry. Not only masonry units have improved their properties, but also mortar mixtures with admixtures, modern tools and machinery have emerged in the industry.

Despite the positive aspects, masonry have lost its structural function in favour of reinforced concrete and steel. This is particularly emphasized in earthquake prone countries, where it is primarily used as cladding system or for non-loadbearing walls. Few exceptions are loadbearing reinforced masonry in North America and structural masonry used in low-rise buildings. The situation in developing countries is quite different as structural masonry is still largely used. This is evident from constant publication of guidelines and manuals for building earthquake safe houses and strengthening existing non-engineering or low quality masonry structures, as highlighted in Arya et al. [2010], Meli et al. [2010], Morton [2008].

Nowadays, in Macedonia the use of masonry as structural material is rather limited and only less important agricultural or farming one-storey buildings can be found, built with concrete masonry blocks and cement mortar. Main role of masonry is given to the non-loadbearing walls and infill walls in reinforced concrete or steel buildings. For this purpose, mainly clay or calcium silicate masonry units are used. There are some grave concerns for using masonry as infill without providing adequate connection to load-bearing structural elements, because Macedonia is earthquake prone country. As Bachmann [2002] discusses, one of the basic principles for the seismic design of buildings is to avoid 'bracing' of frames with masonry infills and to separate the non-structural masonry walls by joints. Unfortunately, this is very rarely practised in today's construction building in the country.

The highest magnitude measured in Macedonia was M7.8 in 1904 Pehchevo earthquake.

2.2 typical masonry buildings in macedonia

Common understanding for dwellings in traditional culture of Macedonians are houses. This term also implies living space for burning fire and space where most important household matters are organized during the day, while at night it is used for sleeping [Trpeski, 2006]. According to historians, there is not enough data how private architecture of the buildings looked like between XV and XVIII century since there are no preserved monuments to inspect this matter. The only thing left is to study the descriptions left by travellers passing through Macedonia. They point out that buildings in the towns were mainly built with wood, whereas stones were used to build public buildings like churches, mosques, hammams, bezistens (covered bazaars) and etc. When writing about simple residential buildings most of the travellers did not found this town's architecture interesting and often they mention low-rise timber houses or adobe houses, mortared with earth and mud. On contrary, houses where Turks lived were described as luxurious with large verandahs, almost looking like palaces.

(a) House in village Tresonche

(b) House in village Vrben

Figure 6: Traditional bondruk construction from Mavrovo region

Starting from the beginning of XX century, many researchers and architects have studied the traditional building techniques in Macedonia. Some of them, not residents of Macedonia, have studied the traditional houses which incorporated important components from oriental building techniques. Thus, they made efforts to set the basics for development of contemporary architecture in former Yugoslavia. However, their selective approach is the main characteristic of the studies. Namely, their studies were focused primarily on bigger and representative residential buildings dominated by traditional Macedonian town house. Macedonian rural architecture and its important primary architectural forms and materials was completely neglected.

2.2.1 *Building materials in Macedonian traditional buildings*

The properties of structural materials used in Macedonia are based on the climate and geographical conditions, terrain configuration, cultural, historic, socio-economic and ethnic factors, as well as traditional building techniques, available building materials and so on. Generally, basic building materials were materials that can be found everywhere: earth, straw, wood and stone.

Earth (or mud) was considered as essential auxiliary material in every building. Often mixed with husks, it was used as bonding material and for plastering. Mud/earth was used as mortar in crushed or dressed stone masonry. Adobe, fired bricks and tiles were produced from locally available clay earth.

Straw was considered as essential material for construction. It was mixed with mud for plastering and rye straw was used for roof coverings because of their lengths. This technique for roofing prevailed until the first half of the XX century.

Wood was used for simple houses and represented the easiest method for building. Using it in complex house types, it had aesthetic function also. In certain mountain regions, wood was used for timber framing where connections were made by tongue and groove

(a) Wood cantilever extension at house in village Vevchani

(b) Wood truss 'santrach' on double wythe wall

Figure 7: Elements of traditional masonry building

without nails. Other buildings were completely erected with wood in the characteristic 'bondruk' construction, Figure 6. Bondruk consists of wood frame infilled with wattle and daub and covered with a white wash. The framing was made from timber beams in vertical, horizontal and slanted direction. Often, instead of soft vegetation, bondruk was infilled with adobe and stone. Characteristic details of the cantilever extensions of the first floor and/or second floor were found in the houses constructed from wood, as shown in Figure 7a.

Figure 6 available at www.build.mk and www.iskonmakedonija.blogspot.com. [Accessed October, 2011]

Figure 7a available at www.iskonmakedonija.blogspot.com. [Accessed October, 2011]

Stone as building material can be found in all ethnographic parts of Macedonia. In some areas stone was used for the whole house, while others used stones for foundations and for the ground floor. Stone walls were single or double wythe with intermediate horizontal wood beams along the height for levelling and connection between wall skins. These beams are connected with cross beams and create wood trusses, also called 'santraches' in Turkish, see Figure 7b. The cavity between the walls was infilled with stone or brick waste pieces bonded with mortar. Stone masonry was also used in inner walls for room separation. Usually, stone units with irregular shape were used. It was natural or crushed, dressed, for façade walls, and manufactured in blocks laid at corners to provide wall stiffening.

Figure 7b taken by the author in the framework of PROHITECH project. [PROHITECH, 2007]

Crushed, roughly and fine dressed stone masonry walls usually were not plastered, but the joints were pointed with fine mortar. Stone was used for roofing as tiles, also. Construction techniques in traditional buildings are familiar with dry stone masonry, where stone units are laid on top of each other without using bonding materials.

Bricks were used as adobe or fire burned. Usually they were combined with stone in the ground floor while bricks were used on the other floors. Wood trusses were used to level the walls and to connect double leaf walls. Sometimes the outer wall was plastered, but mostly in urban areas, while rural brick houses were left without plaster, see Figure 8. In the first half of XX century residential and public buildings were constructed with brick masonry and lime, cement-lime or cement

Figure 8 available at www.build.mk. [Accessed October, 2011]

(a) Brick masonry house in village Vevchani

(b) Brick masonry house in Skopje

Figure 8: Rural vs. urban masonry buildings

mortar. Most of the buildings were built from URM and only small amount of the building stock in urban areas was constructed with confined masonry. Floors were flexible, made with timber framing, or stiff with reinforced concrete slabs. Generally, masonry buildings in urban areas had two to four floors as shown in Figure 9 and Figure 10. These figures illustrate the present state of typical residential buildings in the city of Skopje constructed in the early 50s of the XX century. Those buildings survived Skopje earthquake with small damage. After 1963 Skopje earthquake, reinforced concrete and steel started to replace masonry as structural material.

Figure 9, Figure 10 available at www.build.mk. [Accessed October, 2011]

(a) URM building with bricks on both floors (Madzir Maalo)

(b) URM building with RC floors (Debar Maalo)

Figure 9: Present state of two-storey brick masonry buildings in city of Skopje

(a) Three storey URM building

(b) Four storey URM building

Figure 10: Present state of multi-level brick masonry buildings in city of Skopje

2.3 in-plane behaviour of masonry walls

Throughout their service life building structures are loaded with variety of external actions in all directions. Horizontal actions from lateral loads are of primary importance for masonry buildings. Such loads can be generated from winds and earthquakes and other sources. All structural elements have to be designed to resist these types of loads. In masonry buildings, main structural elements are walls that in combination with other elements like roof, floors, beams and piers transfer the loads to the foundations. Masonry walls are often subjected to in-plane and out-of-plane loads. As the name indicates, in-plane loads act along the middle plane of the wall, whereas out-of-plane loads take actions in perpendicular direction of the wall plane. Consequently, masonry has to be designed to resist both types of loads, i.e. to prevent in-plane and/or out-of-plane failure mechanisms. In addition to the lateral loads, masonry walls are essentially loaded in vertical direction from self-weight, dead and live loads. Therefore, they are subjected to complex stress state. Out-of-plane behaviour is beyond the scope of this thesis.

Unreinforced masonry can resist compressive stresses because of its high compressive strength. But, it has very low tensile strength which makes this structural material very susceptible to shear and flexural stresses generated from lateral loads. Previous studies in the past few decades have reported that this problem can be overcome by adding steel reinforcement. This intervention increases the ductility and such structural material is known as reinforced masonry. Reinforcement bars are usually placed in bed joints and/or inside the wall in the vertical direction inside the hollow units. The disposition of the reinforcements depends on the unit type and the presence of mortar. However, the problem for understanding the real behaviour of masonry becomes more complicated. Namely, masonry is composite material with anisotropic behaviour and by adding reinforcement, the complexity of the problem increases when interaction between masonry components and steel reinforcement has to be taken into account. Moreover, the difficulty of understanding masonry behaviour rises in confined masonry. Confined masonry represents masonry with vertical tie-columns. The basic feature of confined masonry structures are the vertical, reinforced-concrete or reinforced-masonry bonding tie-column elements, which confine the walls at all corners and wall intersections, as well as along the vertical borders of openings. In order to be effective, tie-columns have to be well connected with the bond-beams along the walls at the floor levels.

Many studies refer to masonry walls as 'shear' walls which indicates that these structural elements can fail in shear only. However, there is an inconsistency with this argument. As Voon [2007] discusses, masonry walls can fail by sliding horizontally, in flexure, or in shear. The mode of failure depends on wall aspect ratios, axial compression stress levels, boundary conditions and the strength properties of the materials. Therefore the name 'shear wall' may not be particularly representative since the dominant mode of failure of a shear wall may be other than shear.

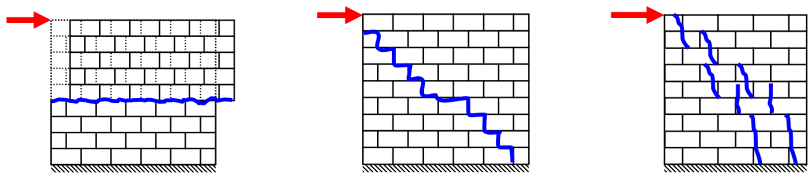

(a) Sliding over bed joint (b) Diagonal head and bed joint failure (c) Block failure

Figure 11: Shear failure modes

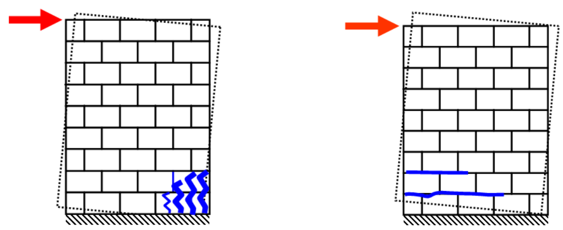

(a) Crushing of blocks (b) Tensile cracking

Figure 12: Compression and tension failure modes

This study concentrates on the in-plane behaviour of unreinforced and strengthened masonry walls. Typical failure mechanisms associated with unreinforced masonry are shown in Figure 11 and Figure 12. Over the past 40 years there has been growing interest in experimental testing of masonry and much information has become available.

Meli [1973] investigated behaviour of masonry panels subjected to lateral loads in one direction and to cyclic loads. Tests were performed on unreinforced, reinforced, confined and infill masonry walls to obtain strength, stiffness, failure modes and post-cracking behaviour. In his study he points out that unreinforced masonry walls had completely brittle failure mode and proposes consideration of linear elastic behaviour for analysis of seismic effects. Also, he alerts about using unreinforced masonry in seismic areas due to catastrophic failures in the past. He found out that reinforced walls falling in bending showed remarkable ductility and elasto-plastic behaviour with little cracking and high deformations under cyclic loads. But, walls falling in shear with diagonal cracking got smaller ductility and brittle behaviour when subjected to high vertical loads. He concludes that for adequate behaviour under cyclic loads, the layout, wall aspect ratio and reinforcement of the walls should be selected in such a way to favour bending failure.

The influence of the applied axial load and the amount of vertical and horizontal reinforcement on the lateral resistance of concrete masonry walls was experimentally evaluated by Shing et al. [1989]. The experimental programme consisted of 16 masonry walls and failure mechanisms, ductility and capability for energy dissipation are discussed. The results showed that the walls that failed in flexure showed greater ductility than the ones that failed in diagonal shear. However, the axial load level had more significant influence on the flexural strength than on the shear strength. The appearance of first major diagonal shear crack depends on the tensile strength of the masonry and the applied vertical load, but not so much on the reinforcement percentage present. The amount of horizontal and vertical reinforcement had influence on the post cracking behaviour. They identified that specimens with low amount of vertical steel reached their maximum resistance right after appearance of the first diagonal cracks. The walls with higher amount of vertical steel sustained $15 - 20\,\%$ additional load. This research highlighted the significance of different design factors on the failure mechanisms of masonry walls which can be used to evaluate the design provisions for reinforced masonry walls.

A comparison of the theoretical and experimental load capacity, stiffness and crack pattern in masonry walls falling in shear was conducted by Angelillo and Olivito [1995]. In their research, they made uniaxial and biaxial compression tests on scaled brick masonry models and tests on brick masonry panels subjected to horizontal loading. They used masonry-like (no tension) model for theoretical

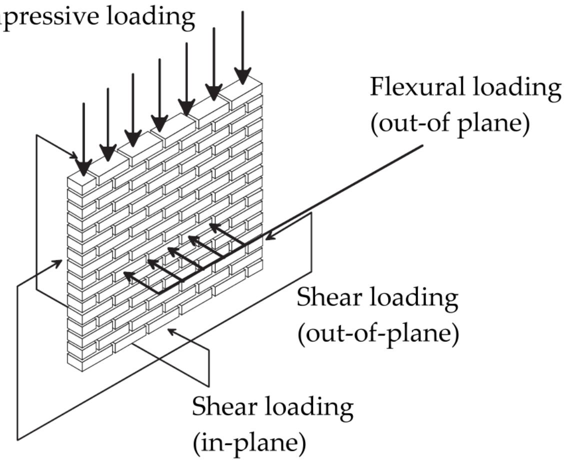

Figure 13: Loading conditions expected on a wall

predictions and introduced sophisticated material laws to analyse phenomena like damage and failure. By assigning elastic-perfectly plastic strength criterion they achieved reasonable predictions for panel global stiffness, fracture pattern and failure mode.

Final conclusion of experimental and analytical evaluation of the seismic behaviour of confined and reinforced masonry walls drawn by Lafuente et al. [1998], does not support the procedure of taking advantage of the inelastic behaviour of the material for seismic resistant design. They suggested discovering other possibilities to achieve ductile mechanisms that provide stable energy dissipating hysteresis cycles. They pointed out that proposed tests in most standards are not suitable to predict the behaviour of masonry walls loaded in-plane with seismic loads and proposed correction factors for cracking resistance of confined masonry walls. This research showed that the presence of reinforcement in the walls does not improve the energy dissipation by inelastic behaviour, but the ultimate load resistance levels were increased. An analytical model for non-linear analysis of masonry walls under monotonic in-plane loads was proposed also.

To get real understanding for masonry behaviour many researchers emphasize the importance for studying experimentally the level of the axial loads applied and the wall aspect ratio. Galasco et al. [2010] highlighted that to provide generally valid results, the selected height of the tested wall samples should be close to a storey height, while the length may influence the expected failure mode. As shown in their study, the level of the axial load shall be decided upon representative value of actual stress levels in inspected types of buildings. For historic stone masonry buildings in Italy, this roughly corresponds to 1/6 of the mean compressive strength of the material and two stress levels of 0.2 MPa and 0.5 MPa were used. As demonstrated by in-plane cyclic shear tests on large undressed double leaf stone masonry walls, they recommend limited deformation capacity associated to both

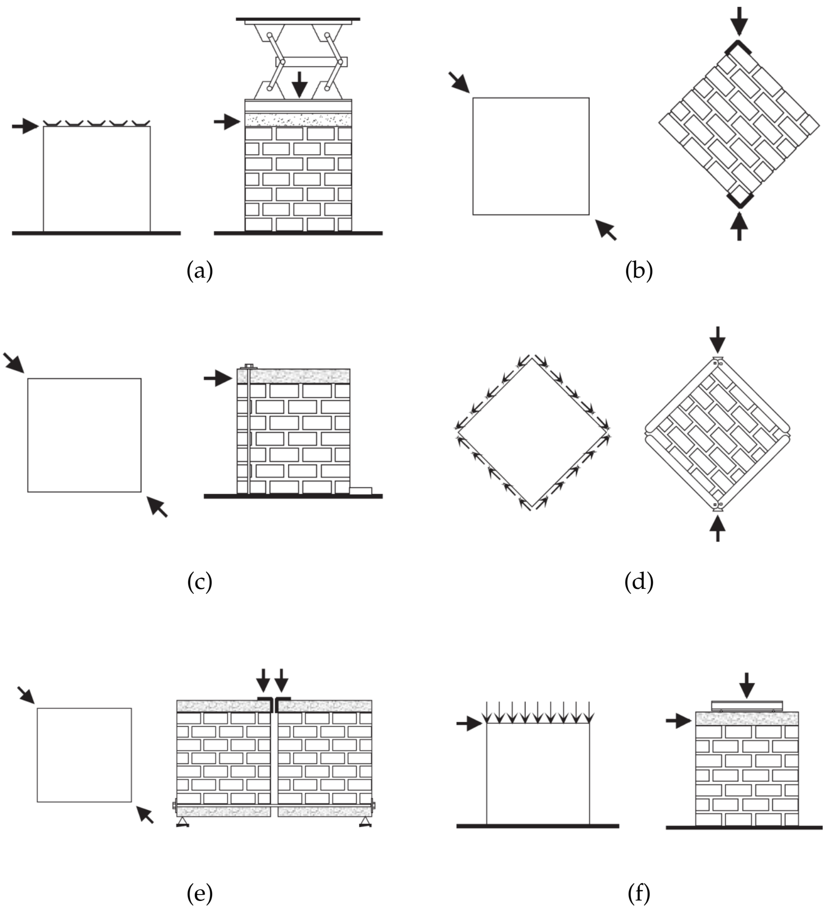

Figure 14: Test set-ups for in-plane shear behaviour

shear and flexure failure mechanisms. Furthermore they suggested representative values for chord rotation capacity of 0.3 % for in-plane shear failure and 0.6 % for in-plane flexural failure.

In a recent review study, Bosiljkov et al. [2010] indicated that the failure modes of structural masonry strongly depend upon the most unfavourable loading conditions that could be expected on a wall panel as illustrated in Figure 13. They also mention that in some situations out-of-plane failure can prevail, but to perform satisfactorily in earthquakes, masonry wall shall have proper in-plane resistance. It is the most important parameter for seismic resistance much needed to avoid collapse of the masonry structure. In their study, they also indicated that the methods used to assess the seismic resistance of unreinforced masonry structures are based on the same principles and numerical models that are used for seismic design of reinforced concrete shear walls and shear-wall structures. Although correct in the linear elastic range, these assumptions cannot be applied in nonlinear range due to composite, heterogeneous and non-linear nature of structural masonry. Another important issue pointed in this research considers absence of harmonised test methods to determine

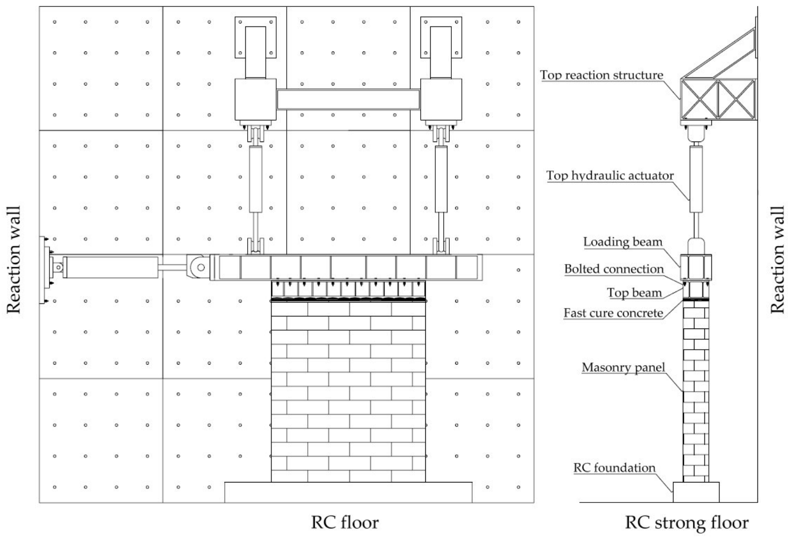

Figure 15: Test set-up proposed by Costa [2007]

the performance and shear resistance of masonry elements subjected to seismic loads. Some referenced test set-ups are shown in Figure 14. Throughout the studies, several different set-ups were used, but none of them simulates the real conditions. Their justification was based on the fact that they reproduced well the static or kinematic boundary conditions which can be interpreted and understood easily.

Figure 14 was first provided by Magenes [1992].

In another study, Costa [2007] developed and proposed new test set-up (Figure 15) and two simplified alternatives for evaluation of the in-plane resistance of autoclaved aerated concrete (AAC) walls. The proposed set-up was based on the test set-up developed for a EU project ESECMaSE and the tests were performed by EUCENTRE at the Structural Mechanics Laboratory of the University of Pavia, in Italy. This set-up ensured fully fixed boundary conditions on the top and the bottom edges of masonry wall specimens and is suitable for simulating masonry buildings with reinforced concrete slabs. The fixed end conditions on the top of the wall were obtained by using mixed displacement/force control system with vertical hydraulic actuators. To avoid the complex control system, two alternative set-ups were proposed. The first one uses simpler control system, while the second one introduces innovative mechanical device to avoid top rotation. The experimental results indicated good displacement capacity and some energy dissipation. The drift limitation of 0.4 % for squat walls and 0.6 % for slender walls was suggested. On the other hand, reinforced AAC walls exhibited improved energy dissipation and largely increased displacement capacity. Also, it was found that vertical reinforcement considerably improved the maximum strength of the walls. For this type of masonry walls, design provisions from Eurocode 6 [2005] gave accurate results and were recommended for computing lateral resistance of AAC walls.

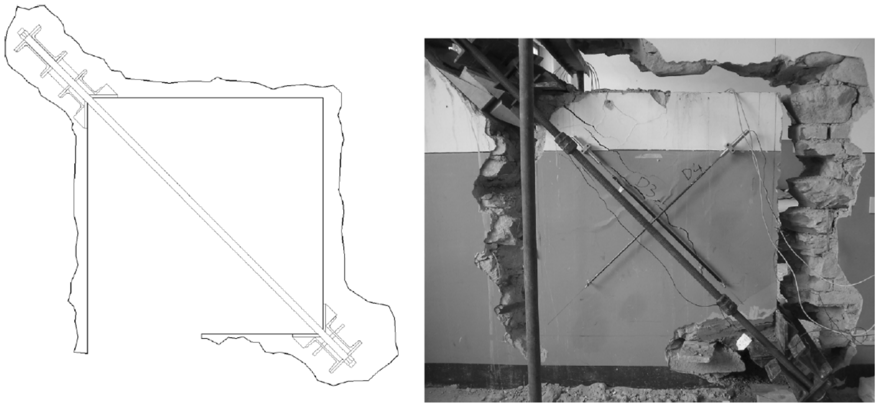

Figure 16: Example of in-situ diagonal compression test

Based on experimental testing of a series of 22 masonry walls and 6 types of hollow clay masonry units subjected to cyclic loads, recently Tomaževič and Weiss [2011] discussed a criterion for robust behaviour required by the codes. Two levels of precompression were used and in correlation of the seismic resistance parameters of the walls and strength properties of the units, no specific robustness indicator has been determined based on the mechanical properties of the tested units. Precompression level was found to be a governing parameter. They demonstrated that the shape and the mechanical characteristics of the tested units have not significant influence on the seismic behaviour of the walls.

As an alternative to laboratory tests to determine tensile strength of masonry walls, in-situ diagonal compression tests can give useful results. Brignola et al. [2009] simulated the behaviour of different masonry typologies to give a numerical interpretation on in-situ experimental results and identify tensile strength, Figure 16. This parameter is very important for seismic safety control of masonry, especially in existing buildings. The experimental tests were performed on 24 masonry panels located in 16 buildings of different villages in the region of Tuscany in Italy. Linear and non-linear analyses were conducted to identify the orthotropic and boundary conditions as well as evolution of the stresses. Through numerical non-linear analysis RILEM and ASTM code interpretations were compared.

In-situ tests proved to be the only reliable method for determination of load-bearing capacity of existing masonry buildings, Figure 17a. As discussed by Tomaževič [1999] this is very important for selection of methods for repair and strengthening especially for buildings located in seismic areas. Sometimes flat-jacks can be used in-situ to determine masonry compressive strength or to evaluate the stress state present in the walls. Other reliable method considered was cutting out specimens from existing walls and testing them in laboratory, as shown in Figure 17b.

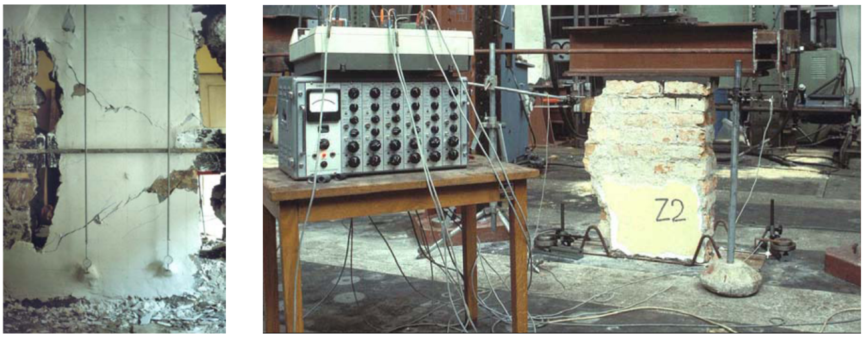

(a) Diagonal shear cracks after in-situ test

(b) Laboratory test on a extracted sample from old brick masonry building

Figure 17: Test methods for verifying masonry properties [Tomaževič, 2007]

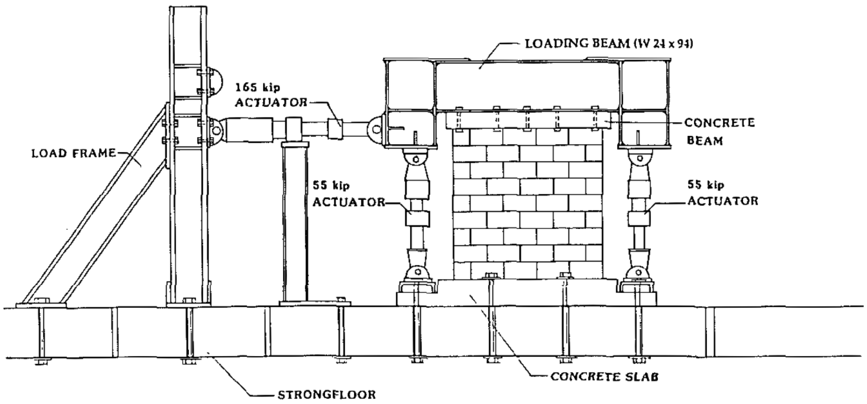

Figure 18: Test set-up by Shing et al. [1989]

2.4 A REVIEW OF TEST SET-UPS FOR IN-PLANE SHEAR BEHAVIOUR

As noted previously, test set-up plays important role in discovering masonry in-plane shear behaviour by experimental tests with cyclic loads. It should be able to provide all necessary parameters about the seismic behaviour of the tested samples, particularly for assessment and performance analysis studies of structural masonry. It is very difficult to construct a single test set-up which represent well the global forces and displacements, crack patterns, failure mechanisms, ductility and energy dissipation capacity, etc. Here, a brief review of the test set-ups used by other authors is presented.

As demonstrated in Figure 18, Shing et al. [1989] used servo controlled hydraulic actuators to apply the vertical and horizontal loads. The lateral displacements were controlled by horizontal actuator connected to a stiff steel frame, whereas vertical actuators were attached to a strong floor in the bottom and stiff steel beam connected to reinforced concrete beam on the top of the wall specimen.

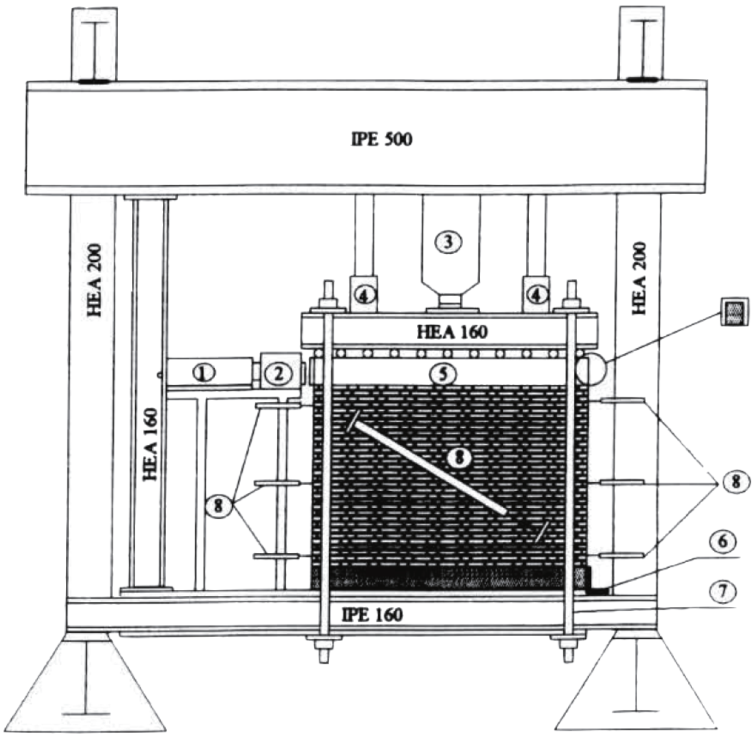

Figure 19: Test set-up by Angelillo and Olivito [1995]

Angelillo and Olivito [1995] used steel test frame to apply vertical and horizontal loads. The rotation of the top beam was prevented with steel rods connected to the bottom steel beam. The application of the vertical loads was by transferring the load from the actuator by means of hydraulic actuator and rollers. This set-up is illustrated in Figure 19.

Gouveia and Lourenço [2007] reported an experimental test set-up within a testing programme designed to study confined masonry with unfilled vertical joints, as shown in Figure 20. It consists of a steel frame, connected to a strong floor, and steel beams, used for transferring horizontal loads on the wall attached to a strong wall. As noted in their article, the top beam was not capable to prevent rotation, and vertical displacements at the edges of the top beam were measured. The reduction of the friction between the top steel beam and the load distributor beam was obtained by using steel rollers. Tests were carried out with constant vertical stress and two full displacement cycles for each amplitude increment to assess strength and degradation.

A special testing device (Figure 21) was used by Stoian et al. [2003] to test masonry shear behaviour and to retrofit the shear capacity using carbon-fibre reinforced polymer (CFRP) composite layers. It consists of a pair of L-shaped steel elements attached to a very stiff concrete block. The steel elements were connected to a strong floor by additional steel frame. Vertical loads were applied on the top of

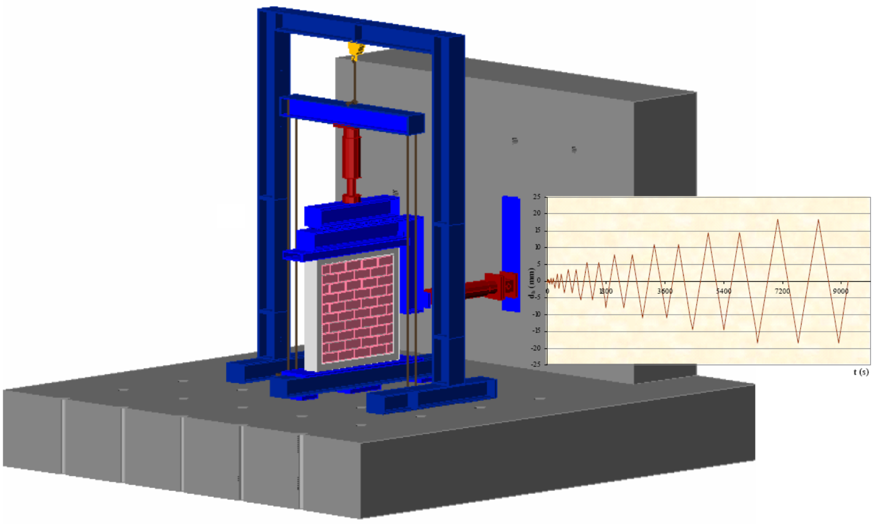

Figure 20: Test set-up referred by Gouveia and Lourenço [2007]

the wall with hydraulic jacks through reinforced concrete bond beam. The horizontal load applied on the wall was transferred from the steel elements by a series of steel bolts embedded in the reinforced concrete bond beam.

In their investigation for retrofitting unreinforced masonry with glass fibre reinforced polymers (FRP), Mahmood et al. [2008] used strong floor-strong wall concept for performing in-plane shear tests. Figure 22 shows the test set-up. For execution of the experiment, test walls were constructed directly on the strong floor by providing proper bonding to the first course of the wall with a layer of strong cement mortar. Vertical loads were applied on the top of the wall by hydraulic jack through four external stressing tendons attached to the strong floor and the top steel beam. Horizontal forces were applied in a displacement controlled manner with double acting hydraulic actuator connected to the strong wall.

In his recent thesis, Haach [2009] reported a test set-up as illustrated in Figure 23. In this study, static cyclic tests on masonry walls were performed under combined vertical and horizontal loads. The bottom reinforced concrete beam of the wall was fully fixed to a steel beam by steel bolts and adjustable clamping angles on both transversal sides to prevent uplifting and slippage. Bottom steel profile was connected to a strong floor by steel anchors. The vertical load was applied by hydraulic actuator and vertical steel cables anchored to the strong floor. The distribution of the vertical load was maintained by stiff steel beam and a set of steel rollers which allowed relative displacement of the wall in respect to the vertical actuator. Additionally, rubber layer was placed between the steel profile and the top reinforced concrete beam to improve the stress distribution. The horizontal load was applied on the top reinforced concrete beam by an actuator with hinges and was transferred to the beam with steel plates. The tests were carried

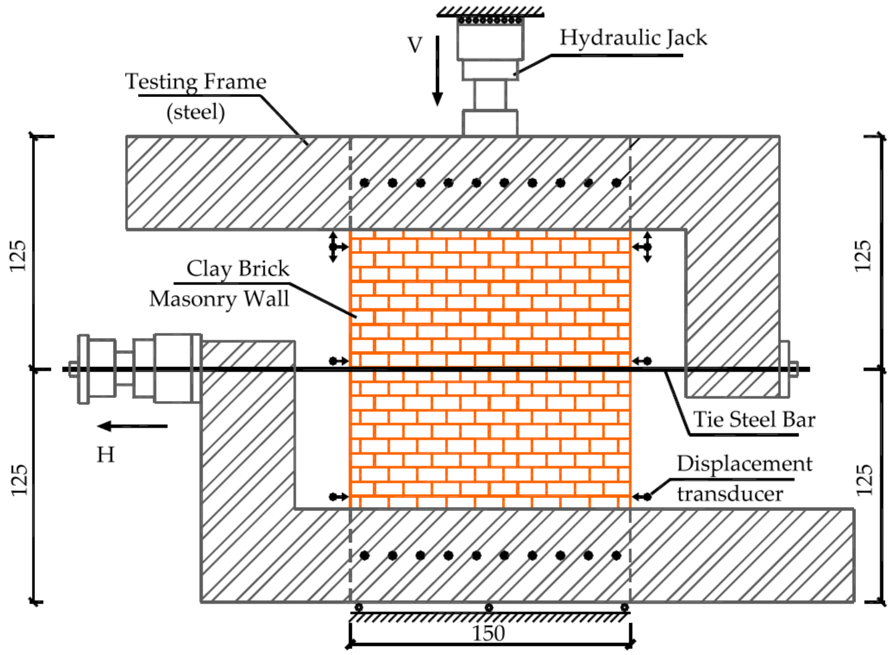

Figure 21: Test set-up by Stoian et al. [2003]

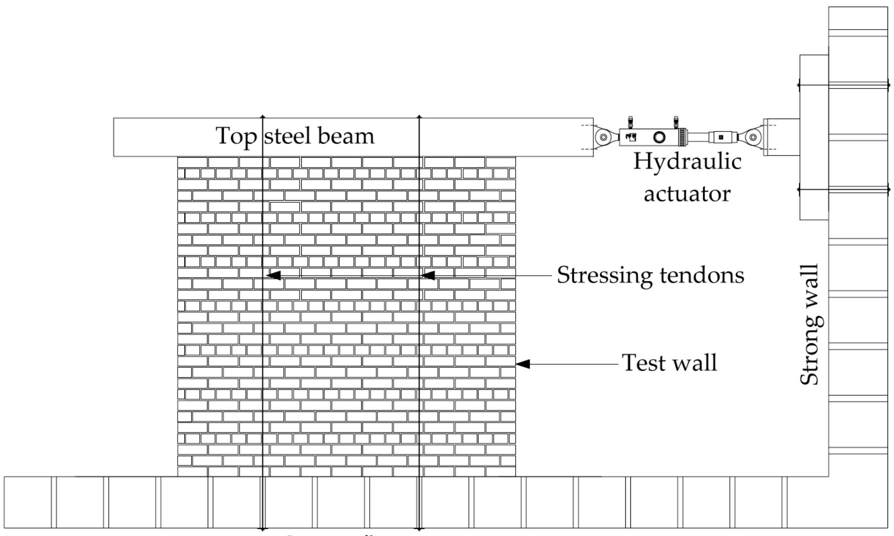

Figure 22: Test set-up by Mahmood et al. [2008]

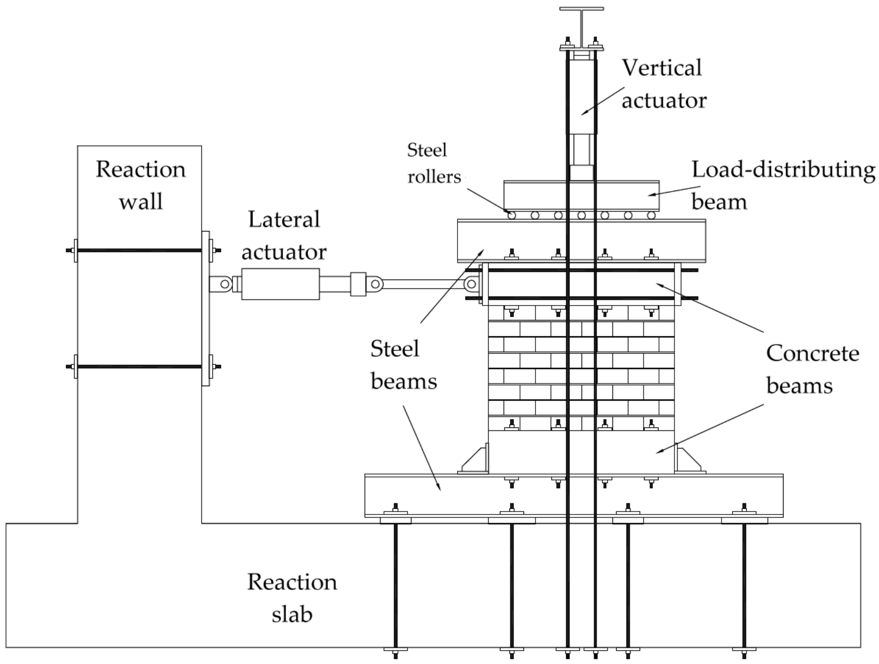

Figure 23: Test set-up by Haach [2009]

out under displacement controlled conditions with two full cycles per displacement increment and constant vertical precompression level.

Some authors performed experimental definition of masonry shear strength by diagonal compression tests and semi-cyclic load application, as reported in Krstevska [2002]. In this research masonry was considered as infill material for reinforced concrete frames. Axial and diagonal compression tests were performed on masonry walls with dimensions 90x100x12 cm and 90x100x25 cm, Figure 24.

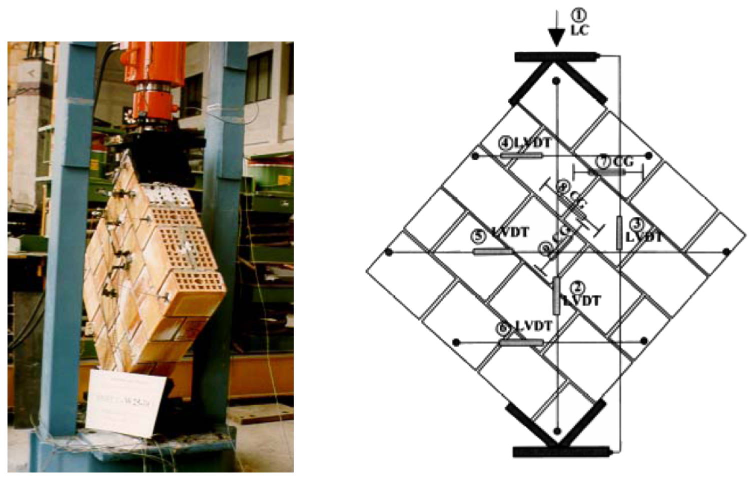

(a) Wall sample tested under diagonal compression

(b) Instrumentation of the tested wall

Figure 24: Test set-up by Krstevska [2002]

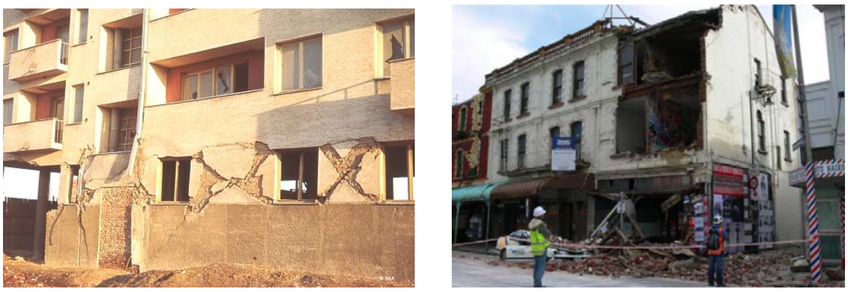

(a) In-plane damage on residential masonry building after 1963 Skopje earthquake [Ambraseys, 1967]

(b) Out-of-plane failure of walls after 2010 Canterbury earthquake [Ingham and Griffith, 2011]

Figure 25: Damage in masonry buildings caused by earthquakes

The effects of the tensile stresses in different directions and shear stresses in the mortar joints were also studied by diagonal compression tests, as discussed in Meli [1973].

2.5 strengthening techniques and materials for masonry

Masonry structures are vulnerable to seismic actions and it is necessary to improve their performance to be able to resist the next earthquake. The most common type of damage to masonry buildings caused from earthquakes are diagonal, horizontal and 'X' shaped cracks causing in-plane failure (Figure 25a) and diagonal cracks in building corners causing out-of-plane failures (Figure 25b).

As defined in Tomaževič [1999], seismic strengthening or upgrading comprises technical interventions in the structural system of a building that improve its seismic resistance by increasing the strength and the ductility. Strengthening a building before an earthquake is called "rehabilitation", whereas strengthening after the earthquake is called "retrofit". Structural restoration of existing masonry buildings represents major activity in the field of construction, mainly because of the requirements to protect impressive number of buildings with outstanding value from ageing, earthquakes and human misuse. In this subsection an overview of techniques for strengthening masonry walls are presented.

The strengthening process of masonry structural elements requires from the design engineer to assure the increase of bearing capacity and/or ductility of the strengthened elements, as identified in Dumova-Jovanoska et al. [2005]. Beside designing according code provisions and engineering design practise, the addition of new elements should ensure proper fixation into the existing structural system. The newly designed structural elements, as well as the repair and strengthening of the existing elements must satisfy the conditions in respect to the historic value and integrity of the structural elements and the

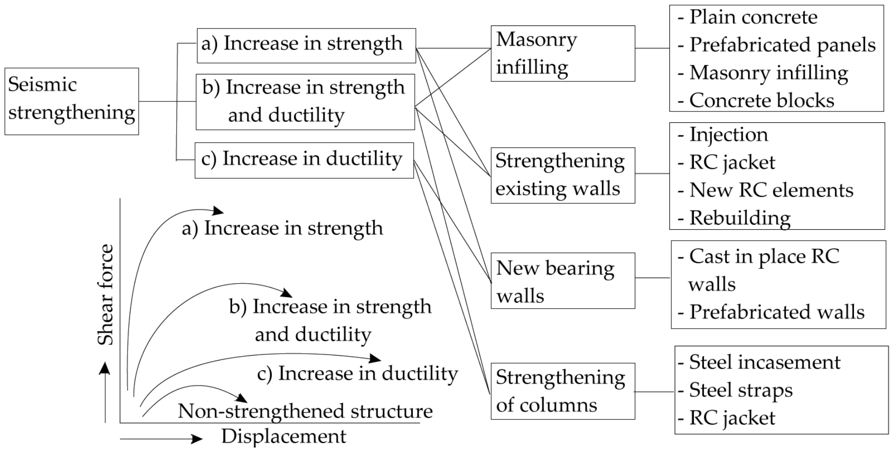

Figure 26: Concept and methodology for seismic strengthening

integral structure. Depending on the selected repair and strengthening solution, a general concept and methodology is shown in Figure 26.

To select appropriate strengthening method, a profound knowledge about the structural behaviour and materials is needed. In the past, many buildings have been repaired and strengthened using engineer's experience and intuition. In a lack of understanding of the causes, there were some cases where cracks were repaired by simple coverings with plaster and mortar. We are witnesses of today's building and reconstruction practice how critical errors have been made in adaptation and accommodation of new living spaces in old buildings. These errors include removal of structural walls in all levels of a building or in the ground floor only, adding new levels when upgrading a building, creating openings in the existing walls and etc., without proper strengthening of the existing structure. Structural strengthening of historic monuments is part of a complex multi-scale approach for conservation and restoration and is not a objective of this research.

Seismic strengthening is complex procedure aiming in strengthening individual structural elements, but also in ensuring good performance of the whole structural system. Hence, the lateral resistance, ductility and energy dissipation capacity of a building should be validated. The technical measures for strengthening of masonry buildings according to Tomaževič [1999] can be classified in two cases, (1) techniques applicable to individual elements, like strengthening masonry walls, and (2) techniques for improving structural integrity, like tying the walls, anchoring and stiffening of floors and roofs to walls. When applying strengthening techniques, a number of important technical criteria should be met. Namely, walls should be uniformly distributed in both orthogonal directions of the building with sufficient number and strength to resist seismic loads. Moreover, the walls should be tied and connected properly together and with the floors which should possess high rigidity in their plane.

2.5.1 *Strengthening of the masonry structural system*

Strengthening of stone masonry buildings mainly consist of interventions which provide appropriate connections between masonry walls and masonry walls to floors. Such measures should provide integral behaviour of the structural system to resist seismic loads. The strengthening methods include: connection of walls in both directions with reinforced concrete (RC) bond beams, stiffening or replacement of flexible floor systems with RC slabs, rebuilding of individual walls, and partial or full injection of cavities and cracks, application of RC jackets and etc.

Similarly to strengthening stone masonry, strengthening of adobe masonry structures is performed by establishing wall to wall and floor and roof to wall connections. Depending on the designed seismic resistance level, adobe masonry strengthening techniques consists of: connections of transverse and longitudinal structural walls by RC jackets, replacement of timber floor structures by RC slabs, rebuilding of individual walls and return of the dislocated walls into their original position. Particular attention has to be paid to insertion of new walls in the buildings which do not have transverse stiffening walls.

2.5.2 *Strengthening of brick, concrete and mixed masonry*

Masonry buildings constructed from bricks, concrete blocks and mixed masonry systems are relatively new buildings that possess certain seismic resistance. Usually their level of damage is lower in contrast with other structures. Most of them are constructed with RC bond beams and columns and have RC floor slabs which satisfy the demands for structural integrity. These structures are strengthened by insertion of vertical RC elements in case these do not exist, injection of cracks, rebuilding of individual walls with cement mortar, application of different coating types and strengthening of the foundations. Masonry structures without vertical RC elements are strengthened by insertion of vertical columns in the ends of the walls and at the intersection points of the structural walls. In the case of systems with no sufficient stiffening transverse walls, these walls have to be inserted. Also the partition walls have to be rebuilt by solid bricks in cement lime mortar with a thickness of 25 cm framed by RC horizontal and vertical bond elements [Dumova-Jovanoska et al., 2005].

2.5.3 *Strengthening materials*

The process of selection of adequate strengthening materials requires satisfactory knowledge on materials available for such application. Traditional materials, although insufficient in providing such solutions, take important part in the procedures of strengthening masonry.

But if designed with care, traditional materials give good results by increasing the seismic resistance and involve low cost expenses, easy application and short time for implementation. In the same time, application of new materials and innovative techniques for strengthening arises very often. During the past years, there has been a large volume of published studies on application of new materials and technologies for strengthening masonry, in particular application of composite materials (FRP) from glass, carbon and kevlar fibres (Stoian et al., 2003; Li et al., 2005; Faella et al., 2010), textile reinforced mortar (TRM), (Papanicolaou et al., 2008; Islam et al., 2011), Shape Memory Alloys (SMA) (Tirelli et al., 2001) and etc. The following subsection describes very briefly the materials often used in traditional techniques for strengthening masonry buildings.

Concrete (cast in-situ) refers to conventional concrete, very often used when strengthening masonry. There have been numerous cases of poor concrete behaviour, caused by volume change and shrinkage in addition to weak contact strength between the new concrete and the old strengthened material. To overcome such problems, conventional cement based concrete should be replaced by high strength concrete with minimum water-cement (W/C) ratio and low slumps. Other admixtures that contribute to higher initial and final concrete strength and provide longer concrete consistency and reduce shrinkage such as superplasticizers are highly recommended. Casting method is very important for cast-in-situ concrete to ensure adequate bonding to the old material. Vibration of the new concrete is necessary to prevent creation of air pockets and voids and to obtain solid volume of concrete. Cast-in-situ concrete with constant volume is another type of strengthening material. It contains expansive admixture that compensate the shrinkage of the mix, but requires special care when designing the mixture and extensive laboratory testing to determine concrete properties. Other similar types of concrete like polymer modified concrete are also used for strengthening masonry.

Shotcrete is essentially concrete with very fine gradation of selected aggregates, that is applied onto strengthening surfaces by gun sprayers. Single or double-side shotcrete with minimum layer thickness of 60 mm is normally used. In combination with a reinforcement, it presents powerful strengthening technique. In contrast to cast-in-situ concrete, it requires highly trained personnel for preparation and application. An advantage over the conventional concrete is the high final strength obtained as a result of high compaction energy during application and low W/C ratio of the mix. Shotcrete can be easily applied on vertical, inclined and overhead surfaces with minimum formwork requirements. Similarly as traditional concreting, detailed surface preparation is necessary to remove any loose material, sand or dust from the surface, to apply a primer or simply wet the surfaces. Such preparation ensures proper bonding between the old and new material. This crucial step in shotcreting is often violated and a main reason for poor bond strength. Adding polymer materials in shape of fibres improves shotcrete material properties, especially influences in reducing cracking due to shrinkage, slightly increases tensile strength and provides better confinement of the shotcrete. Time consumption for application, reduction of available space, disturbance of the occupants, and final wall appearance in addition to added mass that increases seismic inertial forces are the main disadvantages of shotcrete.

ElGawady et al. [2006] performed static cyclic tests on URM walls strengthened using shotcrete to investigate their in-plane behaviour. One single-sided shotcrete specimen and one double-sided specimen were tested in addition to one reference specimen. The same amount of reinforcing bars was used in both cases. The walls were made with hollow clay brick masonry units and weak mortar. Double-sided specimen had shear dowels fixed into drilled holes into the masonry to provide a link between both shotcrete layers. Test results showed increase in the lateral strength of the specimens by factor of 3.6, coupled with more ductile failure and energy dissipation of the double-side specimen.

Previously, Hutchinson et al. [1984] carried out in-plane tests on brick walls strengthened by various methods under a slow cyclic loading. Strengthening methods examined were: prestressing, shotcrete, glass reinforced cement (GRC), steel fibre reinforced concrete (FRC) and ferrocement. Shotcrete was found to be a good solution in respect to the shear behaviour and costs compared on unit basis, but in the same time less economical than GRC and FRC on a strength basis. Other cementitious coatings, such as thin fibre reinforced coatings, were found to be very competitive to other solutions and higher lateral resistance and ductility was identified.

Kahn [1984] conducted a series of diagonal compression tests on old brick masonry panels retrieved from a demolition of an old building and retrofitted by layer of reinforced shotcrete. Seventeen brick panels were tested under a single, static reversed cycle load applied across their diagonal. The purpose of the study was to examine the in-plane behaviour of brick-shotcrete panels and quality of the brick-shotcrete bond and other effect of the most commonly used strengthening technique. In his study Kahn [1984] concluded that wet brick surfaces provided proper bond which ensured development of full composite strength of the panel. Moreover, in contrast to the expectations, the dowels did not improve the composite behaviour or bond of two layer shotcrete brick panels. Shear strength and ductility primarily were dependent on the shotcrete properties and the reinforcement.

Resins and Grouts are traditional materials used for injection of cracks and gluing of thin steel sheets. There is large variety of available products and the components used for injection should be carefully investigated and properly designed. The environmental conditions have influence on the material properties, adhesion and shrinkage effects. Resins and grouts can be injected to fill the cracks and voids by using low or high pressure injection or vacuum injection. In dependence of the crack widths, resins can be used with or without fillers. Two types of grouts are traditionally used for injections, the first one using cement base, and the second one using polymer grout. Resin or grout injection is expensive technique, very time consuming and requires highly trained workforce.

Other types of strengthening materials such as glued metal or FRP straps or sheets, steel shear connectors (anchors), steel reinforcement bars anchored and welded, masonry stitching, construction of new masonry or RC shear walls and others are not discussed in this study.

The primary attention in this research is given to a traditional strengthening technique often used in the building practice in the country and in the wider region, namely strengthening by RC jackets.

2.5.4 *RC jacketing*

Primary investigation in this research is given to a strengthening technique often used to improve the lateral resistance and energy dissipation of the system or in the case of seriously damaged brick- and block masonry walls, as reported by Tomaževič [1999] and Beg [2005]. RC jacketing is strengthening and retrofitting technique that consists of application of single- or double-sided RC walls or coatings. This method is also known as RC coating, RC overlay, RC cladding and RC mesh. This technique is suitable both for stone and brick masonry. Although similar to shotcrete, it has distinctive features elaborated in the following paragraphs.

The execution starts by removing the plaster from the wall face and removing the mortar from the joints between the units at a depth up to 15 mm. This process is crucial to establish good bond between the new and old material. If cracks are discovered in the wall, they are first injected or grouted. If single-side jackets are used, pieces of stone or brick are removed at regular intervals and reinforcing cage is placed and concreted. This provides good shear connection which transfers the loads from the new jacket to the existing wall (Figure 27). If double-side jackets are applied, holes are drilled into the mortar joints at interval of $100 - 150$ mm in both orthogonal directions (Figure 28). Reinforcing anchor ties with diameter of $4 - 6$ mm are placed into the holes to link both RC meshes and then cemented or epoxied. The approximate quantity of anchor ties considered by Tomaževič [1999]

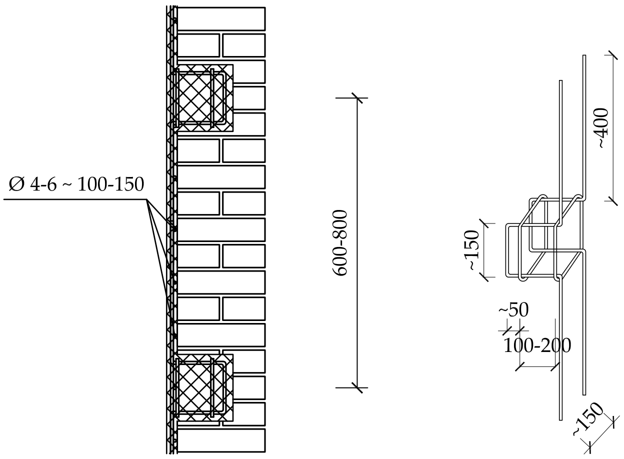

(a) Single-side RC jacket

(b) Reinforcement cage detail

Figure 27: Shear connection of single RC jacket to brick masonry wall

is $4-6$ pieces per m^2, while Sheppard and Terčelj [1980] propose 10 pieces per m^2.

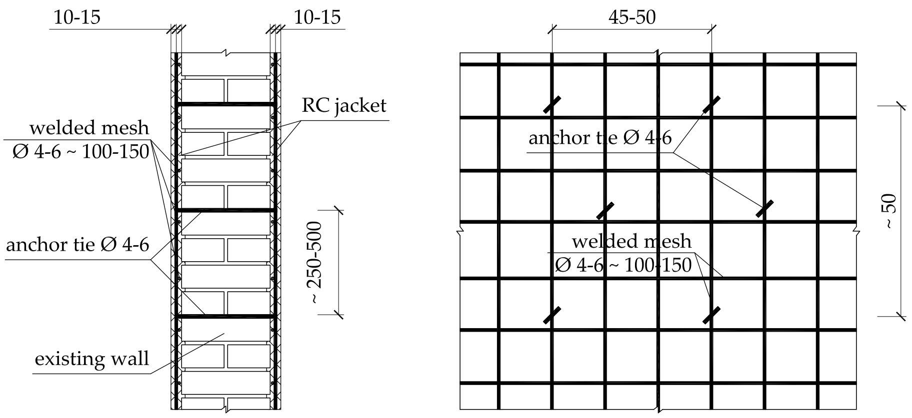

(a) Double-side RC jacket

(b) Anchor tie position

Figure 28: Application of RC jacket to brick masonry wall on both sides

After that, the surface is cleaned from loose material and dust, moistened with water and spattered with cement milk or other cementitious primer. The RC jacket is applied in two layers of cement mortar. The first layer is applied on the prepared surface by casting or by trowel. The thickness of the layer is about $10-15$ mm, and is designed with a compressive strength of $20-30$ N/mm^2. Reinforcing meshes with bar diameter of $4-6$ mm at distance of $100-150$ mm in both directions are placed on the wall and connected to the anchor ties. Usually wire-mesh is used, though single bars can be applied also. The connection to the anchor ties is created with simple wire or by welding. After the reinforcement was placed, the second layer

of cement mortar is applied. Some researchers (eg. Tomaževič, 1999) have recommended that the total thickness of the RC jacket has not to exceed 30 mm. Other authors, (see Dumova-Jovanoska et al., 2005) propose the jacket thickness of $60 - 100$ mm.
The jackets run from the foundation level up to the designed floor level. The reinforcement at each floor level has to be connected to a bond beam or RC slab. If RC bond beams or slabs are not existent, usually they are inserted at floor levels during the strengthening process. The thickness of the bond beam passes the entire section of the jacketed masonry wall, while the height is proportioned according to the structural analysis results. The connection between the jackets and the bond beams are created inside the beam, by connecting (or welding) the longitudinal reinforcement from the jackets with the transversal reinforcement (stirrups) in the beams. Usually, additional reinforcement is placed at the ends of the walls. This aspect is supported by Dumova-Jovanoska et al. [2005] who take into account stress analysis for definition of the additional reinforcement if the ultimate stress due to moment effect is considered referent. In all other cases, it was suggested to place 6 vertical structural reinforcement bars with diameter 14 mm on each side of the wall. In this report it was pointed out that the jackets have to be constructed with pressurized gunite concrete. The portland cement content was defined at 500 kg/m^3 and the lower limit of W/C ratio was assigned to 0.4. For efficient performance during gunite concrete application and to ensure better tube flow, improved adhesion to the wall, increased compactness and better flattening, admixtures for concrete and mortar were proposed. Layers with thickness up to 30 mm of concrete gunite sprayed in circular motion at a distance of $600 - 1000$ mm with a pressure of $2 - 3$ bar were proposed. RC jackets can be applied by simple concreting. In such case, the thickness of the layers has to be $80 - 100$ mm. If concrete is used and poured into forms, the reinforcing mesh with bar diameters of $8 - 10$ mm at a distance of 250 mm have to be used.

Several experimental studies have attempted to explain the effect of strengthening masonry walls by RC jackets and their in-plane behaviour when subjected to horizontal loads. Sheppard and Terčelj [1980] conducted experimental programme for testing masonry walls under combined vertical and horizontal loading. Twenty URM walls and twenty strengthened walls from five different masonry types were tested. Cement grouting of ten walls and application of steel-mesh reinforced cement plaster layer on another ten walls was investigated. In the case of walls strengthened with reinforced plaster layers on both sides, the shear strength was increased to such an extent that the failure mechanism changed from shear to flexure. Large increase of the tensile strength was achieved and the horizontal load-carrying capacity of normal strength masonry was increased by a factor of 2, while in the case of walls with high initial tensile strength, the increase was by a factor of 1.25.

The technical feasibility of RC jacketing applied to confined masonry walls was experimentally investigated by Alcocer et al. [1996], on four full-scale specimen tested under alternated cyclic lateral loads. This study involved variable level of damage, type and size of specimen, wire-mesh diameter and anchor tie bar types. More uniform crack pattern, remarkable increase in lateral strength and deformation capacity and greater dissipated energy in all jacketed specimen was found. Crack pattern and failure mechanisms were governed by shear deformations. More importantly, the amount of steel reinforcement did not have influence on the initial stiffness of the undamaged, jacketed walls. Furthermore, the contribution of the steel welded meshes to the strength, depended on the amount of horizontal reinforcement, applied deformation, anchor type and mortar quality. Maximum design drift ration of jacketed confined masonry walls considered was 0.007. Nine anchor tie bars per m^2 were recommended. It has been demonstrated that RC jacketing is an effective technique for improving seismic resistance of masonry buildings.

An important study of the efficiency of the current techniques for repair and strengthening of historic masonry buildings, following 1997 Umria-Marche earthquake, was presented in Penazzi et al. [2001]. An extensive survey of damaged multiple leaf stone masonry buildings previously repaired and strengthened after the 1979 earthquake was carried out. Structural and material compatibility problems were identified and lack of knowledge of the materials and building construction details, wrong choice of repair technique and its poor application was distinguished as the most sensitive issues in repairing and strengthening historic stone masonry buildings. Wall and pier jacketing was pointed out to be largely applied technique in Italy, used to strengthen and repair stone masonry walls in addition to the fact that it was recommended by the Italian code. The most widespread mistakes and associated damages discovered were: (1) lack of connection between reinforcement meshes and to the floors; (2) missing overlapping distance between two reinforcement meshes; (3) absence or too widely spread anchor ties caused separation of RC layers from the wall; (4) usage of too short anchor bars; (5) presence of steel bar corrosion due to poor concrete cover and (6) lack of uniformity of distribution of the repaired areas in the buildings caused non-uniform stiffness distribution and occurrence of torsion stress.

As summarized by ElGawady et al. [2004], this strengthening technique improves the in-plane lateral resistance of a strengthened wall to 2-3 times in comparison to unreinforced wall, improves lateral displacement while on the same time improves stability of the wall in the out-of-plane direction. Low technology requirements and limited addition of mass were pointed out as main advantages, whereas reduction of space, architectural impact and required architectural finishing were indicated as disadvantages.

Ghiassi et al. [2008] reported that RC coating with reinforced concrete layer applied to brick masonry buildings was one of the most popular strengthening methods in Iran. It was discussed that this method provides good strength and ductility to masonry buildings, and controls crack propagation. The lack of experimental and analytical information on this method was highlighted and conclusion was made that in the practice it is often applied based on empirical recommendations. To investigate analytically the in-plane behaviour of retrofitted masonry wall with RC concrete layer, a novel approach was proposed. RC coated wall was considered as composite material consisting of masonry and reinforced concrete. Biaxial stress-strain relations and failure criteria for masonry were implemented and all failure mechanisms were taken into account. Smear crack approach for reinforced concrete was used. Good agreement of analytical results with existing experimental results was obtained.

The experiments, which showed that RC jacketing improves the lateral capacity, have also indicated the importance of adequate anchoring of jacket reinforcement to the existing masonry. If the connection was not adequate to prevent splitting, the coating separated from the wall at the occurrence of cracks in the masonry wall and buckled.

2.6 DESIGN PROCEDURES

RC jacketing is widely used retrofit and strengthening technique applied to masonry structures. Nevertheless, there are no specific design provisions that predict the lateral capacity of the composite masonry wall elements nor lateral displacements. Over the years, some attempts to establish adequate design provisions have been made, but still none of the modern design codes does not prescribe any specific method for analysis of RC jacketed masonry walls. On contrary, there are many design codes that prescribe design guidelines for URM, reinforced masonry or confined masonry, as well as reinforced concrete.

Since no design model for RC jacketed masonry walls is given in the literature, a primary goal in this research is to investigate if the available design models and concepts for reinforced masonry are suitable for obtaining the bearing capacity of RC jacketed walls. Such concept was proposed due to the similarity of the both structural materials. This is demonstrated by comparing experimentally the obtained results from testing of RC jacketed walls subjected to in-plane cyclic loads and the design models for reinforced masonry given in few codes and provisions. For reference, URM walls were analysed with the selected available code models, also.

This section presents a brief overview of some well known approaches for calculation of the shear strength of unreinforced and reinforced masonry walls.

2.6.1 *Actual regulations in Macedonia (PIOVSP'81 code)*

Actual regulations in Macedonia are based on the 'Code of Technical Regulations for the Design and Construction of Buildings in Seismic Regions' - PIOVSP [1981], first published in Official Gazette of former SFR Yugoslavia. The code was enforced in June 1981, amended in 1982 (Official Gazette 49/82), 1983 (Official Gazette 29/83), 1988 (Official Gazette 21/88), and in 1990 (Official Gazette 52/20).

PIOVSP'81 is still valid in Macedonia.

Section 16, article 89, defines the basic structural system of masonry buildings. As proposed, it should consist of load-bearing walls placed in both orthogonal directions of the buildings and connected together at the level of the rigid floor by horizontal tie-beams. Moreover, this code divides masonry structure types in three categories:

In the references, sometimes tie beams are referred as bond beams.

- Ordinary, plain masonry structures (Unreinforced masonry);
- Masonry structures with vertical RC tie beams (Confined masonry), and
- Reinforced masonry structures.

Provisions regarding masonry materials, wall thickness, wall distribution in plan view, floor structures, and reinforcement details are given in several articles. Two possibilities for analysis and design are offered. If the seismic resistance is estimated by the method of allowable stresses, then the principal stresses in the walls have to be checked. Depending on the wall type, stresses ranging from $\sigma_{allow} = 0.06 - 0.11$ N/mm² are allowed. The principle tensile stresses in the walls are calculated by Eq. 2.1.

$$\sigma = \sqrt{\left(\frac{\sigma_0^2}{4} + (1.5\tau_0)^2\right)} - \frac{\sigma_0}{2} \leq \sigma_{allow} \tag{2.1}$$

where,

τ_0 average shear stress in the wall caused by seismic load

σ_0 average normal stress in the wall caused by vertical load

If the seismic resistance of masonry buildings is controlled by the limit-state method, then the resistance of the building should be compared to the total seismic force calculated according to the provisions in the code, taking into account a safety factor of at least 1.5. The ultimate average shear stress in the walls is calculated with Eq. 2.2.

$$\tau_{0,ult} = \frac{\sigma_{n,ult}}{1.5} + \sqrt{1 + \frac{\sigma_0}{\sigma_{n.ult}}} \tag{2.2}$$

where,

$\tau_{n,ult}$ ultimate average shear stress in the wall at ultimate load

$\sigma_{n,ult}$ principal tensile stress in the wall at ultimate load

The PIOVSP [1981] allows application of cement-lime-sand mortar of class M2.5-M5.0 for construction of masonry buildings in seismic regions. It strictly prohibits usage of cement mortar.

2.6.1.1 *RC jacketed walls*

The repair and strengthening measures applied to masonry buildings are summarized in article 17 in the 'Code for technical regulations for repair, strengthening and reconstruction of buildings damaged in earthquakes' (PSZRV [1985]). These interventions include: strengthening and repairing of the existing structural system, strengthening by reconstruction of individual walls in the structural system, introduction of new walls in the structural system, and tying of the walls at the levels of the floor structures. Article 19 highlights the strengthening techniques for brick and block masonry and allows single- or double sided RC jacketing with thickness of $3-5\,\text{cm}$. Some requirements for the reinforcement of the RC jackets are given in article 21:

- Reinforcement mesh and concrete coating with class MB 30 should be applied;
- The central part of the wall should be reinforced with vertical reinforcement with an area of at least 0.05 % from the total horizontal cross-section of the wall with the jackets;
- On both ends of the wall, the vertical reinforcement with an area of at least 0.05 % from the total horizontal cross-section of the wall is grouped and placed at a length of 1/10 from the length of the horizontal cross-section of the wall. This reinforcement is guided through floor structures and is anchored in the foundations;
- The total area of the vertical reinforcement should not be less than 0.15 % from the total horizontal cross-section of the wall;
- The area of the horizontal reinforcement placed in the jackets should not be less than 0.1 % from the total thickness of the wall per each meter height, and
- The reinforcement mesh in the jackets should be anchored to previously cleaned and prepared wall surface.

For stiffness calculations, the thickness of the wall should be increased by four times the thickness of the RC jackets.

2.6.2 *Tomaževič [1999]*

2.6.2.1 *Unreinforced masonry walls*

Tomaževič [1999] and [2009b] defines the shear strength of masonry as resistance of masonry wall to lateral in-plane loads in the case that the wall fails in shear. It has been highlighted that the parameter describing the shear resistance of the masonry wall depends on the physical model describing the failure mechanism. Shear strength of masonry, based on friction analogy, and diagonal tensile strength of masonry have been pointed out as mechanisms for controlling the masonry resistance. Based on the theory of Turnšek and Čačovič [1971], the in-plane resistance of masonry wall falling with diagonally oriented cracks passing through masonry units in case of brick-masonry wall, or passing through stones and mortar has been explained.
Diagonal cracks at shear failure caused by principal tensile stress corresponding to the vertical and lateral load have been assumed. Tomaževič [1999] assumes ideal elastic, homogeneous, isotropic wall behaviour up to the failure. The corresponding principle tensile stress at maximum resistance of the wall has been defined as 'tensile' or 'referential tensile strength of masonry', (f_t). The principal compressive and tensile stresses caused in the middle section of the wall resulting from combined action of vertical and horizontal loads can be calculated according to Eq. 2.3.

$$\sigma_p = \sqrt{\left(\frac{\sigma_0}{2}\right)^2 + (b\tau)^2} \pm \frac{\sigma_0}{2} \tag{2.3}$$

oriented in the directions of both diagonals of the wall

$$\phi_c = \phi_t = 0.5 \arctan \frac{2\tau}{\sigma_0} \tag{2.4}$$

where,

$\sigma_0 = \frac{N}{A_w}$	average compressive stress in horizontal section of the wall due to constant vertical load
$\tau = \frac{H}{A_w}$	average shear stress in horizontal section of the wall due to horizontal load
A_w	area of the horizontal cross-section of the wall
b	shear stress distribution factor in relation to wall geometry and ratio between vertical load N and maximum horizontal load H_{max}

Assuming the behaviour of the wall up to the maximum horizontal load (H_{max}), as elastic, homogeneous and isotropic, the principal tensile stress (f_t), is calculated:

$$f_t = \sigma_t = \sqrt{\left(\frac{\sigma_o}{2}\right)^2 + (b\tau_{max})^2} - \frac{\sigma_0}{2} \tag{2.5}$$

where,

f_t tensile strength of masonry

τ_{max} average shear stress in horizontal section of the wall at maximum horizontal load H_{max}

Following this approach, the lateral resistance $(H_{u,s})$ of URM wall failing in shear can be evaluated with Eq. 2.6.

$$H_{u,s} = A_w \frac{f_t}{b}\sqrt{\frac{\sigma_0}{f_t} + 1} \tag{2.6}$$

In a recent comparative study Tomaževič [2009b] found that calculation of the shear resistance of masonry based on sliding shear mechanisms do not correlate well with the experimental results, and do not provide accurate information for seismic resistance of URM and confined masonry structures. On the other hand, it has been demonstrated that results from calculations based on the assumption of diagonal tension shear failure mechanisms are in good agreement with the experimental results.

However, shear sliding failure mechanism is considered by Tomaževič [1999]. This was explained as situation occurring in upper storeys of a buildings, at walls with low level of vertical forces and very high level of horizontal forces. In a case of unreinforced masonry, the sliding shear resistance of a wall is calculated by Eq. 2.7.

$$H_{u,sl} = \mu_c \sigma_0 A_w \tag{2.7}$$

where,

μ_c friction coefficient of the unit-mortar interface

Flexural resistance of URM failing with bending failure mode was considered similarly like in Eurocode 6 [2005], by taking into account rectangular compressive stress block in a masonry wall section. To obtain the flexural capacity of the section through corresponding ultimate bending moment (M_{Ru}), equilibrium of sectional forces in the most stressed section of the wall was assessed. The ultimate bending moment can be calculated with Eq. 2.8.

$$M_{Ru} = \frac{\sigma_0 t L^2}{2}\left(1 - \frac{\sigma_0}{0.85 f_k}\right) \tag{2.8}$$

The flexural resistance of the wall $\left(H_{u,f}\right)$ can be determined depending on the boundary conditions:

$$H_{u,f} = \frac{M_{Ru}}{\alpha h} \tag{2.9}$$

where,

α boundary conditions at the bottom and the top of the wall

$$\alpha = \begin{cases} 0.5 & \text{for fixed ended wall} \\ 1.0 & \text{for cantilever wall} \end{cases}$$

The boundary conditions in real buildings are difficult to determine and exactly simulate or implement in a design model. The fixity conditions may change during the ground shaking due to a progressive damage and consequent changes in the rigidities of the wall and the surrounding structural elements. A good description can be established by the three load parameters: normal load N, which is assumed to be constant along the height of the wall; bending moments at the top and the bottom section of the wall, and the horizontal load H.

2.6.2.2 *Reinforced masonry walls*

To improve brittle masonry behaviour when subjected to in-plane horizontal loads, horizontal reinforcements that prevent separation of the wall's cracked parts at shear failure are used. As reported in Tomaževič [1999], reinforced masonry (RM) walls with horizontal and vertical distribution of reinforced bars have been found difficult to model as a result of the complex mechanisms developing at shear failure. Tension of horizontal steel, dowel action of vertical steel, combination of truss and arch-beam action of vertical and horizontal reinforcement and masonry, and interlocking between parts of the walls separated by diagonal cracks have been identified as major failure mechanisms at shear.
Contributions of masonry (H_{R1}), horizontal (H_{R2}) and vertical (H_{R3}) reinforcement have been considered as the main components of the shear strength of RM walls used for practical calculations. Equation 2.10b shows the lateral resistance of RM wall failing in shear.

$$H_{str,s} = H_{R1} + H_{R2} + H_{R3} \tag{2.10a}$$

$$H_{str,s} = A_w \left(\frac{f_t}{\gamma_M b}\right) \sqrt{\frac{\gamma_M \sigma_0}{f_t} + 1} + \Phi A_{sh} \frac{f_{yh}}{\gamma_s} + 1.026 A_{sv} \sqrt{\frac{f_m f_{yv}}{\gamma_m \gamma_s}} \tag{2.10b}$$

where,

Φ	horizontal reinforcement capacity reduction factor
A_{sh}	area of horizontal reinforcement
A_{sv}	area of vertical reinforcement
f_{yh}	yield strength of horizontal reinforcement
f_{yv}	yield strength of vertical reinforcement
f_m	compressive strength of mortar
γ_M	partial safety factor for masonry
γ_s	partial safety factor for steel
γ_m	partial safety factor for mortar

Sliding shear failure mechanism for reinforced masonry can be calculated by taking into account the resistance to shear sliding of masonry and the reinforcement. In such case, the influence of the vertical reinforcement acting in bending has been taken into account in addition to the friction effects. This type of failure occurs in walls with low compression forces, through horizontal cracking developing in wide extension of the wall. This failure mode can occur in the upper storeys of buildings, where vertical loading acting on the wall is low but horizontal loads from the seismic action are considerably high. The sliding shear resistance of reinforced masonry wall can be calculated with Eq. 2.11.

$$H_{str,sl} = \mu\sigma_0 A_w + 1.026 A_{sv}\sqrt{f_m f_{yv}} \tag{2.11}$$

The flexural resistance of reinforced masonry can be calculated by adding the contribution of the reinforcement to the flexural capacity of the cross-section of a unreinforced masonry wall. In case of symmetrically reinforced walls, the flexural resistance can be evaluated by Eq. 2.12.

$$M_{Ru,str} = \frac{\sigma_0 t L^2}{2}\left(1 - \frac{\sigma_0}{0.85 f_k}\right) + \left(l - 2l'\right) A_{sv} f_{yv} \tag{2.12}$$

where,

l	length of the wall's cross-section
l'	distance of wall edges to reinforcement bars

Considering that RC jacketed walls have uniform reinforcement distribution over the wall surface, the Eq. 2.12 can be modified to take into account this distribution, as shown by Eq. 2.13.

$$M_{Ru,str} = \frac{\sigma_0 t L^2}{2}\left(1 - \frac{\sigma_0}{0.85 f_k}\right) + A_{sv} f_{yv}\left(nl - 2\sum_{i=1}^{n} l'_i\right) \tag{2.13}$$

where,

n number of vertical bars $n = L/s$

s horizontal distance between vertical reinforcement bars

The flexural resistance of the wall $(H_{str,f})$ can be determined depending on the boundary conditions:

$$H_{str,f} = \frac{M_{Ru,str}}{\alpha h} \tag{2.14}$$

2.6.2.3 RC *jacketed walls*

Tomaževič [1999] and Beg [2005] provide design criteria guidelines specifying that it is not possible to estimate the lateral resistance of coated wall panels by simple calculation. For practical calculations RC jacketed masonry walls have to be simplified by an equivalent wall with original dimensions and improved mechanical properties. It was proposed to calculate the lateral stiffness of the equivalent wall $(K_{e,eq})$ as a sum of stiffnesses of original wall $(K_{e,w})$ and the jacket $(K_{e,jack})$, as given in Eq. 2.15.

$$K_{e,eq} = K_{e,w} + K_{e,jack} \tag{2.15}$$

In the model, the distinction regarding jacket thickness has been made. For thin jackets, it was proposed to estimate the lateral resistance of the strengthened wall by simple multiplication of the shear resistance of the original wall with an experimentally obtained multiplier. This multiplier has been found as a ratio between the resistance of RC jacketed and original wall. In the case of thick jackets where the thickness of the jacket exceeds 50 mm, no experimental evidence has been found with respect to the behaviour under lateral loads. In such case, the design shear resistance of jacketed wall was defined as a sum of contributions of tension capacity of horizontal reinforcement and dowel capacity of vertical reinforcement of the jacket. In particular, the contribution of the original masonry wall and concrete of the jacketing have been neglected, see Eq. (2.16).

$$H_{sd,eq} = C_{rh} A_{rh} \frac{f_{yk}}{\gamma_s} + C_{rv} A_{rv} \frac{f_{yk}}{\gamma_s} \tag{2.16}$$

where,

$K_{e,eq}$	lateral stiffness of equivalent wall
$K_{e,w}$	lateral stiffness of original masonry wall
$K_{e,jack}$	lateral stiffness of RC jacket
$H_{sd,eq}$	design shear resistance of equivalent wall
A_{rh}, A_{rv}	area of horizontal and vertical reinforcement, respectively
C_{rh}	horizontal reinforcement capacity reduction factor ($C_{rh} = 0.9$)
C_{rv}	vertical reinforcement capacity reduction factor ($C_{rv} = 0.2$)
f_y	yield stress of reinforcement steel
γ_s	partial safety factor for steel ($\gamma_s = 1.0$)

2.6.3 *Eurocode 6 [2005]*

2.6.3.1 *Unreinforced masonry walls*

To determine the shear resistance of unreinforced masonry wall, Eurocode 6 [2005] defines the shear strength of URM walls according to the friction theory, as shown in Eq. 2.17.

$$f_{vk} = f_{vk0} + \mu_c \sigma_d \tag{2.17}$$

where,

f_{vk}	characteristic shear strength of masonry
f_{vk0}	characteristic initial shear strength under zero compressive stress
μ_c	friction coefficient, describing the contribution of the compressive stresses
σ_d	design compressive stress perpendicular to the shear in the member

The code suggests determination of f_{vk0} by experimental tests according to EN 1052-3 [2002] and EN 1052-4 [2000]. The friction coefficient is considered in the code as $\mu_c = 0.4$. This approach corresponds to the Mohr-Coulomb analogy with initial shear strength considered as cohesion of masonry and friction coefficient. The upper limitation of the characteristic shear strength of masonry, given with Eq. 2.18 accounts for possible failure of the units by shear instead of the mortar joints.

$$f_{vk} \leq 0.065 f_b \tag{2.18}$$

where,

f_b	normalized compressive strength of the masonry unit

The design shear resistance calculated by Eurocode 6 [2005], considers only the compressed length of the wall, while tension length being neglected, as shown in Eq. 2.19.

$$H_{u,s} = \frac{f_{vk}}{\gamma_M} t l_c \tag{2.19}$$

where,

$H_{u,s}$ design shear resistance of URM wall

l_c length of the compressed part of the wall, ignoring the part of the wall that is in tension

t thickness of the wall

The length of the compressed part of the wall (l_c), shall be calculated assuming linear stress distribution of the compressive stresses, and ignoring the part of the wall in tension. Any openings and recesses shall be considered. To calculate l_c, the design vertical and horizontal load should be known. For eccentricity of vertical load greater that 1/6 of the wall's length, the length of the compressed part is calculated according to Eq. (2.20).

$$l_c = 3\left(\frac{l}{2} - e\right) \tag{2.20}$$

where,

l total length of the wall

$e = \alpha \frac{H}{N} h$ eccentricity of the vertical load

H horizontal load

N vertical load

h height of the wall

α boundary conditions at the bottom and the top of the wall ($\alpha = 0.5$ for fully fixed wall; $\alpha = 1.0$ for cantilever wall)

The coefficient α provides the position of the moment inflection point along the height of the wall. If a wall resists moment at top and bottom, then there is an inflection point at the mid-height. Cantilever walls loaded at the free end, do not experience inflection points, and therefore the whole height of the wall is taken into consideration.

The flexural resistance of unreinforced masonry walls can be evaluated according to Eurocode 6 [2005] with the same equation as in Tomaževič [1999] (Eqs. 2.8 and 2.9). As pointed out by Gellert [2010] and based on observations of test results, the ultimate bending moment of a cross-section should be reduced with a factor p_v. In such case, the ultimate bending moment can be calculated with Eq. 2.21.

$$M_{Ru} = \frac{\sigma_0 t L^2}{p_v 2}\left(1 - \frac{\sigma_0}{0.85 f_k}\right) \tag{2.21}$$

where,

p_v reduction factor

$$p_v = \begin{cases} 1.3 & \text{for fixed ended wall} \\ 1.0 & \text{for cantilever wall} \end{cases}$$

The flexural resistance of the wall $\left(H_{u,f}\right)$, can be evaluated depending on the boundary conditions:

$$H_{u,f} = \frac{M_{Ru}}{\alpha h} \tag{2.22}$$

2.6.3.2 *Reinforced masonry walls*

When shear failure mechanisms are considered, Eurocode 6 [2005] suggests calculation of the shear resistance of reinforced masonry wall by summing up the contributions of the plain masonry and the horizontal reinforcement only. This simplification is given with Eq. 2.23b.

$$H_{str,s} = H_{R1} + H_{R2} \tag{2.23a}$$

$$H_{sh} = \frac{f_{vk}}{\gamma_M} tl + 0.9 A_{sh} \frac{f_{yh}}{\gamma_s} \leq (2\ MPa)\, tl \tag{2.23b}$$

Distinction in the length of the wall has been made when calculating reinforced masonry walls. In this case, the total length of the wall is taken for calculation of the contribution of the plain masonry.

For simplification, verification of reinforced masonry elements subjected to bending loading should be performed with rectangular stress distribution. The ultimate bending moment can be derived from Eq. 2.24.

$$M_{Ru} = A_{sv} f_{yv} z \leq 0.4 f_k b_w d^2 \tag{2.24}$$

where,

z lever arm between the compressive and tensile force

b_w width of the wall(thickness of the wall)

d effective depth of the section (length of the wall)

$d = \sigma_0 L / 0.38 f_k$

The lever arm for a section when the maximum compression and tension are reached together, may be taken as:

$$z = d\left(1 - 0.5\frac{A_{sv}f_{yv}}{b_w d f_k}\right) \leq 0.95d \tag{2.25}$$

The flexural resistance of the wall $\left(H_{str,f}\right)$, can be determined according to Eq. 2.22.

2.6.4 *FEDRA [2003]*

FEDRA is a computer program, based on finite element method (FEM), for design and analysis of masonry buildings. It represents efficient tool for 3D analysis and design of masonry buildings, entirely based on Eurocode 6 [2005] (EN 1996-1-1:2005). Mixed structural systems are available, and RC elements (columns, beams and slabs) are designed according to Eurocode 2, while timber roof structures according to Eurocode 5. For modelling structural elements of a building, a drawing package has been implemented. The expert system built in the program, does an automatic topology recognition of the structure of the building and automatically produces the structural model, with the load transfers and mesh generations.
Several assumptions have been introduced in the program, such that the seismic loads are defined as static horizontal loads, with a reverse triangular distribution, and for the seismic loading each floor is assumed to be a stiff diaphragm in the horizontal direction. Moreover, the program is designed to be applied at buildings, for which the major part of the loads is taken from the masonry. Also, all horizontal seismic forces are taken from the masonry, and it is assumed that RC columns, if any, do not take any seismic loads. The stiffness of the columns is negligible compared to that of the masonry walls. The shape of the building must be simple and the shape of the slabs about orthogonal. The floors must have enough horizontal stiffness to act as stiff diaphragms in the horizontal direction. Only the bearing walls are entered, not the non-bearing, separation walls.

The solution methodology for masonry walls includes distribution of the total horizontal floor force on the masonry walls using the stiffness of each wall. This stiffness depends on the wall dimensions and the dimensions and positions of the openings. The wall stiffnesses are computed with a finite element analysis (FEA) of each wall, for unit relative displacement between the top and bottom wall ends. After the computation of the horizontal loads, the evaluation of the internal stresses of the walls is done also with FEA, for various load combinations. Design of masonry is done for the ultimate limit state based on Eurocode 6 [2005], chapter 4. All the checks for loading cases $1.35g + 1.50q$ and $1.00g + \psi_2 q +$ earthquake, are done for compression and shear loads. In addition, verification of the slenderness ratio requirements and checks for the strength at stress concentrations are performed according to Eurocode 6 [2005].

Seismic design is based on the concept of equivalent static loads at the level of each floor. It is assumed that each floor acts as a total stiff diaphragm in the horizontal direction. The total seismic force is defined proportional to the total vertical load, by a factor defined as the ratio of the horizontal seismic ground acceleration to the acceleration of gravity g. The distribution of the seismic force is a reverse triangular. At each floor the eccentricity of the horizontal loading is computed. The horizontal load of each floor is applied to the mass centre of the floor, and the building is assumed to rotate around an elastic axis. The elastic axis is defined as the axis passing through the elastic centre of the floor, which is more near to the level $0.8H$, where H is the height of the building.
Unreinforced, *reinforced* and *confined* masonry are designed according to the provisions given in Eurocode 6 [2005].

A specialised design module "Gunites" offers option for design of strengthening walls applied to existing buildings by gunites (concrete jackets). It assists in defining properties for the RC jackets and computes properties of an equivalent wall with increased shear strength. The design shear resistance of RC jacketed masonry wall is calculated by Eq. 2.26.

$$H_{rd} = \left(\frac{0.8 f_{wv} t_w + n f_{rd} t_c \frac{2.00}{1.50}}{\gamma_M T_w} \right) t l_c \tag{2.26}$$

where,

f_{wv}	shear strength of masonry
t_w	thickness of the masonry wall
n	factor taking into account single- $(n = 1)$ or double-sided $(n = 2)$ RC jacket
f_{rd}	shear strength of concrete
t_c	thickness of the concrete jacket
T_w	total thickness of the jacketed wall

The shear strength of reinforced concrete (f_{rd}) is calculated by taking into account the compressive strength of concrete, reinforcement area and yield stress, as shown in Eq. 2.27.

$$f_{rd} = 0.01 \frac{f_{ck}}{\gamma_c} + \frac{A_s}{t_c s} \frac{f_y}{\gamma_s} \tag{2.27}$$

where,

f_{ck} compressive strength of concrete

f_y yield stress of reinforcement steel

A_s area of the reinforcement

s horizontal distance between vertical reinforcement bars

γ_c partial safety factor for concrete

2.6.5 *CSA S304.1-04 [2004]*

Canadian standard CSA S304.1-04 [2004], distinguishes two failure mechanisms related to shear, namely sliding shear and shear/diagonal tensile cracking. Models for calculation of diagonal tension resistance and sliding shear resistance are provided. Furthermore, the code makes a distinction between walls with different geometry aspects. Walls characterized by height/length aspect ratio of 1.0 or higher are considered as flexural shear walls, and walls with a low height/length, or less than 1.0 are denoted as squat shear walls.

2.6.5.1 *Unreinforced masonry walls*

Factored in-plane *shear/diagonal tensile resistance* of URM flexural shear walls $(H_{u,s})$, built in running bond and subjected to the effect of factored shear force $\left(V_f\right)$, and factored bending moment $\left(M_f\right)$, is calculated according to Eq. 2.28.

$$H_{u,s} = \phi_m \left(\nu_m b_w d_v + 0.25 P_d\right) \gamma_g \tag{2.28}$$

where,

ϕ_m material resistance factor for masonry, $\phi_m = 0.6$

v_m shear strength of masonry, given in Eq. (2.29)

b_w overall wall thickness without flanges in the intersection walls, $b_w = t$

d_v effective wall depth

P_d axial compression load on the section being considered, based on 0.9 times dead load, plus axial load N from bending in coupling beams or piers

γ_g factor taking into account partially grouted or ungrouted walls

$$\gamma_g = \begin{cases} 1.0 & \text{for fully grouted masonry (fully solid} \\ & \text{concrete block or solid brick masonry)} \\ A_e/A_g & \text{for all other cases, but not greater than 0.5} \end{cases}$$

A_e effective cross-sectional area of the wall

A_g gross cross-sectional area of the wall

Masonry shear strength attributed to the masonry in running bond is determined according to the following equation:

$$v_m = 0.16 \left(2 - \frac{M_f}{V_f d_v}\right) \sqrt{f'_m} \tag{2.29}$$

where,

f'_m compressive strength of masonry normal to the bed joint at 28 days

$\frac{M_f}{V_f d_s}$ shear span ratio, $0.25 \leq \frac{M_f}{V_f d_s} \leq 1.0$

Sliding shear resistance is generally evaluated for shear along bed joints between courses of masonry (Eq. 2.30) and for shear along bed joint between the support and the first course of masonry (Eq. 2.31). It is given in the code as factored in-plane sliding shear resistance.

$$H_{u,sl} = 0.16\phi_m \sqrt{f'_m} A_{uc} + \phi_m \mu P_1 \tag{2.30}$$

$$H_{u,sl} = \phi_m \mu P_1 \tag{2.31}$$

where,

A_{uc} uncracked portion of the effective cross-sectional area of the wall that provides shear bond capacity

μ friction coefficient

$$\mu = \begin{cases} 1.0 & \text{for masonry-to-masonry or masonry-to-roughened} \\ & \text{concrete sliding plane} \\ 0.7 & \text{for masonry-to-smooth concrete or bare steel} \\ & \text{sliding plane} \end{cases}$$

P_1 effect of axial compression load, $P_1 = 0.9P_d$

Calculation of the in-plane *flexural resistance* due to combined axial load and bending is based on the assumption that the unreinforced masonry walls remain uncracked when the eccentricity resulting from bending about either the major or minor axis exceeds $e \geq 0.33L$ (L—length of the wall). In the same time the maximum stresses must not exceed $\phi_m f_t$ for tension and $\phi_m f'_m$ for compression (f_t—flexural tensile strength of masonry, Table 5 of CSA S304.1-04, 2004). In the case of $e > 0.66L$, the wall can be designed assuming cracked wall sections, using an equivalent rectangular stress block. The flexural resistance can be evaluated with Eq. 2.32.

$$H_{u,f} = \left(0.85\chi\phi_m f'_m\right) t \left(\frac{L}{2} - e\right) 2 \tag{2.32}$$

where,

χ factor used to account for direction of compressive stress in a masonry member relative to the direction used for determination of f'_m. $\chi = 1.0$ for members subjected to compression perpendicular to the bed joints (structural walls)

2.6.5.2 *Reinforced masonry walls*

Factored in-plane *shear/diagonal tensile resistance* of flexural reinforced walls is determined as a combination of contributions of unreinforced masonry and a reinforcement, as shown in Eq. 2.33.

$$H_{str,s} = V_m + V_s \tag{2.33}$$

Masonry shear resistance (V_m), is assessed according to Eq. 2.28 with $d_v \geq 0.8l_w$ for walls with flexure reinforcement distributed along the length, if l_w is the length of the wall. Reinforcement contribution (V_s), is equal to:

$$V_s = 0.6\phi_s A_v f_y \frac{d_v}{s} \tag{2.34}$$

where,

A_v area of horizontal wall reinforcement

f_y yield stress of reinforcement

ϕ_s material resistance factor for reinforcing bars, $\phi_m = 0.85$

s vertical spacing of horizontal reinforcement

The following upper limit for the factored in-plane shear diagonal/tensile resistance $(H_{str,s})$, for flexural walls was prescribed by CSA S304.1-04 [2004]:

$$H_{str,s} \leq maxH_{str,s} = 0.4\phi_m \sqrt{f'_m} b_w d_v \gamma_g \tag{2.35}$$

For *squat shear walls*, the code prescribes increased upper limit for the factored shear diagonal/tensile resistance to account for increased masonry shear resistance with a decrease of height/length aspect ratio. In case of squat shear walls, the following upper limit is applicable:

$$H_{str,s} \leq maxH_{str,s} = 0.4\phi_m \sqrt{f'_m} b_w d_v \gamma_g \left(2 - \frac{h_w}{l_w}\right) \tag{2.36}$$

where, l_w is length of the wall, and valid in case of $\frac{h_w}{l_w} \leq 1.0$.

Sliding shear failure occurs in both flexural and squat shear walls, but it is much more common in squat walls. *Sliding shear resistance* is usually checked at characteristic sections such as in the foundation level, or in upper portions of high-rise flexural walls. Similar to Eq. 2.31, sliding shear resistance of reinforced walls additionally incorporates the factored tensile force at yield of the vertical reinforcement, T_y:

$$H_{str,sl} = \phi_m \mu P_2 \tag{2.37}$$

$$P_2 = P_d + T_y \tag{2.38}$$

$$T_y = \phi_s A_s f_y \tag{2.39}$$

CSA S304.1-04, 2004 distinguishes calculation of *flexural resistance* by evaluation of the moment capacity for the section with concentrated and distributed reinforcement. Simplified wall design model is used to describe the distribution of the forces in the section. It was assumed that the concentrated wall reinforcement yields either in tension or in compression at the wall ends, and the distributed reinforcement yields in tension only. The RC jacketed members can be assumed to correspond to a reinforced members with distributed reinforcement along the length. In such case, the factored moment capacity is given with Eq. 2.40.

$$M_r = 0.5\phi_s f_y A_{vt} L \left(1 + \frac{P_f}{\phi_s f_y A_{vt}}\right)\left(1 - \frac{c}{L}\right) \quad (2.40)$$

where,

A_{vt} total area of distributed vertical reinforcement

c depth of neutral axis

P_f factored axial load N

$$\frac{c}{L} = \frac{\omega + \alpha}{2\omega + \alpha_1\beta_1} \quad (2.41)$$

$$\omega = \frac{\phi_s f_y A_{vt}}{\phi_m f'_m L t} \quad (2.42)$$

$$\alpha = \frac{P_f}{\phi_m f'_m L t} \quad (2.43)$$

The code recommends values for $\alpha_1 = 0.85$ and $\beta_1 = 0.8$.

2.7 EXPERIENCE WITH MASONRY STRENGTHENING IN THE COUNTRY

Masonry strengthening is often applied when there is a need to strengthen the existing buildings, or when the structural walls are seriously damaged. Still, there are not enough theoretical, experimental or numerical investigations of the strengthening techniques applied. The same situation was found in Macedonia. Strengthening by application of RC jackets is almost exclusively used for brick and stone masonry buildings. On the other hand, not so many research efforts have been made in the past to study this strengthening method. This subsection gives an overview of the application and research efforts made in the country regarding masonry strengthening.

One of the first detailed experimental and theoretical investigations in the country was performed by Velkov [1970]. This dissertation deals with the concept of ductilisation of masonry which is understood as a property of the structure to undergo post-elastic deformations, with elastic components. The ductilisation should be analysed for mutual complex actions, effects which normally appear in the structural elements subjected to seismic actions. At the same time, when studying the property of ductilisation, the properties of deformation, strength and energy properties are considered. The ductilisation, as original research concept, was pointed out by the author to possess several advantages over the efforts to explain the behaviour of masonry structures during seismic events only by using the theory of elasticity and the material strength concept. The ductilisation was defined as a measure to improve the deformation capacity and the capacity to absorb seismic energy.

The past earthquakes have demonstrated unfavourable behaviour of

masonry structures during intense ground shaking, great massive failures and large damage to the structural elements. This resulted to limited usage of masonry in seismic areas with big seismic intensities. Structural masonry has a certain strength capacity, which depends on several parameters (quality of material, executions and etc.). However, the deformation properties of masonry are rather limited, especially after crack appearance. Usually, by increasing the deformation, a sudden failure of the structural element is expected, so called a brittle failure. It happens as a result of the brittleness of the masonry. From another point of view, these masonry properties give opportunity to explain the big damage and failure of masonry structures after earthquakes. On the other hand, by using the modern design concepts: the deformation concept, plastic excursions and energy concept, the same unfavourable properties and behaviour of masonry structures and masonry are discovered. This leads to the same conclusion of limited application of masonry in seismic areas. Nevertheless, appropriate measures could be applied that can eliminate the adverse masonry properties. Usually, the solution can be found in combination of masonry with other structural materials, namely in composition with ductile materials.
After the 1963 Skopje earthquake, the author studied thoroughly masonry, both experimentally and theoretically, and especially analysed the damage caused by the recent earthquakes. For the first time in the country, the author proposed usage of strengthened masonry, of so called type 'miks'. This system consists of reinforced concrete core surrounded with two masonry wythe walls. The improved properties of the strengthened masonry with 'miks' system were proved experimentally, particularly the high deformation capacity and approving behaviour for dynamic loadings with high ductility.

Velkov [1970] performed experimental investigations in the Laboratory for testing materials at the Faculty of Architecture and Civil Engineering in Skopje. The experimental programme consisted of test on three unreinforced masonry walls build in solid clay bricks and lime and cement-lime mortar, two confined masonry walls, three walls with reinforced concrete core - 'miks' system, and five walls with reinforced concrete core - 'miks' system, confined with slender reinforced concrete frames. In total, 10 walls were tested in natural wall position, see Figure 29, and two walls were tested in diagonal compression. The experimental test frame is shown in Figure 30. Vertical loads were applied by a system of vertical steel anchors anchored in a reinforced concrete beam. To maintain the vertical load constant during the testing, and even after occurrence of large deformations, a special rubber bearings were developed. In such a way, the influence of the vertical component of the deformation on the variation of the vertical load was reduced to a tolerant value. The testing was performed by application of diagonal loading in half cycles with gradual increase of the force in

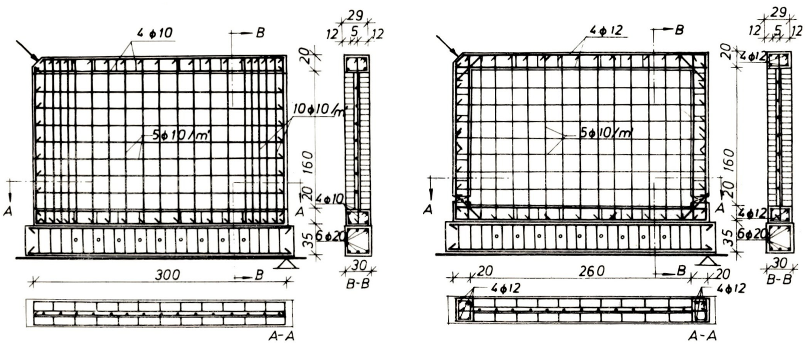

(a) Masonry wall with reinforced concrete core

(b) Confined masonry wall with reinforced concrete core

Figure 29: Masonry walls with 'miks' system

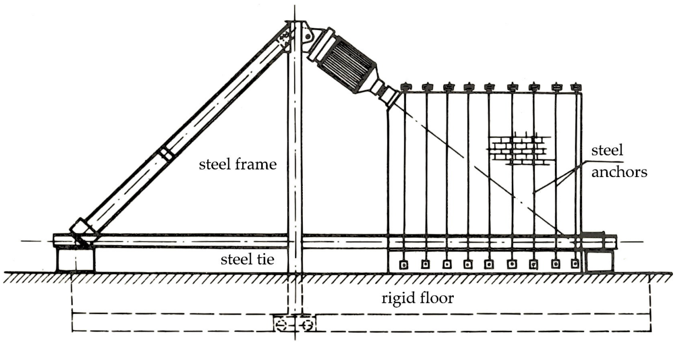

Figure 30: Test set-up by Velkov [1970]

each cycle. The testing continued after appearance of diagonal cracks until final failure of the walls.

Several problems were investigated and analysed by: comparison of the effects of lateral loading on different masonry wall structural systems; detailed study of the obtained ductility derived for different structural systems subjected to load reversals due to a progressive increase of the lateral displacements; studying the effects of masonry ductilisation by combination with structural steel and by confining masonry panels; and studying the proposed structural system - 'confined miks masonry'. The results from the extensive investigations performed, lead to a conclusion that the 'confined miks masonry' system gives the best results regarding the strength and deformability. Also, this system exhibited the largest masonry ductilisation and the author recommends application of this structural system for seismic design of masonry, especially in high buildings. Such structural systems were assessed to have high capacity for energy absorption, high ductility and good strength when exposed to cyclic load reversals in the inelastic range.

Macedonian researchers have gained great experience over the years in experimental analysis and testing of model structures on a shak-

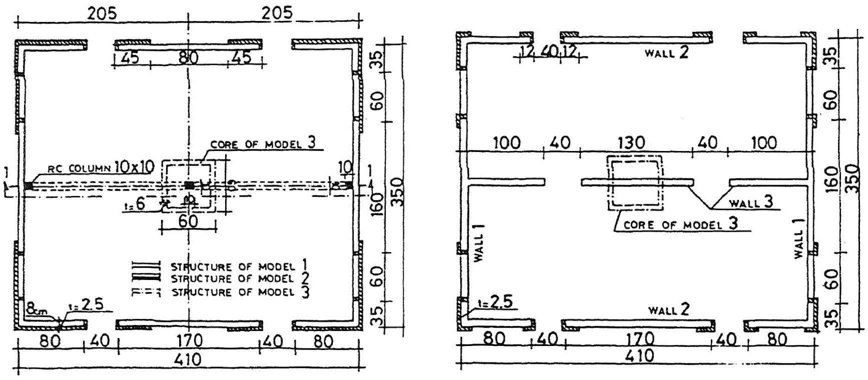

(a) Basement storey of each model

(b) Second and third storey of each model

Figure 31: Plan views of the three models

ing table. Such experiments have been performed at the Institute of Earthquake Engineering and Earthquake Seismology, on a two-component programmable seismic shaking table with size $5x5\,m$ and maximum acceleration, for maximum loading of $40\,t$, of $0.66\,g$. One of the many tests applied on masonry building models, involves testing of structural behaviour of original and strengthened masonry models, performed in the framework of large joint project between the University of Bologna and University "Ss. Cyril and Methodius" in Skopje [Jurukovski et al., 1992]. For the hypothetical prototype building, a true replica, 1/3-scale model was constructed and tested under various earthquake time histories. The hypothetical prototype building consists of mixed structural system (RC beams and columns and brick masonry walls) in the first floor, and classical brick masonry walls in the remaining three stories.

The first model (Model 1) has been built in true-replica as reference model to study its dynamic behaviour under failure conditions. Two strengthened models have been built and tested under the same earthquake records. The first strengthened model (Model 2) applies to the structure of model 1, strengthened by external RC walls and fragments of the RC walls. The second strengthened model (Model 3) applies to the structure of model 1, strengthened by central core, but without strengthening measures applied at model 2. The plan views of the first and the remaining three stories are shown in Figure 31.

The strengthening solution for the model 2 was applied to the external walls, around the corners and the openings. The strengthening consists of one-sided net reinforcement (Q-139) anchored to the wall, and concrete jacket applied over the wall by shotcrete, Figure 32. The reinforcement net with bar diameter Ø $8/15\,cm$ was applied by to the walls and anchored with bars Ø $4\,mm$. The total thickness of the shotcrete was $25\,mm$.

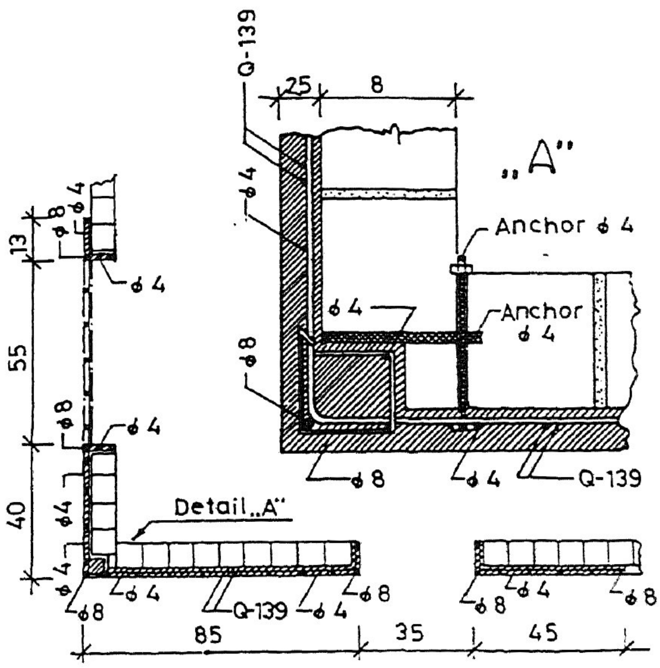

Figure 32: Detail of corner strengthening of model 2

The testing was performed with different earthquake time histories: El Centro 1940, Parkfield 1966, Montenegro 1979 (Bar and Petrovac records) and Friuli 1976 (Breginj record). The sensitivity of the models was assessed in the linear regime with all earthquake records, while the later testing was continued with El Centro, Friuli and Petrovac earthquake records, until the appearance of the first visible cracks. Afterwards, Petrovac record was used in the testing, until the occurrence of considerable damage to the models. The maximum simulated peak acceleration was $0.51\,g$ for model 1, and $1.07\,g$ for models 2 and 3.

The experimental results revealed that model 3 has the highest initial stiffness, followed by the stiffness of model 2, while model 1 has lowest initial stiffness, as expected. One of the interesting results is the stiffness degradation, which was found to be lowest in the model 1, while the models 2 and 3 showed similar behaviour. The prevailing mode shapes were of shear type, for models 1 and 3, and bending type of vibration was detected for the model 2. The viscous damping coefficients, obtained from the frequency response curves, for all models was in a range $2 - 3$. The responses of the models in terms of accelerations and displacements, showed the highest values in model 2 for the same level of peak acceleration. The acceleration time histories recorded on the fourth floor in each model presented no amplification of the model 1, while the amplification factor for model 3 was 2.0 and for model 2 was 3.0. Different damage mechanisms were obtained for the three models. Model 1 was characterised with intensive damage in the first floor, slight damage to the second floor and negligible damage to the remaining floors. Model 2 was

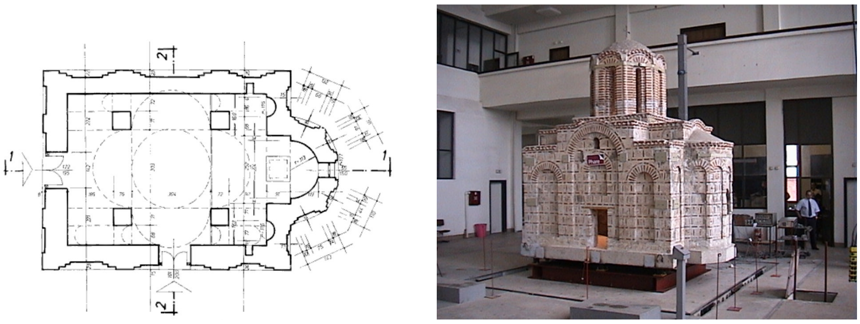

(a) St. Nikita plan view

(b) St. Nikita church model on a shaking table

Figure 33: Tests performed on a model of St. Nikita church

characterized by intensive damage to the masonry in the first three floors, bending failure mechanisms to the RC jacketed walls of the first floor and almost no damage to the upper floors. The third model developed failure mechanism in the masonry of all floors with small cracks observed in the central core. This research pointed out that, the suggested strengthening techniques increase the seismic safety of the prototype building, with both advantages and disadvantages to the two approaches applied. It was suggested that the combination of both strengthening strategies should be considered in practise.

Great experience in repair and strengthening of historical monuments was gathered in the country, also. A remarkable collection of information and data was acquired in the research project for studying the seismic strengthening of Byzantine churches in Macedonia [Gavrilović et al., 2004]. The project was realized in the period 1990-1994 with the objective to develop and test methods for strengthening the structural system of Byzantine churches in order to increase their seismic capacity, by using minimal intervention concepts and minimum incorporation of new elements, and to achieve maximum seismic protection.

Figure 33b courtesy of Prof. V. Sendova

Detailed in-situ field and analytical studies and laboratory tests were performed on the selected prototype 14th century church of St. Nikita in the village of Banjani. Experimental investigations on a scaled model of $1 : 2.75$ were executed to verify experimentally the adopted methodology for repair and seismic strengthening, see Figure 33. The existing prototype structure was found to possess low stability and resistance to seismic intensities that correspond to the design and maximum earthquakes anticipated. After being repaired, the damaged model was structurally strengthened by horizontal belt courses. They were created by incorporating horizontal steel tie rods at three levels in the walls and with filling the surrounding area with injection mixture to provide appropriate bonding contact with the existing masonry. At the base of the dome, a horizontal band was attached. Vertical steel ties were applied in the tambour and anchored to the main walls. In addition, exterior walls were anchored to the foundation with steel ties, and the spaces around the ties were filled with grout to provide positive connections with the walls.

Tambour is a cylindrical or polygonal drum base for a dome.

The effectiveness of the strengthening method was assessed with the results obtained after the repaired and strengthened model was subjected to the same series of dynamic tests. Due to the higher resistance of the strengthened model, higher intensities of accelerations were applied during the testing. In terms of failure mechanisms, the original model suffered damage with separation of the walls and occurrence of vertical cracks. The strengthened model showed different failure mechanisms, with damage in the lower zones of the walls and diagonal cracks. The displacements in the retrofitted model measured at representative points were decreased by half than the original model. It was concluded that the applied strengthening intervention increased the seismic capacity, structural stability and deformability of the structure up to the level of designed protection and it was shown that the structural damage during a major earthquake can be prevented.

The same strengthening concept of "minimal intervention – maximal protection" was applied in several cases, such as the case study of St. Clement's Church at Plaoshnik, Ohrid [Apostolska et al., 2009].

The first temple was build in 863AD, on the bases of an early Christian church, from the 5th or 6th century AD.

Within the investigations performed by Krstevska [2002], tests on small masonry models constructed of ordinary and reinforced masonry, as well as plain and spatial models of structures with masonry infill were performed. The tests were later used to verify the proposed concept of non-linear micro analysis of the structural response of a system with masonry infill. To define the mean mechanical properties, several tests on different masonry wallets were performed, see Figure 34. Those included tests on unreinforced wallets (brick and mortar), plastered unreinforced wallets and tests on masonry wallets reinforced with polymer geogrids of type TENSAR SS30. Vertically perforated bricks with dimensions $250x120x190\,mm$ with 42% holes, compressive strenght of $13.3\,\mathrm{N/mm^2}$ were bonded with M3 class mortar with ratio of cement:lime:sand=1:1:5 and compressive strength of $5\,\mathrm{N/mm^2}$. The wallets were tested under axial and diagonal compression loads. The failure modes were found to be of complex type, with strong influence of the masonry components (bricks, mortar, geogrids). Depending on the testing mode (axial or diagonal compression), different strength properties were obtained. The plastering of the walls significantly increased the bearing capacity of the walls, but after occurrence of cracks, very sharp strength drop was observed.

The strengthening by geogrids increased the bearing capacity with 30% increase detected in diagonal compression tests and 15% increase at axial compression tests.

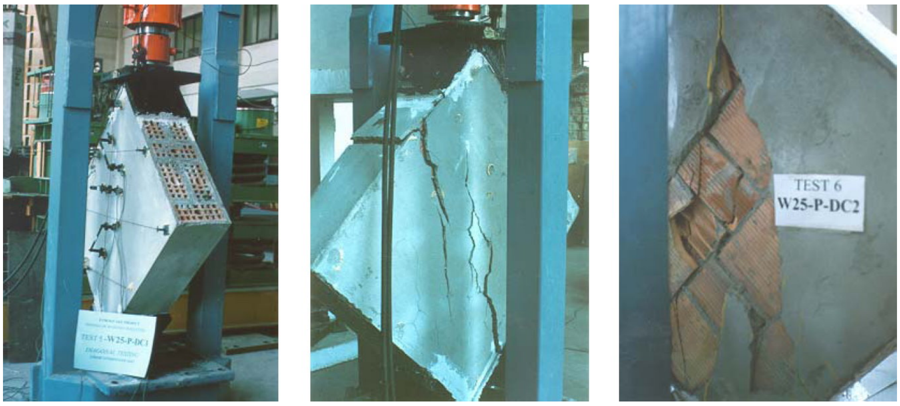

(a) Tests on plastered unreinforced masonry wallets

(b) Tests on strengthened masonry wallets with geogrids

Figure 34: Diagonal compression tests on masonry wallets performed by Krstevska [2002]

The structural strengthening of masonry buildings was often applied in the practice. Usually, it comprises interventions in the existing masonry, strengthening of RC elements, if existing, rebuilding of masonry walls and insertion of vertical and horizontal RC elements at certain levels [Shendova et al., 2005].

To increase the seismic capacity and deformability of existing unreinforced masonry buildings, almost in all cases, horizontal RC elements were incorporated at floor levels, flexible floor diaphragms were replaced with monolithic RC slabs, masonry walls were repaired by injection of existing cracks and the walls were strengthened with RC jackets. A typical example of the applied strengthening techniques is shown in Figure 35 [Bozinovski et al., 1995]. The strengthening of masonry walls with RC jackets was applied on one side (internal) on each critical wall position, see Figure 36. The total thickness of the jackets was 8 cm. The seismic capacity and deformability of the strengthened building were increased about $2-3$ times than the original building.

Beside strengthening of masonry walls with jackets and repair of cracks, often increase of the seismic capacity of a building can be obtained by insertion of new RC shear walls. As reported by Gavrilović

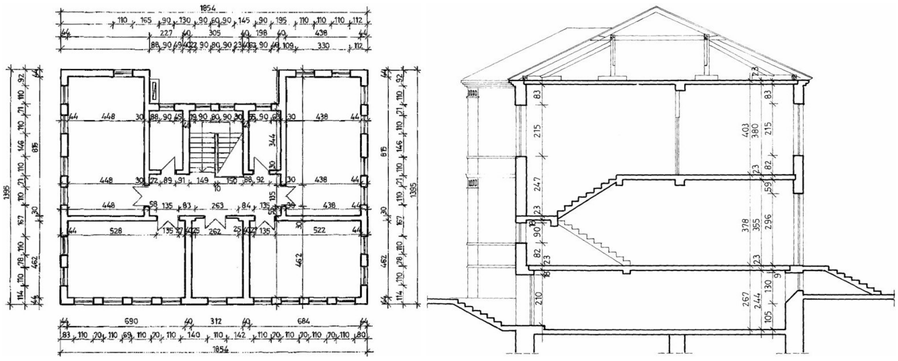

Figure 35: Plan and section view of an existing school building with insufficient seismic capacity

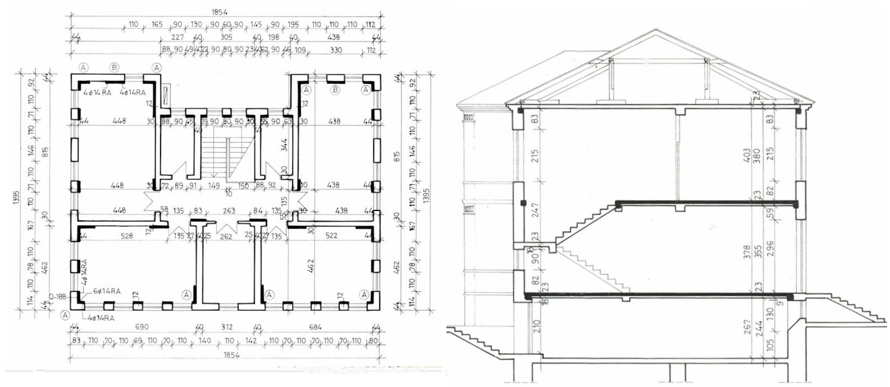

Figure 36: Plan and section view of the strengthened school building

and Bozinovski [1994] the seismic capacity of the strengthened building was assessed to be 4 times higher than the original building, while the deformation capacity was increased twice.

In several cases, where it was found to be appropriate, the masonry buildings were strengthened by combining two methods, application of RC jackets to the masonry walls and tying the new and existing walls with steel ties [Bozinovski et al., 2006]. As can be seen from Figure 37, RC jackets with thickness of 10 cm were applied in wall piers and wall corners on both sides of the external walls. After that, to obtain better structural integrity the jackets were connected with steel ties, running on the bottom side of the floors.

One of the most important research projects, that scientists from Macedonia have participated in, were the activities carried out within the European research project "PROHITECH – Earthquake Protection of Historical Buildings by Reversible Mixed Technologies". This project was fitted into the Sixth European Framework Programme (FP6-2002-INCO-MPC-1), having a duration of four years (2004–2008). Within this project sixteen academic Institutions, belonging to twelve Euro-Mediterranean Countries (Italy, Algeria, Belgium, Egypt, Macedonia, Greece, Israel, Morocco, Portugal, Romania, Slovenia, Turkey) were

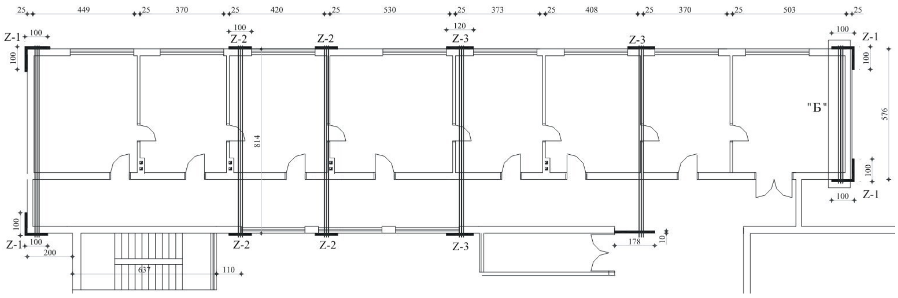

Figure 37: Strengthening of masonry building with rigid floor by RC jackets and steel ties

involved. The research was articulated in four main parts, focusing on "Strategies for interventions", "Selection of material and technologies", Numerical and experimental studies" and "Definition of design criteria". Within that research project, a deep and comprehensive view of the faced issues has been achieved. The techniques were based on the use, which can also be combined, of FRP (Fibre Reinforced Polymers) elements, aluminium-cement based volume expansive mortars, steel collars, steel or aluminium shear panels, steel connectors, whose applications show the advantages of the proposed techniques for the protection of historically valuable buildings, since they allow to both protect the constructions and to preserve their cultural value. The main objective of the project has consisted in the development of sustainable methodologies for the use of Reversible Mixed Technologies (RMTs) in the seismic protection of the existing constructions [Mazzolani, 2009]. University "Ss. Cyril and Methodius" from Skopje participated in this project with Faculty of Civil Engineering as main contractor and Institute of earthquake engineering and engineering seismology (IZIIS) as subcontractor and the relative responsible person was prof. K. Gramatikov. Both institutions were deeply involved in the experimental and numerical activities carried out within the project. The experimental analyses have maybe represented the actual core of the PROHITECH research project. They have provided a very important contribution in the development of RMTs to be applied for the seismic protection of historical buildings.

Within the project, the work has been carried out with the main aim of assessing and setting-up new mixed techniques for the repair and strengthening of historical buildings and monuments belonging to the Cultural Heritage of the Mediterranean basin. The experimental activity has been developed at five different levels, namely full scale tests, large scale models, sub-systems, devices, materials and elements. The full scale experimental tests have been performed on a RC building located in the Bagnoli area in Naples, Italy, the Mustafa Pasha mosque in Skopje, Macedonia, the Gothic cathedral in Fossanova, Italy, the Byzantine St. Nikola church in Psacha, Kriva Palanka, Macedonia and the Beylerbeyi Palace in Istanbul, Turkey. The programme of large

(a) Strengthened large scale model of Mustapha Pasha Mosque with C-FRP elements

(b) Strengthened large scale model of Fossanova Cathedral with FRP cables

Figure 38: Shaking table tests on strengthened large scale models

scale tests has included experiments on the following models: Mustafa Pasha mosque; Fossanova Gothic cathedral; Greek Temple; St. Nikola Byzantine church in Psacha.

The 1:6 scale model of the Mustafa Pasha mosque has been realized at the IZIIS Laboratory in Skopje. The main objective of the experimental investigation has been the study on the effectiveness of the proposed reversible intervention, based on the use of C-FRP elements, see Figure 38a. The experimental campaign on the Mustafa Pasha mosque model has been carried out in three main phases [Krstevska et al., 2009a].

The 1:5.5 scale model of the Fossanova Gothic cathedral has been tested at the IZIIS Laboratory. Shaking table tests have been carried out on the Fossanova model both before and after the consolidation, carried out by means of FRP cables. After the test on the original construction, which has induced damage, the model has been repaired and post-tensioned FRP cables, both horizontal and vertical, have been applied, see Figure 38b. The consolidated model has been subjected to two tests, in which the vertical cables were always active: a first test, with only the superior horizontal cables active; a second test, with all the horizontal cables active [Tashkov et al., 2009b]. The used intervention has increased the seismic resistance of the structure of about three times.

At last, the 1:3.5 scale model of the St. Nikola Byzantine church has been tested on shaking table at the IZIIS Laboratory. A first test on the base isolated model, by means of the ALSC floating - sliding system (Figure 39), has been carried out [Tashkov et al., 2009a]. The protection system has performed adequately, and prevented damages to the model. A second test, in which the seismic isolation has been removed, has led to severely damage the construction.

The numerical analyses have represented the counterpart of the experimental tests described in the above section, since most of them

(a) The model of St. Nikola church with base isolating ALSC system

(b) Details of the ALSC system

Figure 39: Shaking table tests on base isolated St. Nikola church

have been focused on models of the experimented test specimens. Consequently, also for the numerical analyses, the activity has been developed at five levels, from full scale building to materials and elements. Pre- and post-experimental numerical analyses, devoted to support the development of advanced analytical models, have been performed for the large scale models and tested also by the experimental tests. The Mustafa Pasha Mosque and the simulation of the masonry walls has been modelled in cooperation between the University of Naples "Federico II" - Architecture Faculty and the University "Ss. Cyril and Methodius" from Skopje [Lazarov and Todorov, 2009a,b, Landolfo et al., 2009, Dumova-Jovanoska and Churilov, 2009]. The Gothic Cathedral of Fossanova has been modelled at the University of Chieti-Pescara "G. d'Annunzio". The model of the St. Nikola Church in Psacha has been set up at the Faculty of Civil Engineering, University "Ss. Cyril and Methodius" [Kokalanov et al., 2009](Figure 40), and the Greek Temple has been modelled at the National Technical University of Athens.

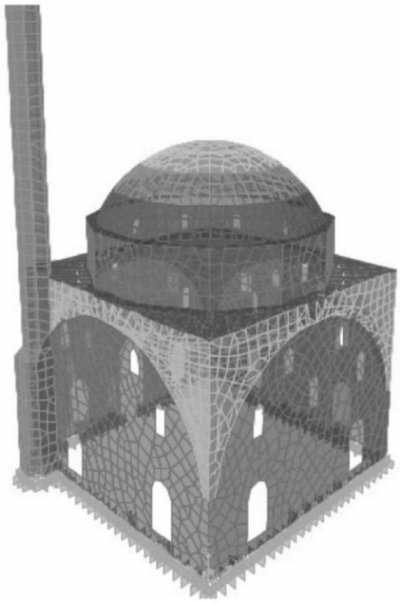

(a) FE model of Mustapha Pasha mosque [Lazarov and Todorov, 2009a]

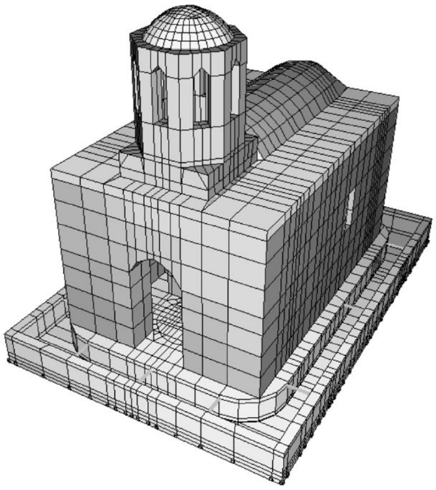

(b) FE model of St. Nikola church [Kokalanov et al., 2009]

Figure 40: Numerical models of the tested large scale models within PRO-HITECH project

Part II

EXPERIMENTAL RESEARCH

Experimental research activities used in the dissertation are elaborated in the following part.
The mechanical and physical properties of the masonry components are identified. The mechanical characteristics of masonry are tested and the results are presented.
Next, the main experimental results considering the in-plane behaviour of unreinforced and strengthened walls are shown.
Finally, a comparison of the behaviour between the strengthened and unreinforced walls is summarized.

3 EXPERIMENTAL BEHAVIOUR OF MASONRY COMPONENTS AND MASONRY

3.1 INTRODUCTION

Masonry is considered as inhomogeneous, anisotropic and composite material due to the components it contains, such as bricks, blocks and mortar. Mortar joints are considered as planes of weakness of masonry structural elements, particularly in case of weak mortar. Primary masonry structural elements are walls, piers and spandrels. Different failure mechanisms can develop in masonry walls when subjected to horizontal loads. They all depend on strength characteristics of the components, wall height/length aspect ratio, vertical stresses and many subtle circumstances, like present environmental effects, freeze/thaw cycles, workmanship during construction, possible damage due to water, moisture, mildew and etc.

However, masonry is the most used building material starting from the ancient time until present. Magnificent architectural masterpieces have been built from masonry, many of them still exist today and resist all unfavourable influences.

Generally, masonry resists the compressive stresses very well, but has low tensile and shear strength. This leads to very early cracking and it is the main reason why unreinforced masonry is not allowed to be used as main structural material in seismic zones with high intensity. In fact, the actual code in Macedonia [PIOVSP, 1981] does not allow URM buildings to be built in seismic zone IX, and at the same time makes limitations to the maximum number of floors allowed in different seismic zones. According to the code, confined and reinforced masonry buildings are allowed to be constructed in seismic zone IX with Gr+2 floors and Gr+7 floors, respectively. But, the design code does not deal with existing buildings and it is rather oriented to a design of new masonry buildings. Moreover, existing masonry buildings are regularly strengthened and repaired, usually in cases of their upgrading or addition of new spaces. This additionally increases the complexity in understanding the behaviour of masonry under in-plane horizontal loads.

To design a new masonry building or repair and strengthen the existing one, it is crucial to have a knowledge and to understand masonry mechanical behaviour. Any experimental, numerical or analytical analysis can be accurate only if mechanical properties of masonry and its components are known. It is fundamental to perform experimental tests on masonry bricks, blocks, mortar samples and wallets to be able to determine the properties from the undamaged state until failure. Later, reliable results can be produced with numerical tools if appropriate and sufficient material properties are established.

Commonly, two types of tests are used to determine the masonry characteristics. Destructive tests (DTs) are performed on samples extracted from a building or in case of a new building on the construction materials to be applied. Sometimes, it is not possible to carry out destructive tests on elements, especially in cases of historical buildings or monuments. On the other hand, non-destructive tests (NDTs) have the great advantage not to provoke any damage to the inspected element, but are limited in the number of properties that can be obtained.

This chapter presents an experimental programme designed to establish the necessary material properties for masonry components. Characterisation of masonry components, their physical properties and behaviour under compressive, tensile and shear loading as well as the shear strength of the unit-mortar interface is elaborated. Masonry components under investigation represent the most common types or bricks and mortar used in the country. Also, the materials for masonry strengthening by application of RC jackets are tested and the results are presented in the following sections.

3.2 EXPERIMENTAL TESTS ON CLAY BRICKS

Unreinforced masonry walls made from solid clay bricks and lime mortar are rather common types of structural elements in Macedonia, in particular in rural areas and in many existing low-rise residential and public buildings. After the 1963 Skopje earthquake and the first code provisions for seismic design and construction, mainly reinforced concrete was used in the building practise, while masonry being ignored. Nevertheless, many unreinforced masonry buildings still remain and many of them were strengthened with RC jackets. The need for identification of this strengthening method for this kind of buildings is evident.

The choice of materials and strengthening method has been designed to recreate the conditions that are representative of what can be found in existing buildings. It was decided to test the properties of selected solid clay bricks produced from different manufacturers currently offered on the market. To compare and account for time dependent effects, such as ageing, and to determine the properties of bricks which can be found in existing buildings, one series of bricks were pulled out from an old building.

Three series of new solid clay bricks were selected and classified in series A, B and C. The fourth series of bricks contained bricks from the old building. Bricks in series A were produced by brick factory "Elenica" from city of Strumica, series B were represented by bricks manufactured by small brick production factory from city of Prilep,

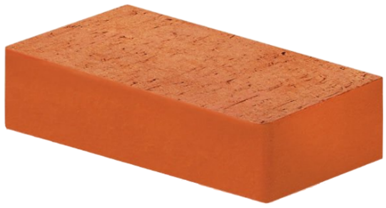

(a) Solid clay brick - series A

(b) Solid clay brick - series B

(c) Solid bricks with vertical holes - series C

(d) Solid frogged bricks - series D

Figure 41: Series of solid clay bricks for testing physical and mechanical properties

and brick in series C were fabricated by brick factory "Kik" from city of Kumanovo. The bricks in series D were solid frogged units extracted from 60 years old, two-floors unreinforced masonry residential building in city of Skopje before its demolition. All bricks were solid clay, and had usual dimensions in length, thickness and height of 250x120x65 mm, except bricks in series C which had rectangular vertical holes (see Figure 41).

3.2.1 *Physical properties*

Physical properties of bricks, such as dimensions and dimensional variability, surface smoothness, corner roundness, presence of cracks, weight and density, water absorption due to capillarity action, and consistence on ice were obtained according to the actual standards in Macedonia. Bricks from series D were not tested for physical properties due to their late arrival in the laboratory. Brick dimensions, surface smoothness, corner roundness, and presence of cracks are necessary parameters to classify the bricks according to MKS B.D1.011.

To classify the bricks in one of the three available quality classes, I, II or III, the brick's shape was obtained by visual inspection, while

(a) Measurement of brick dimensions (b) Weight measurement on brick sample

Figure 42: Control of physical properties on bricks and brick samples

(a) Bricks in drying chamber (b) Testing water absorption

Figure 43: Testing of physical properties of solid clay brick units

the dimensions were measured as requested by the standard (see Figure 42). Surface smoothness and corner roundness were obtained by measurements with metal ruler, and at the same time presence of cracks on the brick's surface was observed. The measurements were conducted on a minimum number of 5 real-scale bricks from series A, B and C, and arithmetical mean value and coefficient of deviation were established. Each brick was measured for dimensions and weight twice. Table 1, Table 2, and Table 3 present the obtained physical properties of the brick units.

The meanings of the symbols in the tables is as follows: L/B/h= length/width/height of brick; SS=surface smoothness on brick plane (a=60-125, b=60-250, c=125-250); CR=corner roundness; Cr=; Md=mass (dry); Ms=mass (saturated); WA=water absorption; Mf=mass after freezing; γ_d=density (dry).

Mass (m) in dry conditions was obtained on previously dried bricks at a temperature of 105±5°C to attain constant mass (see Figure 43a). Constant mass was considered to be attained if two successive measurements in 2 hours interval yielded mass difference no more than 2 %. Mass was measured on each brick at a temperature of 20±5°C on electronic scale with a precision of 0.01 g.

Unit	L	B	H	SS a	SS b	SS c	CR	Cr	Md	Ms	WA	Mf	γ_d
	(mm)	(mm)	(mm)	(mm)	(mm)	(mm)	(mm)	(mm)	(g)	(g)	(%)	(%)	(kg/m³)
A1	252.0	120.0	63.0	±0.5	+1.0	+4.0	3.5	no	3582.2	3974.9	11.0	3582.2	1880.3
	251.0	121.0	64.0										1842.9
A2	250.0	120.0	65.0	+1.0	-1.0	±1.0	2.5	no	3625.7	4027.2	11.1	3625.7	1859.3
	249.0	120.0	65.5										1852.6
A3	249.0	120.0	65.0	+1.0	+1.0	+2.0	6.0	no	3862.3	4301.9	11.4	3862.2	1988.6
	248.0	121.0	63.0										2043.0
A4	250.0	120.0	65.0	±1.0	+2.0	+2.0	3.0	yes	3829.4	4275.5	11.6	3825.5	1963.8
	249.0	120.0	65.0										1971.7
A5	253.0	120.0	65.0	±1.0	-3.0	+2.0	4.0	yes	3705.3	4112.7	11.0	3704.1	1877.6
	252.0	119.0	63.5										1945.8
Mean	250.3	120.1	64.4				3.8		3721.0	4138.4	11.2	3719.9	1922.6
CV (%)	0.62	0.45	1.38				31.80		2.95	3.16	2.35	2.93	3.39

Table 1: Physical properties of brick units from series A

Unit	L	B	H	SS a	SS b	SS c	CR	Cr	Md	Ms	WA	Mf	γ_d
	(mm)	(mm)	(mm)	(mm)	(mm)	(mm)	(mm)	(mm)	(g)	(g)	(%)	(%)	(kg/m³)
B1	242.0	121.0	64.0	±1.0	+3.0	-2.0	7.5	no	3226.8	3689.8	14.3	3218.4	1721.8
	242.0	121.5	66.5										
B2	242.0	122.0	61.5	±1.0	+3.0	+1.0	4.0	no	3226.7	3680.5	14.1	3218.9	1777.1
	242.0	119.5	64.5										
B3	242.0	119.5	67.0	+1.0	+5.0	-3.0	8.0	no	3240.7	3682.9	13.6	3240.7	1672.6
	242.5	121.5	64.0										
B4	238.0	119.5	64.0	+2.0	+5.0	-1.0	6.5	no	3195.9	3696.5	15.7	3183.2	1755.8
	237.0	120.0	63.0										
B5	241.0	122.0	65.0	+2.0	+1.0	-3.0	4.5	yes	3245.8	3713.6	14.4	3235.1	1698.4
	242.0	122.0	65.0										
Mean	241.1	120.9	64.5				6.1		3227.2	3692.7	14.4	3219.3	1719.9
CV (%)	0.76	0.87	2.34				26.13		0.54	0.32	4.68	0.62	2.40

Table 2: Physical properties of brick units from series B

Unit	L	B	H	SS			CR	Cr	Md	Ms	WA	Mf	γ_d
				a	b	c							
	(mm)	(mm)	(mm)	(mm)	(mm)	(mm)	(mm)	(mm)	(g)	(g)	(%)	(%)	(kg/m^3)
C1	254.0	124.0	66.0	±2.0	±0.5	+1.5	2.0	yes	2591.3	2948.9	13.8	2580.5	1246.6
	254.0	124.5	66.0										1241.6
C2	255.0	125.0	66.5	±1.0	±2.0	-3.0	1.0	no	2447.1	2785.7	13.8	2438.1	1154.5
	255.0	125.0	66.0										1163.2
C3	255.0	124.0	66.5	+1.0	±0.5	-3.0	1.0	no	2626.4	2984.5	13.6	2622.9	1249.0
	253.0	124.5	66.0										1263.4
C4	252.0	124.0	66.0	±1.0	±0.5	-2.0	1.0	no	2601.6	2965.8	14.0	2593.8	1261.5
	253.0	123.5	66.5										1252.1
C5	254.0	125.0	63.0	±1.0	±0.5	-2.0	2.0	no	2560.5	2912.0	13.7	2549.3	1280.1
	254.0	124.5	63.0										1285.2
Mean	253.9	124.4	65.6				1.4		2565.4	2919.4	13.8	2556.9	1239.7
CV (%)	0.37	0.39	1.97				34.99		2.45	2.43	0.88	2.50	3.44

Table 3: Physical properties of brick units from series C

Brick density in dry conditions is calculated by a ratio of mass to volume, according to Eq. 3.1.

$$\gamma_d = \frac{m}{V} = \frac{m}{LBh} \tag{3.1}$$

Water absorption was tested on each brick unit placed in special bin in vertical position, laid with the smaller side on a metal plate with holes, Figure 43b. Water with temperature 15-20°C was added into the bin, with water level up to the half-length of the samples. After 2 hours, additional water was added into the bin, up till a level of 3/4 from the brick length. After another 2 hours, water was added to fully submerge the samples. Brick units were submerged in water at a room temperature about 24 hours, and then were pull out, cleaned from excessive surface water with dry clothes and were measured on electronic scale. Water absorption was calculated with Eq. 3.2.

$$WA = \frac{m_1 - m}{m}\, x\, 100 \;\; (\%) \tag{3.2}$$

where,

m dry constant mass of a brick, in kg

m_1 saturated constant mass of a brick, in kg

Consistence on ice was tested on the same brick units used for measuring water absorption. They were placed on a railing in a fridge with constant air flow from all sides. Freezing temperature of -20±2°C was kept constant during the first 4 hours without any interruption of the process. The clear spacing between the bricks was about 2 cm. After the first freezing cycle, the units were pulled out from the fridge and were fully submerged in water with a temperature of 20±5°C for the next 4 hours (thawing cycle). The freeze/thaw cycles were repeated 5 times and brick mass was measured after each freezing cycle. During each cycle, visual inspection was carried out to determine possible damage in the bricks, usually in a form of splitting or disintegration, and all observed changes were noted.

In relation to the obtained results from measurements of dimensions, surface smoothness, corner roundness and presence of crack, all bricks from the first three series were classified in quality class I.
Mass, density, water absorption and consistence on ice, and mechanical properties were determined according to MKS B.D8.011. In agreement with the standard, strength class is determined by mean and single minimum values for compressive strengths on the brick gross cross-section. Adequate values for strength classification are given in MKS B.D1.011 [1987].

3.2.2 *Compressive strength of brick units*

The mechanical properties of brick units are essential for analytical or numerical analysis. The standard MKS B.D8.011 [1987] prescribes testing methods of clay bricks, blocks and slabs. Strength class of bricks i.e. the compressive strength should be determined on 5 brick units taken from an average sample and prepared by following the standard requirements. Tests to determine the compressive strength of brick units and brick samples and bending tensile strength of brick units is presented in the following subsection.

3.2.2.1 *Unit preparation*

Units for testing the compressive strength should be previously prepared according to the procedure given in the standard. Ten full-size brick units were selected for testing, whereof 5 sandwich units were obtained by bonding two bricks together. The bonding was made on the largest side of each brick. Bonding material was cement paste with maximum thickness of 5 mm with 40 % aluminate cement AC 650 and 60 % Portland cement. Bricks from series D needed cement pasting on all surfaces because of voids and curved surfaces obtained during extraction from the existing building, as shown in Figure 44. Testing units were cured in laboratory conditions for 7 days at a room temperature of 15 - 20°C. On the day of the testing, all glued units were examined for possible deviation from flat surface and were placed

(a) Brick sandwich units before testing

(b) Brick sandwich units from series C positioned on steel plate before testing

Figure 44: Brick sandwich units ready for testing

on a steel plate with thickness of 20 mm. No additional adjustments were made since the testing machine was equipped with fine-tuning capabilities.

3.2.2.2 *Test set-up and test procedure*

The method for testing the compressive strength on clay bricks recommended by the standard requires testing of glued units between steel plates with appropriate jacks equipped with a system for load application in uniform manner without any shocks. Servo-hydraulic, automatic controlled 'Form+Test' and 'Interfels' system for testing uniaxial compressive strength (Figure 45), with load capacity of 3000 kN was used to perform all the tests. Load application was automatic with predefined parameter calibration and precompression. The system was equipped with a load cell attached to the vertical actuator and displacement transducers. The load was applied with a constant loading rate of 0.25 $\mathrm{N/mm^2/s}$ until failure. The compressive strength was automatically obtained after the unit failure.

Figure 45 taken from Jovanovski and Josifovski [2006].

3.2.2.3 *Test results and failure modes*

A summary of the test results for obtained compressive strength of the brick units is presented in Table 4. Bricks from series A showed highest mean compressive strength among all brick series of 10.84 $\mathrm{N/mm^2}$. Hollow clay bricks from series C showed lowest coefficient of variation (CV) of 17.1 %. Notably, the bricks from series D demonstrated greatest CV of 36.17 %. This could be explained with the selected bricks for testing extracted from different wall positions, probably load-bearing and non load-bearing.

Surprisingly, all results revealed very low compressive strength and according to MKS B.D8.011 [1987] only units from series A can be classified in the lowest possible strength class, M100, which can be used for load bearing walls. The results for the compressive strength

Figure 45: Testing system for uniaxial compressive strength with capacity of 3000 kN

of the units from the other groups indicated that those units can not be classified in any strength class and can not be used even for non load-bearing walls. Moreover, the actual regulations in Macedonia, PZZ [1991] limit the minimum compressive strength of clay units to be used for load-bearing walls to 10 N/mm^2. On the other hand, Eurocode 8 [2004], for areas with medium and high seismicity, prescribes the minimum normalized compressive strength of masonry units normal to bed face to 5 N/mm^2. Having in mind the dimensions of the units and in accordance to EN 772-1 [2011], conversion of the compressive strength to the normalised compressive strength was obtained by multiplication with a shape factor $\delta = 0.8$. Thus, the normalised compressive strength of units from series A was 8.67 N/mm^2, 3.22 N/mm^2 for series B, 5.14 N/mm^2 for series C, and 4.88 N/mm^2 for series D. Clearly, units from series A and C satisfy the minimum strength requirements as recommended by Eurocode 8 [2004].
Figure 46 illustrates typical failure modes of brick units after compression strength tests. Crushing and partial splitting of units was observed in all tests. Crushing was dominant failure mode in the units from series B, while the units in series C demonstrated vertical cracks at failure.

3.2.3 *Compressive strength of brick specimens*

To compare the results for compressive strength of the units and to consider the influence of the size-effect on the compressive strength

Unit	A (mm^2)	N (kN)	f_{bk} (N/mm^2)
2A1	30496.50	301.92	9.90
2A2	30870.00	404.40	13.10
2A3	30678.75	223.95	7.30
2A4	30492.00	365.90	12.00
2A5	30870.00	367.35	11.90
Mean	30681.45	332.70	10.84
CV(%)	0.55	19.11	18.90

(a) Series A

Unit	A (mm^2)	N (kN)	f_{bk} (N/mm^2)
2B1	30132.00	93.41	3.10
2B2	30253.50	130.09	4.30
2B3	29767.50	77.40	2.60
2B4	29520.00	135.79	4.60
2B5	29889.00	164.39	5.50
Mean	29912.40	120.22	4.02
CV(%)	0.87	25.89	26.01

(b) Series B

Unit	A (mm^2)	N (kN)	f_{bk} (N/mm^2)
2C1	31496.00	/*	/*
2C2	31372.00	241.56	7.70
2C3	31245.50	215.59	6.90
2C4	31119.00	199.16	6.40
2C5	31369.00	147.43	4.70
Mean	31320.30	200.94	6.43
CV(%)	0.41	17.12	17.10

(c) Series C

Unit	A (mm^2)	N (kN)	f_{bk} (N/mm^2)
2D1	29524.00	292.29	9.90
2D2	32385.00	113.35	3.50
2D3	34060.00	224.80	6.60
2D4	30250.00	184.53	6.10
2D5	38500.00	169.40	4.40
Mean	32943.80	196.87	6.10
CV(%)	9.73	30.28	36.17

(d) Series D

Table 4: Uniaxial compressive strength of brick units

A=gross area; N=failure load; f_{bk}=uniaxial compressive strength; *) error in test.

of solid clay bricks, another series of brick specimens cut from whole units was prepared for testing. The brick specimens were cut from units belonging to series A, B and D on a large rock cutting saw. It was decided to prepare 6 cube brick specimens with dimensions 50x50x50 mm from each series (Figure 47a). Units with vertical holes from series C were not included, since their shape does not allows cutting of solid cube specimens. The test set-up and test procedure was the same as for the whole units.

The results obtained are presented in Table 5. The mean compressive strength of specimens from series A was 16.37 N/mm^2, from series B was 9.32 N/mm^2 and from series D was 13.00 N/mm^2 . The increased values for compressive strength ranging from 1.5-2.3 times for corresponding series indicates the significant influence of the size-effect

Spec.	l (mm)	b (mm)	h (mm)	A (mm^2)	Md (g)	γ_d (kg/m^3)	N (kN)	$f_{b,comp}$ (N/mm^2)
A12	54.00	54.30	53.00	2932.20	303.71	1954.29	59.52	20.30
A13	53.50	54.00	53.40	2889.00	299.50	1941.37	51.42	17.80
A22	54.00	54.00	53.50	2916.00	305.39	1957.55	47.24	16.20
A23	54.70	54.50	52.00	2981.15	300.58	1938.98	53.06	17.80
A32	53.60	54.80	50.00	2937.28	289.58	1971.76	40.83	13.90
A33	53.70	54.50	48.20	2926.65	280.75	1990.22	35.71	12.20
Mean	53.92	54.35	51.68	2930.38	296.59	1959.03	47.96	16.37
CV (%)	0.74	0.53	3.79	0.94	2.93	0.90	16.45	16.37

(a) Series A

Spec.	l (mm)	b (mm)	h (mm)	A (mm^2)	Md (g)	γ_d (kg/m^3)	N (kN)	$f_{b,comp}$ (N/mm^2)
B12	54.00	54.00	51.00	2916.00	256.71	1726.18	20.70	7.10
B13	53.40	54.70	53.30	2920.98	262.21	1684.20	27.46	9.40
B22	54.00	54.20	52.00	2926.80	247.28	1624.77	24.00	8.20
B23	54.30	55.00	52.40	2986.50	261.14	1668.71	32.85	11.00
B32	54.00	54.00	52.60	2916.00	261.50	1704.90	25.37	8.70
B33	54.00	54.40	52.50	2937.60	259.78	1684.43	33.78	11.50
Mean	53.95	54.38	52.30	2933.98	258.10	1682.20	27.36	9.32
CV (%)	0.50	0.67	1.33	0.84	2.00	1.87	17.08	16.48

(b) Series B

Spec.	l (mm)	b (mm)	h (mm)	A (mm^2)	Md (g)	γ_d (kg/m^3)	N (kN)	$f_{b,comp}$ (N/mm^2)
D12	52.00	54.00	53.50	2808.00	230.80	1536.33	52.51	18.70
D13	52.20	53.00	53.00	2766.60	223.10	1521.52	63.36	22.90
D22	51.50	54.00	54.00	2781.00	225.00	1498.26	45.33	16.30
D23	50.00	51.50	53.00	2575.00	187.00	1370.21	17.77	6.90
D32	52.00	54.00	53.00	2808.00	205.50	1380.83	18.81	6.70
D33	50.00	53.00	53.00	2650.00	194.20	1382.70	17.23	6.50
Mean	51.28	53.25	53.25	2731.43	210.93	1448.31	35.83	13.00
CV (%)	1.82	1.69	0.72	3.22	7.80	4.93	52.06	50.69

(c) Series D

Table 5: Physical and mechanical properties of brick cube specimens

l/b/h=length/width/height of specimen; A=gross area; Md=mass (dry); γ_d=density (dry); N=failure load; $f_{b,comp}$=uniaxial compressive strength of cube specimens.

(a) Failure mode of the units from series A

(b) Failure mode of the units from series B

Figure 46: Failure modes of brick units subjected to uniaxial compressive stress

(a) Solid cube brick specimens

(b) Failure modes of solid cube specimens

Figure 47: Solid brick cube specimens used for testing compressive strength

on the compressive strength of the tested bricks. However, the values for CV are lower than those calculated for the whole units, except for series D. Characteristic failure modes of brick specimens are shown in Figure 47b. All specimens failed with progressive vertical cracking and splitting, except for specimens in series B which failed by smashing and crushing.

3.2.4 *Tensile flexural strength of brick units*

It has been common practice to determine the tensile flexural strength of building materials, such as concrete or mortar by using prism test specimens and applying three-point bending test. Such analogy was established for testing the tensile flexural strength of the brick units. Without any specific preparation, 5-7 units from all series were selected for testing. Their dimensions, mass and density were obtained as described in subsection 3.2.1.

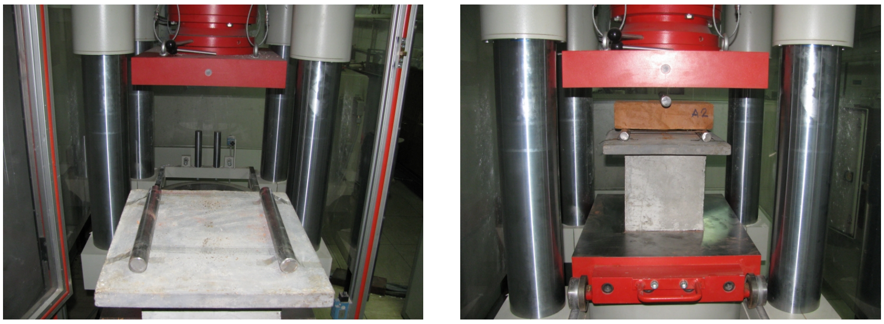

(a) Bottom steel rollers (b) Brick unit ready for testing

Figure 48: Details of testing the tensile flexural strength of brick units

3.2.4.1 *Test set-up and test procedure*

The test set-up used for testing the tensile flexural strength consist of the testing system described in subsection 3.2.2 and illustrated in Figure 45. Boundary conditions were created by steel roller bearings with length of 150 mm and diameter of 10 mm. Two rollers were placed on a stiff steel plate with thickness of 25 mm fixed with sticky tape to prevent accidental movement during preparation and testing. The span between the rollers was $l = 200\,mm$. A brick unit was placed directly on the steel rollers and carefully lined up in the centre. On the top of the unit, another roller was placed freely in the centre of the brick. The test set-up is shown in Figure 48.

Load application was automatic with constant loading rate of $0.25\,\mathrm{N/mm^2/s}$ until failure.

3.2.4.2 *Test results and failure modes*

The tensile flexural strength was obtained automatically through the system's predefined test set-up for testing the tensile flexural strength. Failure load was calculated directly from the obtained tensile flexural strength according to Eq. 3.3 and Eq. 3.4. Table 6 presents the obtained values for tensile flexural strength of brick units and the attained failure load.

$$f_{bt,flex} = \frac{M_{ult}}{W} = \frac{(Nl)/4}{(bh^2)/6} = \frac{3Nl}{2bh^2} \tag{3.3}$$

$$N_{t,flex} = \frac{2bh^2}{3l_{span}} f_{bt,flex} \tag{3.4}$$

where,

$f_{bt,flex}$	tensile flexural strength of a brick
b	unit width
h	unit height
l_{span}	span between supports

Figure 49: Tensile flexural failure mode of brick unit

Typical failure mode of the brick units after the tensile flexural strength test is shown in Figure 49. Brittle behaviour of bricks was noticed with sudden crack occurrence and immediate progressive crack distribution over the height until the complete failure.

3.3 EXPERIMENTAL TESTS ON MORTARS

Mortar is bonding material in masonry composed of binder agents, aggregate and water. As binding materials lime, cement, their combination or other hydraulic binders are usually used, depending on the structural type and building type. Lime mortar was usually used in rural buildings and historic monuments. Lime-cement mortar is the most common type of mortar used in the construction practice in Macedonia. PZZ [1991] declares the minimum strength class of mortars that satisfy the requirements according to JUS U.M2.010 [1992]. For clay brick masonry, the minimum strength class for lime mortar is M1, for cement-lime mortar is M2, and for cement mortar is M10. On the other hand, for construction of masonry buildings in seismic regions only cement-lime mortar is allowed as referred in PIOVSP [1981]. In seismic zones of intensity VII and VIII, mortar with minimum strength class of M2.5 should be used, whilst for zones of intensity IX, M5 is the minimum permitted mortar class. Pure cement mortar without any lime is not allowed. The strength class roughly corresponds to the mean compressive strength after 28 days, and the class number corresponds to the actual value for compressive strength expressed in N/mm^2. Eurocode 8 [2004] prescribes minimum mortar compressive strength of $5\,N/\mathrm{mm}^2$ for unreinforced and confined masonry and $10\,N/\mathrm{mm}^2$ for reinforced masonry.

As stated by Haach [2009], mortar is one of the components of masonry that is responsible for uniform stress distribution, correction of irregularities of units and accommodation of thermal deformations and shrinkage. It plays major role in the final behaviour of the masonry

Unit	γ_d (kg/m^3)	N (kN)	$f_{bt,flex}$ (N/mm^2)
A1	1931.45	6.13	3.60
A2	1827.78	4.00	2.20
A3	1867.17	5.23	3.00
A4	1968.64	4.73	2.80
A5	1965.41	3.58	2.10
A6	1943.74	4.64	2.80
A7	1915.41	3.65	2.10
Mean	1917.08	4.56	2.66
CV (%)	2.52	18.60	19.49

(a) Series A

Unit	γ_d (kg/m^3)	N (kN)	$f_{bt,flex}$ (N/mm^2)
B1	1770.95	2.47	1.60
B2	1644.34	2.70	1.60
B3	1659.08	2.66	1.50
B4	1740.22	2.60	1.60
B5	1690.76	1.48	0.90
B6	1681.69	2.86	1.70
Mean	1697.84	2.46	1.48
CV (%)	2.61	18.46	18.01

(b) Series B

Unit	γ_d (kg/m^3)	N (kN)	$f_{bt,flex}$ (N/mm^2)
C1	1279.55	1.10	0.60
C2	1243.02	1.57	0.90
C3	1242.89	1.61	0.90
C4	1236.50	1.79	1.00
C5	1244.29	1.79	1.00
Mean	1249.25	1.57	0.88
CV (%)	16.15	1.23	16.70

(c) Series C

Unit	γ_d (kg/m^3)	N (kN)	$f_{bt,flex}$ (N/mm^2)
D1	1359.97	5.19	3.00
D2	1369.11	7.46	2.90
D3	1369.37	5.14	2.40
D4	1402.05	2.39	1.40
D5	1443.19	10.97	4.60
Mean	1388.74	6.23	2.86
CV (%)	2.21	45.99	36.31

(d) Series D

Table 6: Tensile flexural strength of solid clay bricks

γ_d=density (dry); N=failure load; $f_{bt,flex}$=uniaxial compressive strength of cube specimens.

(a) Steel mould for mortar specimens

(b) Preparation of mortar specimens in moulds

Figure 50: Preparation of mortar prism specimens for testing physical and mechanical properties

in terms of stresses and strains. Its participation in the compressive and shear strength of masonry is appreciated by many codes.

In this research, lime mortar was used in all subsequent tests and thus, primary physical and mechanical properties were tested. To compare the results with 'stronger' mortar, cement-lime mortar specimens were prepared and tested.

3.3.1 *Preparation of mortar specimens*

Mechanical properties of mortar are important parameters for masonry behaviour under compressive and/or lateral loads. Preparation and testing of compressive and tensile flexural strength of mortar specimens was done according to MKS U.M8.002 [1968] and MKS B.C8.042 [1981]. These standards are similar to the actual EN 1015-11 [1999].

Although the number of mortar specimens required by the standards is 3, mortar properties were tested on 6 lime mortar specimens and 9 cement-lime mortar specimens. Prism mortar specimens with dimensions $lxbxh = 160x40x40$ mm were provided from each mortar type. Prisms were taken from a mortar batch and poured into clean and lubricated steel moulds, see Figure 50. Materials for production of mortars were previously stored in laboratory conditions for few days and the mortar specimens were prepared at stable room temperature of 19°C with relative humidity of 60 %.

For preparation of lime mortar, lime and well aggregated sand were mixed in ratio 1:3, while for cement-lime mortar the ratio cement:lime:sand was 1:1:4 (see Figure 51).To mix and prepare all mortar specimens regular tap water was used. The chemical properties and content of the lime were unknown and originated from individual producer available on the market. Portland cement was provided by "Titan" type PC 30p 45S (conforming EN 197-1, 2000). The content of the cement component was portland cement with additive of natural

(a) Components of cement-lime mortar (b) Mixing cement-lime components

Figure 51: Preparation of cement-lime mortar

or artificial pozzolana and hydraulic binding material produced by grinding of portland cement clinker, gypsum and maximum 30% of additives.

Mix content ratio was roughly obtained and measured while preparation of the mortar paste by using regular shovel. The exact weight portions of components were not specified prior mixing due to the intention to recreate the conditions usually found at constructions sites.

The mortar specimens were taken from the laboratory mortar batch used for building the masonry walls tested later. They were gently tamped in the moulds with a trowel. The specimens were stored at laboratory conditions next to the masonry walls for 48 hours. After that, the lime mortar specimens were stored in the laboratory under foregoing conditions, while the cement-lime specimens were stored at temperature of 20^{o}C and relative humidity of $80 - 90\,\%$.

3.3.2 *Physical properties of lime and cement-lime mortar*

The physical properties of the prepared mortar specimens in terms of dimensions, mass and density were tested twice. The first time, precise measurements of specimen dimensions and mass were taken before testing the tensile flexural strength, and the second time before testing the compressive strength the measurements took place on the two-half's left from the specimens after testing the tensile flexural strength, see Figure 52. The mean density for lime mortar in dry conditions obtained from both tests was $1385\,{}^{kg}/_{m^3}$ with CV of about $1\,\%$. Cement-lime mortar had density of $2084\,{}^{kg}/_{m^3}$ with CV of $2.4\,\%$.

A summary of results for lime mortar is presented in Table 7, and results for the physical properties of cement-lime specimens are shown in Table 8. The meaning of the symbols in the tables is as follows: l/b/h=length/width/height of specimen; A=gross area; Md=mass (dry); γ_d=density (dry).

Spec.	l (mm)	b (mm)	h (mm)	A (mm^2)	Md (g)	γ_d (kg/m^3)
1	40.50	40.00	158.50	6419.25	355.70	1385.29
2	40.20	40.00	159.00	6391.80	349.50	1366.99
3	39.70	38.80	159.00	6312.30	340.90	1391.90
4	40.00	39.50	159.00	6360.00	343.60	1367.73
5	39.70	38.60	159.00	6312.30	343.30	1408.96
6	39.00	40.00	159.00	6201.00	342.30	1380.02
Mean	39.85	39.48	158.92	6332.78	345.88	1383.48
CV(%)	1.18	1.48	0.12	1.11	1.49	1.05

(a) Whole prism specimens

Spec.	l (mm)	b (mm)	h (mm)	A (mm^2)	Md (g)	γ_d (kg/m^3)
1/1	40.00	40.50	88.70	3548.00	196.50	1367.49
1/2	38.60	39.60	77.80	3003.08	163.90	1378.21
2/1	39.00	39.70	81.50	3178.50	175.90	1393.97
2/2	38.80	39.60	84.50	3278.60	181.40	1397.18
3/1	40.00	39.70	82.00	3280.00	180.00	1382.32
3/2	39.20	39.80	76.20	2987.04	166.20	1398.00
4/1	39.30	39.60	81.00	3183.30	173.30	1374.76
4/2	38.30	39.60	79.50	3044.85	168.90	1400.78
5/1	39.20	39.70	81.00	3175.20	176.20	1397.80
5/2	39.00	40.00	77.60	3026.40	165.60	1367.96
Mean	39.14	39.78	80.98	3170.50	174.79	1385.85
CV(%)	1.32	0.67	4.28	5.13	5.30	0.90

(b) Two-half's prism specimens

Table 7: Physical properties of lime mortar

(a) Precise measurement of mortar specimen dimensions (b) Measurement of mortar weight on electronic weight

Figure 52: Primary physical properties on mortar specimens

Spec.	l (mm)	b (mm)	h (mm)	A (mm^2)	Md (g)	γ_d (kg/m^3)
1	41.00	40.00	161.00	6601.00	561.60	2126.95
2	43.00	40.00	161.00	6923.00	550.10	1986.49
3	42.00	40.00	161.00	6762.00	576.80	2132.51
4	42.50	40.00	161.00	6842.50	550.90	2012.79
5	42.50	40.00	161.00	6842.50	572.20	2090.61
6	43.00	40.00	161.00	6923.00	574.40	2074.25
7	41.00	40.00	161.10	6605.10	565.10	2138.88
8	41.00	40.50	161.00	6601.00	565.00	2113.41
9	42.00	40.00	161.00	6762.00	563.50	2083.33
Mean	42.00	40.06	161.01	6762.46	564.40	2084.36
CV(%)	1.86	0.39	0.02	1.85	1.57	2.41

Table 8: Physical properties of cement-lime mortar on two-half's prism specimens

3.3.3 *Tensile flexural strength of of lime and cement-lime mortar*

First, tensile flexural strength test was performed on mortar prism specimens. The test was done according to standardized procedures described in MKS B.C8.022 [1976], MKS B.C8.042 [1981], and EN 1015-11 [1999]. The tests were performed 60 days after the casting.

3.3.3.1 *Test set-up and test procedure*

The test set-up was similar to that used to test the tensile flexural strength of brick units. Six lime mortar specimens and nine cement-lime specimens were tested. Mortar specimens were positioned and carefully aligned on steel rollers with diameter of 10 mm at a distance of 106.7 mm. Steel roller with the same diameter was placed on the top of the specimen and centred. Load was increased automatically from zero without shocks at a loading rate of 0.25 N/mm^2/s until the failure. The tensile flexural strength was obtained automatically with the system's set-up.

3.3.3.2 *Test results and failure modes*

Lime mortar produced quite low tensile flexural strength with a mean value of 0.10 N/mm^2, but high CV of 43.59 %. Although low tensile flexural strength was expected, the high dispersion of results was unusual. On the other hand, the mean tensile flexural strength for the cement-lime mortar specimen was 5.97 N/mm^2 and the CV was 17.14 %. A summary of the results obtained is presented in Table 9. The failure load was calculated with Eq. 3.6 by rearranging the Eq. 3.5.

$$f_{mt,flex} = 1.5\frac{Nl}{bd^2} \tag{3.5}$$

$$N = \frac{f_{mt,flex}bd^2}{1.5l} \tag{3.6}$$

where,

$f_{mt,flex}$	tensile flexural strength of mortar
N	failure load of mortar
b	width of specimen
d	height of specimen
l	length of specimen

All mortar specimens failed by breaking into two halves immediately after reaching the ultimate failure load. Failure mode of mortar specimens is presented in Figure 53. The broken specimens were kept for testing the compressive strength of both mortar types.

MKS B.C8.042 [1981] suggests calculation of the tensile flexural strength of lime mortar as a ratio between the failure load and the

Spec.	N (kN)	$f_{mt,flex}$ (N/mm^2)
1	0.02	0.08
2	0.03	0.10
3	0.05	0.19
4	0.03	0.10
5	0.02	0.08
6	0.01	0.05
Mean	0.03	0.10
CV (%)	41.40	43.59

(a) Lime mortar

Spec.	N (kN)	$f_{mt,flex}$ (N/mm^2)
1	1.40	5.15
2	1.48	5.20
3	1.67	6.00
4	1.41	5.00
5	1.69	6.00
6	1.57	5.50
7	1.55	5.70
8	2.37	8.50
9	1.86	6.70
Mean	1.67	5.97
CV (%)	17.06	17.14

(b) Cement-lime mortar

Table 9: Mortar tensile flexural strength

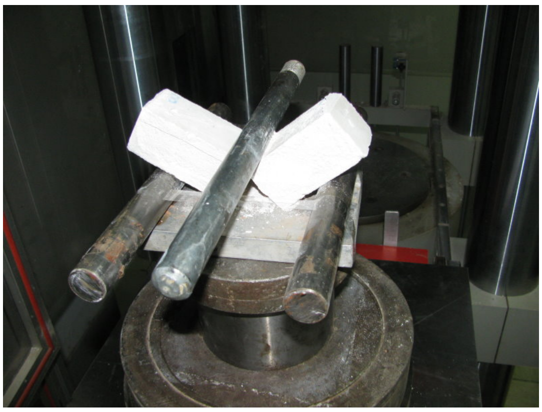

Figure 53: Typical tensile flexural failure mode of mortar specimen

(a) Mortar specimens left from the tensile strength tests

(b) Testing mortar compressive strength

Figure 54: Testing compressive strength of mortar specimens

cross-section area, Eq. 3.7. In that case, the mean value for the failure load of lime mortar specimens was calculated as 0.16 N, while for cement-lime mortar specimens was 10.04 N.

$$N = f_{mt,flex} bd \tag{3.7}$$

3.3.4 *Compressive strength of lime and cement-lime mortar*

Tests for the compressive strength of lime and cement-lime mortar were done according to MKS B.C8.022 [1976], MKS B.C8.042 [1981], and EN 1015-11 [1999]. Specimen's broken halves from the tensile flexural strength test were used to test the compressive strength. The tests were performed right after the tensile flexural tests in the same laboratory conditions.

3.3.4.1 *Test set-up and test procedure*

Mortar specimen halves were first cleaned from any loose material leftover from the previous test, see Figure 54a. The testing system plates were cleaned with soft clothes to remove any dust. Two bearing plates made from stiff steel with dimensions 40.1x40.0 mm and thickness 0.8 mm were used for load application. Both plates were freely placed on the mortar specimens, on the bottom and on the top. The testing system platens were able to align freely when in contact with the steel bearing plates. The bearing plates were arranged on the specimens so that about 18 *mm* of free space was left between the plates and prism cast ends. The absolute flatness of the bearing plates allowed load application over the whole surface of the plates, see Figure 54b.

The vertical load was applied without shocks with a loading rate of 0.03 $N/mm^2/s$ which roughly corresponds to the suggested loading rate in the standards of 50 N/s. Load was increased uniformly until failure of the specimens and the maximum compressive strength

(a) Lime mortar

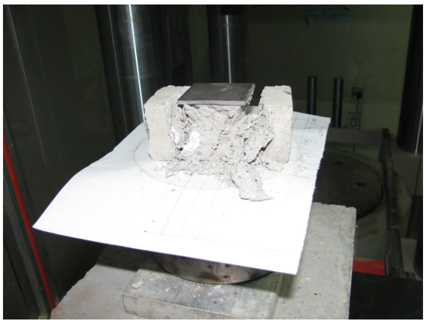

(b) Cement-lime mortar

Figure 55: Compressive failure modes of mortar specimens

was automatically recorded with the testing system set-up. The maximum load applied during the test was calculated by multiplying the maximum compressive strength with the cross-sectional area of the specimen, Eq. 3.8.

$$N = f_{m,comp}bl \tag{3.8}$$

where,

N	failure load
$f_{m,comp}$	compressive strength of mortar
b	width of specimen
l	length of specimen

3.3.4.2 *Test results and failure modes*

Low compressive strength of lime mortar was determined with a mean value of 0.55 N/mm^2 and CV of 12.2 %. On the other hand, cement-lime mortar demonstrated high compressive strength with average of 26.92 N/mm^2, but higher CV than lime mortar of 25.48 %. A summary of the test results is presented in Table 10.

All mortar specimens showed similar failure modes expressed by crushing of the specimen over the whole height in the region where two bearing plates were positioned, as illustrated in Figure 55. According to the strength class offered in the standards, lime mortar could not be classified in any class, while cement-lime mortar could be classified as M20, according to the principle of single minimum value for compressive strength on a gross cross-section.

3.4 EXPERIMENTAL TESTS ON CONCRETE

The basic properties of the concrete used for strengthening masonry wall by RC jacketing were determined experimentally. Normal portland

Spec.	N (kN)	$f_{m,comp}$ (N/mm^2)
1/1	1.77	0.50
1/2	1.50	0.50
2/1	1.91	0.60
2/2	1.64	0.50
3/1	1.97	0.60
3/2	2.09	0.70
4/1	1.59	0.50
4/2	1.52	0.50
5/1	1.59	0.50
5/2	1.82	0.60
Mean	1.74	0.55
CV (%)	11.05	12.20

(a) Lime mortar

Spec.	N (kN)	$f_{m,comp}$ (N/mm^2)
1/1	66.67	20.20
1/2	60.40	18.30
2/1	67.50	19.50
2/2	64.38	18.60
3/1	124.08	36.70
3/2	89.93	26.60
4/1	84.50	24.70
4/2	91.69	26.80
5/1	73.21	21.40
5/2	67.06	19.60
6/1	86.88	25.10
6/2	88.61	25.60
7/1	87.13	26.40
7/2	88.45	26.80
8/1	122.45	37.10
8/2	117.83	35.70
9/1	127.13	37.60
9/2	127.80	37.80
Mean	90.87	26.92
CV (%)	24.92	25.48

(b) Cement-lime mortar

Table 10: Mortar compressive strength

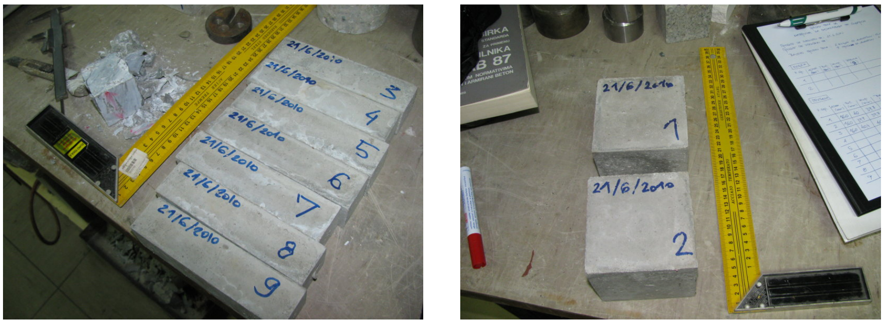

(a) Prism specimens (b) Cube specimens

Figure 56: Casted concrete samples ready for testing

cement "Titan" type PC 30p 45S, fine aggregate with three fractions, and regular tap water were mixed to produce the concrete which was applied on the masonry walls. The grades by volume of cement:sand were 1:3, mixed in concrete mixer and measured by shovel. The mixing took place under laboratory conditions at air temperature of about 25^{o}C with relative humidity of about 45 %. The water portions were added manually. Mix content ratio was obtained manually, by an empirical assessment of the workmen.
Concrete specimens for testing the physical and mechanical properties were taken from the concrete batch. In total, nine prism specimens with dimensions 40x40x160 mm and two cube specimens with dimensions 100x100x100 mm were casted, see Figure 56. Specimens were gently tamped in the moulds with a trowel and were stored in laboratory at a temperature of 20^{o}C and relative humidity of $80 - 90$ %. The same steel moulds used for casting the mortar specimens were applied. Additionally, steel cube moulds were used to cast the cube specimens. All moulds were taken away from the specimens 48 hours after the casting. The tests took place 102 days after the casting. The specimens were stored in the laboratory, near the strengthened walls, until the day of testing.

Specimen dimensions, mass and density were determined prior execution of the tests. Table 11 shows the main physical properties of the concrete prism specimens. The density of concrete prism specimens was about 2150 kg/m^3 with a CV of 0.64 %. The density of the concrete obtained with cube samples was similar, about 2190 kg/m^3, see Table 12. In the tables the meaning of the symbols is as follows: l/b/h=length/width/height of specimen; A=gross area; Md=mass (dry); γ_d=density (dry).

3.4.1 *Tensile flexural strength of concrete*

First, tensile flexural strength of concrete was determined following the same procedure for test set-up and load application as in case

Spec.	l (mm)	b (mm)	h (mm)	A (mm^2)	Md (g)	γ_d (kg/m^3)
1	39.70	40.00	160.00	6352.00	544.70	2143.81
2	39.70	39.90	160.00	6352.00	539.60	2129.06
3	40.00	40.40	160.00	6400.00	553.20	2139.54
4	40.40	40.00	160.00	6464.00	553.10	2139.16
5	40.40	40.00	159.00	6423.60	559.40	2177.13
6	40.30	40.00	160.00	6448.00	557.30	2160.75
7	39.00	40.00	160.00	6240.00	539.20	2160.26
8	38.80	40.00	160.00	6208.00	532.80	2145.62
9	39.20	40.00	160.00	6272.00	538.20	2145.25
Mean	39.72	40.03	159.89	6351.07	546.39	2148.95
CV (%)	1.45	0.33	0.20	1.38	1.65	0.64

Table 11: Dimensions, mass and density of concrete prism specimens

Spec.	l (mm)	b (mm)	h (mm)	A (mm^2)	Md (g)	γ_d (kg/m^3)
1	99.00	100.00	100.00	9900.00	2173.70	2195.66
2	97.50	100.00	100.00	9750.00	2126.70	2181.23
Mean	98.25	100.00	100.00	9825.00	2150.20	2188.44
CV (%)	0.76	/	/	0.76	1.09	0.33

Table 12: Dimensions, mass and density of concrete cube specimens

Unit	N (kN)	$f_{conct,flex}$ (N/mm^2)
1	1.54	5.80
2	1.45	5.50
3	1.52	5.60
4	1.37	5.10
5	1.30	4.80
6	1.45	5.40
7	1.46	5.60
8	1.37	5.30
9	1.36	5.20
Mean	1.42	5.37
CV (%)	5.20	5.34

Table 13: Tensile flexural strength of concrete

N=failure load; $f_{conct,flex}$=tensile flexural strength of prism specimens.

of testing mortar specimens. A predefined test set-up in the testing system for tensile flexural strength on prism specimens was selected. Uniform load was applied until the failure with a loading rate of 0.01 kN/s which corresponds to 0.006 N/mm^2/s. The failure load was calculated according to Eq. 3.6. Table 13 presents the results for the tensile flexural strength of concrete obtained on prism specimens.

Experimental failure mode of concrete after the tensile flexural strength test is shown in Figure 57. The prism specimens broke into two halves in vicinity of the central prism section where the load was applied.

3.4.2 *Compressive strength of concrete*

Tests to determine compressive strength of concrete were performed on concrete prism and cube specimens. Broken prism halves from the tensile flexural strength test were used as specimens for determining the compressive strength. The tests on cube specimens were done on the whole casted specimens without any previous intervention. The same test set-up and procedure for testing was applied as in case of testing mortar. Loading rate was 0.5 N/mm^2/s and the load was increased without shocks until the failure of the specimen. The obtained results are presented in Table 14.

Similar compressive strength was obtained on both tests. Compressive strength obtained on prism specimens gave slightly higher values,

(a) Tensile flexural strength test set-up

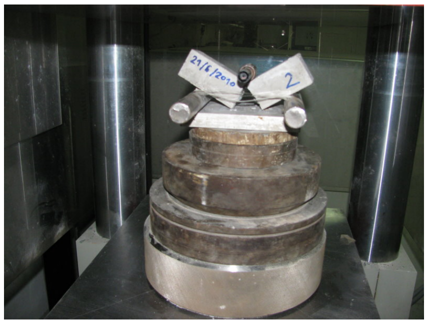

(b) Failure mode of concrete prism specimen

Figure 57: Tensile flexural test set-up and failure mode of concrete

Spec.	$f_{conc,comp}$ (N/mm^2)
1/1	34.30
2/2	29.10
3/1	26.90
4/2	31.60
5/2	31.30
6/1	30.80
7/1	31.00
8/2	28.10
9/2	32.30
Mean	30.60
CV (%)	6.93

(a) Tests on prism specimen

Spec.	$f_{conc,comp}$ (N/mm^2)
1	28.30
2	26.40
Mean	27.35
CV (%)	3.47

(b) Tests on cube specimen

Table 14: Compressive strength of concrete

(a) Compressive failure of prism specimen (b) Compressive failure of cube specimen

Figure 58: Compressive failure modes of concrete

(a) Samples of reinforcement mesh for testing tensile strength (b) Typical tensile failure mode of reinforcement samples

Figure 59: Tensile strength test on bars cut from reinforcement mesh

30.60 N/mm^2 than on cube specimens, 27.35 N/mm^2. But, different variation of the compressive strength could be established if more cube specimens were used for testing.
Prism specimens failed by crushing of the concrete through the whole height of the specimen under the bearing plates and vertical splitting near the steel plate edges, as shown in Figure 58a. Both cube specimens failed similarly, with progression of the vertical cracks from the middle to the outer surface of the specimens, Figure 58b.

3.5 EXPERIMENTAL TESTS ON REINFORCEMENT MESH

The reinforcement wire mesh used for RC jackets applied to masonry walls was produced by "Gamatroniks", factory for reinforcement meshes from city of Delchevo, Macedonia. Wire mesh with bearing bars in both orthogonal directions of type Q-139 was used. The wire mesh was composed of ribbed bars of diameter 4.2 mm placed at a distance of 100 mm in both directions. Reinforcement bars were connected by spot welding in the factory.

Type	Wire diameter		Wire distance		Wire area		Mesh dimensions		Mesh mass	
	long.	trans.	long.	trans.	long.	trans.	length	width		
	(mm)		(mm)		(mm^2)		(mm)		kg/m^2	kg/psc
Q-139	4.2	4.2	100	100	1.39	1.39	6000	2150	2.21	28.732

Table 15: Properties of Q-139 wire mesh

Spec.	Diameter	Breaking		Elongation at break	
		Force	Strength	Diameter	Elongation
	(mm)	(kN)	(N/mm^2)	(mm)	(%)
1	4.20	8.30	599.09	3.50	16.67
2	4.20	12.30	887.80	3.50	16.67
3	4.20	8.00	577.43	3.50	16.67
4	4.20	9.60	692.92	3.00	28.57
5	4.20	7.40	534.13	3.00	28.57
6	4.20	8.00	577.43	3.00	28.57
7	4.20	7.20	519.69	3.50	16.67
8	4.20	7.80	563.00	3.00	28.57
9	4.20	9.80	707.36	3.50	16.67
10	4.20	9.00	649.61	3.00	28.57
Mean	4.20	8.74	630.85	3.25	22.62
CV (%)	/	16.56	16.56	7.69	26.32

Table 16: Reinforcement test results

To determine the mechanical properties of the reinforcement, ten specimens were cut from the mesh. Each specimen had length of 500 mm, see Figure 59a. The tests were performed with a universal tensile testing system EU VEB 40, according to MKS C.A4.002 [1985] which is similar to ISO 6892-1 [2009]. Basic physical properties acquired from the producer are presented in Table 15. Test results are shown in Table 16.

Failure modes of all specimens were similar and are shown in Figure 59b.

Figure 60: Test set-up for compressive strength of masonry

3.6 COMPRESSIVE STRENGTH OF MASONRY

3.6.1 *Wallet UMWC-1*

Masonry uniaxial compressive strength was tested on one wallet (UMWC-1) with dimensions 1200x1200x250 mm and three wallets (UMWC-2) with dimensions 520x320x125 mm built with bricks from series A and lime mortar with grading 0:1:3. Average joint thickness in all wallets was 10 mm for vertical joints and 12 mm for horizontal joints. The bricks had compressive strength of 10.84 N/mm^2 and the lime mortar possessed compressive strength of 0.55 N/mm^2.

3.6.1.1 *Test set-up and test procedure*

UMWC-1 was tested with similar wall test set-up arrangement used for the in-plane cyclic shear tests of masonry walls. The wallet was built right on the spot designated for testing, and no movement on the wallet was produced whatsoever. The wallet was placed over a RC beam which was fully fixed to a strong floor by steel anchors. Any movement of the bottom RC beam was prevented with steel supports wrapped around both ends of the bottom RC beam. The top beam was placed over the wallet 28 days after the casting. It was glued to the wallet with a layer of lime mortar. The top beam was carefully positioned in the centre of the wall to ensure that no additional bending moment is introduced to the wallet and to provide

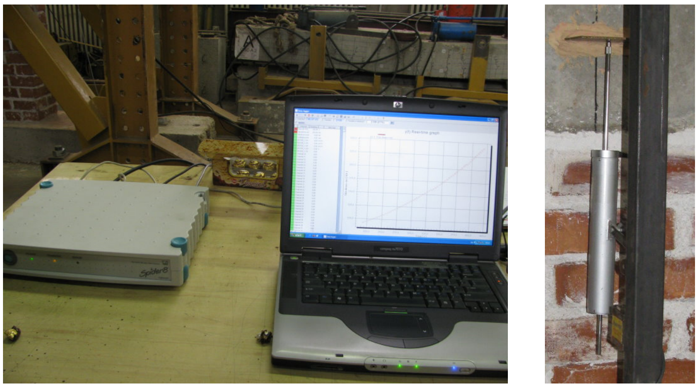

(a) Data acquisition system

(b) Kyowa DT-50A

Figure 61: Details of the test set-up and testing procedure

uniform load transfer of the vertical load, see Figure 60. The top RC beam produced a prestressing load of 4.14 kN (0.42 t).

The load was applied by one vertical hydraulic actuator with capacity of 500 kN, positioned in the centre of the top RC beam. The load was increased manually with uniform loading rates controlled by a load cell positioned between the actuator and the beam. The vertical actuator was supported by a horizontal stiff steel beam. Data acquisition was automatic with data acquisition system (DAQ) consisting of transducer, DAQ hardware and personal computer.

PC-based data acquisition with Spider8 multi-channel PC measurement DAQ from HBM was used, see Figure 61a. The system was fully PC-controlled through an LPT connection. It contained separate A/D converter for each channel and a sampling rates of up to 9600 values/s per channel was used. Eight channel Spider8 DAQ was used for all tests. It consisted of sensors, signal conditioning, analog-to-digital conversion and filters for every measurement channel. Catman®Professional software was used to set-up and control the tests.

Vertical displacement at the top RC beam was monitored and recorded. Kyowa DT-A 50 mm displacement transducer (DT) was used to measure the absolute displacement in the direction of the load application, see Figure 61b. The DT was mounted on a separate steel frame independent of the main testing frame and the wall. Thus, any relative displacements from the vertical actuator and connecting testing frame had not influence on the displacements of the wallet. Kyowa DT-50A displacement transducers had nonlinearity and hysteresis within ±0.5 % RO, repeatability of 0.3 % RO or less and rated output of 1.5 $^{mV}/_{V}$ 3000 $^{\mu m}/_{m}$. Factory produced 4-conductor $(0.08\,\mathrm{mm}^2)$ chloroprene shielded cable with length of 5 m with RS-232 connector plug was used to connect the DT to DAQ.

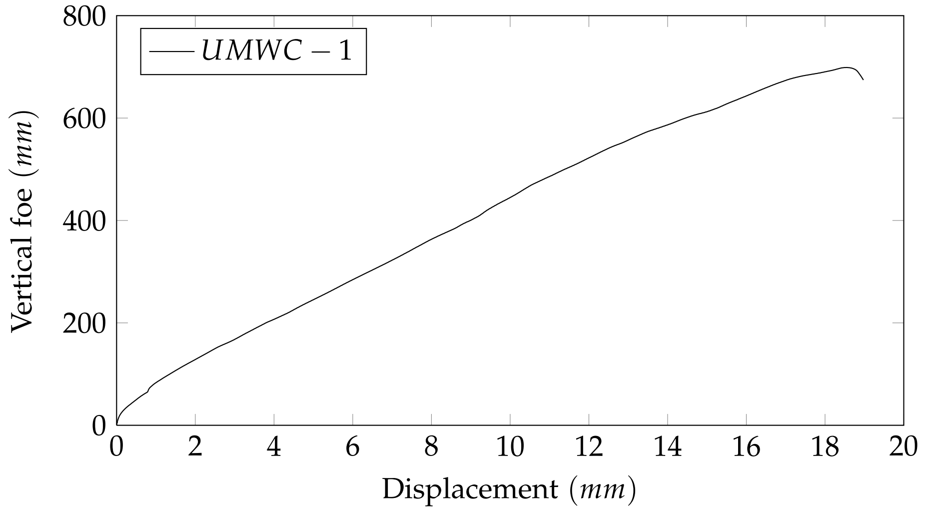

Figure 62: UMWC-1 Force-displacement curve

3.6.1.2 *Test results and failure mode*

Tests were carried out in controlled laboratory conditions, 40 days after building the wallet. Axial compression test was conducted with average load application rate of 0.6 $^{kN}/_{s}$. The whole test lasted 15 : 32 min. The main results presented by force-displacement $(P - \Delta)$ curve and stress-strain $(\sigma - \epsilon)$ curve are shown in Figure 62 and Figure 63.

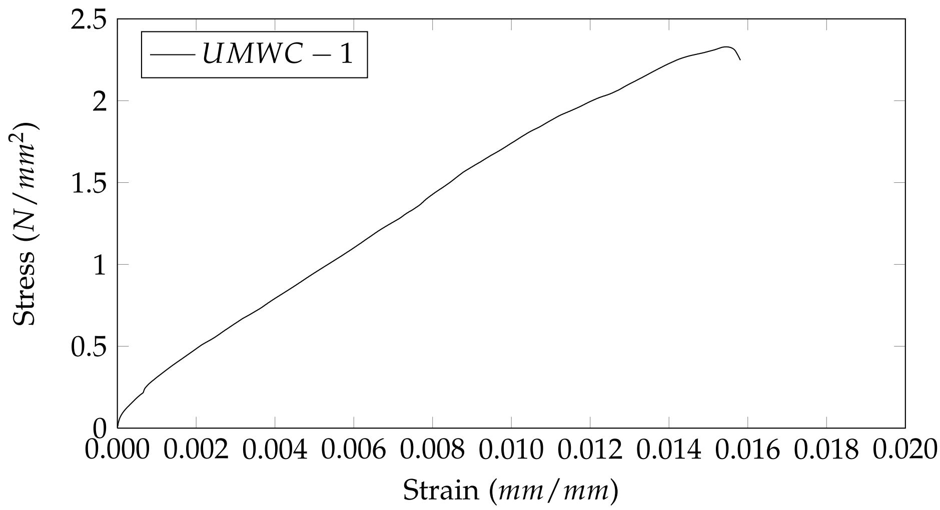

Figure 63: UMWC-1 Stress-strain curve

The wallet presented ultimate load of 705.6 kN and ultimate displacement of 18.7 mm. Masonry compressive strength was calculated according to Eq. 3.9.

$$f_{m,test} = \frac{F_{max}}{A_w} \tag{3.9}$$

Wallet	$f_{mas,test}$ N/mm²	$f_{k,test}$ N/mm²	$E_{m,test}$ N/mm²	$f_{k,EC6}$ N/mm²	$E_{m,EC6}$ N/mm²
UMWC-1	2.35	1.96	200.00	2.09	2085.23

Table 17: Mechanical properties of masonry related to compressive strength and modulus of elasticity obtained from wallet UMWC-1

$f_{mas,test}$=compressive strength of masonry, $f_{k,test}$=characteristic compressive strength of masonry, and $f_{k,EC6}$=characteristic compressive strength of masonry according to Eurocode 6 [2005], $E_{m,test}$=modulus of elasticity of masonry, $E_{m,EC6}$=modulus of elasticity of masonry according to Eurocode 6 [2005].

where,

$f_{m,test}$ compressive strength of masonry

F_{max} ultimate compressive load

A_w loaded cross-section of the masonry wallet

In Table 17, results for the compressive strength are presented. The characteristic compressive strength of masonry was obtained by dividing the compressive strength of masonry with 1.2, while the characteristic compressive strength of masonry specified according to Eurocode 6 [2005] was determined from Eq. 3.10.

$$f_k = 0.55 f_b^{0.7} f_m^{0.3} \tag{3.10}$$

$f_b = 8.67$ N/mm² from Table 4a and $f_m = 0.55$ N/mm² from Table 10a.

where,

f_k characteristic compressive strength of masonry

f_b normalized mean compressive strength of bricks, in the direction of the applied load ($\delta = 0.8$)

f_m compressive strength of mortar

It was observed that the values calculated according to Eurocode 6 [2005] were 6.39 % higher than the characteristic compressive strength obtained with the test. This indicates that good agreement was found between the experimental values and those suggested by Eurocode 6 [2005].
Masonry modulus of elasticity was expressed as secant modulus from the strains in the measuring position occurring at a stress equal to one third of the maximum stress achieved, as suggested by EN 1052-1 [1999]. Equation 3.11 was used to calculate the modulus of elasticity and the result is presented in Table 17. The short term secant modulus of elasticity of masonry for use in structural analysis suggested by Eurocode 6 [2005], $E_m = 1000 f_k$, largely overestimates the obtained experimental value, see Table 17. In spite of this, a confident conclusion

for the modulus of elasticity could be drawn, if the compressive strength tests were performed on at least three wallet specimens.

$$E_m = \frac{F_{max}}{3\epsilon A_w} \tag{3.11}$$

where,

E_m modulus of elasticity of masonry

ϵ strain at a stress level equal to 1/3 of the ultimate stress

Although the compressive strength tests was not executed by following standardized test procedures, it was used as a benchmark of the new experimental test set-up. Also, the obtained results can not be directly correlated with the prescribed test procedures due to the load concentration in the middle of the wall which resulted from the non-uniform distribution of the vertical load.

However, the results confirmed the well known brittle behaviour of masonry. Masonry wallet UMWC-1 demonstrated brittle and fragile behaviour when subjected to uniaxial compressive stresses. Vertical cracks first appeared in the first top course of the bricks and started to propagate along the height of the wall, spreading towards the vertical edges of the wallet. The vertical cracks passed mainly through the units when the tensile stresses reached the tensile strength of the bricks. However, few vertical cracks were noticed between the units and the vertical mortar joints due to exceedance of the bond strength between them, see Figure 64. Owing to the direct application of the vertical actuator onto the RC beam, concentrated load appeared to prevail in the wallet which caused local vertically oriented cracks in the top RC beam, just beneath the vertical actuator. It could be concluded that the RC beam does not provide uniform load distribution over the whole transversal cross section.

3.6.2 *Wallets UMWC-2*

The compressive strength of masonry was determined by tests on a series of wallets according to EN 1052-1 [1999]. Three wallets with dimensions 520x385x125 mm were assembled in the laboratory. Masonry materials were taken from the same consignment used for erecting the masonry walls tested under cyclic loads. Masonry units from series A and lime mortar with grading 0:1:3 were used to build wallet samples. Masonry components had the same mechanical properties as described in subsection 3.6.1. The mortar head and bed joints had thickness of about 15 mm. The wallets were build on a flat surface on a laboratory floor. Prior assembling, the bricks were submerged into water and left for a minute to absorb water. To ensure flat surfaces for load distribution, parallel faces and right angles to the main axis of the wallet, wooden moulds were used. After construction, the wallets

Figure 64: Failure mode at the end of the compressive test on wallet UMWC-1

were cured in controlled laboratory conditions next to the masonry walls, see Figure 65. The compression tests were performed at the age of 117 days after construction of the wallets.

3.6.2.1 *Test set-up and test procedure*

The wallets were tested in the testing system used for testing the uniaxial compressive strength (Figure 45). First, the wallets were carefully aligned in the testing system and full contact between the testing machine and both top and bottom surfaces of the wallets was ensured. No additional compensating layer was used, owing to the fact that the system was equipped with self-levelling and pinned conditions

Figure 65: Wallets UMWC-2 for testing masonry compressive strength

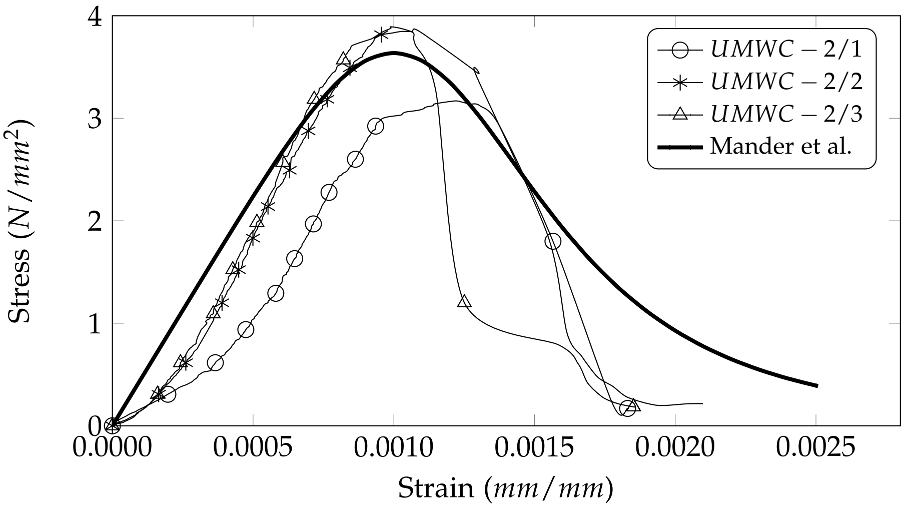

Figure 66: Stress-strain ($\sigma - \epsilon$) curves for UMWC-2 wallets

of the compression plates. Next, the load was applied in a uniform way without any sudden shocks. Loading rate was 0.0025 N/mm^2/s which is the minimum recommended rate for low strength units. The failure of the wallets was reached after $12 - 13$ min from the beginning of the loading. Masonry modulus of elasticity was obtained from the built-in displacement transducer in the head of the vertical actuator of the testing machine. This slightly deviates from the procedure suggested in EN 1052-1 [1999] where devices for measuring changes in the height should be applied on the wallets. Nevertheless, the system automatically records the load and the deformation changes in time, as well as the maximum load reached. The testing system ensures that the whole cross-section of the wallet was loaded uniformly.

3.6.2.2 *Test results and failure modes*

All wallets presented similar behaviour under axial compression loads in terms of maximum load and deformation capacity. The wallet UMWC-2/1 presented a deviation from the other two wallets with respect to the stiffness and the maximum load. Still, its ultimate deformation capacity was close to other wallet samples, see Figure 66. The main mechanical properties obtained by the tests are provided in Table 18.

The characteristic compressive strength of masonry calculated according Eq. 3.10 on page 104 and given in Table 17 in average was about 31 % higher and is within a range of $21 - 36$ % higher from the test results. An important notice regarding the ratio of modulus of elasticity of masonry and the characteristic compressive strength of masonry can be drawn. In absence of tests, Eurocode 6 [2005] recommends the ratio of $E_m/f_k = K_E$ to be taken as 1000. The mean coefficient K_E obtained by the tests was 939.24 which was about 6 % lower than

Wallet	F_{max} (kN)	$f_{mas,test}$ N/mm^2	$f_{k,test}$ N/mm^2	E_{test} N/mm^2	$E_{test}/f_{k,test}$
UMWC-2/1	206.00	3.17	2.64	2089.83	791.30
UMWC-2/2	250.00	3.85	3.21	3181.27	992.56
UMWC-2/3	253.00	3.89	3.24	3353.41	1033.86
Mean	236.33	3.64	3.03	2874.84	939.24
CV (%)	9.09	9.09	9.09	19.46	11.28

Table 18: Mechanical properties of masonry related to compressive strength and modulus of elasticity obtained from UMWC-2 wallets

the recommended value. It can be noted that the suggested value in Eurocode 6 [2005] corresponds well with the experimental results. However, the actual values for modulus of elasticity of masonry may vary in wide range between $100\,f_k \leq E_m \leq 2000\,f_k$ as discussed by Tomaževič [2009a].

In deficiency of good analytical model for masonry, a stress-strain model for confined concrete subjected to uniaxial compressive loading and confined by transverse reinforcement developed by Mander et al. [1988] was used to compare the test results. The model takes into account any general type of confining steel, either spiral or circular stirrups, or rectangular stirrups with or without additional cross ties. All relations were lumped into single equation used for stress-strain ratio. Cyclic loading and effects of strain rate were also included in the model. Figure 66 shows the resulting stress-strain curve obtained by Eqs. 3.12a to 3.12c and a comparison with the experimental stress-strain curves. Good agreement was found between the theoretical model and the test results.

$$\sigma_m = \frac{f_{m,test}\epsilon_m r}{r - 1 + \epsilon_m^r} \tag{3.12a}$$

$$r = \frac{E_m}{E_m - E_{sec}} \tag{3.12b}$$

$$E_{sec} = \frac{f_{m,test}}{\epsilon_m^{'}} \tag{3.12c}$$

where,

σ_m stress level for compressed masonry

ϵ_m strain level for compressed masonry

r ratio of mean modulus of elasticity for masonry to secant modulus of elasticity

$\epsilon_m^{'}$ strain at maximum stress level

(a) Wallet UMWC-2/1 (b) Wallet UMWC-2/3

Figure 67: Failure modes of wallets UMWC-2

Figure 67 shows the obtained failure modes after testing the compressive strength. All wallets exhibited similar failure modes and brittle failure. The masonry wallets initially showed strengthening behaviour, followed by elastic behaviour until appearance of the first cracks. Vertical cracks occurred first, followed by cracks in the unit-mortar interface. After reaching the compressive strength of the bricks, extensive cracking and crushing of the units and the mortar was obtained.

3.7 INITIAL SHEAR STRENGTH OF MASONRY

As composite material, masonry can present different failure modes, depending on the geometry, material and the load factors. Generally, it can fail in compression, tension, bending or shear. This study focuses on shear failure of masonry, with a special attention to diagonal tensile cracking. One of the most important material properties are diagonal tensile strength of masonry and characteristic shear strength of masonry. Many failure and material models are based on these properties. Also, the design codes employ the characteristic shear strength of masonry for verification of elements subjected to shear, (PZZ [1991], Eurocode 6 [2005], CSA S304.1-04 [2004] or AS 3700 [2011]).
The diagonal tensile strength of masonry is very hard to predict. In most cases it is obtained experimentally by shear tests or diagonal tests. Some design approaches and codes neglect the diagonal tensile strength of masonry, while others are based on it [Turnšek and Čačovič, 1971].
According to Eurocode 6 [2005] the characteristic shear strength of masonry is obtained from the characteristic initial shear strength of masonry and a portion of the vertical stress, see Eq. 3.13, for all joints filled and Eq. 3.14 for perpend joints unfilled. The characteristic initial shear strength of masonry is suggested to be determined from tests, following the recommendations given in EN 1052-3 [2002] or EN 1052-

4 [2000]. In this study, the characteristic initial shear strength was determined according to EN 1052-3 [2002].

$$f_{vk} = f_{vk0} + 0.4\sigma_d \tag{3.13}$$

$$f_{vk} = 0.5f_{vk0} + 0.4\sigma_d \tag{3.14}$$

3.7.1 *Test set-up and test procedure*

According to EN 1052-3 [2002] principle, the initial shear strength of masonry has to be derived from the strength of small masonry specimens tested to destruction. The specimens have to be subjected to shear under four-point load, with precompression perpendicular to the bed joints. Thereafter, four different failure modes are considered to give valid results. The initial shear strength has to be defined from a linear regression curve crossing zero normal stress.

Tests were conducted on nine specimens with dimensions lxbxh = 225x118x251 mm (Figure 68b) prepared from solid clay bricks (series A) and lime mortar. The properties of the masonry components are given in 3.6.1. All specimens had three courses of units with one unit in length and a 10 mm thick joint between them. The specimens were cured in laboratory within controlled environment conditions without any pre-compression of the specimens. Each specimen was tested at the age of 114 days.

The testing machine shown in Figure 45 was used to apply the vertical load. Special steel frame apparatus was constructed following the recommendations given in the standard, see Figure 68a. Steel plates with thickness of 20 mm supported by steel roller bearings with diameter of 20 mm were used to support the specimens. Roller bearings were fixed to the plates by welding. On top of the middle brick, another sandwich of rollers and plates welded together was positioned to introduce shear forces into the interfaces. First, normal forces were applied to the triplet specimens by means of steel plates and rods, see Figure 68c.

To determine the characteristic initial shear strength of masonry, three different levels of precompression were applied. Normal forces with intensity 6, 18 and 30 kN acting as precompression loads were applied to the specimens to obtain precompressive stresses of approximately $f_{pi} = 0.2$, 0.6 and 1.0 N/mm². The precompression loads were kept constant with external hydraulic jack and monitored with a load cell.

Shear stresses in the unit-mortar interface were introduced by gradually increasing the shear forces until the failure. Shear strength of masonry was recorded by the system, while the applied shear forces were calculated with Eq. 3.15.

$$F_{i,max} = f_{voi} A_i \tag{3.15}$$

(a) Test set-up for initial shear strength

(b) Nine triplet specimens curing in laboratory

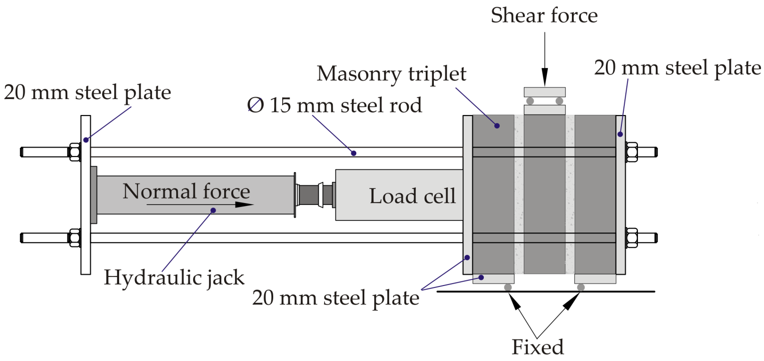

(c) Test test-up sketch

Figure 68: Test set-up and specimens for determination of initial shear strength

where,

$F_{i,max}$	maximum shear force attained at individual specimen
f_{voi}	shear strength of an individual specimen
A_i	cross-sectional area of a specimen parallel to the bed joints

3.7.2 *Test results and failure modes*

The main test results indicating the initial shear strength of tested triplet specimens are presented Table 19. As expected, low shear strength of masonry specimens was obtained. The results of the individual shear strength (f_{voi}) against the normal compressive stress (f_{pi}) were plotted on a graph shown in Figure 69. From a linear regression analysis, the initial shear strength (f_{vo}) at zero normal stress was obtained. Actually, the initial shear strength which coincides with the initial cohesion (f_{vo}) has negative value which indicates negligible shear strength. For practical applications of masonry of type such as the tested one, the initial shear strength can be assumed zero. The obtained coefficient of friction strongly depends on the unit-mortar

Spec.	l (mm)	b (mm)	h (mm)	f_{pi} (N/mm^2)	$F_{i,max}$ (kN)	f_{voi} (N/mm^2)
1	117.00	225.00	250.00	0.20	6.44	0.11
2	115.00	225.00	252.00	0.20	5.80	0.10
3	116.00	226.00	252.00	0.20	7.02	0.12
4	118.00	225.00	252.00	0.60	23.79	0.40
5	120.00	223.00	251.00	0.60	24.70	0.41
6	119.00	223.00	251.00	0.60	24.49	0.41
7	119.00	227.00	250.00	1.00	36.89	0.62
8	120.00	228.00	251.00	1.00	42.17	0.70
9	119.00	227.00	250.00	1.00	38.08	0.64
Mean	118.11	225.44	251.00	/	/	/
CV (%)	1.41	0.73	0.33	/	/	/

Table 19: Results from testing shear strength of masonry

surface contact and it was obtained as $\mu = 0.6667$, which gives characteristic angle of internal friction of $\alpha = 33.66^0$.

According to EN 1052-3 [2002], triplet specimens should fail with one of the following failure modes:

- A.1 Shear failure in the unit/mortar bond area either on one or divided between two units faces;
- A.2 Shear failure only the mortar.

If failure is obtained as:

- A.3 Shear failure in the unit, or
- A.4 Crushing and/or splitting failure in the units, then

further specimens have to be tested until the specimens reach shear failures A.1 or A.2 for each precompression level, or the result may be used as a lower bound to the shear strength for each precompression level.

All triplet specimens failed similarly. The shear failure occurred mainly in mortar joints with predominant type of fracture A.1 as indicated in the standard, see Figure 70. After exceeding the unit-mortar bond strength, the specimens demonstrated failure in the joint with relative movement of the middle brick. The low shear strength of the specimens was noted during positioning the specimens for testing. In few cases, bricks were completely detached from the mortar. In those situations, new triplet specimens were constructed.

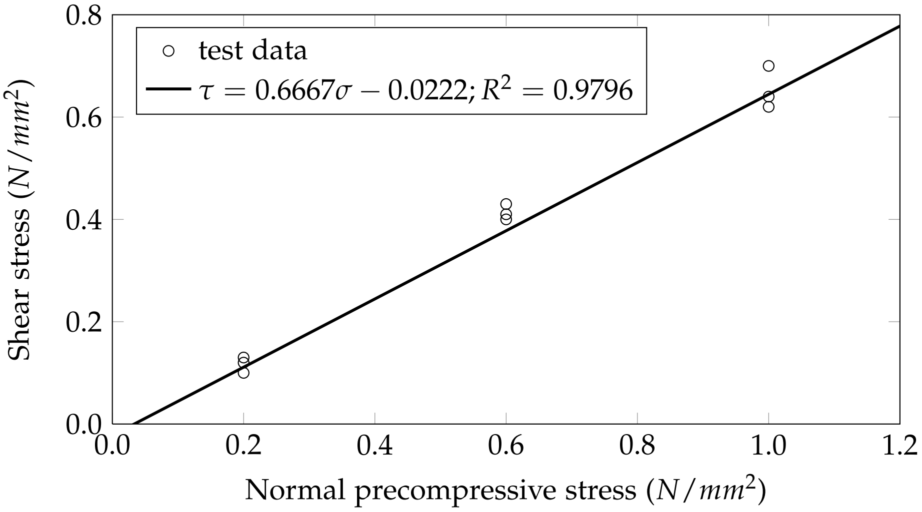

Figure 69: Shear vs. normal stress

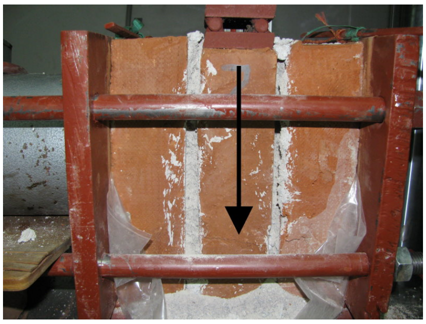

(a) Shear failure in the unit-mortar interface

(b) A.1 type of failure obtained in the triplet specimen

Figure 70: Failure mode of triplet specimens

γ_d ($^{kg}/_{m^3}$)	$f_{b,m}$ ($^{N}/_{mm^2}$)	f_b ($^{N}/_{mm^2}$)	$f_{bt,flex}$ ($^{N}/_{mm^2}$)
1922.6	10.84	8.67	2.66

(a) Solid clay bricks

γ_d ($^{kg}/_{m^3}$)	f_m ($^{N}/_{mm^2}$)	$f_{mt,flex}$ ($^{N}/_{mm^2}$)
1384.67	0.55	0.10

(b) Lime mortar

Table 20: Summary of the physical and mechanical properties of masonry components

γ_d=density (dry); $f_{b,m}$=mean compressive strength of brick; f_b=normalized mean compressive strength of brick; $f_{bt,flex}$=mean tensile flexural strength of brick; $f_{mt,flex}$=mean tensile flexural strength of mortar; f_m=compressive strength of mortar.

The characteristic initial shear strength and characteristic angle of internal friction should be obtained by multiplying the initial values with 0.8.

3.8 SUMMARY AND CONCLUSIONS

In this chapter, the physical and mechanical characteristics of masonry and its constituents were determined by tests. Materials used for strengthening masonry with RC jackets, concrete and reinforcement, were also tested to find out their properties.
Four types of clay bricks were tested, solid, frogged solid and solid with vertical holes. Two types of mortar were tested, lime and cement-lime mortar. Additionally, one concrete mix and one reinforcement type were used to determine their characteristics. The compressive and tensile flexural strength of all constituents were obtained by standardized test methods. The compressive and initial shear strength of masonry were determined also. The modulus of elasticity for masonry was obtained through standardized tests on three wallet specimens. A comparison of the obtained results with data from literature or suggested by the codes was carried out where applicable.

The results for obtained properties of masonry and its components were summarized and presented in Table 20 and Table 21, for further reference. In the following chapters, solid clay bricks from series A and lime mortar were used.

From the experimental results the following conclusion can be made:

- A large difference in the compressive strength of solid bricks was obtained, meaning that the material and the process for brick production has great influence. Solid frogged bricks showed compressive strength comparable with other series. A significant influence on the compressive strength of the bricks has the specimen size for testing. An increase in the compressive strength of cut specimens in the range of 1.5-2.3 times for corresponding

f_k (N/mm^2)	E (N/mm^2)	f_{vk0} (N/mm^2)	α $(^0)$
3.03	2874.84	0.00	34

Table 21: Summary of the mechanical properties of masonry

f_k=characteristic compressive strength of masonry; E=modulus of elasticity of masonry; f_{vk0}=characteristic initial shear strength of masonry, under zero compressive stress; α=characteristic angle of internal friction.

series was obtained when compared to the compressive strength of the whole units.

- Obtained tensile flexural strength of the bricks indicated large scatter in the results between the series. The tensile flexural strength was in a range of 25 % and 37 % from the compressive strength of the bricks from series A and B, respectively. The highest ratio of 47 % was obtained for frogged solid bricks, while only 14 % was determined for the hollow bricks.

- Big difference in the compressive strength and tensile flexural strength between lime mortar and cement-lime mortar was obtained. Notably, the ratio of tensile flexural strength to compressive strength in both mortar types was similar, about 20 %.

- The compressive behaviour of masonry built with solid clay units and lime mortar appeared to be very brittle. Compared to the approach given in Eurocode 6 [2005], a difference of about 31 % in the compressive strength of masonry was found out. However, good agreement between the experimental and the estimated modulus of elasticity suggested in the code was obtained. Besides, the compressive stress-strain diagram was well described with a model developed for confined reinforced concrete.

- The initial shear strength of masonry was tested by shear tests according to EN 1052-3 [2002]. Results revealed that the initial shear strength of lime masonry under zero compressive stress is negligible. In that case, the characteristic shear strength of masonry, as suggested in Eurocode 6 [2005], can be related only to the design compressive stress perpendicular to shear at the level under consideration. Since it depends on the stress state, the shear strength as defined by Eurocode 6 [2005] cannot be considered as a mechanical characteristic of masonry [Tomaževič, 2009b].

4 EXPERIMENTAL BEHAVIOUR OF MASONRY WALLS

4.1 INTRODUCTION

In masonry buildings, the main structural elements which resist the lateral forces due to wind and earthquake are walls and piers. Although often referenced in literature as shear walls, the term 'shear' may not be representative since it indicates the dominant failure mode. In relation to the geometry ratio, material properties, boundary conditions and normal stress levels, masonry walls can fail in compression, flexure or shear. In case when masonry walls are subjected to in-plane lateral loads, then shear failure mechanisms prevail.

If the normal compressive stresses in a wall are low and the wall has mortar with low strength characteristics, then the seismic forces acting in-plane of the wall may cause sliding failure of the wall. Sliding failure mode in URM can occur either along the length of the wall or in part of it. Usually, this failure happens in the upper stories of a building and rarely causes total collapse of a building. Partial damage was often observed as a result of sliding in the upper stories due to low levels of normal compressive stresses and high accelerations.
Most common failure mode developing in the ground story of a building caused by the seismic forces is failure by diagonally oriented cracks as shown in Figure 25a. Such a failure is usually called diagonal tension shear failure [Tomaževič, 2009b]. At this level, normal compressive stresses are high, and depend on the wall configuration and the number of floors. Diagonal tension shear failure is represented by cracks oriented at bed- and head-joints, or passing through the units or partly through the units and partly following the joints. This failure mode often causes total collapse of the buildings made from URM.
Out-of-plane failure of walls is also possible to develop, especially after exceeding the tensile bond strength of head joints and friction resistance of bed joints. Such walls show predominant flexure failure mode when subjected to out-of-plane loads and are usually known as 'flexure' walls. Out-of-plane failure modes are not considered in this study.

In this research SMW acronym is used to denote strengthened masonry wall with RC jackets.

To prevent shear failure of the walls and to improve the seismic resistance of a building by increasing the strength and ductility, technical interventions for strengthening or seismic upgrading are used. Different strengthening methods for UMWs are available, of which the most common is application of RC jackets. Although often used, research on the behaviour of SMWs are rarely found and therefore little is known about the mechanical behaviour of the walls. This situation points out that a research effort has to be made to obtain better understanding for the behaviour of SMWs. The deficit of experimental investigations on SMWs resulted from the huge interest of the building industry in reinforced concrete, where 'old' structural masonry in buildings was totally replaced with RC structural elements.

In this chapter, an experimental research to study the structural behaviour of strengthened masonry walls with RC jackets is presented. Tests on walls were performed under in-plane cyclic lateral loads. The main aim of the experimental research was to correlate masonry walls to different structural situations. Therefore, wall geometry and normal compressive stress levels were varied. Due to the limited amount of financial support for the experimental part, four unique SMWs were tested. To compare the strengthening effects, four UMWs with same geometry, boundary and stress conditions were tested. Also, all tests were performed in the laboratory for testing structures and materials at Faculty of Civil Engineering, University "Ss. Cyril and Methodius" in Skopje.

4.2 EXPERIMENTAL PROGRAM

The experimental program was based on in-plane static cyclic loading tests. This simplification in the interpretation of the seismic loading was due to the high costs of testing if the actual restraints of masonry walls are to be simulated. During earthquakes, horizontal and vertical effects initiated on individual walls change frequently in an alternate, cyclic manners. Due to the restraining effects in both horizontal wall ends, additional compressive stresses develop in the walls at each loading cycle and prevent creation of diagonal tension cracks in both wall ends. Such situation usually triggers formation of diagonal tension cracks in the middle section of the walls. Hence, walls in a laboratory are usually tested under controlled levels of vertical loads and controlled boundary conditions as fully fixed or as cantilevers.

4.2.1 *Materials and geometry of masonry specimens*

For acquiring useful information it is important to identify the minimum number of tests that can provide appropriate combinations of the relevant parameters. In particular, for the purpose of definition of the wall's geometry and vertical load levels, several typical ground floor plans of existing building were studied. As a result of the limitations in the laboratory facilities and the budget funds, two geometry configurations appropriate for the laboratory test set-up were selected. The lengths of the walls were 1460 mm and 2520 mm, and the height of the walls which strongly depends on the load application configuration in the testing frame, was fixed to 1820 mm.

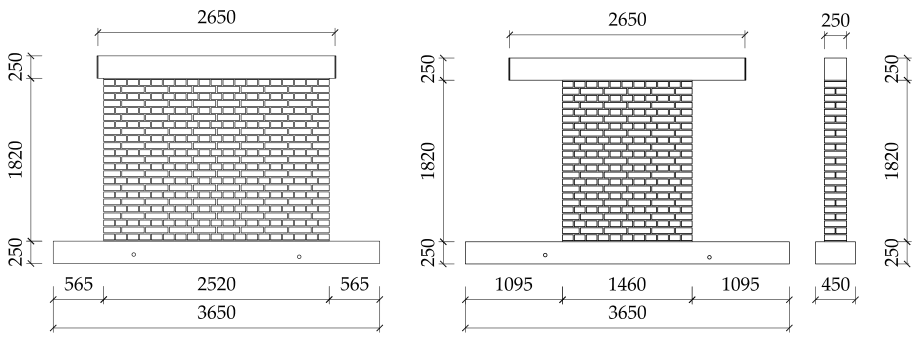

(a) Squat wall (b) Tall wall

Figure 71: Geometry of the walls for in-plane testing

Wall	l (mm)	h (mm)	t (mm)	σ_0 (N/mm^2)	σ_0/f_k
UMW1	2520	1820	250	1.0	0.33
UMW2	1460	1820	250	1.0	0.33
UMW3	2520	1820	250	0.5	0.17
UMW4	1460	1820	250	0.5	0.17
SMW1	2520	1820	250	1.0	0.33
SMW2	1460	1820	250	1.0	0.33
SMW3	2520	1820	250	0.5	0.17
SMW4	1460	1820	250	0.5	0.17

Table 22: Details of the tested walls

In total, eight walls with solid clay bricks and lime mortar were constructed. These walls were specifically developed for the experimental research purposes of this thesis. The walls were built with the same type of materials referred to in chapter 3 for mechanical characteristics. Two geometry aspect ratios h/l of 0.7 (squat walls) and 1.2 (tall walls) were used. The wall geometry in longitudinal and transversal section is shown in Figure 71.

From the inspected prototype buildings of up to three stories, normal stresses close to 1.0 N/mm^2 were calculated in the ground floor walls. To provide results of general validity, two vertical load levels were decided, with intensities of 0.5 N/mm^2 and 1.0 N/mm^2. The geometry details and vertical precompression levels defined as a ratio of normal compressive stress to compressive strength of masonry are presented in Table 22.

All walls were constructed in a laboratory. They were build on a bottom RC beam with dimensions 3650x450x250 mm. Another RC beam with dimensions 2650x250x250 mm for transferring the vertical and horizontal loads was used and placed on the top of the walls. Both

RC beams were pre-casted in a factory from concrete of type MB30 ($f_c = 30\,N/mm^2$) and were reinforced with 3 Ø 12 mm, RA 400/500-2 reinforcement bars in both top and bottom layers. Transversal reinforcement in shape of rectangular stirrups Ø 8/100/200 mm were provided in both beams. Steel plates ≠ 250.250.10 mm and bars Ø 10 mm were used to anchor the plates to both transversal cross-sections of the top beam and to provide good contact between the horizontal actuators and the beam. Additional structural hooks from reinforcement bars for lifting and transporting the specimens were casted in the beams. The bottom beam contained two vertical circular openings with diameter of 60.3 mm on each side. High strength steel anchors were used to fix the beam to the strong floor. Two horizontal openings with same diameter and length of 450 mm were provided in the bottom beam to support the lifting of the test walls and transporting to the test position.

4.2.2 *Construction of the specimens*

Due to the limited space in the laboratory for storing and manipulating the large wall specimens, the construction of the walls was divided into two periods. Previously, the RC beams were delivered by the concrete factory "Karpos" from Skopje. Their designed compressive strength was achieved in the factory.
First, UMWs were constructed from December 21, 2009 to December 24, 2009. In the second period, SMWs were constructed from June 21, 2010 to July 27, 2010. The second period was essentially divided in two subperiods. In the first one, UMWs were constructed. In the second, at the age of 28 days, RC jackets were applied to the walls. The construction of the specimens was carried out in three phases:

A. Construction of unreinforced masonry walls;

B. Application of RC jackets on unreinforced masonry walls;

C. Positioning and bonding of the top RC beams.

4.2.2.1 *Construction of UMWs*

A thin layer of lime mortar was laid on the bottom RC beam for levelling the first course of bricks. Before putting into contact with the mortar, the bricks were fully soaked into tap water. This was necessary step to provide good bond between the bricks and the mortar, and to prevent early drying of the mortar. The first course of bricks was levelled in their respective position within the course. All vertical joints were filled with mortar. The bed joints were created with the help of timber sticks cut to the required dimensions to maintain the specified thickness of the joints. Levelling of the following courses in vertical direction was maintained by timber planks fixed to the

(a) Laying of the first course of bricks

(b) Laying the second course of bricks and filling the head joints with mortar

Figure 72: Details of construction of UMWs

(a) Soaking of the bricks before construction

(b) Levelling the courses in both orthogonal directions

Figure 73: Details of construction and levelling the courses in the walls

bottom RC beam and supported diagonally. Horizontal levelling was performed by ropes, which were previously arranged in absolute horizontal position. Details from construction of the walls are shown in Figure 72 and Figure 73.

The top RC beam was positioned in the centre of each wall and was bonded with the wall 3-4 days before testing of each wall. Bonding was provided with special cementitious admixture with strength class M80 (brand name Eksmal-1, produced by "Ading" A.D. Skopje). Bonding material consists of one-component expansive and self-flowing ready-mix grout. It is used for sealing anchors, bearings of crane girders and bridge structures and reaches high strength in short time. After 24 hours, approximated compressive strength declared by the manufacturer was $35 - 40\,{}^{N}/_{mm^2}$ and the bending strength was $5 - 7\,{}^{N}/_{mm^2}$. The declared compressive strength after 28 days was $70 - 80\,{}^{N}/_{mm^2}$, the bending strength was $11 - 12\,{}^{N}/_{mm^2}$, while the bond strength was $3 - 4\,{}^{N}/_{mm^2}$. Due to the soft, liquid and self compacting properties, the bonding material was casted in timber moulds on the top of the wall. After 30 min, the RC beam was lifted by overhang crane, carefully positioned in the centre of the wall and laid down on the bonding material. No additional anchorage between the beam and the wall was used.

4.2.2.2 *Construction of SMWs*

Construction process of the SMWs was carried out in several steps. Firstly, UMWs were constructed following the same procedure described previously. The second phase was initiated after 28 days, which was estimated time for the lime mortar to reach its full strength.

Secondly, connecting anchors for both reinforcement meshes with diameter of ∅ 6 mm and length of 280 mm were inserted in the wall. Plain steel anchors with yield strength of 500 N/mm^2 with chess-board distribution at a distance of 500 mm were used. Depending on the mortar strength, connecting anchors can be inserted into pre-drilled holes or can be hammered directly in the assigned locations. Since the lime mortar was soft, anchors were easily inserted with slight hammer kicks. No additional epoxy or cementitious was used. Approximately, 4 anchors per m^2 were used for all walls, see Figure 74.

Thirdly, small length pieces of reinforcement bars with diameter of 15 mm were positioned over the anchors on both sides of the wall and were welded on the spot. Owing to the fact that 30 mm thick layers of concrete jackets were casted, this technical intervention was used to secure the reinforcement meshes at the specified distance of 15 mm from the wall. In particular, the meshes were positioned in the centre of the jacket. Spot welded wire mesh ∅ 4.2/100 mm was welded on the connecting anchors and the distance bars. Reinforcement wire-mesh was cut in dimensions to fully cover the entire surface of the wall. The reinforcement meshes were not restrained into the beams, and were anchored only in the wall, see Figure 75.

The fourth step comprised positioning of timber moulds for casting the concrete. Timber planks and beams were used on both sides to maintain the moulds in vertical position. The transversal surfaces on both sides of the walls were left without RC jackets. Moulds were positioned at a distance of 30 mm from the wall. The top side of the wall was left open to allow pouring of the concrete into the moulds.

In the fifth step, concrete mix was prepared in the laboratory. Fine aggregate with maximum aggregate size of 8 mm and portland cement (brand name Titan, produced by cement factory Usje A.D. Skopje) was used to prepare the concrete. Regular tap water was used for mixing the concrete components. The concrete was prepared manually with cement to sand ratio of 1:3. The fresh concrete was transported by cart and poured into the moulds with baskets. Because the space between the moulds and the wall was tight for internal vibration of the concrete, external vibration by manual hammering on the moulds during concreting was applied. This was necessary to prevent concrete segregation and air voids in the concrete jacket. Details of preparation and casting of the concrete for the jackets are shown in Figure 76.

(a) Marking locations for connecting anchors

(b) Hammering anchors into UMW

(c) Disposition of the connecting anchors for reinforcement meshes

(d) Close-up view of the connection anchor

Figure 74: Details of construction of connecting anchors

(a) Welding of reinforcement bar pieces over the anchors

(b) Close-up view of welded reinforcement bar over anchors and welded wire-mesh to anchors

Figure 75: Details of construction of the reinforcement wire mesh

(a) Preparation of concrete for the jackets

(b) Transport of fresh concrete

(c) Casting of concrete into moulds

(d) External vibration of concrete by hammer

Figure 76: Details of preparation and casting of concrete for the jackets

In the last step, the specimens were cured in the laboratory under controlled environmental conditions. Moulds were removed 16 hours after the casting. During the following 7 days, wet polyester blankets were used to keep the humidity level of the wall and to avoid premature water evaporation. The walls were cured in the laboratory for 28 days by constant wetting of the surfaces with tap water. This was necessary because during the curing period the outside temperature was close to $40\,^{0}C$ and maintaining stable temperature conditions inside the fully operational laboratory was very hard. After the age of 28 days, the walls were stored in the laboratory until the day of testing.

4.2.3 *Test set-up and testing procedures*

For execution of the static cyclic tests of the masonry walls, upgrading of the present test set-up frame was carried out. The existing steel testing frame was designed for application of vertical loads only, and needed to be redesigned to take into account the horizontal loads. The former frame configuration consisted of four steel I shaped columns (profile I25) and two connecting transversal beams with variable section profile I44 at the supports and I33 in the centre. Stiff steel beam with complex cross-section and height of 400 mm was positioned between the transversal beams. It was used to support the vertical

(a) SMW after removal of the moulds

(b) Protection of a wall with wet blankets on both sides

Figure 77: Curing of the constructed SMWs

loads generated by the vertical actuators. Such space frame configuration was modified and additional steel elements were designed and installed. The new steel testing frame is shown in Figure 78.

For application of the horizontal loads, two horizontal supporting stiff steel beams I 380.190.15...1250 mm with additional stiffening ribs of the steel rib were designed. These beams were positioned in horizontal direction and located at both ends of the testing frame, see Figure 79a. Both beams were connected with two steel beams with hollow square cross-section 160.160.6...2710 mm, Figure 79b. These beams were braced to the supports and jointed with steel plates $\neq$ 273.12...359 mm, see Figure 79c. The K bracing consisted of four hollow square profiles 150.150.6...2201 mm. All stiffening and bracing elements were welded on the spot. Testing frame was fixed to the 500 mm thick RC floor in the laboratory. Eight high strength steel anchors with diameter of $\emptyset$48 mm 8.8 (M48) were used to fix the testing frame to the strong floor. As a result of the testing configuration, the maximum wall dimensions were limited to 2590x1820 mm.

The tests were carried out according to the test set-up shown in Figure 80. The bottom RC beam was fixed to the strong floor with two anchor bolts. To avoid uplifting and slippage of the beam, additional clamping devices were designed and attached to the beam, see Figure 81. Three extra bolts were used to fix each clamping device to the floor. The empty space between the clamping devices and the bottom RC beam was filled with Eksmal-1 bonding material.

Normal compressive loads were applied by two vertical actuators with capacity of 500 kN. The vertical load was transferred on a stiff steel load distribution beam positioned over a series of steel roller bearings over the top RC beam. The roller bearings had diameter of 24 mm and length of 250 mm. They were distributed in horizontal distances of 100 mm over a steel plate with thickness of 15 mm. This

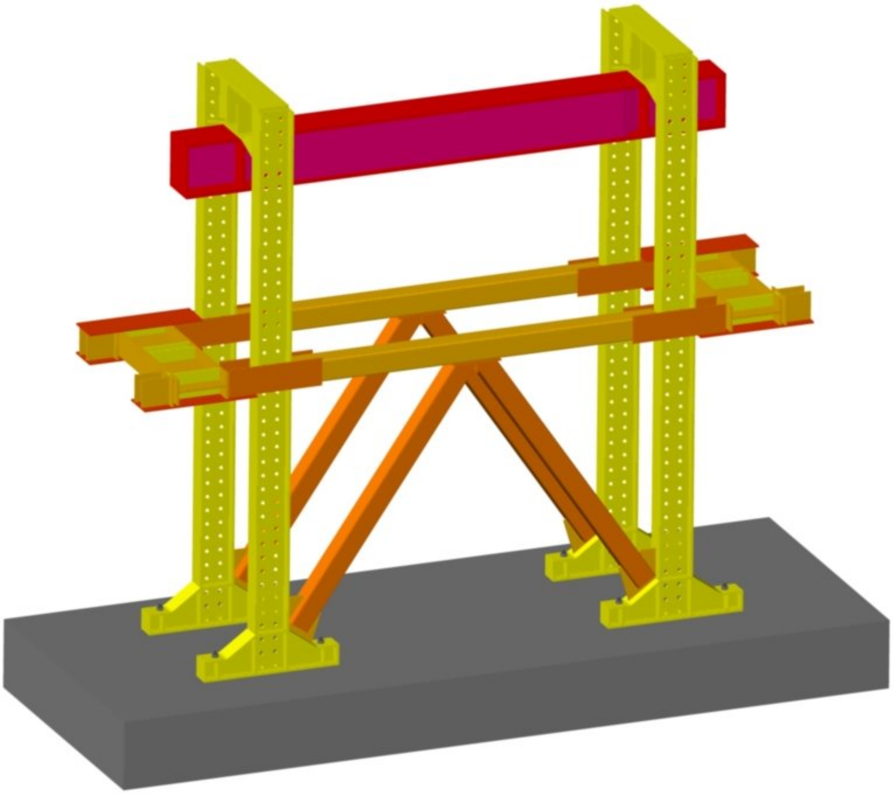

Figure 78: 3D view of the testing frame

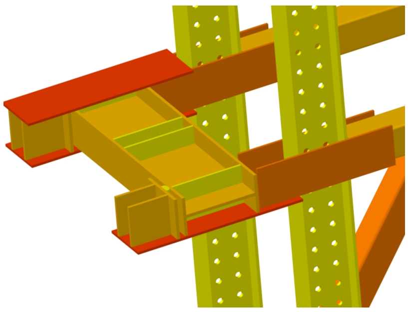

(a) Detail of the supporting elements for the horizontal actuators

(b) Detail of the K bracing

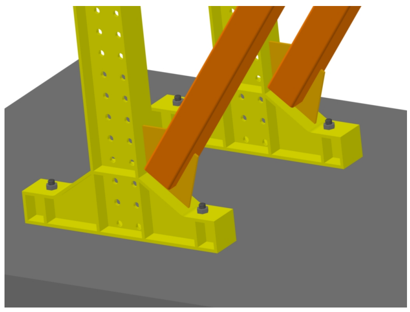

(c) Detail of the supports and the K bracing

Figure 79: Details of upgraded steel testing frame

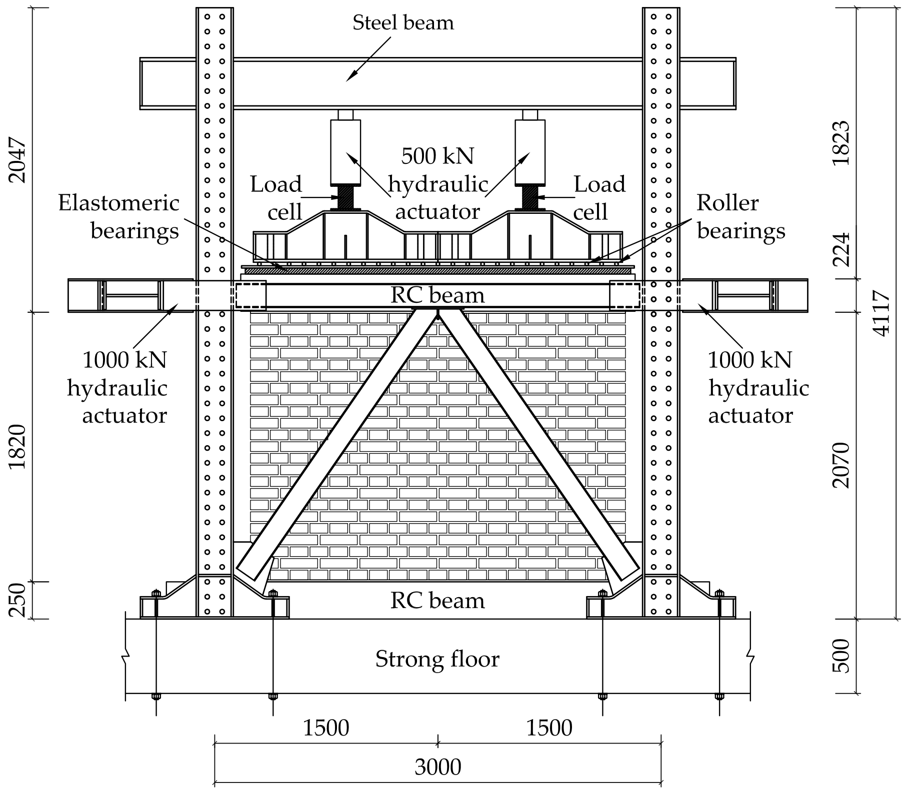

Figure 80: Test set-up for in-plane horizontal cyclic loading

intervention was necessary to allow relative displacements of the wall from induced horizontal loads and to retain the vertical actuators in their position. To obtain uniform vertical load distribution over the whole horizontal cross-section of the wall, elastomeric rubber bearings with thickness of 40 mm were inserted between the top RC beam and the steel plate.

All these test set-up measures were taken to assure as much as possible fully fixed boundary conditions on the bottom and top of the walls. The vertical load level was constantly monitored and manually controlled to achieve the desired constant level of the axial stresses. Both vertical actuators were connected to an oil pump through a relief valve. The connections between the vertical actuators allowed operation of the both actuators in the same time by compensating the oil pressure in the actuators. Consequently, depending on the direction of the horizontal load application, one actuator operated with decrease in the oil pressure, while the other had increased the oil pressure. However, no additional measures were taken to prevent any possible rotation of the top of the walls.

Lateral loads were simulated with horizontal actuators with capacity of 1000 kN positioned on both sides of the wall. These actuators were installed in specially designed supports and were secured with steel rings. Before application of the loads, careful alignment of the horizontal actuators with respect to the middle plane of the wall was

Figure 81: Clamping device for the bottom RC beam

performed. Such alignment was crucial in order not to impose any undesired bending moments due to eccentricity of the loadings.

The main steps of the adopted test procedure were divided in several steps, as follows:

A. Initially, a vertical compressive load was applied by two vertical hydraulic actuators under a force controlled rate of about $0.5\,kN/s$. The vertical actuators were connected with a series of connectors allowing control of both actuators with one hydraulic pump. Vertical loads were manually applied until the desired level of vertical load was reached. After reaching the designed load levels in normal direction of the wall, the hydraulic actuators were kept to maintain constant vertical load.

B. Afterwards, the horizontal load was manually applied on the top RC beam by the horizontal actuators with loading rates of $0.2 - 0.5\,kN/s$ until reaching the specified displacement increments. Thus, the cyclic load test were carried out under displacement controlled increments. Cyclic lateral displacements with step-wise increased amplitudes repeated three times at each specified increment have been used to simulate the in-plane lateral seismic loads. Typical lateral displacement-time history is presented in Figure 82.

C. Test data related to the horizontal displacements and the horizontal load were acquired automatically with the data acquisition system shown in section 3.6.1. The displacements produced by the vertical loads were monitored manually and recorded separately.

D. During the tests, the main events were registered manually and by photographs. These involve appearance of cracks, progressive opening of the cracks, delamination and other phenomena.

E. To protect the measuring equipment from possible damage, the tests were stopped before complete collapse of the walls and in

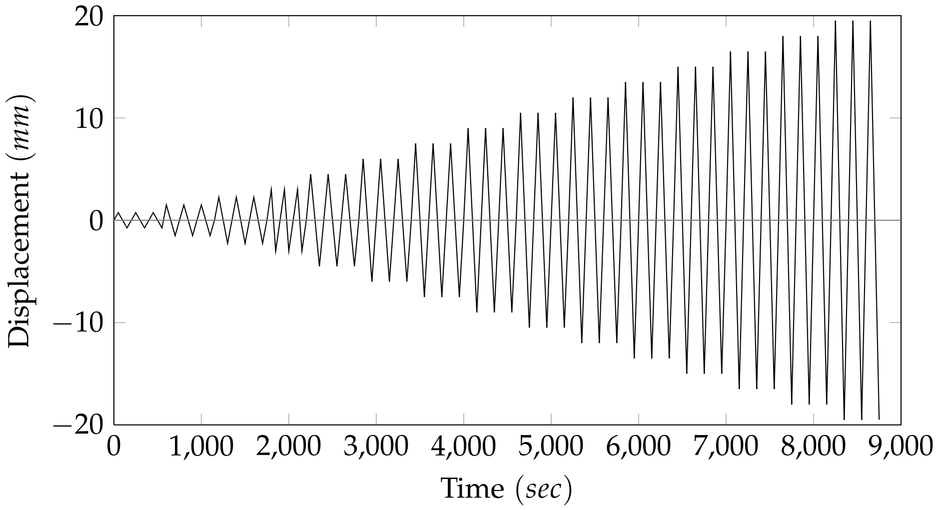

Figure 82: Imposed horizontal displacement time-history

most cases after decrease of the horizontal load of 20 % from the maximum horizontal load obtained for each wall.

4.2.4 *Instrumentation*

The horizontal and vertical displacements under cyclic loading have been instrumented with a set of displacement transducers. The distribution of the instruments is shown in Figure 83. Kyowa displacement transducers DT-50A (with capacity of 50 mm) were used at the measurement points DT 1, DT 5, DT 6, DT 7 and DT 8. The points DT 2 and DT 2′ were instrumented with Kyowa DT-100A transducers (capacity-100 mm). These transducers were used to measure the horizontal absolute displacements from a steady point. Vertical relative displacements were measured at points DT 3 and DT 4 with dial gage-equipped displacement transducers, DT-D (capacity -50 mm).

For characteristics of Kyowa DTs and DAQ system, see section3.6.1

DT 1 was placed directly on the clamping device to monitor possible slippage of the bottom beam. At the measurement points DT 2 and DT 2′, external steel frames were positioned in the front and in the back side of the wall to accommodate the transducers. Glass plate pieces with dimensions 100x100 mm were glued in the centre of the top RC beam with their plane normal to the plane of the wall. DTs 5 to 8 were mounted on other external steel frames to assure fixed reference points for measurement. Similarly, glass plates were attached on the wall to provide alignment and smooth contact. To record the vertical displacements and to monitor possible wall rotation, relative displacements were instrumented at points DT 3 and DT 4. Steel wire was used to span the distance between the top and bottom RC beams. DT 3 and DT 4 were located on the strong floor, thus enabling steady reference points.

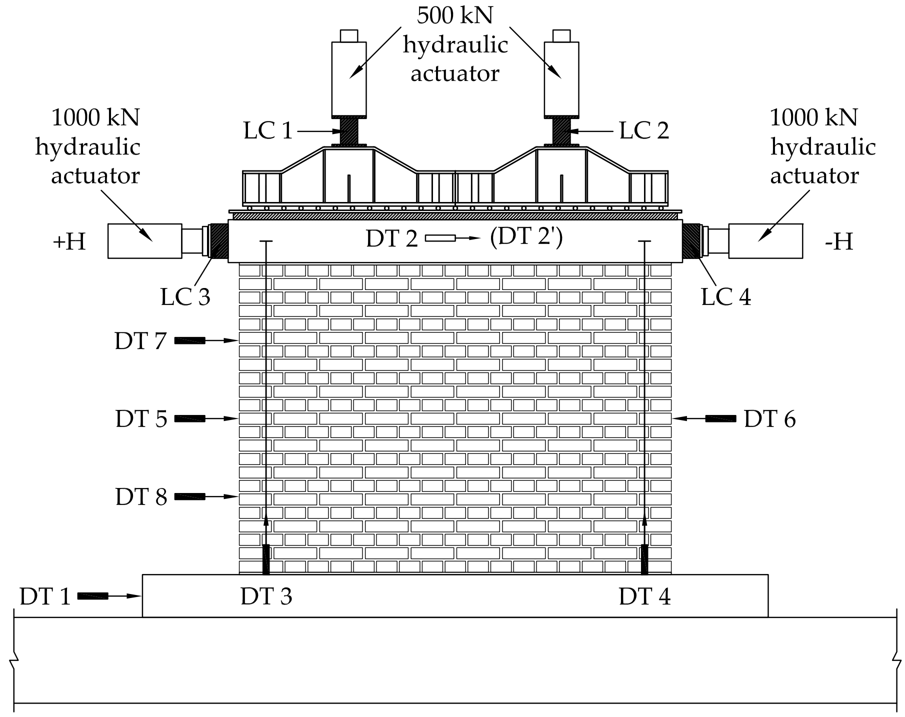

Figure 83: Instrumentation of the walls with displacement transducers and load cells

Applied forces were instrumented with load cells located between the actuators and the load application point. Custom made load cells LC 1 and LC 2 were used for the vertical actuators. Horizontal actuators were equipped with appropriate set of load cells mounted directly on the actuator head.

All displacement transducers and load cells were calibrated prior execution of each test. The actuators were calibrated and checked twice during the testing period. Data acquisition was automatic with 8 channel Spider8, PC-based DAQ unit. The horizontal displacements at points DT 2, DT 2′, DT 5 and DT 6, as well as the horizontal forces obtained with the load cells LC 3 and LC 4 were automatically stored in digital form with the computer software. Other measured values were manually recorded after each displacement cycle.

4.3 TEST RESULTS FOR UNREINFORCED MASONRY WALLS

Following the test procedure described in section 4.2.3, large amount of experimental data was acquired during the tests. The most important results are summarized and presented through the obtained failure modes, force-displacement hysteresis curves, envelopes of force-displacement curves with capacity (resistance) degradation of the walls at repeated cycles of loading, characteristic limit states, stiffness degradation and energy dissipation capacity. All results regarding UMWs and SMWs are presented in individual subsections.

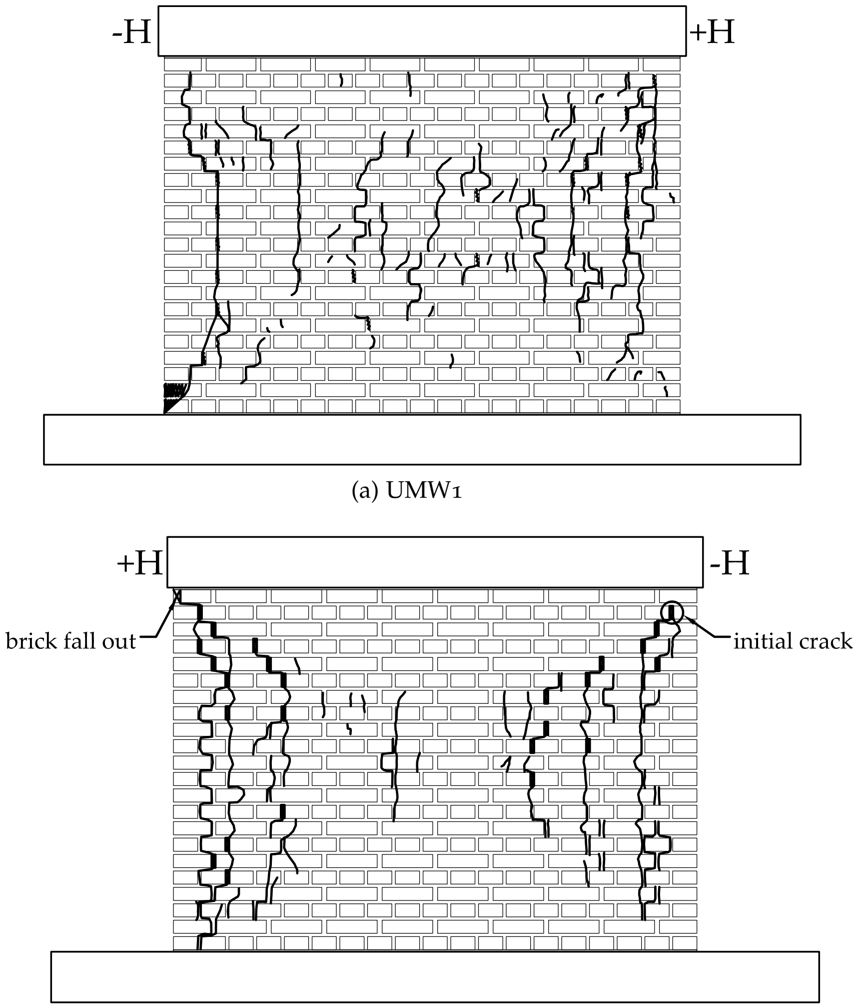

(a) UMW1

(b) UMW3

Figure 84: Cracking patterns of squat unreinforced masonry walls

4.3.1 *Failure modes*

As expected, all walls failed in shear with similar failure mechanisms. Shear failure was due to the formation of diagonally oriented cracks in the bricks or passing trough the bricks or in the brick-mortar interface. No local buckling or crushing of the bricks was observed except for crushing of the bricks in the bottom left corner of the wall UMW1 and small brick fall-out in the top left corner of the wall UMW3. The cracking pattern obtained at the end of the tests is presented in Figure 84.

However, a difference in the crack pattern was noticed for squat and tall walls. In particular, walls UMW1 and UMW3 presented mainly vertically oriented cracks passing through the bricks or along the head joints. At ultimate state, the cracking pattern with 'hour-glass' shape was observed. Initially, vertical cracks started to develop in the vertical planes closest to wall edges and subsequently started to propagate to the centre of the wall. Walls UMW2 and UMW4 demonstrated typical diagonally oriented cracks, see Figure 85.

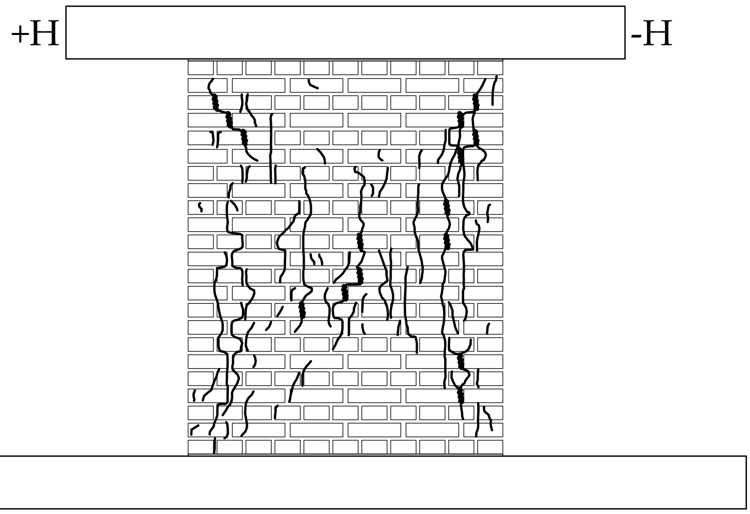

(a) UMW2

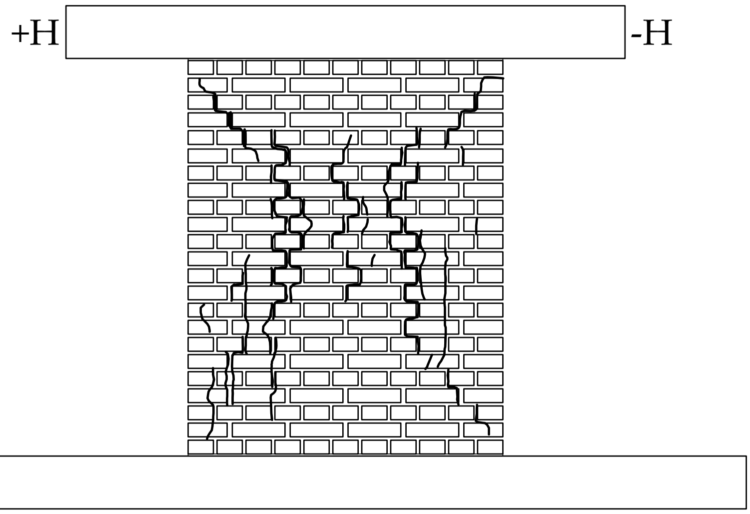

(b) UMW4

Figure 85: Cracking patterns of tall unreinforced masonry walls

On the basis of the observed failure mechanisms, three limit states have been defined. The limit states characterise the behaviour of unreinforced masonry wall specimens tested under in-plane horizontal loads. These are:

1. Crack limit, identified by presence of the first cracks in the walls passing through the bricks or along the head joints (H_{cr}, d_{cr});

2. Maximum resistance, defined by the maximum obtained resisting horizontal force and corresponding displacement (H_{max}, d_{Hmax}), and

3. Ultimate limit, characterised by the maximum attained displacement of the wall and corresponding ultimate horizontal force (H_{dmax}, d_{max}).

4.3.2 *Force-displacement diagrams*

Force-displacement diagrams defined as a relation of the horizontal load to absolute horizontal displacement are considered one of the most important information to understand the global behaviour of the tested walls. In the following section, a general discussion about the global behaviour of unreinforced masonry walls will be presented supported by analysis of the force-displacement hysteresis loops.

All tested walls showed symmetrical force-displacement curves with respect to positive and negative displacements, see Figure 86 and Figure 87. The first cracks in the walls UMW1 and UMW2 were detected almost at same displacements, but in the capacity a difference of up to four times was obtained. This correlation was not established for the walls UMW3 and UMW4. The level of precompression showed correlation with the geometry of the walls. For instance, in the case of walls with equal aspect ratio, the walls loaded with higher precompression level achieved higher lateral capacity. This behaviour has been observed in other studies, also (Vasconcelos, 2005, Haach, 2009, Tomaževič and Weiss, 2011). Such behaviour can be explained by the higher principle tensile stresses needed to generate failure of the walls. If compared in relation to the precompression level, then the walls loaded with equal vertical loads showed higher capacity up to 2 times. The capacity that was acquired at the ultimate limit state leads to the same conclusions. The walls with high precompression level showed higher energy dissipation.
On the other hand, the displacement levels at all limit states did not show apparent relations in terms of geometry and precompression levels. The squat walls demonstrated that the precompression level has no significant influence on the ultimate displacements. Actually, greater ultimate displacement was obtained for the wall UMW3 in comparison to the wall UMW1. However, the tall walls showed dependence on the precompression level. The wall UMW2 exhibited greater ultimate displacement than the wall UMW4. Therefore, no particular trends could be established for the elastic secant stiffness of the tested walls.

The test results in terms of the identified three limit states and corresponding lateral capacity, displacement and rotation angle are summarized in Table 23.

Rotation angle (θ) has been defined as a ratio of the displacement, at each limit state, to the height of the wall. A summary of the test results in terms of lateral capacity and deformation capacity for each limit state is presented in Table 24. Also, the ratio between the measured

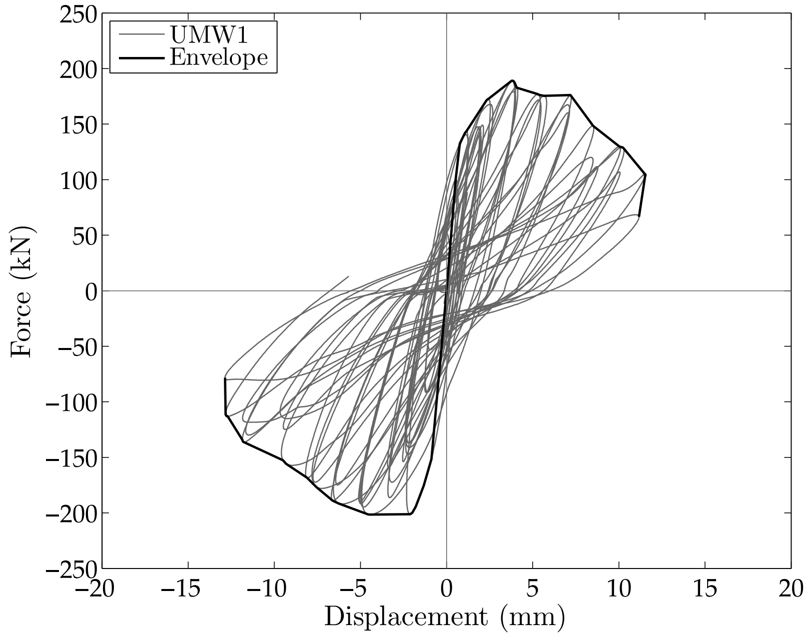

(a) UMW1

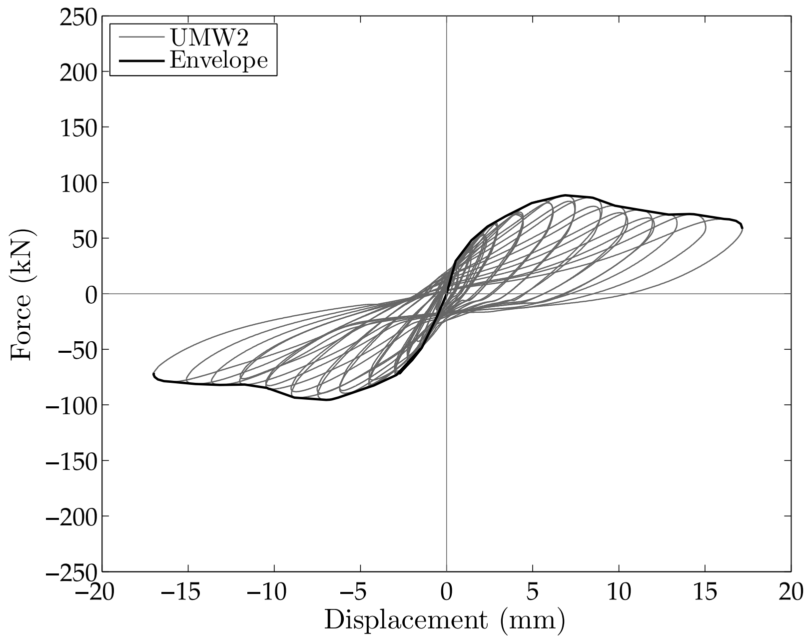

(b) UMW2

Figure 86: Force-displacement hysteresis loops for walls with precompression level $\sigma_0/f_k = 0.33$

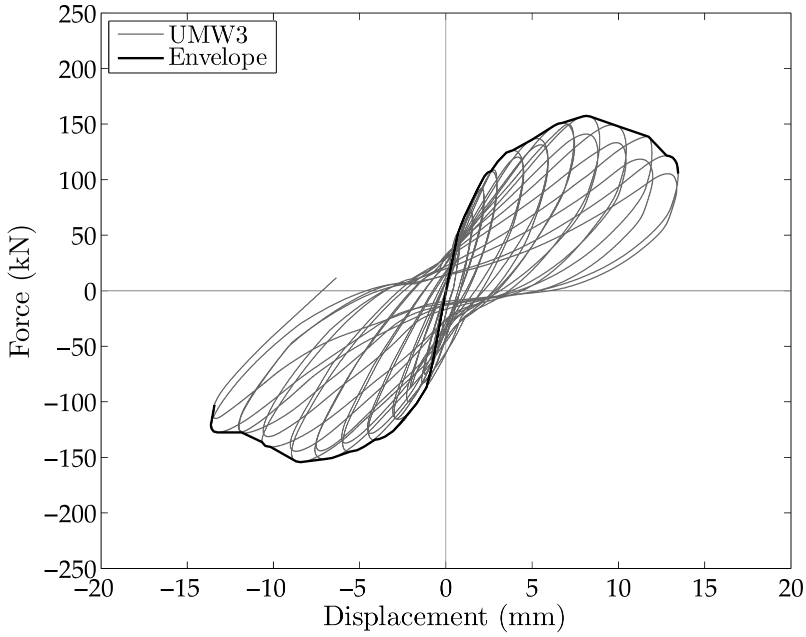

(a) UMW3

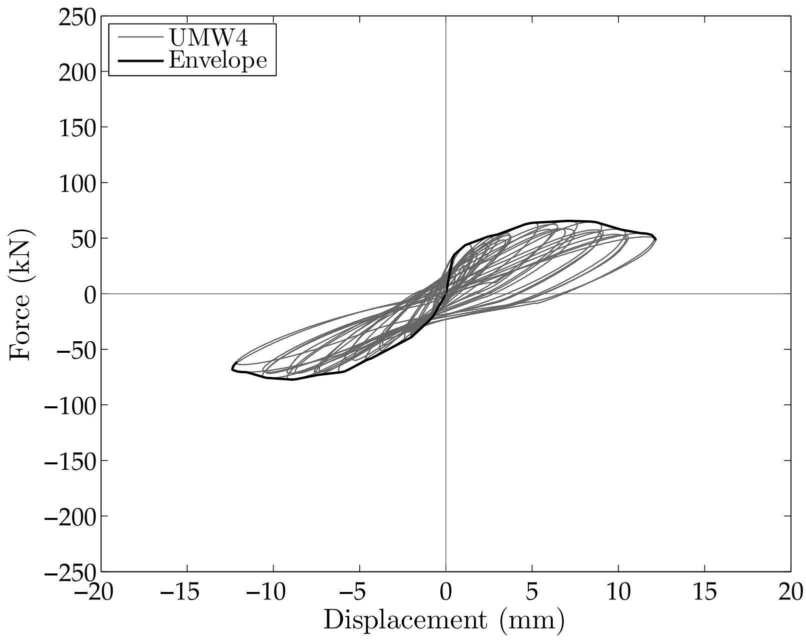

(b) UMW4

Figure 87: Force-displacement hysteresis loops for walls with precompression level $\sigma_0/f_k = 0.17$

Spec.	Dir.	Crack limit			Maximum resistance			Ultimate resistance		
		d_{cr}	H_{cr}	θ_{cr}	d_{Hmax}	H_{max}	θ_{Hmax}	d_{max}	H_{dmax}	θ_{dmax}
	(+/-)	(mm)	(kN)	(%)	(mm)	(kN)	(%)	(mm)	(kN)	(%)
UMW1	+	0.54	100.23	0.03	3.80	189.14	0.21	11.51	105.08	0.63
	-	0.64	105.64	0.04	6.60	189.06	0.36	12.70	113.04	0.70
UMW2	+	0.58	25.69	0.03	6.88	88.54	0.38	16.10	67.28	0.88
	-	0.54	20.02	0.03	6.98	95.57	0.38	15.60	79.23	0.86
UMW3	+	0.70	51.96	0.04	8.14	157.35	0.45	12.86	105.31	0.71
	-	0.79	66.51	0.04	8.43	154.37	0.46	13.35	115.00	0.73
UMW4	+	0.80	32.24	0.04	7.09	65.46	0.39	11.56	51.16	0.64
	-	0.69	19.04	0.04	8.91	77.23	0.49	11.77	63.78	0.65

(a) Test results for positive and negative loading direction

Spec.	Crack limit			Maximum resistance			Ultimate resistance		
	d_{cr}	H_{cr}	θ_{cr}	d_{Hmax}	H_{max}	θ_{Hmax}	d_{max}	H_{dmax}	θ_{dmax}
	(mm)	(kN)	(%)	(mm)	(kN)	(%)	(mm)	(kN)	(%)
UMW1	0.59	102.94	0.03	5.20	189.10	0.29	12.11	109.06	0.67
UMW2	0.56	22.86	0.03	6.93	92.06	0.38	15.85	73.26	0.87
UMW3	0.75	59.24	0.04	8.29	155.86	0.46	13.11	110.16	0.72
UMW4	0.75	25.64	0.04	8.00	71.35	0.44	11.67	57.47	0.64

(b) Averaged test results with respect to loading direction

Table 23: Test results for UMWs: lateral capacity, displacement and rotation angle at limit states

Spec.	σ_0/f_k	H_{cr}/H_{max}	H_{dmax}/H_{max}	$\theta_{cr}/\theta_{Hmax}$	$\theta_{dmax}/\theta_{Hmax}$	$\theta_{dmax}/\theta_{cr}$
UMW1	0.33	0.54	0.58	0.11	2.33	20.52
UMW2	0.33	0.25	0.80	0.08	2.29	28.30
UMW3	0.17	0.38	0.71	0.09	1.58	17.59
UMW4	0.17	0.36	0.81	0.07	1.46	21.60
Mean	/	0.38	0.72	0.09	1.91	22.00
CV(%)	/	27.62	12.74	19.07	20.72	17.83

Table 24: Lateral capacity and deformation capacity for UMWs at characteristic limit states

values for lateral capacity and the rotation angle at the attained crack limit state and at ultimate state are given.

Analysing the results presented in Table 24 with respect to the influence of the precompression level on squat walls (UMW1 and UMW3), the ratio of the load acting on the wall at initiation of cracking $\left(H_{cr}/H_{max}\right)$ shows difference of 42 % in favour of the wall with higher precompression level (UMW1), as expected. On contrary, this trend was not observed for tall walls (UMW2 and UMW4). In fact, they showed opposite trend with a difference of $-30\,\%$ in favour of the wall UMW4.
The ratio of the ultimate load to the maximum load $\left(H_u/H_{max}\right)$ observed at squat walls varies significantly in range of $0.58 - 0.71$, while for tall walls constant ratio was obtained.
The displacement capacity of the walls showed a relation with the level of precompression stresses. The rotation of all the walls at cracking limit states presented similar values, while at ultimate limit state the walls with higher σ_0/f_k exhibited 55 % greater rotations at the top of the walls. The displacement capacity, expressed with regard to the rotation of the walls at the ultimate rotation and the attained maximum capacity $\left(\theta_u/\theta_{Hmax}\right)$ is relatively small for unreinforced masonry walls with a mean value of 1.91. The ratio of rotation at ultimate state to rotation at cracking limit state for all walls varies in close range with a mean value of 22.00. This indicates formation of cracks, and thus plastic behaviour of the walls from the very beginning of application of the horizontal load.

Based on the idea that the shear capacity of a wall is governed by the tensile strength, the equations have been implemented in actual seismic codes [PZZ, 1991]. The equations have been derived on the basis of elementary theory of elasticity by taking into account the assumption that the masonry wall is an elastic, homogeneous and isotropic panel. With the respect to the assumption, the wall behaviour until the maximum value of the horizontal load is elastic and at

Spec.	Shear cracking		Maximum capacity	
	τ_{cr} (N/mm^2)	$f_{t,cr}$ (N/mm^2)	τ_{max} (N/mm^2)	$f_{t,max}$ (N/mm^2)
UMW1	0.163	0.057	0.300	0.173
UMW2	0.063	0.009	0.252	0.127
UMW3	0.094	0.037	0.247	0.197
UMW4	0.070	0.021	0.195	0.135
Mean	0.098	0.031	0.249	0.158
CV(%)	40.72	58.04	14.90	18.03

Table 25: Shear and tensile strength of UMWs at cracking limit state and maximum capacity

that moment the principal tensile stress, called 'tensile' or 'referential tensile strength' [Tomaževič, 2009b] of masonry is given with Eq. 4.1.

$$f_{t,max} = \sqrt{\left(\frac{\sigma_0}{2}\right)^2 + (b\tau_{max})^2} - \frac{\sigma_0}{2} \tag{4.1}$$

where,

f_t tensile strength of masonry

σ_0 average compressive stress in the horizontal section of the wall

b shear stress distribution factor

τ_{max} average shear stress in the horizontal section of the wall at maximum horizontal load H_{max}

The shear stress distribution factor (b) has been defined to depend on the wall geometry and the ratio between the vertical load and the maximum horizontal load. The usual range of b is $1.1 \leq b = h/L \leq 1.5$ [Tomaževič, 2009b, Bosiljkov et al., 2010]. For calculation and comparison of the shear and tensile strength obtained at cracking limit state and maximum capacity presented in Table 25, b has been adopted as 1.5.

Analysing the results for shear and tensile strength of unreinforced masonry walls at the attained maximum capacity, significantly higher values for the shear strength have been calculated in comparison to the tensile strength of masonry. Shear strength has been related to the compressive stress with increasing trend, which means that the walls loaded with higher compressive stresses have higher shear stresses. The tensile strength of masonry was related to the shear strength. By increasing the shear strength, the tensile strength of masonry will increase. The relations between the shear and the tensile

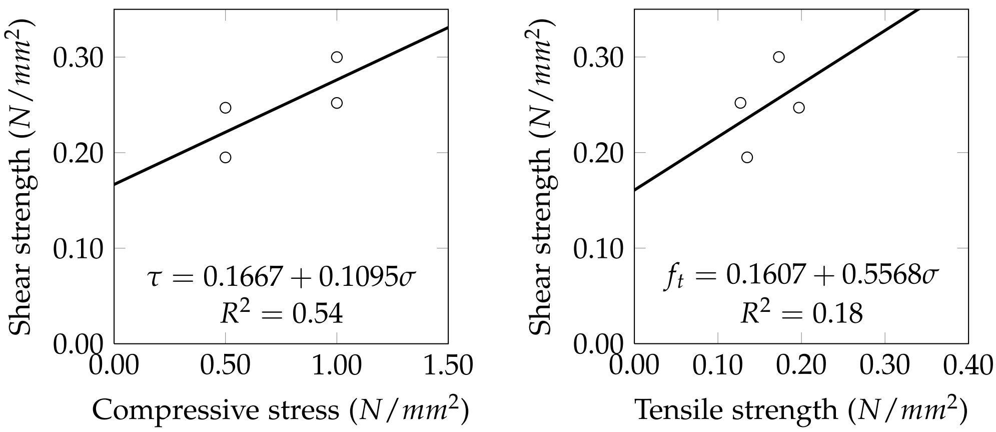

(a) Shear strength vs. compressive stress

(b) Tensile strength vs. shear strength

Figure 88: Relations of shear strength to compressive stress and shear strength to tensile strength for UMWs

stresses and the compressive stresses have been plotted in Figure 88. However, the results presented have to be used cautiously, since only two series of values have been used to fit the linear least square regression. Poor values for the approximation have been obtained in both cases $\left(R^2 = 0.54 \text{ and } R^2 = 0.08\right)$. The obtained coefficient of friction of the walls (0.1095) is rather different from the coefficient found experimentally to be 0.6667, see Section 3.7.

4.3.3 *Stiffness degradation and energy dissipation capacity*

These parameters were considered important for numerical modelling of the behaviour of masonry walls subjected to cyclic loads and for evaluation of their seismic performance.

Stiffness degradation is expected to occur at shear failure modes due to reversed cyclic loads. Generally, it is low at masonry walls failing with bending. The stiffness degradation parameter is particularly important at ultimate limit state, since the horizontal loads are distributed to the walls according to their stiffness. After failure of the first wall, the load transfer is changed and different distribution is obtained related to the residual wall stiffness.

The energy dissipation capacity of the walls is also important parameter in cyclic response analysis. This capacity is usually evaluated through the coefficient of equivalent viscous damping (CEVD) $\left(\xi_{eq}\right)$, calculated by equating the energy dissipated in a vibration cycle of the actual structure and an equivalent viscous system [Chopra, 2007]. It is generally used to represent dissipated energy in the elastic range, although in some research studies the energy dissipated in inelastic deformations has been modelled as equivalent viscous damping.

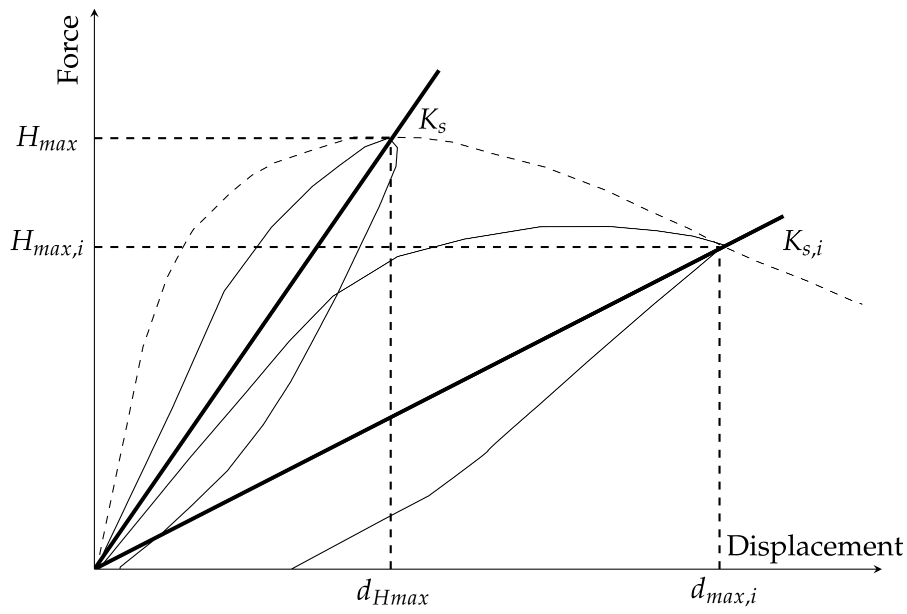

Figure 89: Calculation of stiffness degradation

4.3.3.1 *Stiffness degradation*

To evaluate the damage occurring in the walls during the cyclic load reversals, secant stiffness $(K_{s,i})$ was calculated for each cycle. The secant stiffness at each loading cycle was calculated according to Eq. 4.2. Figure 89 illustrates the procedure for calculation of the secant stiffness.

$$K_{s,i} = \frac{H_{max,i}}{d_{max,i}} \tag{4.2}$$

where,

$K_{s,i}$ secant stiffness at i cycle

$H_{max,i}$ horizontal load at maximum displacement at i cycle

$d_{max,i}$ maximum displacement at i cycle

Figure 90 shows the development of the stiffness degradation. It can be noticed that all walls demonstrate decreasing of the secant stiffness with increasing horizontal displacements. This trend follows a power function. Some differences in the stiffness degradation are noticed up to 50 % of the maximum horizontal displacements. After that, all walls show same rate of stiffness degradation for each displacement level. Except UMW4, all walls demonstrate small increase of the stiffness in the second cycle and subsequent decrease in the following cycles. This aspect happens in the range of $K_{s,i}/K_s = 2 - 4$. Wall UMW4 exhibits highest stiffness degradation, particularly after the third cycle and immediate decrease in the next loading cycles.

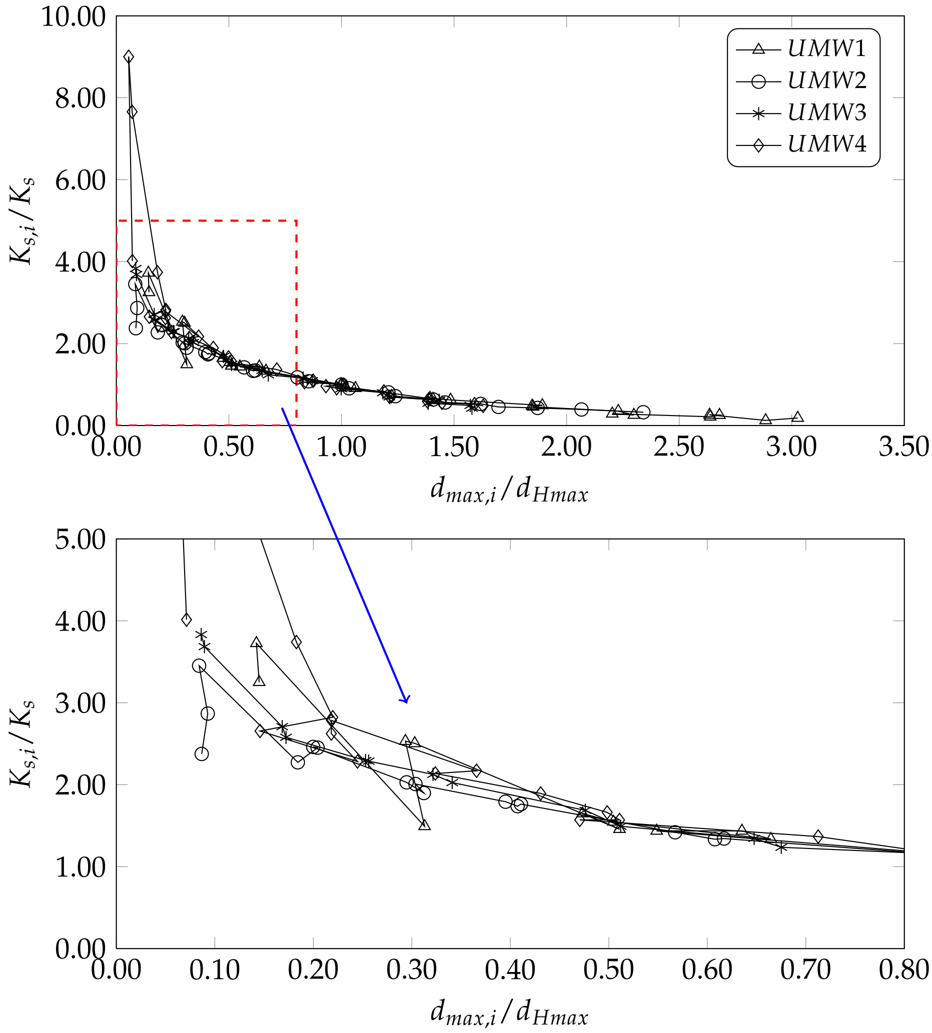

Figure 90: Stiffness degradation for the positive part of the diagrams

Tomaževič [1999] highlights that the stiffness degradation of masonry walls subjected to in-plane cyclic loads follows a power function according to Eq. 4.3.

$$\frac{K_{s,i}}{K_s} = \alpha_1 \left(\frac{d_{max,i}}{d_{Hmax}} \right)^{\beta} \tag{4.3}$$

where,

K_s	secant stiffness at elastic limit
d_{Hmax}	displacement at maximum horizontal load
α_1, β	stiffness degradation parameters

Stiffness degradation parameters α_1 and β depend on the horizontal load history and compression stresses caused by the vertical load on the top of the wall. It was suggested to determine these parameters experimentally, or in lack of test results, values of $\alpha_1 = 0.3$ and

$\beta = -0.85$ can be used for the case of walls loaded with vertical precompression level up to $\sigma_o / f_k = 0.2$.
The parameters α_1 and β were obtained by regression analysis of the experimental curves for all walls and the values of $\alpha_1 = 0.74$ and $\beta = -0.97$ were calculated.

4.3.3.2 *Energy dissipation capacity*

To analyse the possible differences in the behaviour of the walls due to different geometry aspect ratio and vertical compressive stresses, the energy dissipation capacity has been assessed from the experimentally obtained hysteretic relations between the horizontal load and the horizontal displacements.

Viscous damping concept has been used to describe energy dissipation of various mechanisms such as cracking, non-linear behaviour, interaction with other elements, and etc., and it represents the combined effect of all dissipation mechanisms. This has been done for practical reasons since there is no direct relationship of the damping with real physical phenomena. It also simplifies the solution of the fundamental differential equation of motion represented by Eq. 4.4.

$$m\ddot{u} + c\dot{u} + ku = 0 \tag{4.4}$$

where,

c damping coefficient

The proportionality of the damping coefficient c to the velocity implies that this factor represents viscous damper. This approach has been used for simplicity and easy solution of the differential equation without any special physical reason. Dividing the Eq. 4.4 by m yields

$$\ddot{u} + 2\xi\omega_n\dot{u} + \omega_n^2 u = 0 \tag{4.5}$$

where,

ξ damping ratio or fraction of critical damping, $\xi = \frac{c}{2m\omega_n}$

ω_n natural frequency of vibration of the system, $\omega_n = \sqrt{\frac{k}{m}}$

m mass of the system

The equivalent viscous damping coefficient has been divided in two parts, according to Eq. 4.6.

$$\xi_{eq} = \xi_0 + \xi_{hyst} \tag{4.6}$$

where,

ξ_0 initial viscous damping in the elastic range

ξ_{hyst} equivalent viscous damping ratio due to hysteretic behaviour

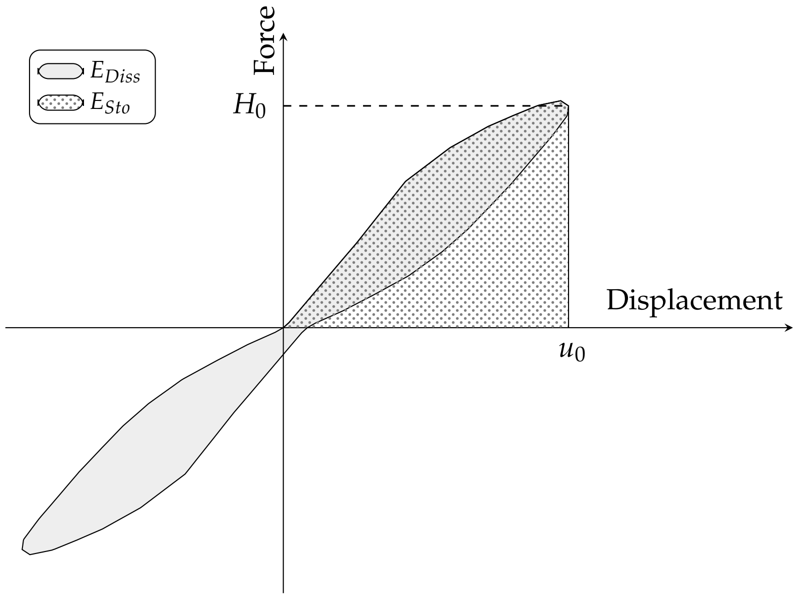

Figure 91: Dissipated and stored potential energy

Initial viscous damping can be estimated by measuring amplitude decay from tests in laboratories or in-situ [Chopra, 2007], but in practice it is usually defined as a constant damping in the range between 2 % and 5 %. This coefficient is assumed to represent different sources of energy dissipation in the elastic range. Application of constant damping in the inelastic range may be inappropriate attributable to several reasons. The hysteretic models incorporate the full structural energy dissipation in the inelastic range and other mechanisms contribute to the variation of the damping such as foundation damping which is reduced upon entering the inelastic range. Since the initial damping is out of the scope of this research, in further analysis it has been assumed zero, and the CEVD has been estimated dependant only to hysteretic behaviour.

The concept of dissipated (E_{Diss}) and stored (E_{Sto}) energy has been used to approximate the equivalent viscous damping corresponding to the hysteretic behaviour, see Figure 91. The dissipated energy in the walls is given by the area E_{Diss} enclosed by the hysteresis loop in one cycle of loading. The stored potential energy was defined by the displacement amplitude and the horizontal load obtained in the same loading cycle. By equating both energies, the value of the CEVD can be obtained, as shown in Eq. 4.7.

$$\xi_{eq} = \xi_{hyst} = \frac{1}{4\pi} \frac{\omega_n}{\omega} \frac{E_{Diss}}{E_{Sto}} \tag{4.7}$$

To obtain correct values for the CEVD, it has to be determined from tests at $\omega = \omega_n$, when the response of the system has been found to be most sensitive to damping. Hence, and for simplicity reasons,

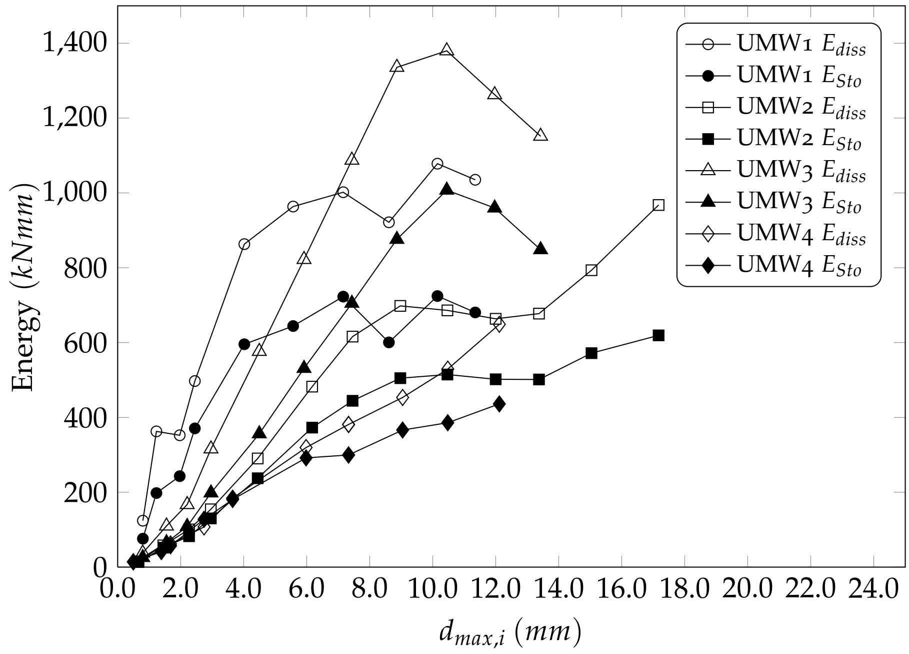

Figure 92: Dissipated and stored potential energy for the positive part of the diagram of UMWs

often the Eq. 4.7 specializes to Eq. 4.8. However, this research uses calculation of E_{Sto} according to Figure 91.

$$\xi_{eq} = \xi_{hyst} = \frac{1}{4\pi}\frac{E_{Diss}}{E_{Sto}} = \frac{1}{2\pi}\frac{A_{hyst}}{H_o u_o} \tag{4.8}$$

The calculated values of stored potential energy, dissipated energy and CEVD for characteristic limit states identified on the positive part of the diagram are given in Table 26.

In terms of energy dissipation capacity, all walls exhibited similar behaviour, as observed from Table 26 and Figure 92. The averaged values for each target displacement and corresponding dissipated and stored energy for the positive part of the force-displacement diagrams are shown in Figure 92. It has been characterized with moderate increase of the dissipated energy up to the level of the maximum horizontal load and slight decrease until the ultimate limit state. The walls UMW2 and UMW4 showed moderate increase of the dissipation capacity after reaching the maximum load. This indicates that the walls posses subsequent dissipation capacity, not utilized during the tests.

The evolution of the CEVD in the sequential displacement cycles is illustrated in Figure 93. The value of ξ_{eq} was estimated within the range of $5 - 15\,\%$ with an average of $13.1\,\%$ for all walls.

Spec.	Crack limit				Maximum resistance				Ultimate resistance			
	E_{hyst} $(kNmm)$	E_{Sto} $(kNmm)$	E_{hyst}/E_{Sto}	ξ_{eq} (%)	E_{hyst} $(kNmm)$	E_{Sto} $(kNmm)$	E_{hyst}/E_{Sto}	ξ_{eq} (%)	E_{hyst} $(kNmm)$	E_{Sto} $(kNmm)$	E_{hyst}/E_{Sto}	ξ_{eq} (%)
UMW1	129.04	92.92	1.39	11.05	743.94	600.14	1.24	9.86	1169.35	884.17	1.32	10.52
UMW2	20.07	16.34	1.23	9.77	664.90	463.15	1.44	11.42	967.64	619.31	1.56	12.43
UMW3	31.76	17.99	1.76	14.04	1417.95	946.09	1.49	11.93	1054.70	775.57	1.36	10.82
UMW4	64.41	49.95	1.29	10.26	502.73	372.83	1.34	10.73	577.10	414.86	1.39	11.07

Table 26: Values of stored energy, dissipated energy and coefficient of equivalent viscous damping for UMWs

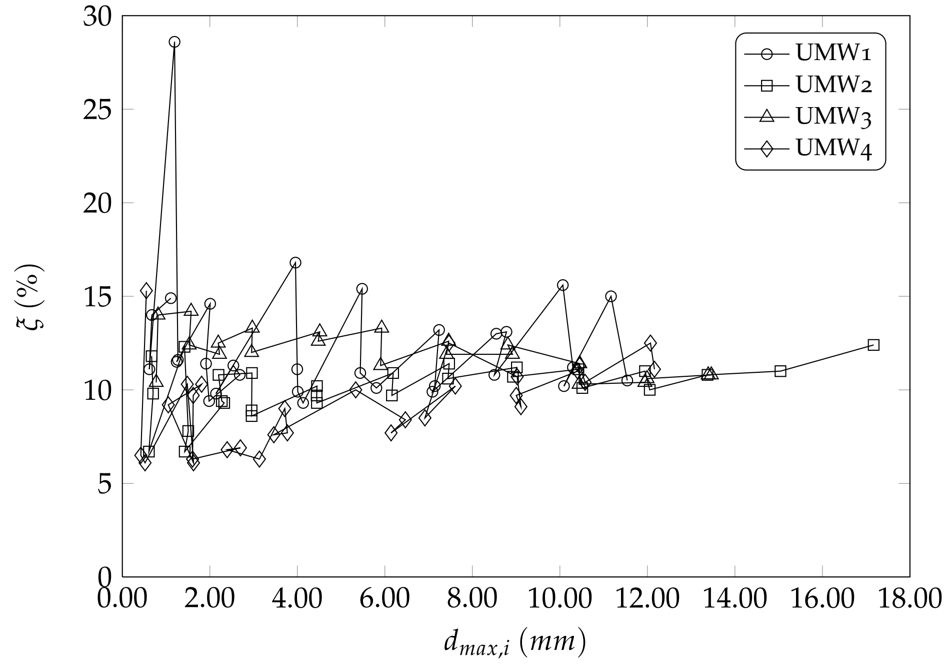

Figure 93: Coefficient of equivalent viscous damping (ξ_{eq}) for the positive part of the diagram of UMWs

4.3.4 *Seismic performance of unreinforced masonry walls*

Seismic events are considered as a main competent actions on buildings in seismic areas. Their cyclic horizontal effects cause extensive bending and shear stresses in masonry walls and almost in every scenario they exceed the elastic range of masonry materials. To satisfy the demand for avoiding brittle behaviour, masonry structural walls should feature sufficient deformation and energy dissipation capacity. Considering the anisotropic and inhomogeneous material behaviour, the analysis of masonry walls in the non-linear range presents challenging task.

To simplify the analysis and design, the masonry is assumed as elastic, homogeneous and isotropic material and the forces, stresses and strains are usually determined on the gross cross-section of the walls. The experimental hysteretic behaviour of a masonry wall loaded with a combination of vertical load and horizontal load applied in reverse cycles is normally represented by and idealized diagram. Tomaževič [1999, 2009b] suggested two multi-linear idealizations of the experimental force-displacement results in form of a bi- or trilinear capacity curve. The simpler, bilinear idealization was accepted as the most common approach for assessment of in-plane seismic performance of masonry walls [Gellert, 2010, Haach, 2009, Costa, 2007, Magenes, 2006, Vasconcelos, 2005, Bosiljkov et al., 2003]. Bilinear idealization has been used in this study, see Figure 94.

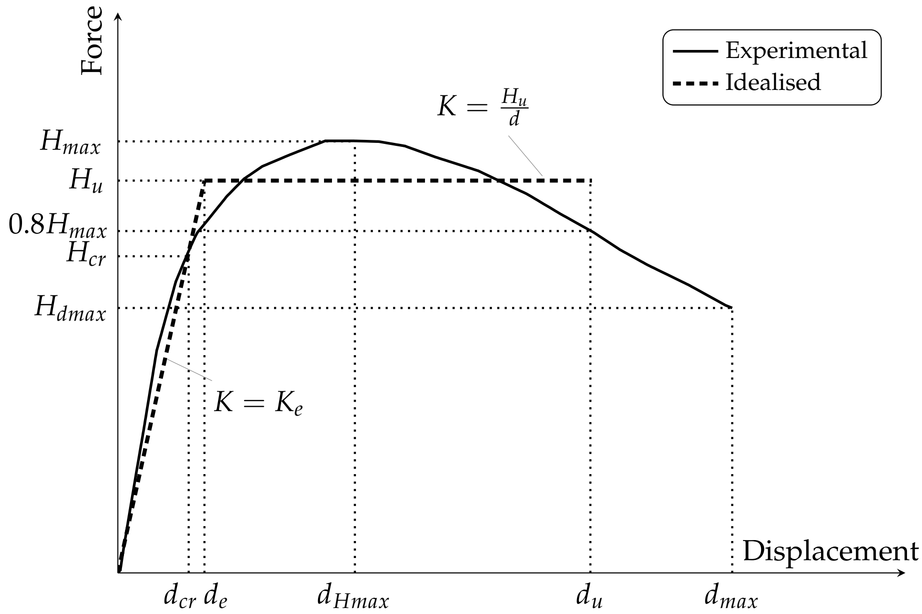

Figure 94: Bilinear idealisation of experimental capacity envelopes

To idealise the experimental results, three limit states identified previously have been used, namely: crack limit, maximum resistance and ultimate resistance. For each limit state, associated displacements and corresponding horizontal loads have been obtained, as shown in Table 23.

Initial slope of the idealised envelope has been defined with the secant stiffness at the formation of the first cracks. It was calculated by dividing the load corresponding to the first crack (H_{cr}) by the corresponding displacement (d_{cr}). Thus, the effective stiffness was calculated with Eq. 4.9.

$$K_e = \frac{H_{cr}}{d_{cr}} \tag{4.9}$$

The ultimate load of the idealised envelope (H_u) has been evaluated by using the principle of equal energy dissipation capacity of the experimental and the idealised wall. It was assumed that the areas enclosed below the experimental, the idealised curves and the X axis were equal. With the known effective stiffness K_e, the ultimate load was calculated from Eq. 4.10.

$$H_u = K_e \left(d_{max} - \sqrt{d_{max}^2 - \frac{2A_{env}}{K_e}} \right) \tag{4.10}$$

where,

A_{env} area below the experimental envelope curve

The elastic displacement (d_e) results from the ratio of the ultimate load (H_u) and the elastic stiffness (K_e), see Eq. 4.11. The ultimate

Spec.	Dir. (+/-)	d_{cr} (mm)	H_{cr} (kN)	K_e (kN/mm)	H_u (kN)	d_e (mm)	d_u (mm)	θ_u (%)	μ_u
UMW1	+	0.54	100.23	185.61	161.48	0.87	8.37	0.46	9.62
	-	0.64	105.64	165.06	172.89	1.83	8.79	0.48	4.80
UMW2	+	0.58	25.69	44.29	73.90	1.67	14.64	0.80	8.77
	-	0.54	20.02	37.07	83.56	2.30	16.80	0.92	7.30
UMW3	+	0.70	51.96	74.23	135.10	1.82	12.53	0.69	6.88
	-	0.79	66.51	84.19	136.51	1.61	13.59	0.75	8.44
UMW4	+	0.80	32.24	40.30	57.79	1.43	11.95	0.66	8.33
	-	0.69	19.04	27.59	65.86	2.36	12.15	0.67	5.15

Table 27: Summary of the obtained results after bilinear idealisation of UMWs

displacement (d_u) and the ultimate drift (θ_u) have been defined at a displacement intersecting the descending branch of the experimental envelope diagram at a horizontal load level equal to 80 % of the ultimate load (H_u), see Figure 94. Hence, with the bilinear idealisation of the experimental results in form of force-displacement diagrams, it was possible to obtain the ductility of the walls. Ductility (μ_u) was considered as an essential property of structures subjected to cyclic loads, see Eq. 4.12.

$$d_e = \frac{H_u}{K_e} \tag{4.11}$$

$$\mu_u = \frac{d_u}{d_e} \tag{4.12}$$

The results from the idealisation of the force-displacement diagrams for unreinforced masonry walls are shown in Table 27. The graphical presentation of the bilinear idealisation of the tested walls is illustrated in Figure 95. A comparison of the idealized curves with the idealisation proposed in different design codes is given in Chapter 5.

As can be seen from the Table 28, the average ratio of H_u/H_{max} was 0.87, which is very close to the value of 0.9 suggested by Tomaževič [1999]. This ratio indicates that in case of bilinear idealisation, the horizontal capacity of the unreinforced masonry walls should be reduced by 13 % during seismic analysis.

From the data given in Table 28 the values for ultimate ductility factor showed wide scatter within a range of $4.8 - 9.6$. No significant correlation of the ultimate ductility factor could be established with respect to the geometry and precompression levels of the tested walls. However, in practical applications for verification of seismic capacity of unreinforced masonry buildings, the ultimate ductility (μ_u) is limited to avoid excessive damage to masonry walls. Although experimental

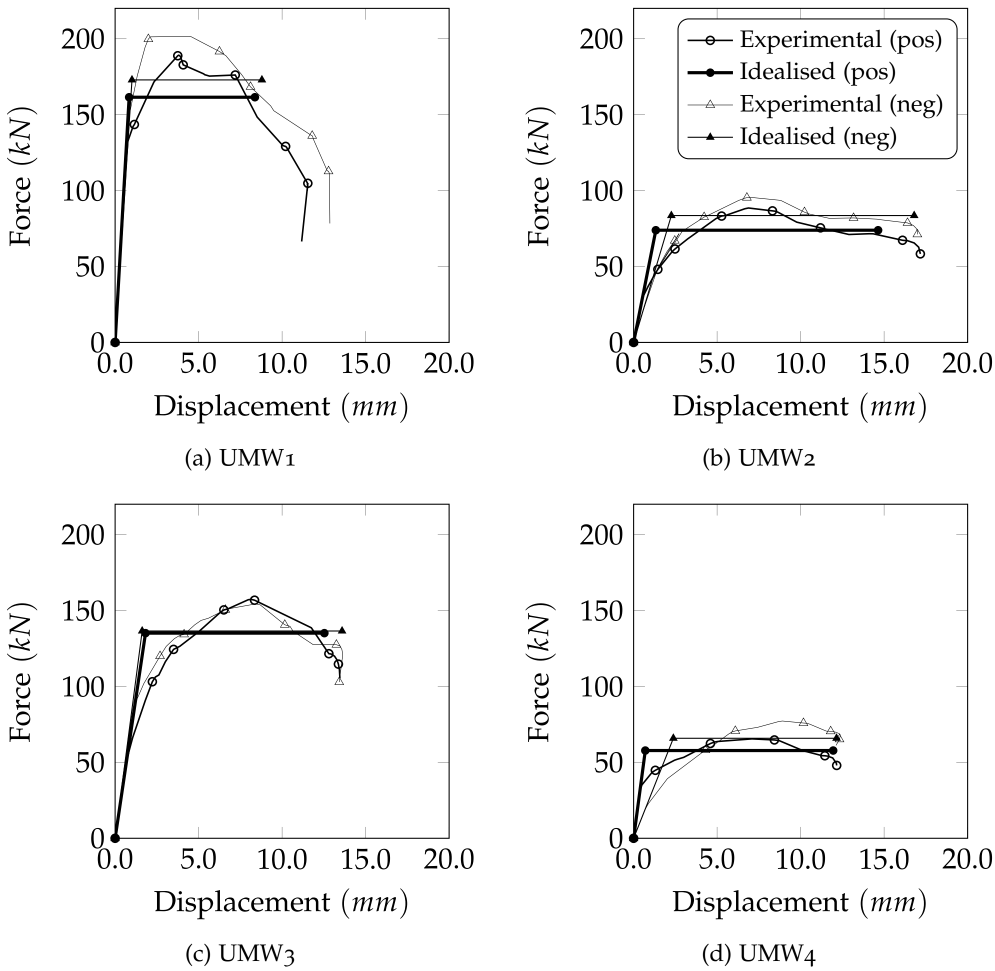

Figure 95: Bilinear idealisation of the experimental UMWs walls in positive and negative direction of loading

results can indicate larger values, Tomaževič [1999] recommended values for ultimate ductility factor of $\mu_u = 2.0 - 3.0$ for the case of unreinforced masonry walls.

To compare the results for the elastic stiffness, a linear elastic theoretical model assuming the total deformation (d) of fixed ended masonry walls partly due to bending and partly to shear was used, as shown in Eq. 4.13.

$$d = \frac{Hh^3}{12EI} + \frac{\kappa Hh}{GA} \tag{4.13}$$

Spec.	Dir. (+/-)	H_u/H_{max} (kN)	K_e (kN/mm)	$K^1_{e,theo}$ (kN/mm)	$K^2_{e,theo}$ (kN/mm)
UMW1	+	0.85	185.61	303.44	250.08
	-	0.91	165.06		
UMW2	+	0.83	44.29	133.84	115.04
	-	0.87	37.07		
UMW3	+	0.86	74.23	303.44	250.08
	-	0.88	84.19		
UMW4	+	0.88	40.30	133.84	115.04
	-	0.85	27.59		

Table 28: Ratio H_u/H_{max} and theoretical effective stiffness for UMWs

where,

H horizontal load causing unit deformation

h height of the wall

L length of the wall

E modulus of elasticity of masonry

G shear modulus of masonry

I moment of inertia of the wall's cross-section, $I = tL^3/12$

A gross area of horizontal cross-section of the wall, $A = tL$

κ shear coefficient, for rectangular cross-section $\kappa = 1.2$

If the relation for A, I and the value of κ are substituted in Eq. 4.13 and it is rearranged to express the effective stiffness, the Eq. 4.14 is obtained. In this calculations, the modulus of elasticity was obtained from Table 21 and the shear modulus of masonry was calculated with the expression $G = E/2(1+\nu)$ considering $\nu = 0.15$.

$$K^1_{e,theo} = \frac{GA}{1.2h\left[1+\alpha'\frac{G}{E}\left(\frac{h}{L}\right)^2\right]} \tag{4.14}$$

where,

α' coefficient determining the position of the bending moment's inflection point along the height of the wall

$$\alpha' = \begin{cases} 0.83 & \text{for fixed ended wall} \\ 3.33 & \text{for cantilever wall} \end{cases}$$

As Table 28 shows, the elastic theory largely overestimates the effective stiffness $\left(K^1_{e,theo}\right)$ of the walls. This indicates strong anisotropic

behaviour of unreinforced masonry.
For practical applications, the effective stiffness derived from elastic theory can be reduced to better match the experimental results. As pointed out by Gellert [2010], based on analysis of several experimental results, the effective stiffness can be calculated by considering reduced moment of inertia, as presented by Eq. 4.15. Yet, the calculated effective stiffness of the walls $\left(K^2_{e,theo}\right)$ with the reduced moment of inertia (I_E) was higher than the stiffness obtained experimentally. Based on the obtained experimental results, a correction factor p_k is proposed to calculate the stiffness, see Eq. 4.16. The factor p_k varies from $0.3 - 0.7$. It is therefore recommended that the stiffness of the walls should be calculated by multiplying the stiffness obtained with the reduced moment of inertia $\left(K^2_{e,theo}\right)$ by the factor $p_k = 0.5$.

$$I_E = \frac{I}{\left(1 + \frac{3.64EI}{h^2GA}\right)} \tag{4.15}$$

$$K_p = p_k K^2_{e,theo} \tag{4.16}$$

The most striking results to emerge from the data were the obtained values for the shear modulus (G_{test}) of unreinforced masonry. A pure conventional definition of the shear modulus was found by rearranging the Eq. 4.14. Thus, the shear modulus of masonry presented in Table 29 was calculated with Eq. 4.17, taking into account the modulus of elasticity $E = 2874.84\,N/mm^2$ from Table 21. The resulting ratio between the shear modulus and modulus of elasticity is presented also. As can be seen, the actual values are within the range of $6 - 25\,\%$ of the modulus of elasticity. The findings of the current study do not support the values for the shear modulus of 40 % of E as recommended by Eurocode 6 [2005]. It is therefore likely that the recommended G/E ratio might lead to unreasonable distribution of seismic loads onto the masonry walls. Hence, for practical applications it is proposed to consider the value of $G = 0.13E$ which was calculated as a mean value from the experimental results. Similar suggestions can be found in Tomaževič [2009b].

$$G_{test} = \frac{K_e}{\frac{A}{1.2h} - \alpha' \frac{K_e}{E}\left(\frac{h}{L}\right)^2} \tag{4.17}$$

4.4 TEST RESULTS FOR STRENGTHENED MASONRY WALLS

The same procedure for testing described in section 4.2.3 was used to investigate the behaviour of the strengthened masonry walls. The results are presented in the same form as for unreinforced walls.

Spec.	Dir.	Experimental		Eurocode 6
		G_{test}	G_{test}/E	$G = 0.4E$
	(+/-)	(N/mm^2)		(N/mm^2)
UMW1	+	712.49	0.25	1149.94
	-	626.17	0.22	
UMW2	+	300.77	0.10	
	-	246.32	0.09	
UMW3	+	267.70	0.09	
	-	305.28	0.11	
UMW4	+	270.39	0.09	
	-	178.29	0.06	

Table 29: Correlation between the experimentally obtained and recommended shear modulus of unreinforced masonry

4.4.1 *Failure modes*

The strengthening method brought to a change in the failure modes of the walls if compared to the unreinforced walls. All SMWs failed with predominantly compression failure in the bottom corner areas. Notable failure mode was separation of the RC jacket from the masonry wall and lifting of the specimen from the bottom RC beam in the direction of load application. Generally, the walls developed bending failure mode and after reaching the tensile and bond strength between the wall and the bottom beam they started to rotate in each displacement cycle as rigid bodies. Another important finding was the separation (or pealing) of the jackets from the masonry. This investigations were set out with the aim of assessing the behaviour of the RC jacketed masonry material and for that reason no connection was established between the reinforcement in the jackets and the bottom and the top RC beams. The intention was to study the response of the new material rather than to study the response of the strengthened masonry wall as a structural element.
In this research it was confirmed that separation of the jackets is associated with their mutual connection and connection to the masonry. The findings of the current research are consistent with the recommendations for the number of anchors given by Tomaževič [1999] and Sheppard and Terčelj [1980]. The cracking pattern in the final stage of testing is presented on a mesh pattern, as shown in Figure 96 and Figure 97.

The presented cracking pattern was observed on the outer face of the jackets. The wall SMW1 demonstrated cracking in the bottom corners of the wall. Bending of the vertical reinforcement in a plane normal

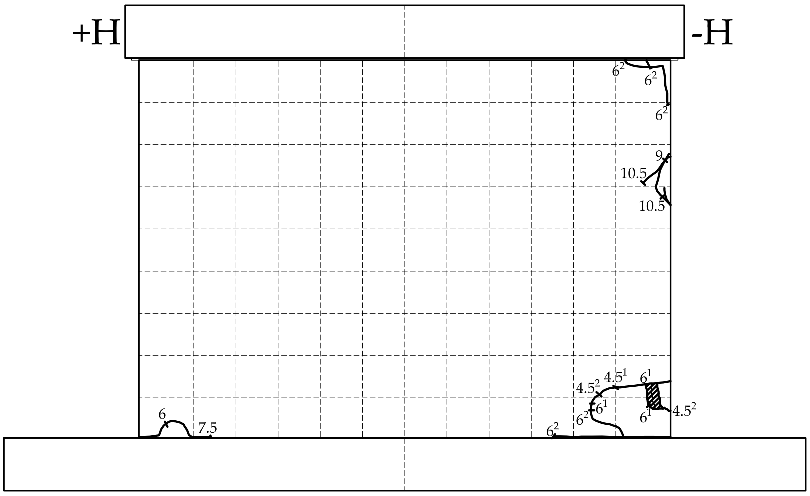

(a) SMW1

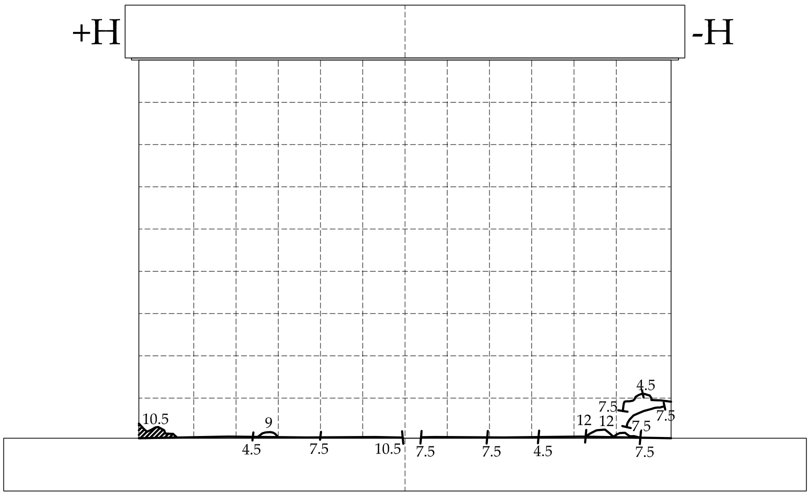

(b) SMW3

Figure 96: Cracking patterns of squat strengthened masonry walls

to the wall plane at a displacement cycle of 4.5 mm was observed. SMW3 showed typical bending failure mode with development of horizontal crack in the connection plane of the wall and the bottom RC beam. Some toe cracking caused by the compression stresses was obtained in the bottom corner. The tall wall loaded with higher vertical load failed with pronounced separation of the jacket from the wall. During this failure, the encased masonry was squeezed from the jackets within a range of $3-5$ cm. Similarly to lightly loaded squat wall, SMW3, the wall SMW4 showed characteristic bending failure with horizontal cracking at the bottom RC beam due to exceeding of the tensile strength. The typical failure modes obtained during the tests are shown in Figure 98.

Since the walls did not show many cracks on their outer surface and to obtain full knowledge of the damage state in the masonry wall, it was decided to remove the RC jackets from the walls prior their

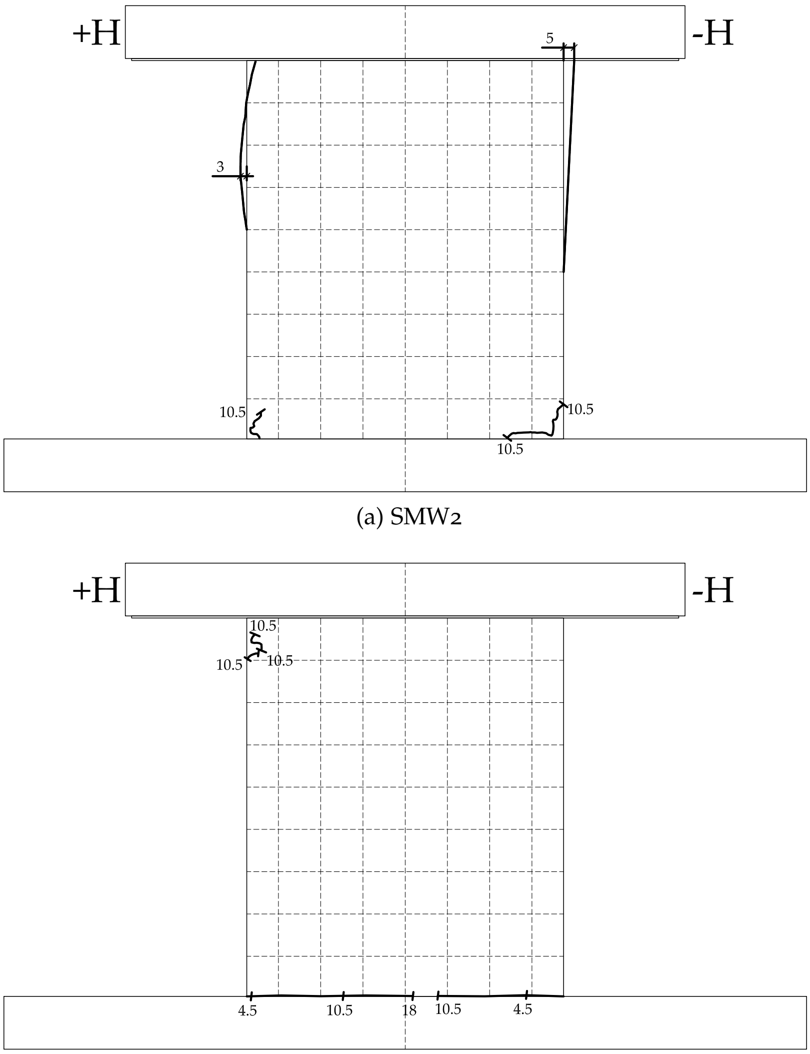

(a) SMW2

(b) SMW4

Figure 97: Cracking patterns of tall strengthened masonry walls

complete demolition. The jackets were carefully removed from the masonry by using power hammer. The most interesting finding was that the walls loaded with higher precompression level exhibited cracking in the masonry wall. The most extensive cracking was obtained at tall wall SMW2, see Figure 99. On contrary, the walls subjected to lower precompression stresses did not suffered any particular damage in the masonry. A possible explanation for this might be that the walls with lower precompression level behaved as one compact element and the shear and tensile strength were not exceeded. From the imprint on the inner surface of the jackets it can be concluded that the bond strength between the concrete and masonry was not exceeded. The separation of the jackets was due to splitting of the bricks in the vertical direction with respect to the wall. This result may be explained by the fact that the splitting strength of the bricks was achieved. It can therefore

(a) Toe cracking and bending of horizontal reinforcement

(b) Horizontal crack between the bottom RC beam and the wall and uplifting of the wall

(c) Separation of RC jackets from masonry walls

(d) Squeezing of encased masonry wall from RC jackets

Figure 98: Failure modes of strengthened masonry walls

be concluded that the splitting strength of the bricks is important mechanical property which can control the separation failure mode.

4.4.2 *Force-displacement diagrams*

The obtained force-displacement curves are presented as hysteresis loops in Figure 100 and Figure 101. Analysing the wall behaviour in relation to the level of the precompression load, the specimen SMW1 exhibited higher maximum capacity up to 32 % in comparison to SMW3, as expected. The second set of walls (SMW2 and SMW4) showed similar maximum capacity with a difference of about 9 % in favour of SMW2. The forces obtained in the ultimate limit state showed opposite trend. The walls loaded with precompression level of $\sigma_0/f_k = 0.17$ demonstrated higher ultimate forces than the corresponding walls loaded with $\sigma_0/f_k = 0.33$.

(a) Cracking pattern for SMW1

(b) Cracking pattern for SMW2

Figure 99: Experimental cracking pattern for strengthened masonry walls (masonry part)

In terms of deformation capacity, the first cracks in the walls SMW3 and SMW4 were reached almost at same displacements. SMW1 started to crack first among the walls, while SMW2 was last. Quite different and inconsistent results for displacements at maximum horizontal forces were obtained. SMW1 showed the maximum capacity at very low level of displacements, 2.76 mm, while for SMW4 maximum capacity was reached at displacement of about 17.19 mm. As for ultimate displacements, the specimens loaded with lower precompression levels showed greater displacement capacity when compared to the corresponding walls loaded with higher vertical forces. This difference varies in the range of $32 - 84\,\%$ and indicates that the level of precompression has opposite influence on the ultimate displacements. A notable trend of the elastic secant stiffness was observed. Namely, the stiffness depends on the level of precompression as expected. The ultimate rotation angle (θ_{dmax}) was within the range of $0.67 - 1.15\,\%$. The test results with parameter for identified limit states are summarized in Table 30. A summary of the averaged results for positive and negative loading direction related to the lateral capacity and deformation capacity for each limit state is presented in Table 31.

As can be seen from the Table 31, the ratio of the force on the wall at the beginning of the first cracks to maximum force (H_{cr}/H_{max}) was dependent on the geometry and the vertical precompression levels, as expected. The squat walls showed higher load capacity than the tall walls. The same conclusion can be drawn regarding the vertical precompression levels. The higher the vertical load, the greater capacity was obtained.

The ratio of the ultimate load to the maximum load was shown to be

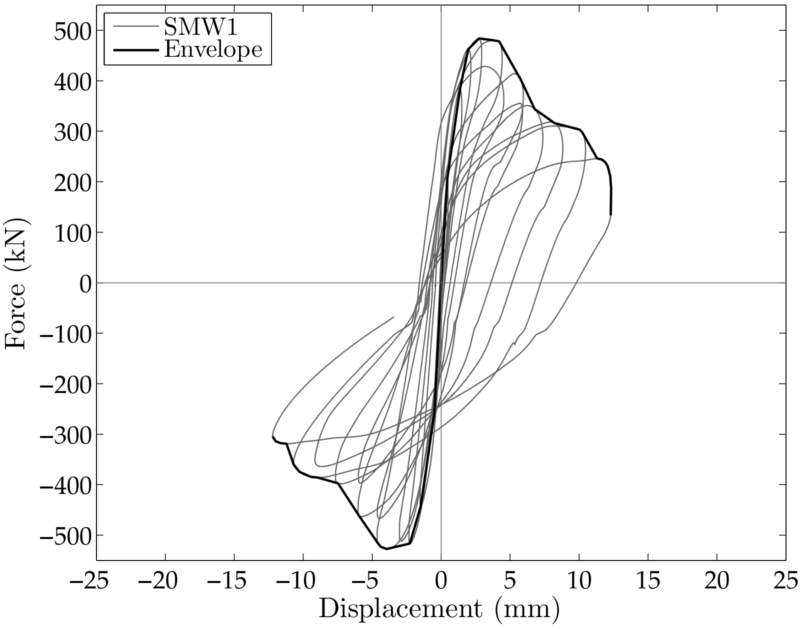

(a) SMW1

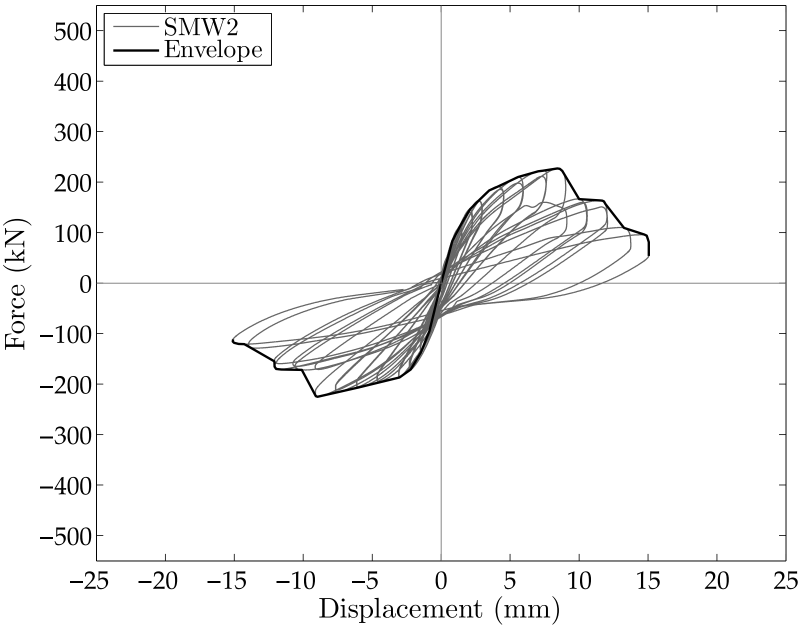

(b) SMW2

Figure 100: Force-displacement hysteresis loops for walls with precompression level $\sigma_0/f_k = 0.33$

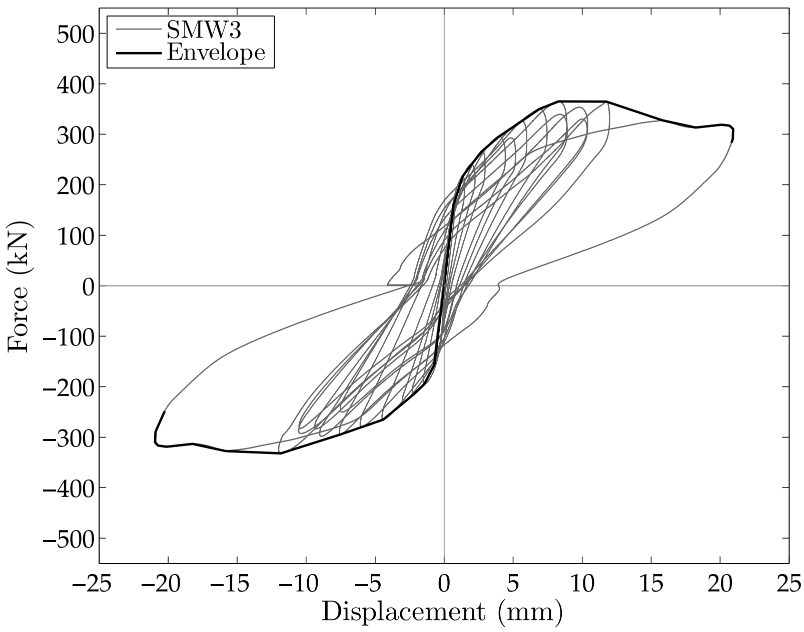

(a) SMW3

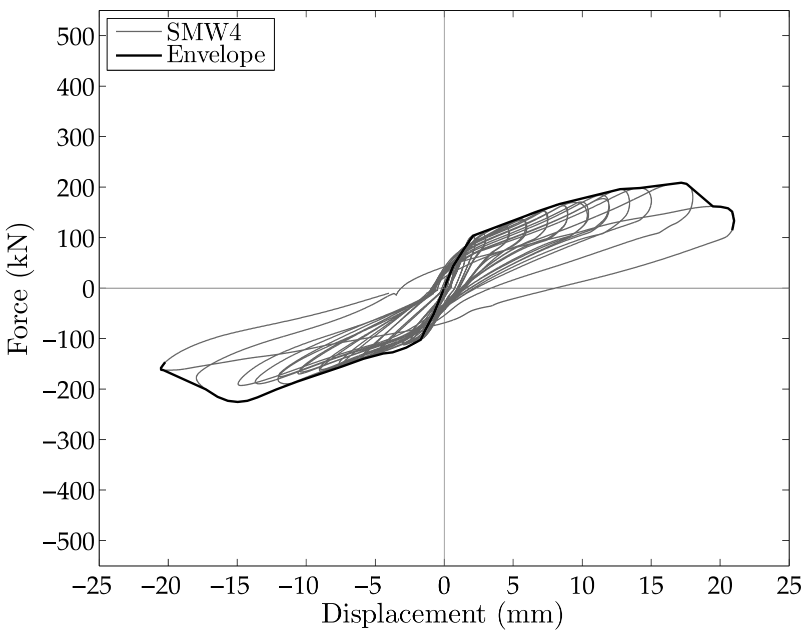

(b) SMW4

Figure 101: Force-displacement hysteresis loops for walls with precompression level $\sigma_0/f_k = 0.17$

Spec.	Dir.	Crack limit			Maximum resistance			Ultimate resistance		
		d_{cr}	H_{cr}	θ_{cr}	d_{Hmax}	H_{max}	θ_{Hmax}	d_{max}	H_{dmax}	θ_{dmax}
	(+/-)	(mm)	(kN)	(%)	(mm)	(kN)	(%)	(mm)	(kN)	(%)
SMW1	+	0.45	207.31	0.02	2.76	483.79	0.15	12.33	188.20	0.68
	-	0.49	258.59	0.03	3.94	527.15	0.22	12.22	304.30	0.67
SMW2	+	0.81	83.28	0.04	8.42	227.18	0.46	15.05	53.80	0.83
	-	0.85	94.89	0.05	8.96	225.14	0.49	15.11	115.60	0.83
SMW3	+	0.68	160.67	0.04	8.29	365.15	0.46	20.95	310.10	1.15
	-	0.72	156.44	0.04	11.83	332.09	0.65	20.95	310.10	1.15
SMW4	+	0.66	43.80	0.04	17.19	208.62	0.94	21.01	133.10	1.15
	-	0.77	51.92	0.04	14.97	225.52	0.82	20.52	157.90	1.13

(a) Test results for positive and negative loading direction

Spec.	Crack limit			Maximum resistance			Ultimate resistance		
	d_{cr}	H_{cr}	θ_{cr}	d_{Hmax}	H_{max}	θ_{Hmax}	d_{max}	H_{dmax}	θ_{dmax}
	(mm)	(kN)	(%)	(mm)	(kN)	(%)	(mm)	(kN)	(%)
SMW1	0.47	232.95	0.03	3.35	505.47	0.18	12.28	246.25	0.67
SMW2	0.83	89.09	0.05	8.69	226.16	0.48	15.08	84.70	0.83
SMW3	0.70	158.56	0.04	10.06	348.62	0.55	20.95	310.10	1.15
SMW4	0.72	47.86	0.04	16.08	217.07	0.88	20.77	145.50	1.14

(b) Averaged test results with respect to loading direction

Table 30: Test results for SMWs: lateral capacity, displacement and rotation angle at limit states

Spec.	σ_0/f_k	H_{cr}/H_{max}	H_{dmax}/H_{max}	$\theta_{cr}/\theta_{Hmax}$	$\theta_{dmax}/\theta_{Hmax}$	$\theta_{dmax}/\theta_{cr}$
SMW1	0.33	0.46	0.49	0.14	3.66	26.12
SMW2	0.33	0.39	0.37	0.10	1.74	18.17
SMW3	0.17	0.45	0.89	0.07	2.08	29.93
SMW4	0.17	0.22	0.67	0.04	1.29	29.04
Mean	/	0.38	0.61	0.09	2.19	25.81
CV(%)	/	25.40	32.22	40.52	40.77	17.95

Table 31: Lateral capacity and deformation capacity for SMWs at characteristic limit states

Spec.	Shear cracking		Maximum capacity	
	τ_{cr}	$f_{t,cr}$	τ_{max}	$f_{t,max}$
	$\left(N/mm^2\right)$	$\left(N/mm^2\right)$	$\left(N/mm^2\right)$	$\left(N/mm^2\right)$
SMW1	0.370	0.247	0.802	0.803
SMW2	0.244	0.120	0.620	0.555
SMW3	0.252	0.203	0.553	0.617
SMW4	0.131	0.068	0.595	0.676
Mean	0.249	0.159	0.643	0.663
CV(%)	33.88	43.73	14.83	13.81

Table 32: Shear and tensile strength of SMWs at cracking limit state and maximum capacity

proportionally dependent on the geometry and inversely proportional to the precompression level. The squat walls showed higher ratios when compared to the tall walls, while the walls with lower precompression level exhibited higher ratio H_{dmax}/H_{max}.
The displacement capacity at all limit states was proportionally dependent on the geometry ratio and the precompression level. The rotation of the walls was about 2 times higher at squat walls if compared to the tall walls and $26-43\,\%$ higher in walls with higher σ_0/f_k.

To compare the results for shear and tensile strength obtained experimentally on the jacketed walls, two limit states, shear cracking and maximum capacity, are presented in Table 32. The tensile strength was calculated according to Eq. 4.1, and by assuming elastic, homogeneous and isotropic behaviour of the strengthened walls. The shear strength was related to the level of compressive stresses and geometry with increasing trend. The tensile strength was estimated to be proportionally related to the level of precompression for all walls except for SMW4. The relation between the shear strength and the tensile strength was found to be directly dependant on the compressive stresses. The relations of the shear strength to the compressive stresses and between the shear and tensile strength are shown in Figure 102.

Poor values for approximation with linear least square regression were obtained in both cases $\left(R^2 = 0.52 \text{ and } R^2 = 0.66\right)$. The coefficient of friction for SMWs found experimentally was 0.2739 which gives characteristic angle of internal friction of $\alpha = 15.32\,^\circ$.

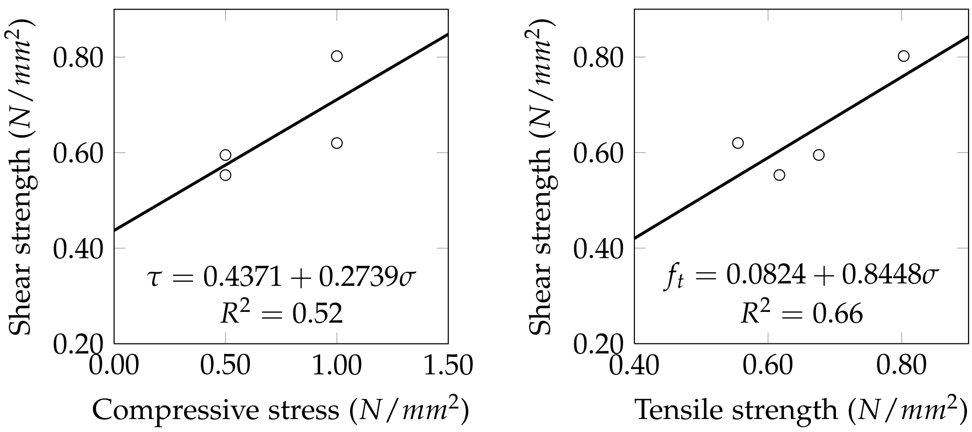

(a) Shear strength vs. compressive stress (b) Shear strength vs. tensile strength

Figure 102: Relations of shear strength to compressive stress and shear strength to tensile strength for SMWs

4.4.3 *Stiffness degradation and energy dissipation capacity*

The parameters for evaluation of the seismic performance of RC jacketed masonry walls were estimated through degradation of stiffness and the capacity for dissipation of input energy.

4.4.3.1 *Stiffness degradation*

Following the procedure shown in subsection 4.3.3, the secant stiffness was calculated for each cycle, see Figure 89. The development of the stiffness degradation with increasing displacement cycles is illustrated in Figure 103. All walls demonstrate similar stiffness degradation with increasing horizontal displacements. The trend of stiffness degradation complies to a power function with no noticeable differences among the walls. SMW2 shows slight deviation from the other walls within the range of $(0.9 - 1.7)$ $d_{max,i}/d_{Hmax}$. This is evident from the force-displacement hysteresis diagram for SMW2 (Figure 100) where imbalance of one hysteresis loop was observed.

Stiffness degradation parameter α_1 and β required with Eq. 4.3 were calculated by regression analysis of the experimental curves for all walls. This analysis resulted in $\alpha_1 = 0.74$ and $\beta = -0.97$ with fine approximation parameter of $R^2 = 0.92$.

4.4.3.2 *Energy dissipation capacity*

Experimental hysteretic loops were used to analyse the behaviour of the jacketed walls due to different geometry and loading conditions. Similarly to unreinforced masonry walls, viscous damping concept has been used to estimate the energy dissipation capacity. The equivalent viscous damping coefficient with zero initial viscous damping was

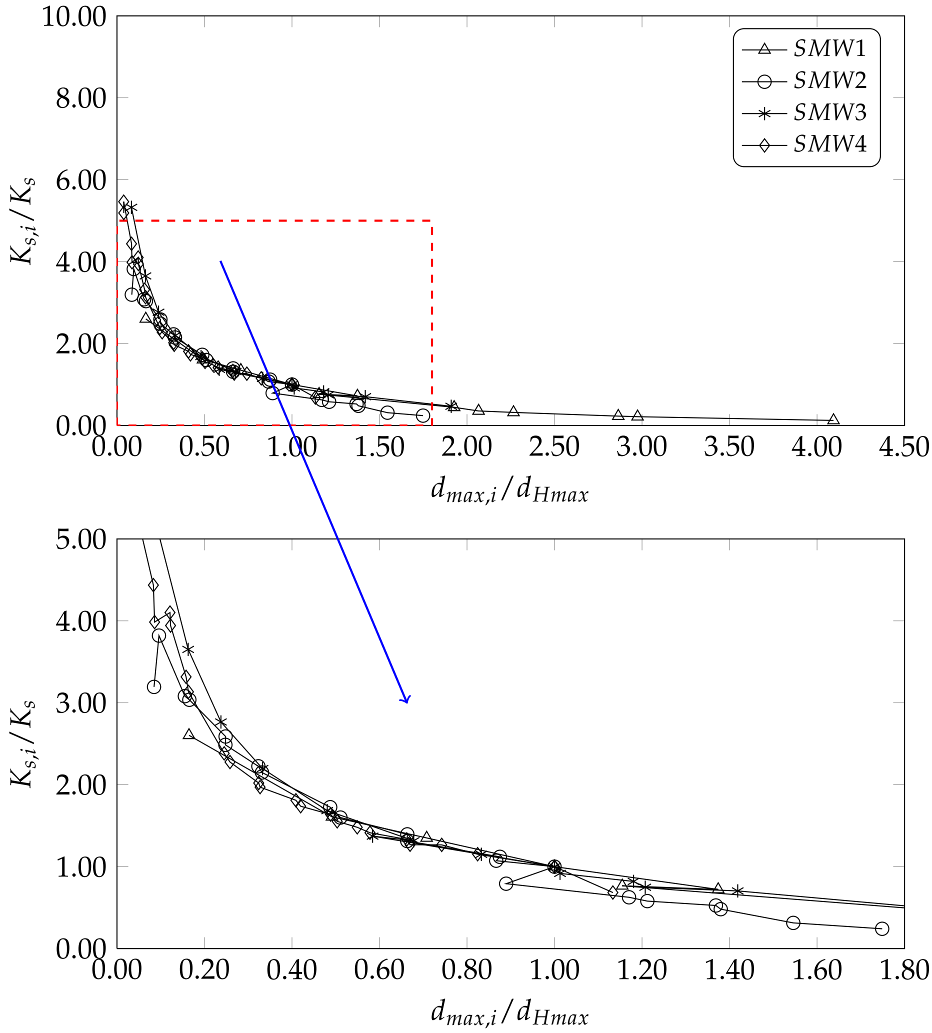

Figure 103: Stiffness degradation for the positive part of the diagrams

assumed. Thus, the energy dissipation capacity is attribute to hysteretic damping, only. The CEVD has been approximated with respect to Eq. 4.7 and Figure 91. The values for the stored potential energy (E_{sto}), dissipated energy (E_{hyst}) and the equivalent viscous damping coefficient (ξ_{eq}) for the identified limit states are shown in Table 33.

All walls demonstrated similar behaviour with respect to the capacity for dissipation of the stored potential energy. It is characterized by lower coefficient of equivalent viscous damping at maximum resistance limit state if compared to the crack limit and ultimate resistance. SMW4 shows deviation from the behaviour of other walls due to its typical bending failure without shear cracks in the masonry. Significantly lower ξ_{eq} than other wall specimen was observed for maximum resistance and ultimate resistance limit states. Figure 104 shows relations of the averaged target displacements and the corresponding dissipated and stored energy for the positive part of the

Spec.	Crack limit				Maximum resistance				Ultimate resistance			
	E_{hyst} $(kNmm)$	E_{Sto} $(kNmm)$	E_{hyst}/E_{Sto}	ξ_{eq} (%)	E_{hyst} $(kNmm)$	E_{Sto} $(kNmm)$	E_{hyst}/E_{Sto}	ξ_{eq} (%)	E_{hyst} $(kNmm)$	E_{Sto} $(kNmm)$	E_{hyst}/E_{Sto}	ξ_{eq} (%)
SMW1	79.04	74.45	1.06	10.39	1142.48	1330.03	0.86	6.84	5754.60	3040.91	1.89	15.06
SMW2	56.55	43.78	1.29	10.28	1384.47	1402.19	0.99	7.86	2141.66	1094.77	1.96	15.06
SMW3	82.85	76.84	1.08	8.81	2399.36	2584.17	0.93	7.39	8313.43	6020.60	1.38	10.99
SMW4	32.40	21.34	1.52	12.08	2899.03	2442.17	1.19	6.23	3354.87	2705.52	1.24	6.23

Table 33: Values of stored energy, dissipated energy and coefficient of equivalent viscous damping for SMWs

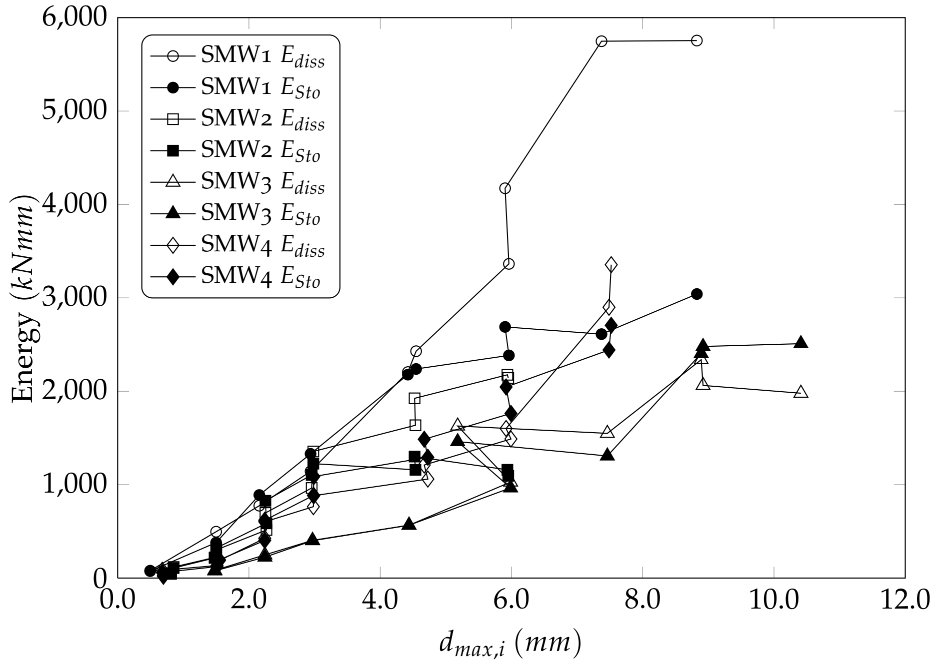

Figure 104: Dissipated and stored potential energy for the positive part of the diagram of SMWs

force-displacement diagrams. The highest energy dissipation capacity was obtained for SMW1, while the lowest for SMW3 and SMW4.

The evolution of the CEVD in the sequential displacement cycles is illustrated in Figure 105. The value of ξ_{eq} varied similarly for all walls within the range of $6 - 12\,\%$ up to maximum displacement of 6.00 mm. After that, a wide scatter in the evolution of the ξ_{eq} was acquired. The average ξ_{eq} estimated for SMWs was 8.8 %.

4.4.4 *Seismic performance of strengthened masonry walls*

For simplified analysis and design, the experimental force-displacement capacity envelopes have been idealised with bilinear curve, as shown in Figure 94. Despite of the obvious inhomogeneity and anisotropic behaviour, RC jacketed walls were considered as elastic, homogeneous and isotropic material for simplicity reasons. To idealise the test results, governing parameters for the identified limit states shown in Table 30 have been used. A summary from the idealisation results for the strengthened masonry walls is presented in Table 34 and Figure 106.

The geometry ratio and the level of precompression have influence on the overall performance of the strengthened walls, and thus on the ultimate force in the idealised bilinear relation of the horizontal force to the horizontal displacement on the top of the wall. As expected, the higher the vertical precompression levels, the higher ultimate forces were obtained. The same remark is valid if the geometry ratio

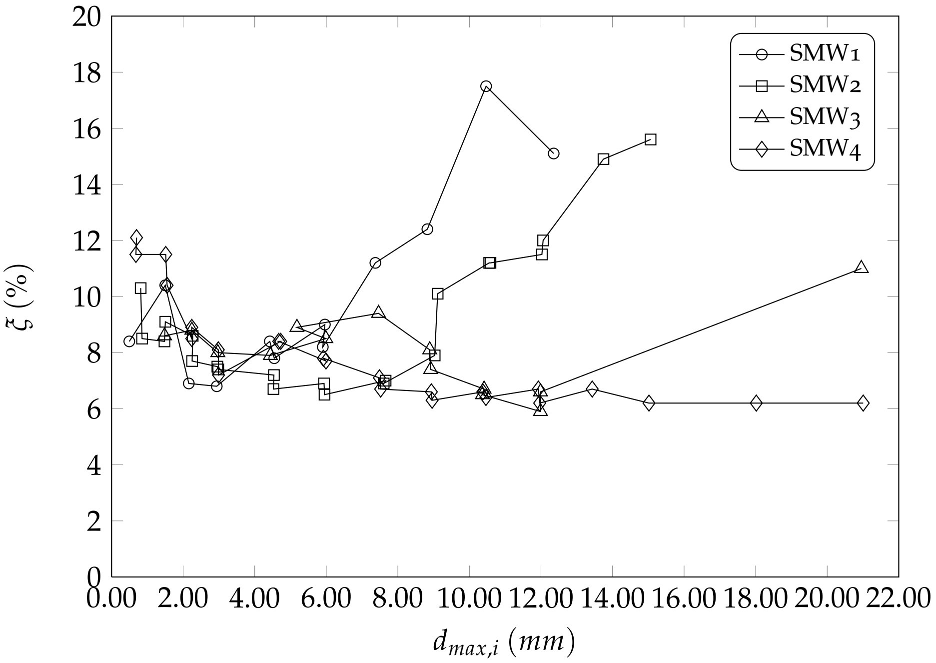

Figure 105: Coefficient of equivalent viscous damping (ξ_{eq}) for the positive part of the diagram of SMWs

Spec.	Dir. (+/-)	d_{cr} (mm)	H_{cr} (kN)	K_e (kN/mm)	H_u (kN)	d_e (mm)	d_u (mm)	θ_u (%)	μ_u
SMW1	+	0.45	207.31	460.69	363.96	0.79	6.04	0.33	7.65
	-	0.49	258.59	527.73	427.59	0.83	6.90	0.38	8.31
SMW2	+	0.81	83.28	102.81	171.65	1.67	9.67	0.53	5.79
	-	0.85	94.89	111.64	179.58	1.68	9.94	0.55	5.92
SMW3	+	0.68	160.67	236.28	326.54	1.38	20.92	1.15	15.14
	-	0.72	156.44	217.28	299.02	1.36	20.53	1.13	15.10
SMW4	+	0.66	43.80	66.36	169.21	2.55	19.26	1.06	7.55
	-	0.77	51.92	67.43	175.83	2.57	18.89	1.04	7.35

Table 34: Summary of obtained results after bilinear idealisation of SMWs

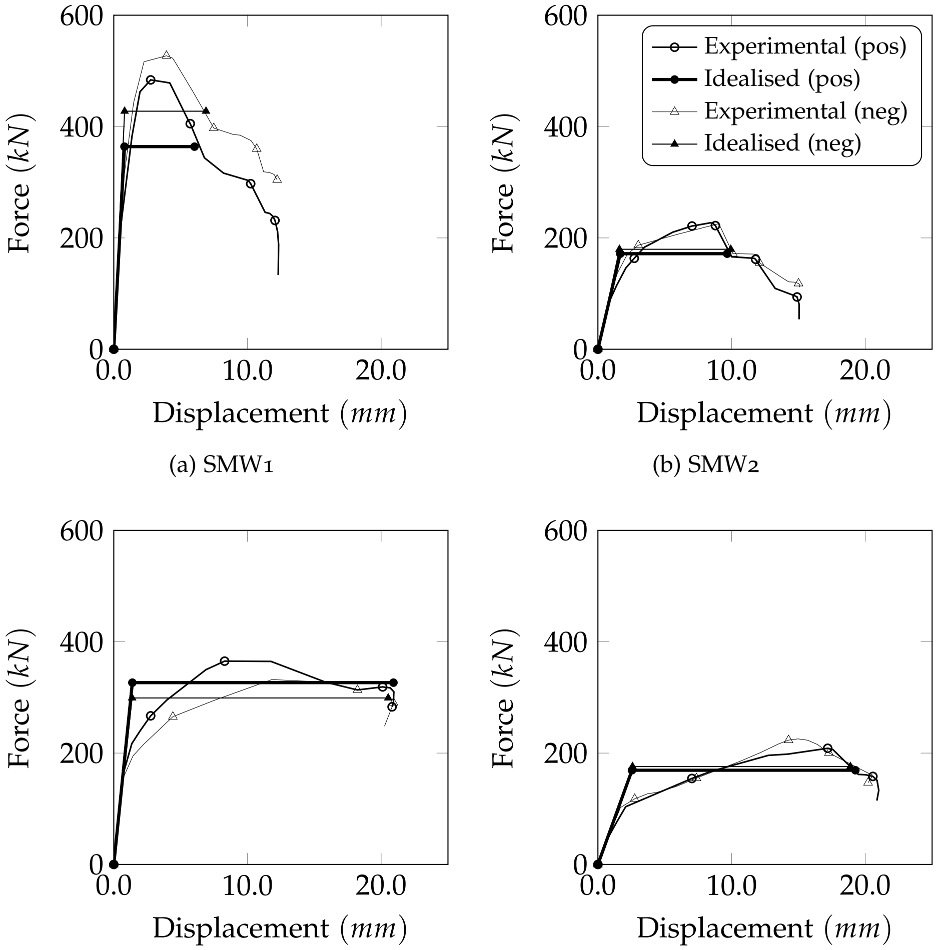

(a) SMW1 (b) SMW2 (c) SMW3 (d) SMW4

Figure 106: Bilinear idealisation of the experimental SMWs walls in positive and negative direction of loading

is compared. The squat walls presented higher ultimate forces than the tall walls. But, if the walls with the same geometry and different precompression levels are compared, an interesting result is revealed. As can be seen from the data in Table 34 the vertical stresses applied on the walls have no significant influence on the ultimate forces. This is more evident for the tall walls SMW2 and SMW4.

Comparison of the deformation capacity of the walls reveals inversely proportional relation to the vertical stresses. The walls subjected to lower vertical stresses showed greater displacements, both in elastic and ultimate limit states. This could be explained with the predominant bending failure mode of the walls, which generates large deformation capacity.

The ultimate ductility factor obtained from the idealisation was within the range $6 - 15$ with an average of $\mu_u = 9$. A correlation of the ductility factor, wall geometry ratio and the precompression level has been

Spec.	Dir. (+/-)	H_u/H_{max} (kN)	K_e (kN/mm)	$K^1_{e,theo}$ (kN/mm)	$K^2_{e,theo}$ (kN/mm)
SMW1	+	0.75	460.69	888.23	405.87
	-	0.81	527.73		
SMW2	+	0.76	102.81	391.77	149.27
	-	0.80	111.64		
SMW3	+	0.89	236.28	888.23	405.87
	-	0.90	217.28		
SMW4	+	0.81	66.36	391.77	149.27
	-	0.78	67.43		

Table 35: Ratio H_u/H_{max} and theoretical effective stiffness for SMWs

found. The results of this study showed that the ductility decreases with increasing vertical stresses and increases for lower ratio for h/L. Since, no recommendations for practical application could be found in the literature, the suggested ultimate ductility factor by Tomaževič [2009a] for reinforced masonry of $\mu_u = 4.0 - 5.0$ could be used.

The average ratio of $H_u/H_{max} = 0.81$ indicates that in case of bilinear idealisation, the horizontal capacity of the strengthened masonry walls should be reduced by 19 % during seismic analysis, see Table 35.
The experimental elastic stiffness has been compared with the theoretical stiffness calculated with Eq. 4.14. In absence of test results, the modulus of elasticity was determined with Eq. 4.18 and the shear modulus was calculated with the expression $G = E/2(1+\nu)$ considering $\nu = 0.15$. Eq. 4.15 was used to calculate the reduced moment of inertia due to evolution of the damage in the walls and to estimate the effective stiffness.

$$E_{SMW} = \frac{E_{UMW} t_{UMW} + 2E_c t_c}{t_w} \tag{4.18}$$

where,

E_{SMW}	modulus of elasticity for strengthened masonry
E_{UMW}	modulus of elasticity for unreinforced masonry
E_c	modulus of elasticity of concrete ($E_c = 31500\,N/mm^2$)
t_{UMW}	thickness of masonry wall
t_c	thickness of concrete jackets
t_W	total thickness of strengthened wall

The results presented in Table 35 show that both theoretical approaches overestimate the effective stiffness determined from the test results. By using the reduced moment of inertia, good correlation with

Spec.	Dir.	Experimental	
		G_{test}	G_{test}/E_{SMW}
	(+/-)	(N/mm^2)	
SMW1	+	1740.02	0.21
	-	2019.54	0.24
SMW2	+	679.21	0.08
	-	744.20	0.09
SMW3	+	855.14	0.10
	-	783.60	0.09
SMW4	+	422.80	0.05
	-	430.07	0.05

Table 36: Correlation between the experimentally obtained and recommended shear modulus of strengthened masonry

the test results was obtained for the walls loaded with $\sigma_0/f_k = 1.0$. This study confirms that the stiffness is related to the geometry and the level of vertical stresses acting on the wall.

To associate the shear modulus of strengthened masonry walls to the elastic modulus, the Eq. 4.17 was used. Table 36 illustrates the estimated shear modulus and its relation to the modulus of elasticity calculated as $E_{SMW} = 8415.19\,N/mm^2$. The actual values of the ratio G_{test}/E_{SMW} are in the range of $5-24\,\%$ of the modulus of elasticity. Thus, for practical applications it is proposed to use the calculated average value from the tests $G = 0.11E$.

4.5 COMPARISON OF THE BEHAVIOUR OF STRENGTHENED AND UNREINFORCED MASONRY WALLS

The effects of the strengthening intervention on the behaviour of masonry walls have been compared to the in-plane seismic behaviour of the unreinforced brick masonry walls. First, a comparison of the obtained force-displacement hysteresis loops is presented, followed by analysis of the effects in terms of lateral capacity, lateral deformation, stiffness degradation and energy dissipation capacity.

Significant improvement of the shear capacity of SMWs compared to UMWs was achieved, see Figure 107. The maximum forces observed at the strengthened specimens were higher than the corresponding forces obtained in the unreinforced specimens within the range of $123-204\,\%$, see Table 37. The same effects were noticed in the other two limit states. The highest effect of the strengthening to the lateral capacity was obtained at the tall wall loaded with moderate level of vertical stresses $\sigma_0 = 0.5\,N/mm^2$ (SMW4).

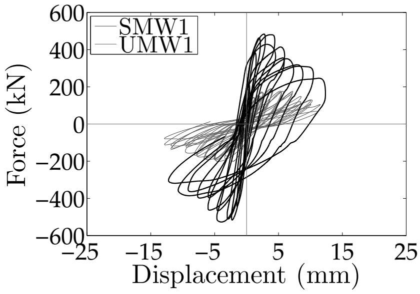

(a) UMW1-SMW1

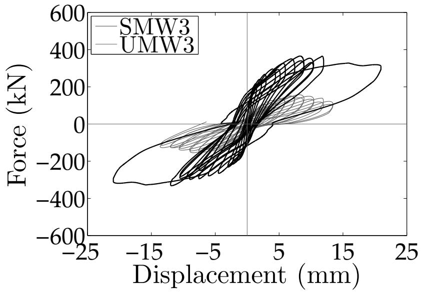

(b) UMW3-SMW3

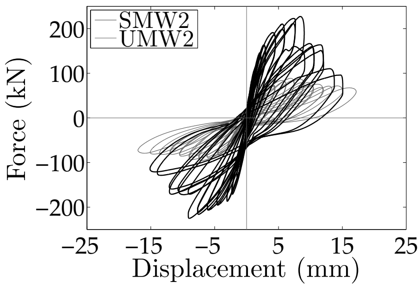

(c) UMW2-SMW2

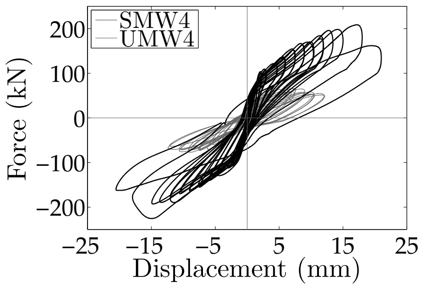

(d) UMW4-SMW4

Figure 107: Comparison of force-displacement hysteresis loops of UMWs and SMWs

The deformation capacity in the ultimate limit state of the strengthened walls was increased with significant improvement in the walls loaded with $\sigma_0 = 0.5\,{}^{N}/_{\mathrm{mm}^2}$. One unanticipated finding was that the deformation capacity of the walls loaded with high vertical stresses was not improved. Moreover, for the tall wall SMW2 it was decreased for about 5 %, although positive effect was obtained for the other limit states. The strengthened walls presented higher effective stiffnesses than the related unreinforced walls. Their relation was obtained within a range of $97 - 186\,\%$. Except in SMW4, the effect of strengthening gave similar increase in the stiffness. It is evident from the Table 37 that the stiffness was almost equally increased for squat walls, while the tall ones demonstrated dependence on the geometry aspect.

The geometry configuration shows influence on the shear behaviour of the strengthened walls. The tall walls exhibited higher maximum capacity if loaded with moderate vertical stresses. The effectiveness of the strengthening method is more significant when applied on squat walls subjected to high vertical stresses. With respect to the deformation capacity, the strengthening method is more effective on walls loaded with low vertical stresses and any geometry configuration. In general, the results from the tests showed that the strengthening method leads to a significant improvement in the shear resistance of the jacketed walls.

The results of this study indicate very similar stiffness degradation of unreinforced and strengthened masonry walls. The stiffness degrad-

Spec.	Crack limit			Maximum resistance			Ultimate resistance			
	d_{cr}	H_{cr}	θ_{cr}	d_{Hmax}	H_{max}	θ_{Hmax}	d_{max}	H_{dmax}	θ_{dmax}	K_e
	(%)	(%)	(%)	(%)	(%)	(%)	(%)	(%)	(%)	(%)
SMW1/UMW1	-20.3	126.3	0.0	-35.6	167.3	-37.9	1.4	125.8	0.0	181.9
SMW2/UMW2	48.2	289.7	66.7	25.4	145.7	26.3	-4.9	15.6	-4.6	163.6
SMW3/UMW3	-6.7	167.7	0.0	21.4	123.7	19.6	59.8	181.5	59.7	186.3
SMW4/UMW4	-4.0	86.7	0.0	101.0	204.2	100.0	78.0	153.2	78.1	97.1

Table 37: Comparison of the force-deformation capacity on averaged test results (positive and negative loading direction)

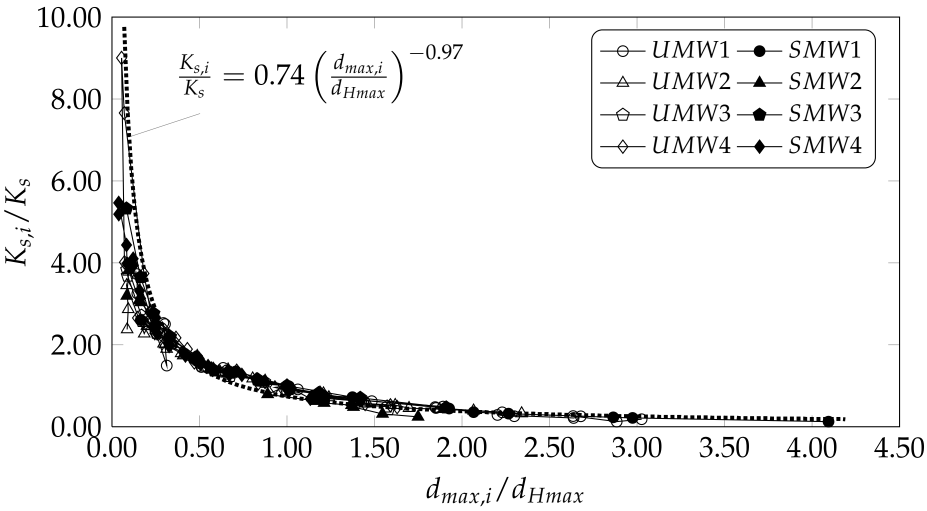

Figure 108: Comparison of stiffness degradation for positive part of the diagrams

ation was found to follow a power function, given by Eq. 4.3. A plot of the evolution of the stiffness with increasing displacements and the obtained power function is illustrated in Figure 108.

The coefficient of equivalent viscous damping (ξ_{eq}) showed wide scatter. It is interesting to note that in the eight walls tested in this study, the unreinforced walls generally demonstrated higher values for ξ_{eq}. The average ξ_{eq} for the UMWs was 13.1 %, while the strengthened walls showed 8.8 %. A decrease in the damping of 33 % was obtained. The damping of the strengthened walls is lower due to the failure mode obtained in contrast to the damping values of the unreinforced walls. An increase of damping could be obtained if the vertical reinforcements is anchored to the top and bottom beams. In such a way, the ductility of the reinforcement will be fully utilized as well as the ductility of the walls can be increased. The strengthened walls SMW1 and SMW2 showed higher values in comparison with the correspond-

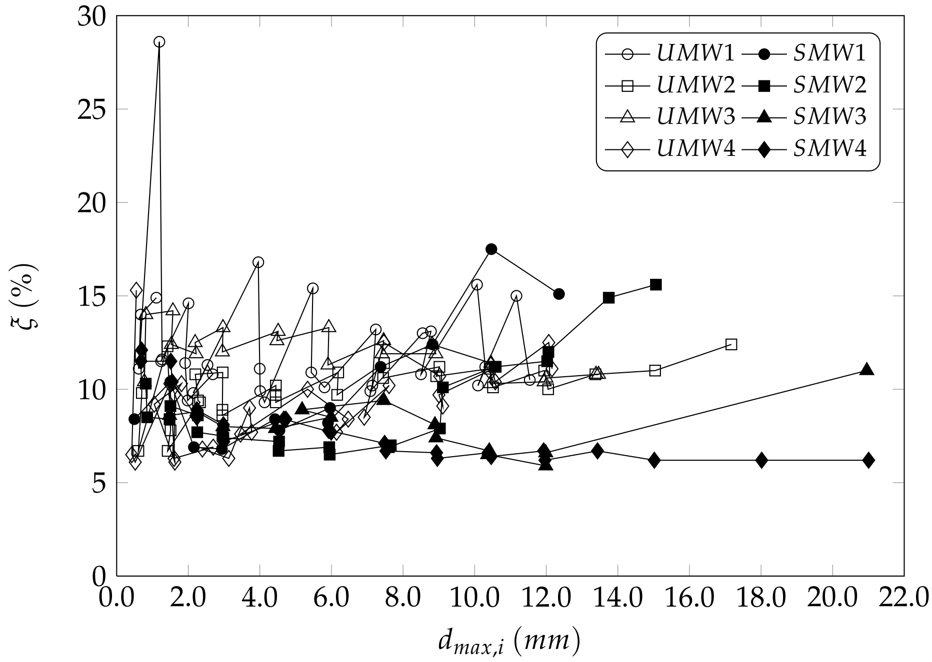

Figure 109: Comparison of coefficient of equivalent viscous damping (ξ_{eg}) for positive part of the diagrams

ing unreinforced walls only after displacement cycles greater than 9 mm, as illustrated in Figure 109 .

The bilinear idealisation of the experimental results revealed interesting effects related to the ultimate ductility factor (μ_u). The data presented graphically in Figure 110 revealed higher ductility of unreinforced walls loaded with vertical stress of $\sigma_0 = 1.0\,\mathrm{N/mm^2}$ than the strengthened walls. The ductility of the squat wall loaded with vertical stress of $\sigma_0 = 0.5\,\mathrm{N/mm^2}$ was dramatically increased, while the tall wall showed similar ductility factor for both materials.

Figure 111 compares the results obtained from the bilinear idealisation of the experimental force-displacement envelope curves. From

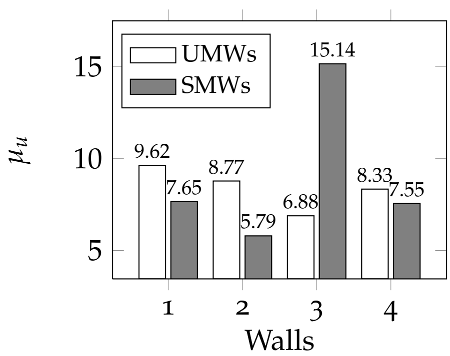

(a) Positive part of the diagrams

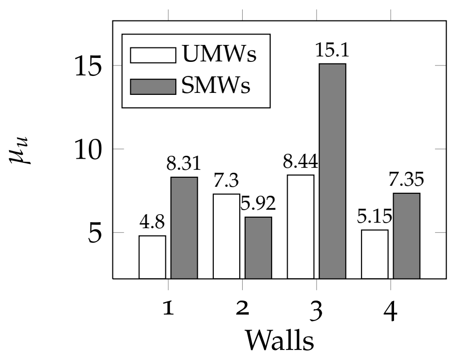

(b) Negative part of the diagrams

Figure 110: Comparison of the ultimate ductility factor (μ_u)

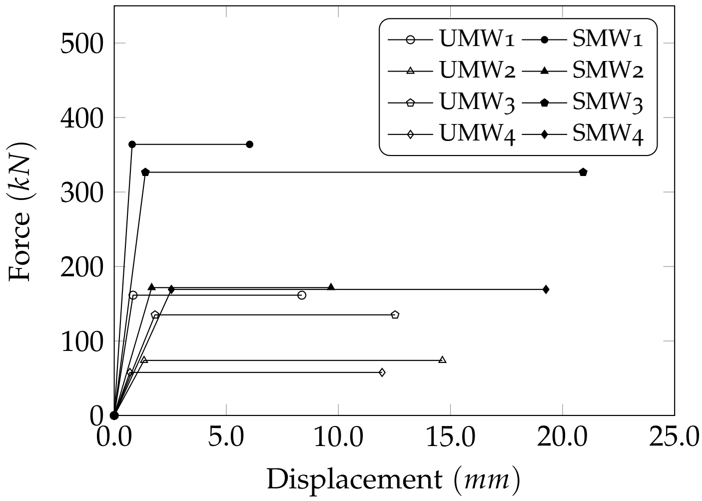

(a) Positive part of the diagrams

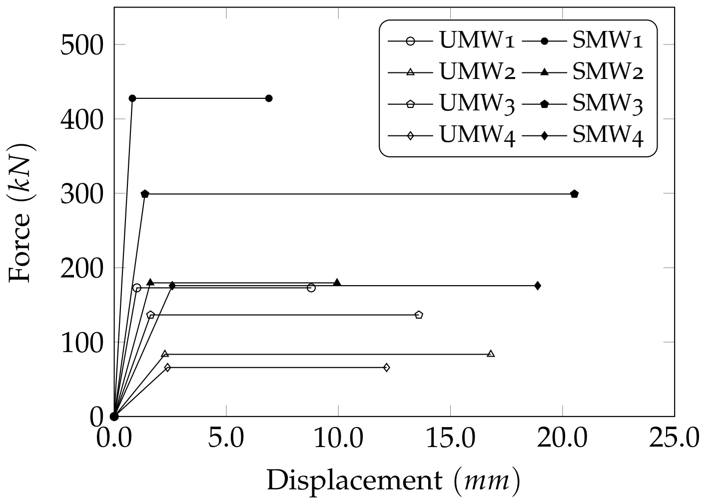

(b) Negative part of the diagrams

Figure 111: Comparison of the idealised force-displacement curves

the graph it can be seen that the strengthening improves the lateral capacity of the walls. The deformation capacity of the walls is not proportionally improved for all walls. Evidently, the precompression level has significant influence on the ultimate displacements, yielding larger displacements at unreinforced walls loaded with high level of vertical stresses than the related strengthened walls. The strengthened walls loaded with moderate level of vertical stresses exhibited higher ultimate displacements than the unreinforced walls.

4.6 SUMMARY AND CONCLUSIONS

This dissertation has investigated the in-plane shear behaviour of unreinforced and strengthened masonry walls subjected to constant vertical stresses and horizontal cyclic loads. Two geometry aspect ratios and two vertical load levels have been varied on masonry wall specimens. In total, four unreinforced clay brick masonry walls have been tested in laboratory on a steel testing frame. Correspondingly, strengthened masonry walls with double sided RC jackets have been subjected to the same testing procedures applied to the unreinforced walls. The aim of the experimental study was to analyse and study the differences in the lateral capacity and deformation of the walls, as well as to find out the stiffness degradation relations and energy dissipation capacity. For practical applications, the experimental curves have been idealised with bilinear relations with three governing parameters, elastic stiffness (K_e), displacement at elastic limit (d_e) and ultimate displacement (d_u). Some of the major findings from this study are outlined in the following paragraphs.

A. This study has found that the tested unreinforced masonry walls within these investigations failed with predominant shear failure modes, characterised by diagonally oriented cracks in the bricks, passing through the bricks or in the brick-mortar interface. The strengthened walls failed with bending failure modes and appearance of cracks mainly in the bottom parts of the concrete jackets and separation of the jackets from the masonry. The masonry encased with the jackets showed diagonal cracks in the ultimate limit state. The change of the failure mode has significant influence on the seismic behaviour of the strengthened walls, because bending failure is desired failure mode with respect to the shear failure.

B. The test results allowed clear identification of three characteristic limit states: crack limit, maximum resistance and ultimate limit. These limit states have been used to compare the behaviour of the walls through different stages of damage evolution.

C. The cracking pattern for the UMWs depends on the geometry aspect ratio. The squat walls $(h/l = 0.7)$ failed with mainly vertically oriented cracks, while the tall walls $(h/l = 1.2)$ showed typical diagonal cracks. The level of the vertical stresses influence the cracking in the masonry encased by the jackets. SMWs loaded with high level of vertical stresses, $\sigma_0 = 1.0\,N/mm^2$, presented cracks in the masonry as well as on the outer concrete surfaces. All strengthened walls showed separation of the jackets after exceeding the splitting strength of the bricks.

D. The tested walls loaded with high level of vertical stresses exhibited higher capacity, but the ultimate displacements have been decreased. In this study, the squat walls showed higher load capacity than the tall walls, with a ratio of the ultimate load to the maximum load dependent on the geometry and precompression levels.

E. The calculated average shear strength of the unreinforced walls at maximum resistance was $\tau_{max} = 0.249\,N/\mathrm{mm}^2$ with tensile strength $f_{t,max} = 0.158\,N/\mathrm{mm}^2$, while the strengthened walls presented $\tau_{max} = 0.643\,N/\mathrm{mm}^2$ and $f_{t,max} = 0.663\,N/\mathrm{mm}^2$. The strengthening method gave improvement in the mechanical properties of the walls.

F. The findings of this study suggest that the ratio of the ultimate load to the maximum load (H_{dmax}/H_{max}) for both materials was similar. The observed mean ratio at unreinforced walls was 0.72, while for strengthened walls ratio of 0.61 was found. It denotes that the failure of the walls happens closely after reaching the maximum capacity, within a range of $30 - 40\,\%$ from the maximum horizontal load.

G. Similar findings for both materials were obtained with regards to the ratio of the rotation at ultimate state to the rotation at cracking limit state $(\theta_{dmax}/\theta_{cr})$. The mean value for all UMWs was in the range of 22.00, while for SMWs it was about 26.00. It indicates nonlinear behaviour of the material from the initial state until the failure of the specimens.

H. One of the more significant findings to emerge from this study is that the stiffness degradation of all walls follows a power function. Identical parameters of the power function were discovered, $\alpha_1 = 0.74$ and $\beta = -0.97$. Thus, the identification of the stiffness degradation can be used for numerical or analytical modelling of the behaviour of masonry walls subjected to cyclic loads and for seismic performance studies.

I. The capacity for dissipation of the input energy was estimated from the force-displacement hysteresis curves. It was evaluated through the coefficient of equivalent viscous damping by taking zero the initial viscous damping in the elastic range. The obtained value of ξ_{eq} in average was 13.1 % for UMWs and 8.8 % for SMWs, indicating decrease of 33 %.

J. Theoretical stiffness (K_e) calculated on the basis of the elastic theory, largely overestimates the experimentally obtained stiffness. Both, uncracked and cracked sections were considered for calculation of the K_e.

K. On the basis of the experimental results and the elastic theory, the ratio of the shear modulus to elastic modulus was calculated. The G/E ratio for UMWs has been found equal to 0.13. Recommended shear modulus of $G = 0.4E$ given in Eurocode 6 [2005] is valid if the compressive loading is predominant one. Similarly, the ratio of G/E for SMWs was 0.11. Therefore, the present study confirms previous findings and contributes to additional evidence that suggests that lower values for G/E should be applied for practical applications, rather than those suggested in the codes.

L. For simplification and practical application in seismic capacity verification, the experimental results were idealised with bilinear relations of force to displacement. The findings of this study confirm larger experimental results for the ultimate ductility factor than those given in the literature recommendations. The mean ductility for UMWs was $\mu_u = 7.0$ and $\mu_u = 9.0$ for SMWs. These values are approximately 2 times higher than suggested by Tomaževič [2009a].

Finally, a number of important limitations in the experimental program need to be considered. First, due to limited budget for testing, only a small number of variable parameters were investigated. The most important limitation lies in the fact that to have statistically significant results, at least three specimens should be tested with same material, boundary, geometry and loading conditions. Nevertheless, the findings in this study confirm that the strengthening method improves the lateral capacity of the walls and thus contributes in achieving proper in-plane strength for seismic verification of masonry buildings.

Part III

ANALYTICAL RESEARCH

Available analytical models in the literature for unreinforced and reinforced masonry walls with respect to the failure modes are compared with the experimental results. A numerical simulation by using static nonlinear analysis and capacity spectrum method have been used to describe and study the behaviour of an existing masonry building.

5 ANALYTICAL EVALUATION OF SEISMIC BEHAVIOUR OF MASONRY WALLS

5.1 INTRODUCTION

This chapter investigates current and code defined design procedures for in-plane shear and bending in masonry walls. Analytical models and procedures considered in section 2.6, include shear capacity design and bending design procedures in the design codes PIOVSP [1981], Eurocode 6 [2005], CSA S304.1-04 [2004], provisions given by Tomaževič [1999] and proposed design equations developed in FEDRA [2003]. Predicted shear and bending resistance of unreinforced and reinforced masonry walls were compared with the lateral capacity of the walls obtained from the experimental investigations (chapter 4). Bending resistance was included due to mixed failure modes of the strengthened walls.

Design provisions for masonry structures exists in many building standards in the world. They consider differences in unit format, mortar type and quality, different assumptions for structural behaviour under shear and bending loads, directions of loading and safety factor verification concepts. Moreover, the standards treat unreinforced, confined and reinforced masonry with separate provisions. There are no available design provisions for strengthened masonry with RC jackets, and only some building recommendations can be found.

The analytical models and code provisions used today and found in the literature describe different failure mechanisms and determine limit capacity of the masonry walls under combination of axial and shear loading. Generally, simple idealization of the limit strength domain is used. Their accuracy is connected to the choice of reference stresses, shear, normal or main principal stresses and their combinations. Definition of the reference and critical stresses in a masonry cross-section can be considered related to masonry as composite material or its constituents. This is the main reason to incorporate different mechanical properties of the structural walls in different analytical models. Most design codes use the original models, others modify them or include additional parameters.

Having in mind that all tests were executed in laboratory conditions, the evaluation of the efficiency of a particular model or provision was made by comparing the calculated lateral resistance $\left(H_{x,y}\right)$ for each wall with the maximum experimental resistance (H_{max}). This was executed by neglecting the safety factors given in the codes. The subscripts in the calculated resistances were defined with the following

Spec.	Dir.	Test	Tomaževič [1999]		
		H_{max}	$H_{u,s}$	$H_{u,f}$	$H_{u,sl}$
	(+/-)	(kN)	(kN)	(kN)	(kN)
UMW1	+	189.14	143.11	533.61	252.00
	-	189.06			
UMW2	+	88.54	82.73	179.11	146.00
	-	95.57			
UMW3	+	157.35	141.71	351.48	126.00
	-	154.37			
UMW4	+	65.46	81.68	117.98	73.00
	-	77.23			

Table 38: Theoretical maximum forces for UMWs according to Tomaževič [1999]

meaning: x denotes type of material (u−unreinforced, str−strengthened (reinforced)), and y stands for type of failure mechanisms (s−shear, f−flexure, and sl−sliding shear).

5.2 LATERAL RESISTANCE OF UNREINFORCED MASONRY WALLS

A comparison between the lateral resistance obtained through tests and the lateral strength given by analytical formulation is given. Detailed description of the models was given in section 2.6, and only the main results are discussed here. The main test results regarding material properties given in chapter 3 are taken into account.

5.2.1 *Tomaževič [1999]*

The formulation for unreinforced masonry walls suggested by Tomaževič [1999] and based on Turnšek and Čačovič [1971] theory have been applied. Shear, bending and sliding shear failure mechanisms have been considered to test the effectiveness of the predicted values. The summary of the calculated lateral resistance with predominant shear, flexural and sliding shear forces are summarized in Table 38.

It is apparent from this table that the experimental lateral capacity is very near to the predicted shear resistance. From the observed failure modes during the tests, the failure of the walls has been determined to result from presence of diagonal shear cracks. The predicted flexural and sliding shear resistances are far from the experimental capacity, although for UMW3 and UMW4 the predicted sliding shear resistance is close to the experimental one. In general, the theoretical flexural res-

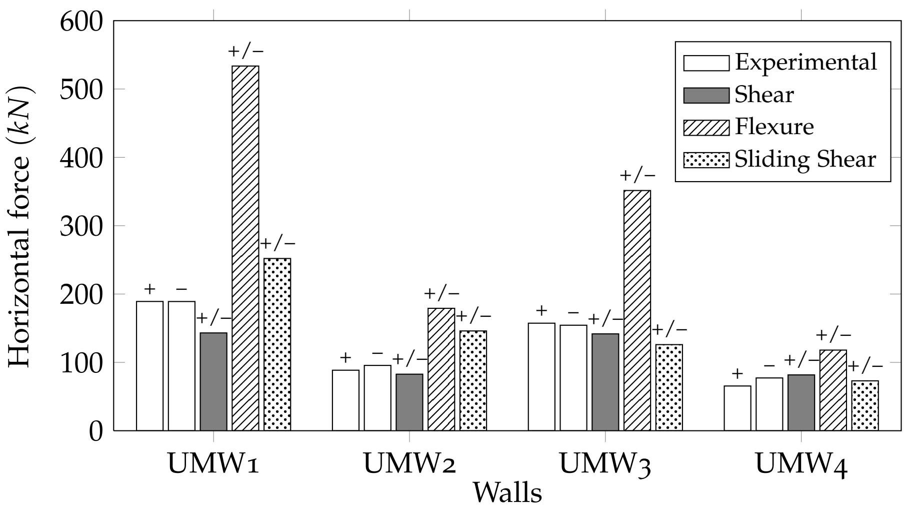

Figure 112: Comparison between experimental and theoretical resistance for UMWs according to Tomaževič [1999]

Spec.	Test	Tomaževič [1999]		
	$H_{max,mean}$ (kN)	$H_{max,mean}/H_{u,s}$ (%)	$H_{max,mean}/H_{u,f}$ (%)	$H_{max,mean}/H_{u,sl}$ (%)
UMW1	189.10	-24.32	182.19	33.26
UMW2	92.06	-4.93	46.04	28.53
UMW3	155.86	-7.48	103.45	-15.79
UMW4	71.34	5.47	24.66	0.87

Table 39: Difference between the experimental and predicted capacity for UMWs according to Tomaževič [1999]

istances presented higher values then the values obtained by the tests, see Figure 112. The predicted sliding shear resistance for the walls loaded with $\sigma_0 = 1.0\,{}^{N}/_{\mathrm{mm}^2}$ are higher then the experimental, and for the walls loaded with $\sigma_0 = 0.5\,{}^{N}/_{\mathrm{mm}^2}$ are closer to the experimental, although the cracking pattern for those walls indicated diagonal shear failure.

The percentage difference between the mean experimental lateral capacity for both loading directions and the predicted resistance for the characteristic failure modes is presented in Table 39.

5.2.2 *Eurocode 6 [2005]/DIN Eurocode 6/NA [2011]*

The design models for verification of unreinforced walls subjected to shear and bending loading proposed in Eurocode 6 [2005] was applied to all tested walls. Without taking into account any national annex (NA) of the country in use, the code suggests verification of the shear

Spec.	Dir.	Test	DIN Eurocode 6/NA [2011]		
		H_{max}	$H_{u,s}$	$H_{u,f}$	$H_{u,sl}$
	(+/-)	(kN)	(kN)	(kN)	(kN)
UMW1	+	189.14	212.15	416.33	252.00
	-	189.06			
UMW2	+	88.54	122.91	139.75	146.00
	-	95.57			
UMW3	+	157.35	170.10	271.83	126.00
	-	154.37			
UMW4	+	65.46	98.55	91.24	73.00
	-	77.23			

Table 40: Theoretical maximum forces for UMWs according to DIN Eurocode 6/NA [2011]

behaviour by considering sliding shear behaviour of masonry, only. Other failure modes regarding shear are not included, but are left to the national authorities for the country in use to decide upon. Since at the moment, Macedonia has not yet accepted the Eurocodes as national codes, and considering the failure mechanisms observed in the tests, in this subsection shear diagonal failure mechanisms are considered through the recommendations given in DIN Eurocode 6/NA [2011]. The code allows calculation of the shear resistance by taking into account the characteristic shear strength of masonry calculated as the lesser value between the sliding shear and the diagonal shear strength, according to Eqs. 5.1a to 5.1c.

$$f_{vk} = min\left\{f_{vlt1}; f_{vlt2}\right\} \tag{5.1a}$$

$$f_{vlt1} = f_{vk0} + 0.4\sigma_0 \tag{5.1b}$$

$$f_{vlt2} = 0.45 f_{bt,cal}\sqrt{1 + \frac{\sigma_0}{f_{bt,cal}}} \tag{5.1c}$$

where,

$f_{bt,cal}$ calculation tensile strength of masonry units
$f_{bt,cal} = 0.040\frac{f_{st}}{1.25}$ for solid bricks

f_{st} average compressive strength of masonry units in relation to compressive strength class (given in DIN Eurocode 6/NA [2011], Table NA.5)

The other important issue regarding prediction of the shear resistance of unreinforced masonry walls according to Eurocode 6 [2005] is the length of the compressed part of the wall (l_c), ignoring the

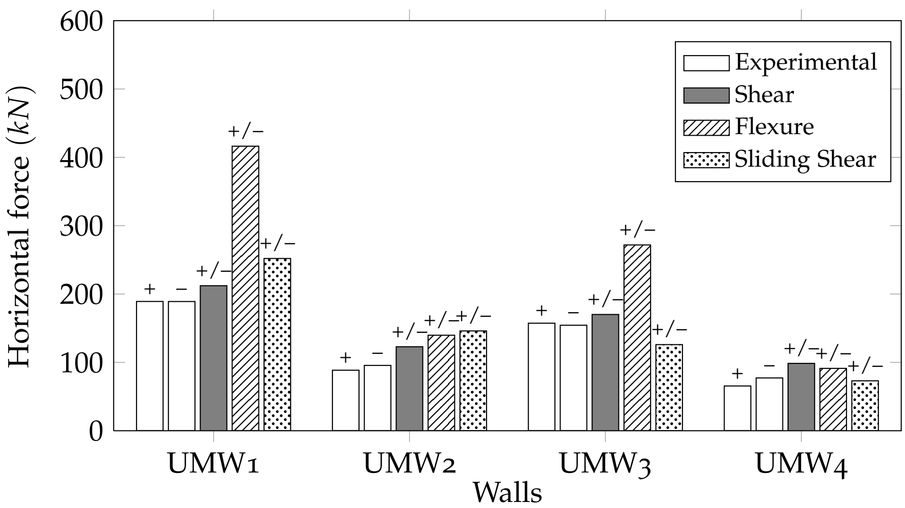

Figure 113: Comparison between experimental and theoretical resistance for UMWs according to DIN Eurocode 6/NA [2011]

part of the wall that is in tension, see section 2.19. The length of the compressed part depends on the current stress state present in the wall and could be determined only if the vertical and the horizontal loads are known. For this research it was decided to adopt l_c equal to the length of the wall. The values of the shear, flexural and sliding shear strength for $l_c = L$ are summarized in Table 40.

From the results presented in Table 40 we can see that the predicted shear resistance calculated through shear strength considering diagonal shear gave closest values to the observed test values. The values for flexural and sliding shear resistances are higher than those obtained from the tests. Generally, the predicted shear and flexural resistances were higher than the experimental values. The sliding shear was obtained with the same values as in the previous model, because they use the same definition for this failure mode. The models presented logical results considering the observed failure modes. For verification purposes the smallest value of $H_{u,s}$, $H_{u,f}$ and $H_{u,sl}$ is usually adopted as governing parameter which defines the possible failure mode and corresponding wall resistance.

The percentage difference between the mean experimental lateral capacity and the predicted resistance for the characteristic failure modes is presented in Table 41. Interestingly, the calculated percentage difference for flexural resistance of specimen UMW4 was closer to the experimental capacity than the value calculated for the shear resistance.

To check the ability of the suggested model to predict the shear resistance with a known stress state, the length of the compressed part of the wall was calculated with respect to the obtained experimental horizontal loads. In addition, the length of the compressed part of the wall was monitored and controlled to be less than the initial

Spec.	Test	DIN Eurocode 6/NA [2011]		
	$H_{max,mean}$ (kN)	$H_{max,mean}/H_{u,s}$ (%)	$H_{max,mean}/H_{u,f}$ (%)	$H_{max,mean}/H_{u,sl}$ (%)
UMW1	189.10	12.19	120.17	33.26
UMW2	92.06	16.32	25.22	28.53
UMW3	155.86	7.53	61.33	-15.79
UMW4	71.34	14.39	10.52	0.87

Table 41: Difference between the experimental and the predicted capacity for UMWs according to DIN Eurocode 6/NA [2011]

length of the wall. If higher length was obtained, then the resistance was calculated with the initial wall length. The obtained results are summarized in Table 42.

There was significant positive effect in the evaluation of the shear resistance by taking into account the compressed length of the wall. This was effective only for walls loaded with $\sigma_0 = 0.5\,N/\mathrm{mm}^2$, the walls from the other series gave higher values for l_c than the original wall length. On the other hand, the difference between the values obtained from the tests and the calculated values for sliding shear resistance was increased.

5.2.3 *CSA S304.1-04 [2004]*

All provisions for unreinforced walls provided in the code are considered for calculation of the predicted wall resistance. The provisions take into account the type of wall (squat or flexure wall), and specify maximum shear resistance $(H_{u,s-max})$ given with Eqs. 5.2a to 5.2b.

$$H_{u,s-max} = 0.4\phi_m \sqrt{f'_m} t l \gamma_g \text{ for flexure walls} \tag{5.2a}$$

$$H_{u,s-max} = 0.4\phi_m \sqrt{f'_m} t l \gamma_g \left(2 - \frac{h}{l}\right) \text{ for squat walls} \tag{5.2b}$$

Also, the code allows calculation of the sliding shear resistance in two cases, between masonry units and between the supports and the first course of the masonry units. The corresponding resistances $(H_{u,sl,wall})$ and $(H_{u,sl,supp})$ were calculated and are presented in Table 43 together with the other resistances. Material resistance factor for masonry was $\phi_m = 0.6$ and the factor taking into account fully grouted masonry $\gamma_g = 1.0$. It is interesting to see that the calculated flexural resistance for all walls is the lowest resistance between all considered failure modes, see Figure 114. It would result in wrong prediction of the possible failure mode of the actual walls.

Spec.	Dir.	Test	DIN Eurocode 6/NA [2011]			
			$l_c = L$		$l_c = 3\left(\frac{L}{2} - \frac{H_{max}\alpha h}{N}\right)$	
		H_{max}	$H_{u,s}$	$H_{u,sl}$	$H_{u,s}$	$H_{u,sl}$
	(+/-)	(kN)	(kN)	(kN)	(kN)	(kN)
UMW1	+	189.14	212.15	252.00	212.15	252.00
	-	189.06				
UMW2	+	88.54	122.91	146.00	122.91	146.00
	-	95.57				
UMW3	+	157.35	170.10	126.00	163.10	120.81
	-	154.37			164.84	122.11
UMW4	+	65.46	98.55	73.00	81.73	60.54
	-	77.23			69.84	51.74

Table 42: Comparison of the theoretical maximum forces according to the tests, DIN Eurocode 6/NA [2011] for different lengths of the compressed part of the wall

Spec.	Dir.	Test	CSA S304.1-04 [2004]			
		H_{max}	$H_{u,s}$	$H_{u,f}$	$H_{u,sl,wall}$	$H_{u,sl,supp}$
	(+/-)	(kN)	(kN)	(kN)	(kN)	(kN)
UMW1	+	189.14	177.46	118.92	483.28	378.00
	-	189.06				
UMW2	+	88.54	98.07	39.92	279.99	219.00
	-	95.57				
UMW3	+	157.35	134.93	116.31	294.28	189.00
	-	154.37				
UMW4	+	65.46	73.43	39.04	170.49	109.50
	-	77.23				

Table 43: Theoretical maximum forces for UMWs according to CSA S304.1-04 [2004]

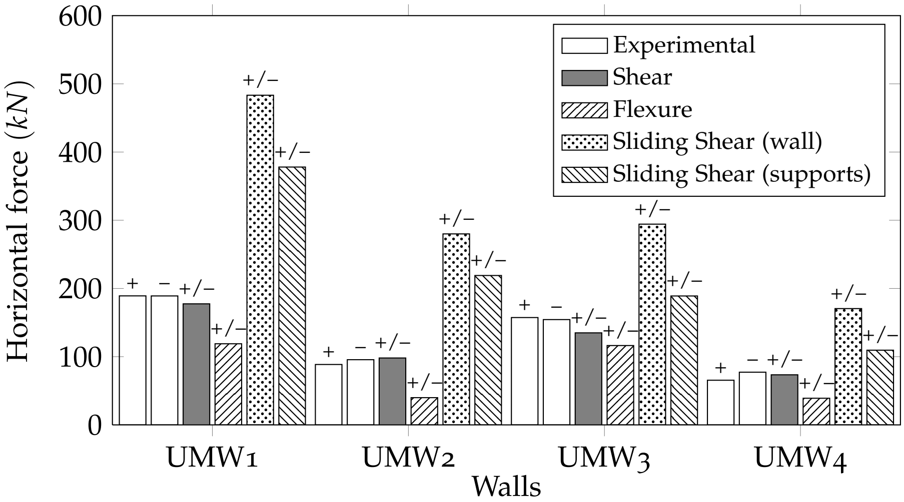

Figure 114: Comparison between experimental and theoretical resistance for UMWs according to CSA S304.1-04 [2004]

From the results presented in the table, it is obvious that the equations that predict the shear resistance by taking into account the diagonal tensile failure give the best results. Also, the shear resistance is better predicted for the walls with lower precompression load ($\sigma_0 = 0.5\,{}^{N}/{}_{\mathrm{mm}^2}$). The other models which predicted flexural resistance and sliding shear resistance are far from the experimental results. The percentage difference of the predicted resistances to the experimental results is shown in Table 44.

Spec.	Test	CSA S304.1-04 [2004]			
	$H_{max,mean}$ (kN)	$H_{max,mean}/H_{u,s}$ (%)	$H_{max,mean}/H_{u,f}$ (%)	$H_{max,mean}/H_{u,sl,wall}$ (%)	$H_{max,mean}/H_{u,sl,supp}$ (%)
UMW1	189.10	-6.16	-37.11	155.57	99.89
UMW2	92.06	3.18	-27.57	99.39	67.13
UMW3	155.86	-11.07	-20.91	73.20	17.52
UMW4	71.34	1.10	-17.08	52.43	20.18

Table 44: Difference between the experimental and predicted capacity for UMWs according to CSA S304.1-04 [2004]

5.3 LATERAL RESISTANCE OF STRENGTHENED MASONRY WALLS

Analytical formulation for reinforced masonry given in the codes and provisions was used to compare the resistance with the lateral resistance of the strengthened walls obtained through tests. The models used were described in detail in section 2.6, and only the main results

Spec.	Dir.	Test	Tomaževič [1999]			
		H_{max}	$H_{str,s-mas}$	$H_{str,s-hr}$	$H_{str,s-vr}$	$H_{str,s}$
	(+/-)	(kN)	(kN)	(kN)	(kN)	(kN)
SMW1	+	483.79	362.35	47.18	12.18	421.71
	-	527.15				
SMW2	+	227.18	208.68	47.18	7.06	262.91
	-	225.14				
SMW3	+	365.15	355.08	47.18	12.18	414.44
	-	332.09				
SMW4	+	208.62	204.36	47.18	7.06	258.59
	-	225.52				

Table 45: Theoretical maximum shear forces for SMWs according to Tomaževič [1999]

are discussed here. The material properties used for calculation in the analytical models were given in previous chapters.

5.3.1 *Tomaževič [1999]*

Although it is very difficult to predict the behaviour of reinforced masonry due to the complex mechanisms that develop, Tomaževič [1999] suggests a model for shear resistance which considers individual material contributions to the resistance of the reinforced wall $(H_{str,s})$. Following this approach, Table 45 presents the shear resistance obtained by calculation of the contributions of masonry $(H_{str,s-mas})$, horizontal $(H_{str,s-hr})$ and vertical reinforcement $(H_{str,s-vr})$.

Good correlation with the experimental results was obtained. The contribution of the reinforcing steel to the total resistance was within a range of $16-27\,\%$, attributing the major part of the shear resistance to the masonry. Generally, slight overestimation of the predicted resistance ranging from $13-24\,\%$ was acquired. The wall SMW1 presented the only underestimation obtained with the analytical model.

Table 46 shows the calculated values for flexural resistance and sliding shear resistance of reinforced masonry walls with values of individual contributors to the total resistance. The model for predicting the flexural resistance largely overestimates the experimental values, particularly for the squat walls (UMW1 and UMW3). On the other hand, the estimated sliding shear resistance with the suggested model gives lowest values among the calculated resistances. This could lead to a wrong conclusion that the strengthened walls will fail by sliding shear if the model for reinforced masonry is applied.

Spec.	Dir.	Test	Tomaževič [1999]					
		H_{max}	$H_{str,f-mas}$	$H_{str,f-vr}$	$H_{str,f}$	$H_{str,sl-mas}$	$H_{str,sl-vr}$	$H_{str,sl}$
	(+/-)	(kN)	(kN)	(kN)	(kN)	(kN)	(kN)	(kN)
SMW1	+	483.79	533.61	556.81	1090.42	252.00	12.18	264.18
	-	527.15						
SMW2	+	227.18	179.11	186.91	366.02	146.00	7.06	153.06
	-	225.14						
SMW3	+	365.15	351.48	556.81	908.29	126.00	12.18	138.18
	-	332.09						
SMW4	+	208.62	117.98	186.90	304.88	73.00	7.06	80.06
	-	225.52						

Table 46: Theoretical maximum flexural and sliding shear forces for SMWs according to Tomaževič [1999]

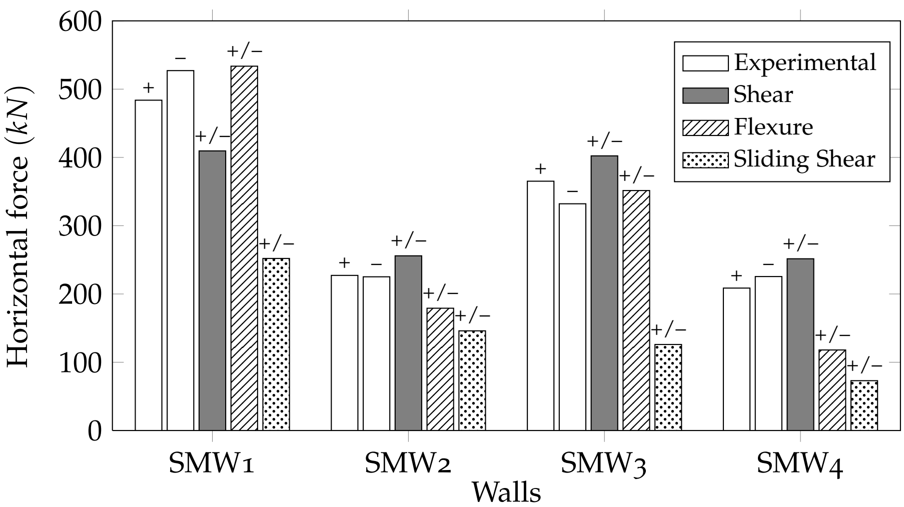

Figure 115: Comparison between experimental and theoretical resistance for SMWs according to Tomaževič [1999]

Spec.	Dir.	Test	Tomaževič [1999]		
		H_{max}	$H_{str,s}$	$H_{str,f}$	$H_{str,sl}$
	(+/-)	(kN)	(kN)	(kN)	(kN)
SMW1	+	483.79	409.53	533.61	252.00
	-	527.15			
SMW2	+	227.18	255.86	179.11	146.00
	-	225.14			
SMW3	+	365.15	402.26	351.48	126.00
	-	332.09			
SMW4	+	208.62	251.54	117.98	73.00
	-	225.52			

Table 47: Summary of theoretical maximum forces for SMWs according to Tomaževič [1999]

From the data in Table 46 we can see that there is significant contribution of the vertical reinforcement to the total flexural resistance of the reinforced masonry section. The contribution of the vertical reinforcement to the sliding shear resistance is rather small with an amount of $5 - 10\,\%$ from the contribution of the masonry. In the case of the tested strengthened walls, the vertical reinforcement present in the jackets was not fixed to the bottom or top beam. Hence, the resistance of the vertical reinforcement due to expected dowel effect could not be fully realized. Having in mind this, the comparison between the predicted and the experimental resistance was made by ignoring the contribution of the vertical reinforcement, see Figure 115. The proposed formulas by Tomaževič [1999] considers the reinforcement within the walls. In case of jacketed walls the bond strength between the masonry and the jackets should be included in the design model.

Therefore, Table 47 presents the shear, flexural and sliding shear resistance by including masonry contribution only. From this data, and the percentage difference between the predicted and the experimental resistance shown in Table 48, we can see that the models for shear and flexural resistance give close results to the experimental results. The differences expressed in percentage from the experimental values are similar for both models, with only slight advantage in the prediction for the flexural resistance. This results in a positive correlation between the obtained failure modes during the tests, and the prediction of the possible failure. As the results indicate, mixed failure mode is predicted, and that was the failure mode derived from the tests, shear failure in the masonry and flexural failure in the jackets.

Spec.	Test	Tomaževič [1999]		
	$H_{max,mean}$ (kN)	$H_{max,mean}/H_{str,s}$ (%)	$H_{max,mean}/H_{str,f}$ (%)	$H_{max,mean}/H_{str,sl}$ (%)
SMW1	505.47	-18.98	5.57	-50.14
SMW2	226.16	5.87	-9.31	-15.86
SMW3	348.62	10.61	0.57	-44.04
SMW4	217.07	6.82	-19.60	-28.50

Table 48: Difference between the experimental and predicted capacity for SMWs according to Tomaževič [1999]

5.3.2 *Eurocode 6 [2005]/DIN Eurocode 6/NA [2011]*

Similar approach for prediction of the resistance of reinforced masonry section suggested by Tomaževič [1999] was used in regulations given in Eurocode 6 [2005]. This involves estimation of the shear resistance by summing up the contributions of the masonry and the vertical reinforcements. The bending failure was included in the model for predicting the flexural resistance of reinforced masonry $(H_{str,f})$, where the total resistance of the section is attributed to the vertical reinforcement. In this case, masonry was ignored. Having in mind that the shear resistance suggested in Eurocode 6 [2005] is based on sliding shear failure mode $(H_{str,sl})$, in this section shear diagonal failure mechanisms are introduced through the shear strength of masonry as proposed in DIN Eurocode 6/NA [2011]. Thus, the shear resistance $(H_{str,s})$ was derived as a sum of contributions of the masonry failing with shear diagonal cracking and the vertical reinforcement.

Table 49 presents the results obtained from analytical analysis of the reinforced masonry sections and compares them with the experimental data. It is apparent from the table that the influence of the horizontal reinforcement has significant contribution to the shear resistance of the walls. The results of this study showed that the predicted shear resistance by including the vertical reinforcement was close to the experimental and good prediction was obtained by considering shear diagonal cracking as main failure mode. If the influence of the vertical reinforcement is ignored due to the lack of connection between the bars and the bottom beam, than the calculated resistance is far from the experimental.

On the other hand, the flexure resistance model considers vertical reinforcement only and the results shown in Table 50 give higher values than the experimental results. The highest resistance was calculated for SMW1, and for all other walls the predicted resistance was in the range of $13 - 21\,\%$ from the experimental results. Prediction of the sliding shear resistance was comparable with the experimental data.

Spec.	Dir.	Test	DIN Eurocode 6/NA [2011]		
	(+/-)	H_{max} (kN)	$H_{str,s-mas}$ (kN)	$H_{str,s-vr}$ (kN)	$H_{str,s}$ (kN)
SMW1	+	483.79	212.15	141.53	353.68
	-	527.15			
SMW2	+	227.18	122.91		264.45
	-	225.14			
SMW3	+	365.15	170.10		311.63
	-	332.09			
SMW4	+	208.62	98.55		240.08
	-	225.52			

Table 49: Theoretical maximum shear forces for SMWs according to DIN Eurocode 6/NA [2011]

Spec.	Dir.	Test	DIN Eurocode 6/NA [2011]			
	(+/-)	H_{max} (kN)	$H_{str,f}$ (kN)	$H_{str,sl-mas}$ (kN)	$H_{str,sl-vr}$ (kN)	$H_{str,sl}$ (kN)
SMW1	+	483.79	941.61	252.00	141.53	393.53
	-	527.15				
SMW2	+	227.18	309.83	146.00		287.53
	-	225.14				
SMW3	+	365.15	458.02	126.00		267.53
	-	332.09				
SMW4	+	208.62	147.51	73.00		214.53
	-	225.52				

Table 50: Theoretical maximum flexural and sliding shear forces for SMWs according to Eurocode 6 [2005]

Spec.	Dir.	Test	DIN Eurocode 6/NA [2011]		
		H_{max}	$H_{str,s}$	$H_{str,f}$	$H_{str,sl}$
	(+/-)	(kN)	(kN)	(kN)	(kN)
SMW1	+	483.79	212.15	416.33	252.00
	-	527.15			
SMW2	+	227.18	122.91	139.75	146.00
	-	225.14			
SMW3	+	365.15	170.10	271.83	126.00
	-	332.09			
SMW4	+	208.62	98.55	91.24	73.00
	-	225.52			

Table 51: Summary of theoretical maximum forces for SMWs according to Eurocode 6 [2005]

Spec.	Test	DIN Eurocode 6/NA [2011]		
	$H_{max,mean}$	$H_{max,mean}/H_{str,s}$	$H_{max,mean}/H_{str,f}$	$H_{max,mean}/H_{str,sl}$
	(kN)	(%)	(%)	(%)
SMW1	505.47	-58.039	-17.64	-50.14
SMW2	226.16	-20.43	-17.09	-15.86
SMW3	348.62	-35.32	-15.19	-44.04
SMW4	217.07	-23.45	-24.89	-28.50

Table 52: Difference between the experimental and predicted capacity for SMWs according to DIN Eurocode 6/NA [2011]

The best match was obtained for SMW4. However, by ignoring the contribution of the vertical reinforcement, quite different situation was obtained. In this case, the flexural resistance could not be calculated by equations provided in Eurocode 6 [2005]. That's why the predicted flexural resistance in Table 51 was estimated by considering the contribution of the unreinforced masonry only (Eq. 2.22). As shown in Figure 116 no correlation could be established between the experimental and analytical models given in DIN Eurocode 6/NA [2011].

Table 52 compares the percentage difference between the experimental and the predicted resistance. All analytical models give lower predictions for the corresponding resistance, ranging from $15 - 60\,\%$ from the experimental data.

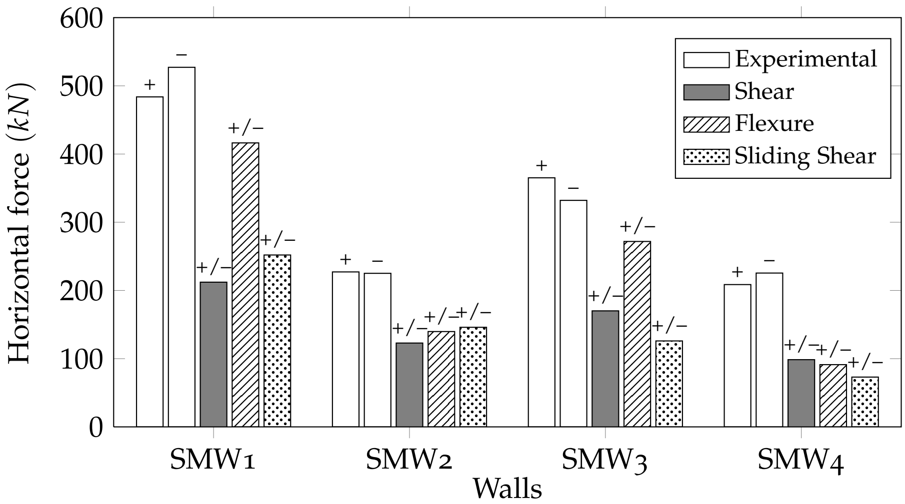

Figure 116: Comparison between experimental and theoretical resistance for SMWs according to DIN Eurocode 6/NA [2011]

5.3.3 *CSA S304.1-04 [2004]*

Similarly to the previous provisions and code regulations, CSA S304.1-04 [2004] combines the contributions of the individual materials to provide equations that can predict the resistance of a reinforced masonry wall for different failure modes. The shear/diagonal tension resistance was calculated according to the equations given in the code, as shown in Table 53. This table provides the contributions of the masonry and the horizontal reinforcements to the total capacity of the walls. It could be seen that the influence of the reinforcement was high and leads to unrealistic results. The code provides shear/-diagonal tension resistance limits for flexure and squat walls. This limits are considered in the analysed walls since the calculated resistance was higher than the limit resistance. Generally, the predicted shear/diagonal tension resistance was lower than the experimental data.

Table 54 presents the results obtained from the analysis with the analytical models for bending and sliding shear failure modes. Flexural resistance has been calculated from the resistance of the vertical reinforcement according to the code provisions. Sliding shear resistance has been estimated in two horizontal sections, at the foundation and in the upper portions of the walls. The resistance at the foundation depends on the friction behaviour between the wall and the bottom RC beam. The sliding shear resistance in the wall body depends on the masonry and the vertical reinforcements. The results of this analysis showed that the model for sliding shear resistance was closest to the test values. This means that generally the wall will fail in sliding shear, and the percentage difference was in a wide range of $3 - 54\,\%$ from the experimental capacity. This is opposite to the observed failure

Spec.	Dir.	Test	CSA S304.1-04 [2004]			
		H_{max}	$H_{str,s-mas}$	$H_{str,s-hr}$	$H_{str,s}$	$H_{str,s-max}$
	(+/-)	(kN)	(kN)	(kN)	(kN)	(kN)
SMW1	+	483.79	177.46	1616.87	1794.33	269.04
	-	527.15				
SMW2	+	227.18	98.07	936.76	1034.83	121.99
	-	225.14				
SMW3	+	365.15	134.94	1616.87	1751.81	269.04
	-	332.09				
SMW4	+	208.62	73.43	936.76	1010.19	121.99
	-	225.52				

Table 53: Theoretical maximum shear forces for SMWs according to CSA S304.1-04 [2004]

mechanisms during the tests, where a combination between flexure and shear diagonal failure was noticed.

Spec.	Dir.	Test	CSA S304.1-04 [2004]		
		H_{max}	$H_{str,f}$	$H_{str,sl,wall}$	$H_{str,sl,supp}$
	(+/-)	(kN)	(kN)	(kN)	(kN)
SMW1	+	483.79	473.59	520.00	384.92
	-	527.15			
SMW2	+	227.18	158.97	332.62	241.82
	-	225.14			
SMW3	+	365.15	291.12	349.91	214.81
	-	332.09			
SMW4	+	208.62	97.72	234.07	143.27
	-	225.52			

Table 54: Theoretical maximum flexural and sliding shear forces for SMWs according to CSA S304.1-04 [2004]

If we consider the actual conditions of the vertical reinforcement and the lack of connection with the bottom beam, the predicted resistances were found to depend on masonry resistance only. In this case, the analysis showed that again the governing case is sliding shear in the masonry wall.

As shown in Figure 117, there is significant difference between the test and the predicted capacities. This leads to an conclusion that

Spec.	Dir.	Test	CSA S304.1-04 [2004]			
		H_{max}	$H_{str,s}$	$H_{str,f}$	$H_{str,sl,wall}$	$H_{str,sl,supp}$
	(+/-)	(kN)	(kN)	(kN)	(kN)	(kN)
SMW1	+	483.79	177.46	118.92	483.28	378.00
	-	527.15				
SMW2	+	227.18	98.07	39.92	279.99	219.00
	-	225.14				
SMW3	+	365.15	134.94	116.31	294.28	189.00
	-	332.09				
SMW4	+	208.62	73.43	39.04	170.49	109.50
	-	225.52				

Table 55: Summary of theoretical maximum forces for SMWs according to CSA S304.1-04 [2004]

Spec.	Test	CSA S304.1-04 [2004]			
	$H_{max,mean}$	$H_{max,mean}/H_{str,s}$	$H_{max,mean}/H_{str,f}$	$H_{max,mean}/H_{str,sl,wall}$	$H_{max,mean}/H_{str,sl,supp}$
	(kN)	(%)	(%)	(%)	(%)
UMW1	505.47	-64.89	-76.47	-4.39	-25.22
UMW2	226.16	-56.64	-82.35	23.80	-3.17
UMW3	348.62	-61.29	-66.64	-15.59	-45.79
UMW4	217.07	-66.17	-82.02	-21.46	-49.56

Table 56: Difference between the experimental and predicted capacity for SMWs according to CSA S304.1-04 [2004]

the provided analytical model for reinforced masonry is not able to capture the effects of strengthened masonry with RC jackets.

The percentage difference between the mean experimental resistance and the theoretical predicted resistance for all failure modes is given in Table 56. The predicted resistances are calculated by ignoring the contribution of the vertical reinforcement as an attempt to recreate the experimental conditions. Clearly, no correlation could be established between the test and the predicted forces.

5.3.4 *FEDRA [2003]*

The specialized design module "Gunites" was used to compare the proposed model with the experimental results obtained from the in-plane cyclic tests of RC jacketed masonry walls. The model is based on the equivalent shear strength of the wall, computed by introduction

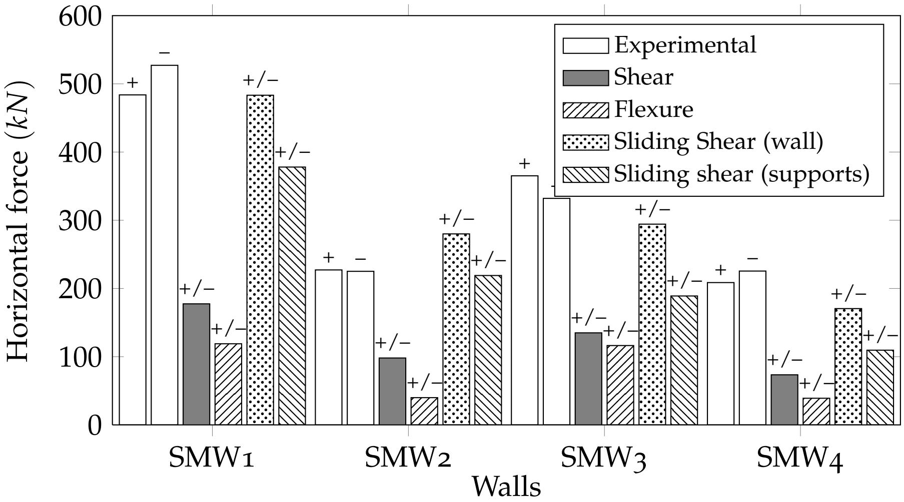

Figure 117: Comparison between experimental and theoretical resistance for SMWs according to CSA S304.1-04 [2004]

of shear strength contribution of masonry and reinforced concrete. The model is based on the prestandard provisions of Eurocode 2 and these provisions are not contained in the final version of Eurocode 2. The analysis was performed with slight rearranging of the relations used in the program and without considering any partial safety factor. The calculated shear strength of concrete was $f_{rd} = 2.949\,{}^{N}/_{mm^2}$ and the corresponding shear strength of the jacketed walls was $f_{vk,jack} = 0.761\,{}^{N}/_{mm^2}$. The results from this analysis are presented in Table 57.

The results from the analysis are compared with the experimental results considering two cases for the length of the compressed part (l_c) of the walls. In the first case, the length of the compressed part of the wall has been considered equal to the length of the wall. In the second case, the length of the compressed part of the wall has been calculated with respect to the maximum horizontal forces obtained experimentally.

The current analysis found that the length of the walls included in the calculation of the shear resistance has significant influence. The results indicate that the length of the compressed part of the wall should be taken equal to the length of the wall. In such case, the predicted shear resistance was found to be closer to the experimental resistance. The percentage difference was in a range of $-5 \div 25\,\%$ from the experimental data. It is interesting to note that the calculated length of the compressed part for SMW4 was found to be negative, which suggests that the whole length of the wall is in tension.

5.4 SUMMARY AND CONCLUSIONS

The present analysis was designed to propose the most appropriate analytical method for predicting the resistance of unreinforced and

Spec.	Dir.	H_{max}	$l_c = L$		$l_c = 3\left(\frac{L}{2} - \frac{H_{max}\alpha h}{N}\right)$	
			$H_{str,s}$	$H_{max,mean}/H_{str,s}$	$H_{str,s}$	$H_{max,mean}/H_{str,s}$
	(+/-)	(kN)	(kN)	(%)	(kN)	(%)
SMW1	+	483.79	479.46	-5.15	320.32	-33.79
	-	527.15			284.57	-46.02
SMW2	+	227.18	277.78	10.21	93.38	-58.90
	-	225.14			96.29	-57.23
SMW3	+	365.15	479.46	25.88	117.08	-67.94
	-	332.09			171.59	-48.33
SMW4	+	208.62	277.78	12.01	0	N/A
	-	225.52			0	N/A

Table 57: Theoretical maximum shear forces for SMWs according to FEDRA [2003]

strengthened masonry walls. Due to the limited experimental programme, and lack of tests which study the behaviour of strengthened masonry walls with RC jackets, this analysis was undertaken to study and evaluate if the available design methods for reinforced masonry could be applied in a case of jacketed masonry walls. Moreover, the similarity between both structural materials, reinforced masonry and jacketed masonry (without anchorage to the beams) lead to the idea that the seismic resistance of the jacketed masonry can be obtained by taking the contributions of the main components. Therefore, the suggested analytical models from Tomaževič [1999] and the design code provisions given in Eurocode 6 [2005], CSA S304.1-04 [2004] and FEDRA [2003] were applied. Several important findings from this analysis are summarized in the following paragraphs.

A. The lateral behaviour of the tested unreinforced masonry walls can be simulated well by all inspected analytical models, see Figure 118. From the bar graph we can see that the predicted values for maximum shear force in the walls considering diagonal shear failure are simulated with success. The percentage difference between the mean experimental shear capacity and the theoretical resistance was within the range of $3 - 38\,\%$ depending on the wall geometry, the precompression level and the analytical model used. Within this investigations, it was found that the diagonal shear failure model given in CSA S304.1-04 [2004] predicted the maximum resistance of the walls very closely to the test results. The model proposed by Tomaževič [1999] gave reliable results, and the model given in DIN Eurocode 6/NA [2011] presented the highest difference from the experimental data. This was particularly notable for the tall walls (34 % and 38 %),

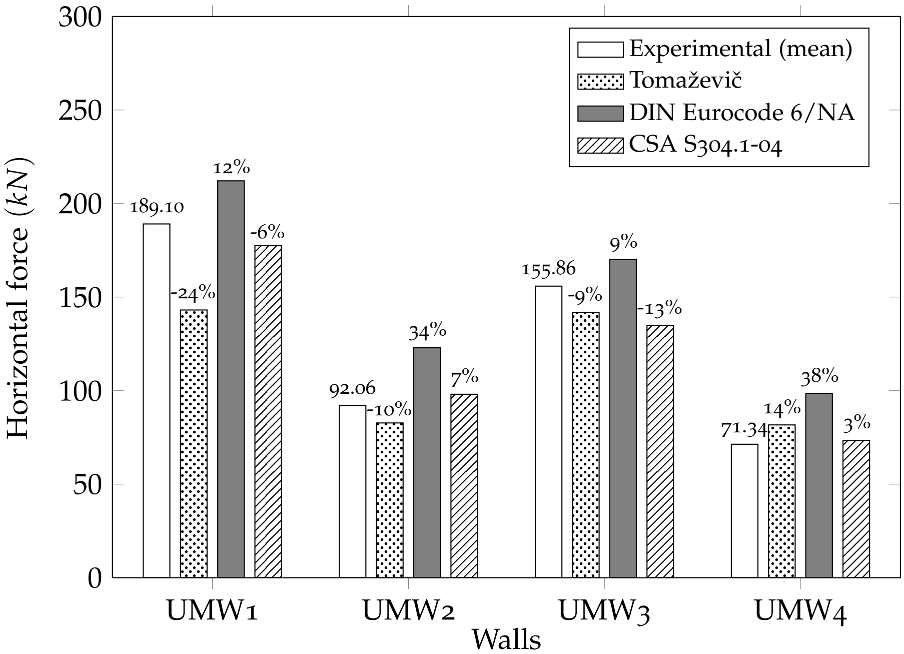

Figure 118: Comparison between experimental shear behaviour and predictions by analytical models for UMWs

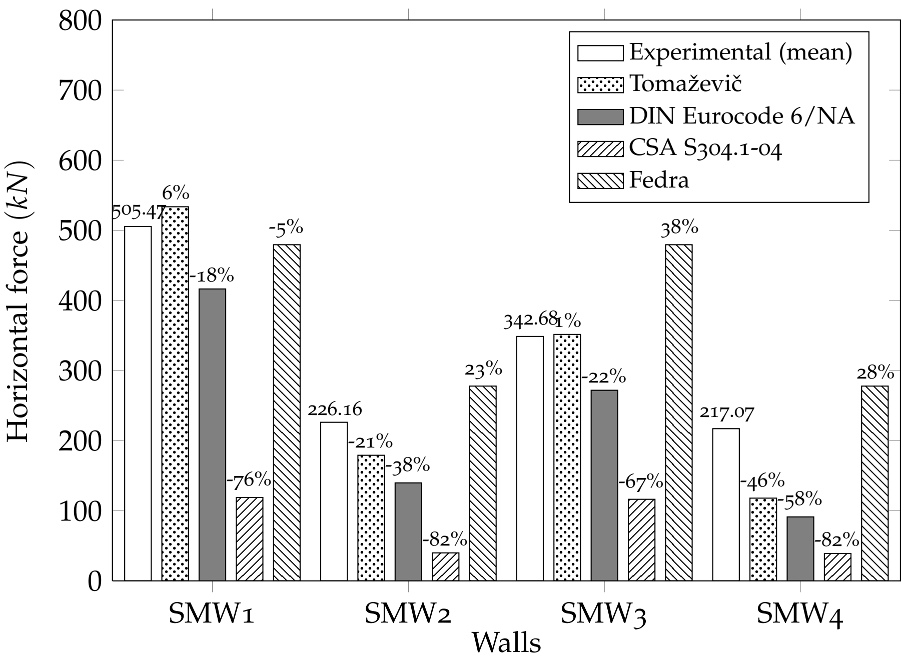

Figure 119: Comparison between experimental shear behaviour and predictions by analytical models for SMWs

while for the squat walls the predicted values were very close to the experimental values.
The model by Tomaževič [1999] gave lower capacities than the experimental one, for all walls except for UMW4. On the other hand, the model given in DIN Eurocode 6/NA [2011] presented higher capacities than the experimentally obtained results. Interestingly, CSA S304.1-04 [2004] model provided lower capacities than the experimental capacity for the squat walls, and higher capacities for the tall walls.

B. The correlation between the test results for the strengthened masonry walls with RC jackets and the analytical models for reinforced masonry is presented in Figure 119. Comparisons between the results was made without considering the contribution of the vertical reinforcement. This was due to the fact that the vertical reinforcements in the tested walls were not anchored to the bottom and top RC beam. The main idea was to study the seismic behaviour of the new strengthening material, rather than to investigate the structural strengthening on the element level. Therefore, the models which base the prediction for the maximum resistance on the contribution of the vertical reinforcement only, can not be applied. In such case, their theoretical values were based on the contribution of the masonry. The flexural resistance calculated with the analytical models has been compared with the experimental resistance of the walls which failed by mixed shear and flexural failure mode. The shear failure was detected in the walls with higher precompression load, but in general all strengthened walls failed by bending and separation of the jackets.
By comparison with the experimental results, the most accurate analytical model for predicting the failure mode and the maximum resistance was the model proposed by Tomaževič [1999]. This model was particularly precise for squat walls giving only $1-6\,\%$ difference from the experimental values. The higher disagreement was obtained for the tall walls. DIN Eurocode 6/NA [2011] predicted relatively well as a result of the contribution of the masonry failing in diagonal shear, while as in case with CSA S304.1-04 [2004] the contribution of the steel was ignored.
Overall, good prediction was shown with the model found in FEDRA [2003]. But, it is based on the shear strength of the jacketed masonry section and it is not applicable for the failure mechanisms shown by the tested walls.

C. The findings from this analysis make a contribution in analysis and design of strengthened masonry walls with RC jackets. The results suggested that the analytical model for reinforced masonry walls proposed by Tomaževič [1999] can be used to determine the shear resistance of walls made from jacketed masonry.

D. The proposed analytical model can be further improved by taking into account the bond strength between the masonry and the jackets. This is particularly important if the analytical model is applied on the structural element level and the anchorage of the reinforcement mesh into the foundations, bond beam and/or slab is fully utilized.

E. For simplification reasons, the maximum lateral capacity of the strengthened masonry walls with RC jackets can be simulated by simple multiplication of the shear resistance of the unreinforced masonry walls by an experimentally obtained multiplier (Γ). It was defined as a ratio between the resistances of RC jacketed and unreinforced walls, and can be taken as $\Gamma = 2 - 3$. However, this approach does not take into account the failure mode of the walls.

6

APPLICATION OF THE CHOSEN ANALYTICAL MODEL FOR ANALYSIS OF MASONRY BUILDINGS

6.1 INTRODUCTION

The importance of numerical modelling and analysis of masonry structures is increasing over the past decade. A great significance was given to the sophisticated numerical tools that can predict the behaviour of a structure from the elastic region, occurrence of cracks and stiffness degradation, to the complete loss of the strength. To completely understand the collapse mechanisms and to assess the structural safety within reliable limits, a precise constitutive models in addition to an advanced methods for solving systems of equations resulting from finite element discretizations are often needed. Consequently, the use of the finite element method is assumed for global behaviour simulation of a masonry structure. Recently, numerical research in masonry is focused on advanced numerical tools since the difficulty for application of the existing numerical tools is increased due to several characteristics of structural masonry.

The solution of certain structural analysis problem is normally achieved by establishing idealization of the material behaviour. The description of the material behaviour, together with the geometry idealization (2D or 3D), enables inclusion of complex effects for the masonry behaviour as well as more expensive solutions. The idealizations which are commonly applied to the behaviour of masonry material are elastic, plastic and non-linear material behaviour.
The recommended approach in engineering practise and analysis of masonry structures is to perform non-linear analysis after linear analysis. Basically, the linear analysis can predict the sections of a structure which are more susceptible to non-linearities and consequently study that part in detail with non-linear material behaviour. However, the resources for application of non-linear analysis methods to masonry buildings are difficult considering the complex behaviour of the masonry.

This chapter presents an application of the chosen analytical models for simplified non-linear analysis of masonry buildings by using a displacement-based verification method. The methodology for analysis is illustrated on an existing masonry building. First, the dynamic characteristics of the building were determined by ambient vibration tests and experimental analysis methods. The test results were used to update the material properties of the initial calculation model through a manual updating technique by matching the test results and the results from numerical modal analysis. The updated material parameters were used in the displacement-based method for analysis on the basis of Capacity Spectrum Method (CSM). The analytical models based on DIN Eurocode 6/NA [2011] and Tomaževič [1999] for unreinforced and reinforced masonry walls were chosen, considering the correlation of the results from the previous chapter. They were applied on the existing masonry building to verify its seismic capacity. For research purposes of the thesis, the chosen analytical models were implemented in the software package MINEA [2011], through a newly developed analysis module. A comparison of results for the two cases of structural material (unreinforced and strengthened) applied to the building are presented.

The following sub-chapters give introduction to the applied methods and give a summary of the main issues regarding the applied design concept. The ambient vibration tests are not prerequisite for the later non-linear analysis, but a good assessment of the material properties of the existing buildings can be achieved.

6.2 INTRODUCTION TO AMBIENT VIBRATION TESTING

The design and construction of complex structures and the new trend of predicting damage in existing structures, stimulated structural engineers to develop appropriate experimental tools to evaluate the structural behaviour over the time, by using monitoring techniques (a process called Structural Health Monitoring). With respect to the monitoring process, static and dynamic data are collected, which can later be used for numerical analysis, such as the model updating process or damage identification.

The aim of the static monitoring is to observe phenomena with small variations on time, such as the displacement variations during construction, a crack or tilt progress, or monitor the environmental conditions. On the other hand, the aim of dynamic monitoring is to observe fast time-dependant phenomena. Dynamic monitoring systems also allow modal identification in terms of identifying resonant frequencies, damping and mode shapes. Static monitoring is beyond the scope of this work and only dynamic monitoring will be addressed next.

6.2.1 *Operational modal analysis*

For structural dynamic monitoring, depending on the excitation source, two different groups of techniques are currently used, namely, Input-Output and Output-Only techniques. Input-Output techniques are based on the estimation of a set of Frequency Response Functions (FRFs) relating an applied force to the corresponding response at several points along the structure.

Testing civil engineering structures with forced vibration generally requires a large amount of specialized equipment and trained personnel, making the tests difficult and expensive. Additionally, when automated health monitoring systems are implemented, force vibration tests are not suitable alternative. For these reasons, simpler tests in which the structures are excited just by ambient vibrations, called Output-Only techniques, are desirable and often used.

During the last years, the technological developments in the field of sensors made feasible the accurate measurement of the low levels of dynamic responses, strongly stimulating the development of the Output-Only identifications methods, also called Operational Modal Analysis (OMA). Output-Only methods are based on the premise that the wind, traffic and human activities can adequately excite a structure. The main assumption of the Output-Only identification methods is that the ambient excitation input is a Gaussian white noise stochastic process in the frequency range of interest. Due to the nature of the excitation, the response includes not only the modal contributions of the ambient forces and the structural system, but also the contribution of the noise signals from undesired sources. In this way, the measurements reflect the response from the structural system and also from the ambient forces, meaning that the identification techniques must have the ability to separate them. Output-Only modal identification methods are divided in two groups, namely, non-parametric methods, essentially developed in the frequency domain, and parametric methods, developed in the time domain.

Calculation models based on Finite Element Method (FEM), which are usually used for dynamic analysis of buildings, present idealized models of the structure, constructed in a suitable way to represent structure's behaviour under different dynamic loads, like: earthquakes, strong winds, explosions and etc. They can be controlled by experimental tests on buildings in real size through ambient and forced vibrations [Ivanović et al., 2000]. Both methods can be used to identify the dynamic properties of the structural system of the building, namely: natural frequencies, damping coefficients and mode shapes.

Ambient vibration tests (AVT) describe the linear behaviour of structures because the amplitudes of vibration are small. These tests can be used to determine the structural behaviour of damaged buildings and their components, and also to develop structural models and time and amplitude dependant analysis algorithms for structural health monitoring and structural control studies. The basic advantage of the ambient vibration tests over forced based tests is the light and mobile equipment used to perform the tests and the small number of operators involved in the process. The most common sources of ambient vibrations are: wind, soil, micro tremors and different local periodical or random excitations (traffic or heavy machinery). Forced vibration tests are performed by attracting large forces acting on the inspected buildings which can produce useful response amplitudes. These forces are created with vibration devices usually positioned on the top of the building. This causes significant excitation of modes of oscillation with greater amplitudes at the higher levels of the building.

6.2.2 *Ambient vibration tests in practice*

Ambient vibration tests are conducted in Macedonia for more than 30 years. Generally, they are performed on structures with significant cultural, historical, political and economical values: historic monuments, dams, bridges and etc. Buildings were rarely tested, except buildings which according to PIOVSP [1981] are classified in out-of-category and category I. Over those years, many tests on structures with ambient vibrations were performed and an extensive knowledge has been gained.

Based on the fact that the resonant frequencies, mode shapes and damping coefficients of the structures are considered the most important parameters in seismic design, an experimental procedure for definition of the dynamic properties of the structures has been introduced in the design practise in the country since 1970s. The pioneers of ambient vibration testing in Macedonia, the Institute of earthquake engineering and engineering seismology (IZIIS), performed test on more than 200 structures (buildings, dams, bridges, schools) in real scale and many test on large scale models.

Many important buildings have been tested in city of Skopje, also. As reported by Krstevska and Tashkov [2003], more than 40 buildings with different structural systems have been tested experimentally by full scale testing methods - forced and ambient vibrations. Five storey large panel buildings in 'Karposh 4' settlement, 12 storey QBE building, 10 storey residential buildings in 'Aerodrom' settlement, MRT building, Skopje Bussiness Centre have been tested, to name but a few.

Seismic stability of the industrial facilities are considered of highest importance and their normal operation after big earthquakes must be ensured. Therefore, many experimental tests have been carried out on such buildings. Ambient vibration tests are often the most appropriate testing methods. In-situ testing by ambient vibrations has been performed on the machinery building of Beauharnis powerhouse by an expert team from IZIIS [Tashkov et al., 2007, Krstevska et al., 2010]. The identified dynamic properties enabled construction of appropriate large scale model of the structure, later tested on a shaking table.

The influence of the storage materials on the structural behaviour of the industrial facilities is one of the most important parameters in structural and seismic design. An example of the changing natural frequencies and mode shapes of the RC silo structure in relation to the amount of grain in the silo was experimentally tested and presented by

Tashkov and Krstevska [1998]. The ambient vibration testing method was applied on the silo structure composed of 30 octagonal main cells and 18 inter-cells, creating the dimensions of the silo in plan view of $17.3x61\,m$ and a height over the terrain of $39.1\,m$. The performed tests on an empty and full silo revealed that the natural frequencies of the full silo were about 40% lower than the natural frequency of the empty silo. Also, the identified damping coefficients were found greater in the case of full silo, than those obtained for an empty silo. However, the mode shapes of vibrations were not significantly influenced by the amount of grain present in the silo.

The understanding of the seismic behaviour of a structure becomes much easier if the dynamic properties are know. The experimental tests can improve and verify the numerical models used for evaluation of the seismic stability of a structure. By using light and mobile testing equipment, as well as sophisticated data processing software, fast and reliable results can be obtained. Such methodology has been applied to one of the most important monuments in the world database of historical heritage, the Old bridge in Mostar, Bosnia and Herzegovina. The demolished original 16th century bridge has been completely reconstructed in 2003, maintaining the original structural materials and visual appearance as the original bridge. The simple arch system of the bridge, with $29\,m$ in length and $13.5\,m$ in height has been tested by ambient vibrations in transversal, longitudinal and vertical direction in 22 points along the bridge [Krstevska et al., 2009b].

Another historical building tested with ambient vibrations was the Presidential Palace in Baku. This stone masonry building with irregular shape has been tested and analysed in longitudinal and transversal directions in the frequency domain up to $25\,Hz$ [Krstevska and Tashkov, 2009]. With the performed 87 tests, the dominant frequencies and the damping coefficients of the building were identified.

Many successful examples of ambient vibration testing methods applied to important buildings have been presented during the years. The experimental investigations supported by the numerical studies with tuned FE models represent powerful technique for structural analysis and seismic design, but also for reconstruction and strengthening of the existing buildings. A typical example can be found in Aras et al. [2011], where the modulus of elasticity in the numerical model of the historical Beylerbeyi masonry palace was adjusted in correlation with the experimental results.

6.3 DISPLACEMENT-BASED ANALYSIS OF MASONRY BUILDINGS

The adopted approach for non-linear static analysis and seismic design of masonry buildings is based on the capacity spectrum method. A new displacement-based design concept has been developed by the Chair for Structural Statics and Dynamics, RWTH University of

Aachen [Gellert et al., 2008, Butenweg et al., 2009]. This concept follows the new trend in the seismic design of structures, performance based design, which examines the deformation properties of a structure. It was generalized to 3D buildings considering torsional effects and the modified structural vibration shape because of its stiffness degradation. The analysis procedure is based on the capacity spectrum method by comparing the seismic action with the loading capacity of the building, considering the non-linear behaviour with its post peak capacity. Masonry failure modes and the hysteretic damping are considered and the concept does not require additional use of empirically determined correction coefficients. The non-linear push-over curve of the entire building is obtained from a the force-displacement curves of the individual masonry walls.

6.3.1 *Capacity spectrum method*

The capacity spectrum method was originally developed in 1975 by Freeman et al. [1975]. It requires definition of the force-displacement capacity of a building and a corresponding site response spectrum. The procedure consists on finding the displacement demand during the ground motion of a building in the inelastic range by the point where both the demand and the capacity curves intersect. The effective damping $\left(\xi_{eff}\right)$ is used to define the demand spectral value which corresponds to the damping that occurs when the structures is pushed into the inelastic range. In this procedure it is viewed as a combination of viscous and hysteretic damping. The effective damping is obtained from $\xi_{eff} = \lambda\xi_0 + 0.05$, where λ is a modification factor to account for the approximation involved in describing the hysteretic response of the building by the bilinear idealisation of the capacity curve. It ranges from $0.3 - 1.0$ depending on the type of the structural system, being 0.3 for systems with poor and unreliable hysteretic behaviour and 1.0 for well-detailed elements with stable hysteresis loops. The value of 0.05 represents the viscous damping inherent in the system.

An iterative procedure is applied to obtain the displacement demand of the building. To initiate the process, the initial stiffness and an arbitrary value of the effective damping (for instance $\xi_{eff} = 5\,\%$) are used. With these values a displacement demand is obtained from the demand acceleration-displacement spectra for this period of natural vibration and 5 % damping, corresponding to point (0) in Figure 120. The displacement demand for this period and damping is obtained, marked as δ_0. From the intersection point of the displacement demand and the capacity curve, a new effective period $T_{eff}\,(1)$ compatible with this displacement is obtained and the effective damping $\xi_{eff}\,(1)$ is computed. A new calculation cycle is initiated. It uses the new period and damping value to obtain new displacement demand, δ_1. The procedure is repeated until the displacement demand δ_m matches

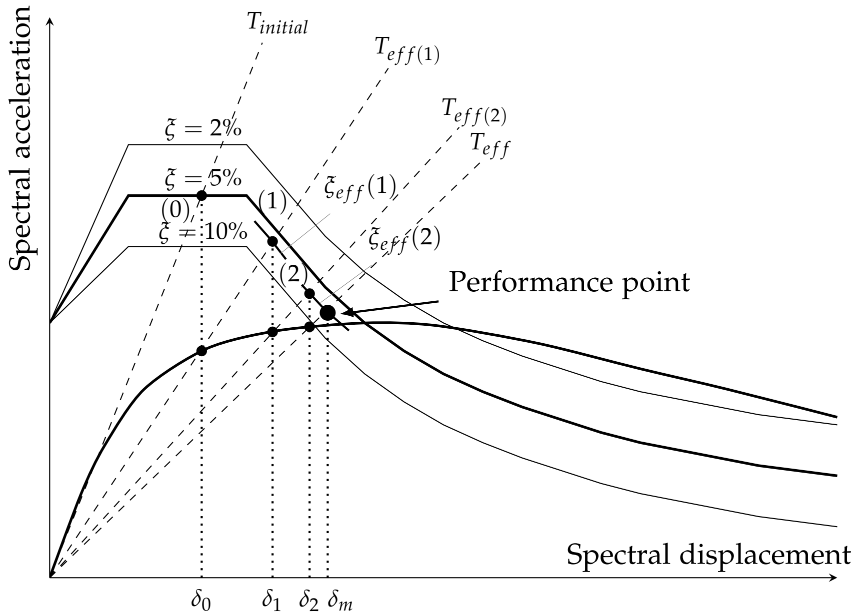

Figure 120: Capacity spectrum method

the spectral value for the period T_{eff} and the damping ξ_{eff} employed. The displacement demand δ_m is compatible with the strength and the stiffness of the building and the ground motion.

6.3.2 *Capacity curves of individual masonry walls*

The developed analysis concept requires definition of the capacity curves of the individual masonry walls from the ground floor of the building. These curves can be determined by experimental investigation, numerical simulation and analytical computation.

Based on the obtained test results from chapter 4 and the bilinear idealisation of the experimental results, analytical formulation for the capacity curves of the individual masonry walls was used. The analytical models according to DIN Eurocode 6/NA [2011] and Tomaževič [1999] considering diagonal shear, flexural and sliding shear failure modes was implemented in the new module. Three parameters are necessary for developing the capacity curve for each wall : *initial stiffness*, *maximum resistance* (load bearing capacity) and *ultimate displacement*, see Figure 121. A database that consists the capacity curves and damping curves at different levels of the vertical load and different height to length ratios was created.

6.3.3 *Capacity curve of the building*

The capacity curve of the entire building can be determined from the capacity curves of the individual walls in the direction of the

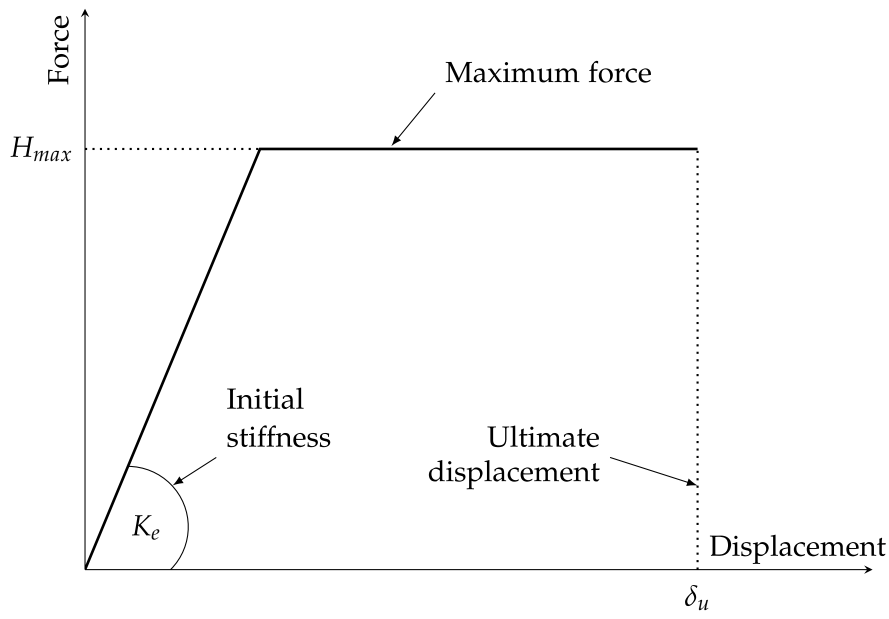

Figure 121: Bilinear capacity curve with necessary parameters

seismic action. Hence, several approximations are made. The structure is assumed to have continuous walls over the height of the building. The upper floors are considered to behave linearly elastic, and the failure modes are limited to the walls from the ground floor. The floor slabs are assumed to be fully rigid horizontal diaphragms which transfer the horizontal forces from the seismic action to the masonry walls.

For symmetrical ground plans with symmetrical mass distribution the capacity curve of the building can be computed by simple superposition of the capacity curves for the individual masonry walls. In case of unsymmetrical ground plans, the torsional effects have to be considered as a result of the rotation and displacement perpendicular to the direction of action. Therefore, the capacity curve is determined by using double iterative algorithm. First, a displacement step is imposed to the ground floor (let's assume in x- direction), see Figure 122. With the imposed displacement, the resulting forces in all masonry walls are evaluated and the resulting moment is computed. Then, double iterative algorithm is applied with a procedure consisting of rotating and translating the system around the mass centre until the floor finds an equilibrium, $\sum M = 0$, $\sum F_y = 0$. The resulting pair of the imposed displacement and the reaction force in the direction of the action create one point from the capacity curve of the building. The whole curve is calculated by repeating the described procedure.

This approach is sufficiently accurate for buildings with few floors. A more refined approach can be applied to take into account stiffness change of all floors.

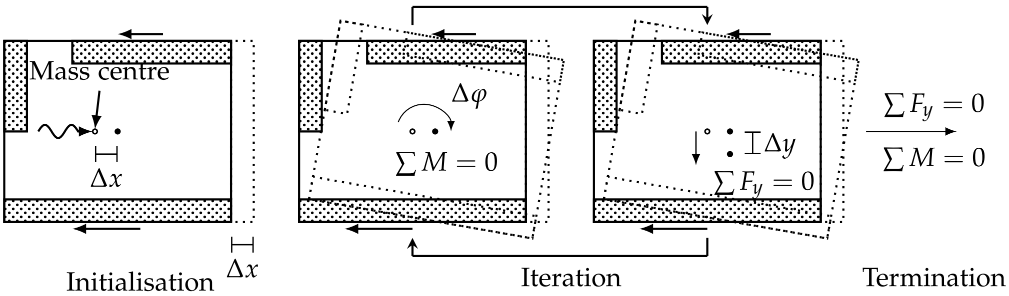

Figure 122: Calculation of the building capacity curve by iterative algorithm

6.4 DEVELOPMENT OF A NEW ANALYSIS MODULE IN MINEA SOFTWARE

For the analysis purposes performed later, each wall needs to be described by a capacity curve. As described earlier, the capacity curve of a wall needs three parameters: initial stiffness, maximum resistance and ultimate displacement.

6.4.1 *Initial stiffness*

The lateral initial stiffness, (K_e), of a wall is defined with secant stiffness at the formation of the cracks. It is calculated as a sum of the lateral deformations from bending and shear deformations on the wall generated from a lateral load. In this sense, Eqs. 4.13 and Equation 4.14 were considered in the module. Reduced moment of inertia was used, according to Eq. 4.15. Thus, the following formulas were used to calculate the lateral stiffness for fully fixed boundary conditions:

$$K_e = \frac{H_u}{d} \tag{6.1a}$$

$$d = \frac{H_u h^3}{12EI_E} + \frac{\kappa H_u h}{GA_W} \tag{6.1b}$$

and the reduced moment of inertia was given as

$$I_E = \frac{I_w}{\left(1 + \frac{3.64EI_w}{h^2GA_w}\right)} \tag{6.1c}$$

6.4.2 *Maximum resistance*

The maximum resistance was obtained with respect to the failure modes for unreinforced and reinforced masonry walls, as presented in Chapter 2.6. It was obtained by adopting the lowest of the resistances calculated for a wall failing in shear or bending. The models for unreinforced and strengthened masonry walls proposed in DIN

Eurocode 6/NA [2011] and Tomaževič [1999] were used to calculate the maximum resistances for each wall.

According to the provisions given by Tomaževič [1999], the maximum resistance of the walls falling in *shear* was calculated with respect to Eq. 6.2.

$$H_{u,s} = C_h \left(H_{um} + H_{ur} \right) \tag{6.2}$$

where $H_{u,s}$ is the maximum resistance of unreinforced masonry wall; C_h is the maximum resistance degradation factor, $(C_h = 0.85)$; H_{um} is the resistance of the masonry; and H_{ur} is the resistance of the reinforcement.
The resistance of masonry was calculated by using Eq. 2.6, where the tensile strength of masonry f_t was evaluated with Eq. 2.5. For the shear stress distribution factor b, three limit states were considered:

$$b = \begin{cases} 1.1 & if\, ^{\mathrm{h}}/_{\mathrm{L}} \leq 1.1 \\ ^{\mathrm{h}}/_{\mathrm{L}} & if\, 1.1 < ^{\mathrm{h}}/_{\mathrm{L}} < 1.5 \\ 1.5 & if\, ^{\mathrm{h}}/_{\mathrm{L}} \geq 1.5 \end{cases} \tag{6.3}$$

The contribution of the reinforcement was introduced through the resistances calculated for the horizontal and the vertical reinforcement. The calculation of the H_{ur} was based on Eq. 2.10a by summation of H_{R2} and H_{R3}, according to Eq. 6.4.

$$H_{ur} = 0.3 A_{sh} f_{yh} + 1.026 A_{sv} \sqrt{f_m f_{yv}} \tag{6.4}$$

The formulas for *bending* resistance of unreinforced and reinforced masonry wall were implemented in the analysis module, also. The formulation given in Eqs. 2.8 and 2.9 were used for unreinforced walls, and the Eqs. 2.14 and 2.13 were used for reinforced masonry walls.

The design provisions for maximum resistance of masonry walls given in Eurocode 6 [2005] and DIN Eurocode 6/NA [2011] were implemented in the analysis module as a second option for definition of the capacity curves.

The *shear* resistance calculation of unreinforced masonry walls was according to Eq. 2.19, while two ultimate criteria for calculation of the characteristic shear strength of masonry (f_{vk}) were established. Namely, the analysis value of f_{vk} was adopted as the smallest between f_{vlt1} and f_{vlt2} which consider sliding shear failure (f_{vlt1}) and diagonal shear failure of masonry (f_{vlt2}), where

$$f_{vlt1} = f_{vk0} + 0.4 \sigma_0 \tag{6.5}$$

$$f_{vlt2} = 0.45 f_{bt,cal} \sqrt{1 + \left(\frac{\sigma_0}{f_{bt,cal}} \right)} \tag{6.6}$$

The calculation tensile strength of the masonry units, $f_{bt,cal}$, was adopted in relation to the unit type according to DIN Eurocode 6/NA [2011]. Due to the fact that the shear resistance of the unreinforced walls depends on the stress state governed by the level of the vertical and horizontal loads, a simplification for calculation of the length of the compressed part of the wall (L_c) was made. In MINEA [2011], the L_c was considered to be equal to the wall length L. This assumption was supported by the fact that the horizontal loads needed for calculation of the actual stress state inside the wall are not known prior to distribution of the horizontal forces on each wall. This distribution is not performed in MINEA [2011], because only the individual capacity curves of the walls are needed as input parameter.

The shear resistance of reinforced masonry walls was implemented according to the formulas given in Eurocode 6 [2005] and DIN Eurocode 6/NA [2011] without any modification.

The *bending* resistance of unreinforced and reinforced masonry walls was also included in the analysis module. Therefore, the Eq. 2.22 was used to calculate the bending resistance of unreinforced walls, while the ultimate bending moment was taken according to Eq. 6.7. The factor p_v depends on the boundary conditions on the top and bottom wall edges, and according to Gellert [2010], the values of $p_v = 1.3$ for fully fixed walls, and $p_v = 1.0$ for cantilever walls were assumed in the module.

$$M_{Ru} = \frac{q_0 L^2}{2 p_v} \left(1 - 1.15 \frac{q_0/t}{f_k} \right) \tag{6.7}$$

The bending resistance of reinforced masonry walls was implemented according to Eq. 2.24.

6.4.3 *Ultimate displacement*

The deformation capability described by the ultimate displacement values has been defined as a drift limit (θ_u) from the wall height according to Eq. 6.8 and Table 60.

$$d_u = \theta_u h \tag{6.8}$$

For implementation of the ultimate displacements, several drift limits defined in the literature and design codes have been considered. The drift ratios given in EN 1998-3 [2005], DIN Eurocode 6/NA [2011], OPCM 3274 [2005] and FEMA 273 [1997] were adopted. Referenced drift limits for shear and bending failure modes are given in Table 58 and Table 59 for two damage states: significant damage (SD) and near collapse (NC).

Reference	Unreinforced masonry		Reinforced masonry	
	SD(%)	NC(%)	SD(%)	NC(%)
EN 1998-3 [2005]	0.40	0.53	N/A	N/A
DIN Eurocode 6/NA [2011]	N/A	0.40 $\sigma_0 \leq 0.15 f_k$ 0.30 $\sigma_0 > 0.15 f_k$	N/A	N/A
OPCM 3274 [2005]	0.40	N/A	$1.5 \cdot (0.40)$	N/A
FEMA 273 [1997]	0.30	0.40	FEMA 273	FEMA 273

Table 58: Referenced drift limits θ_u for shear failure

Reference	Unreinforced masonry		Reinforced masonry	
	SD(%)	NC(%)	SD(%)	NC(%)
EN 1998-3 [2005]	0.80	1.07	N/A	N/A
DIN Eurocode 6/NA [2011]	N/A	$0.6\alpha\,(h^2/L)$	N/A	N/A
OPCM 3274 [2005]	0.80	N/A	$1.5 \cdot (0.80)$	N/A
FEMA 273 [1997]	$0.30\,(h/L)$	$0.40\,(h/L)$	FEMA 273	FEMA 273

Table 59: Referenced drift limits θ_u for bending failure

see FEMA 273, Table 7-5.

The drift ratio for reinforced masonry has been defined according to FEMA 273 [1997] for non-linear static procedures. Here, FEMA 273 [1997] guidelines for reinforced masonry walls were used as a reference to limit the ultimate displacements. This was done considering the fact that no reliable limit values for reinforced masonry walls were defined in other design provisions studied previously.

6.4.4 *General software description and features*

MINEA software was developed by Dr.-Ing. Christoph Butenweg and his associates (SDA-engineering GmbH). It offers solution for effective analysis of masonry buildings under vertical and horizontal loads

Failure mode	Unreinforced θ_u (%)	Reinforced θ_u (%)
Diagonal shear+Sliding shear	$0.4\ (\sigma_0 \leq 0.15\, f_k)$ $0.3\ (\sigma_0 > 0.15\, f_k)$	acc. FEMA 273 table 7-5
Bending	$0.4\,(h/l)$	acc. FEMA 273 table 7-5

Table 60: Ultimate displacements implemented in MINEA

from earthquakes and wind. It features integrated database structure, with databases for masonry materials. Depending on the requirements of the specific project, the calculations can be performed on 2D or 3D models.

The seismic action can be described by a design spectrum according to DIN 4149-04 [2005] and a user supplied free spectrum. The seismic action can be applied in arbitrary direction of the ground plan or the program can automatically determine the weakest direction of the building and apply the horizontal loads. The damping from code defined spectra can be defined as hysteretic or constant viscous damping, while for free spectra the damping has to be included in the spectra.

The building is assumed to be composed of continuous walls along the height and the upper floors are considered as linear elastic.

The torsional effects are considered according to the code regulations.

The materials are classified according to their mechanical properties. A database of code defined and user supplied materials is available within the program. The building is defined in the plan view by including the continuous walls only. The openings, piers and spandrels are not considered and the walls with openings should not be defined in the calculation. The walls are entered through a graphical environment by indicating start and end points of each wall. The floor slab is created within the graphical window by indicating the floor contour points. Openings in the floors can be considered.

The load distribution on the walls is performed according to corresponding areas of influence.

The results are presented in tabular and graphical form. The graphical presentation of the results shows the diagrams of the capacity curves for the individual walls, the capacity curve of the entire building, the diagram from CSM with identified Performance point, the frequency distribution and the damping of the building.

6.5 Practical application

For practical application of the presented seismic verification concept, all input data can be provided by a database containing the capacity curves of the individual walls and the appropriate damping ratios. Depending on the loading conditions and the length to height ratio, a matrix of available data can be build up for each unit mortar combination. By using a feasible interpolation algorithm the buildings capacity curves can be calculated for arbitrary wall configurations as well as for the geometry and loading conditions of the individual walls.

The presented displacement-based seismic verification concept has been applied to an existing public building. The used methodology consists of FEM updating and definition of a mathematical model. It is based on estimation and identification of the structural parameters by ambient vibration measurements due to missing material data for the building. The experimental results were used for modal updating of the material parameters for the initial finite element calculation model with the help of the extracted natural frequencies and the mode shapes. Model updating by variation of several key material parameters was performed. However, modal updating and ambient vibration testing are not necessary for the non-linear analysis, because the eigenfrequencies in the elastic range of the building do not influence the results of the nonlinear calculations. Finally, a model which reflects the real bearing capacity of the building was obtained and used for structural seismic safety verification.

A flow chart describing the methodology is presented in Figure 123. The methodology was established on dynamic-based assessment which involves analytical and operational modal analysis. The analytical modal analysis consists of identification of dynamic properties using the FEM . The finite element model was created according to the available geometry and material data. Operational modal analysis considers extraction of modal parameters (natural frequencies, damping and mode shapes) from output-only experimental data obtained by ambient vibration tests. The need for model updating was checked by comparing the difference between FEM and OMA results. If the difference is less than certain established criteria, than the FE model is optimal. On contrary, the model needs updating. Usually it is done by modifying selected parameters in FE model until calculation results do not match experimental.

6.5.1 *Description of the building*

The proposed methodology has been applied on the public masonry building of the primary school "Vojdan Chernodrinski" in Skopje, Macedonia [Dumova-Jovanoska et al., 2011]. This building was selected for research and application of the developed methodology as a typical example of a building from the city of Skopje due to several reasons. The building was constructed before the catastrophic 1963 Skopje earthquake and according to PIOVSP [1981] it is classified in category I. It is extremely important for such buildings to survive future earthquakes without serious damage of the structural system and to protect the lives of the residing young children.

To perform a dynamic analysis of an existing building with adequate mathematical model, it is necessary to search for the available data describing the building's geometry, as well as data for the construction material and mass distribution in the plan and along the height of the building. Therefore, the original design project documentation of the building was discovered from the Archives of Macedonia. Although incomplete, it was useful to determine some necessary parameters. It

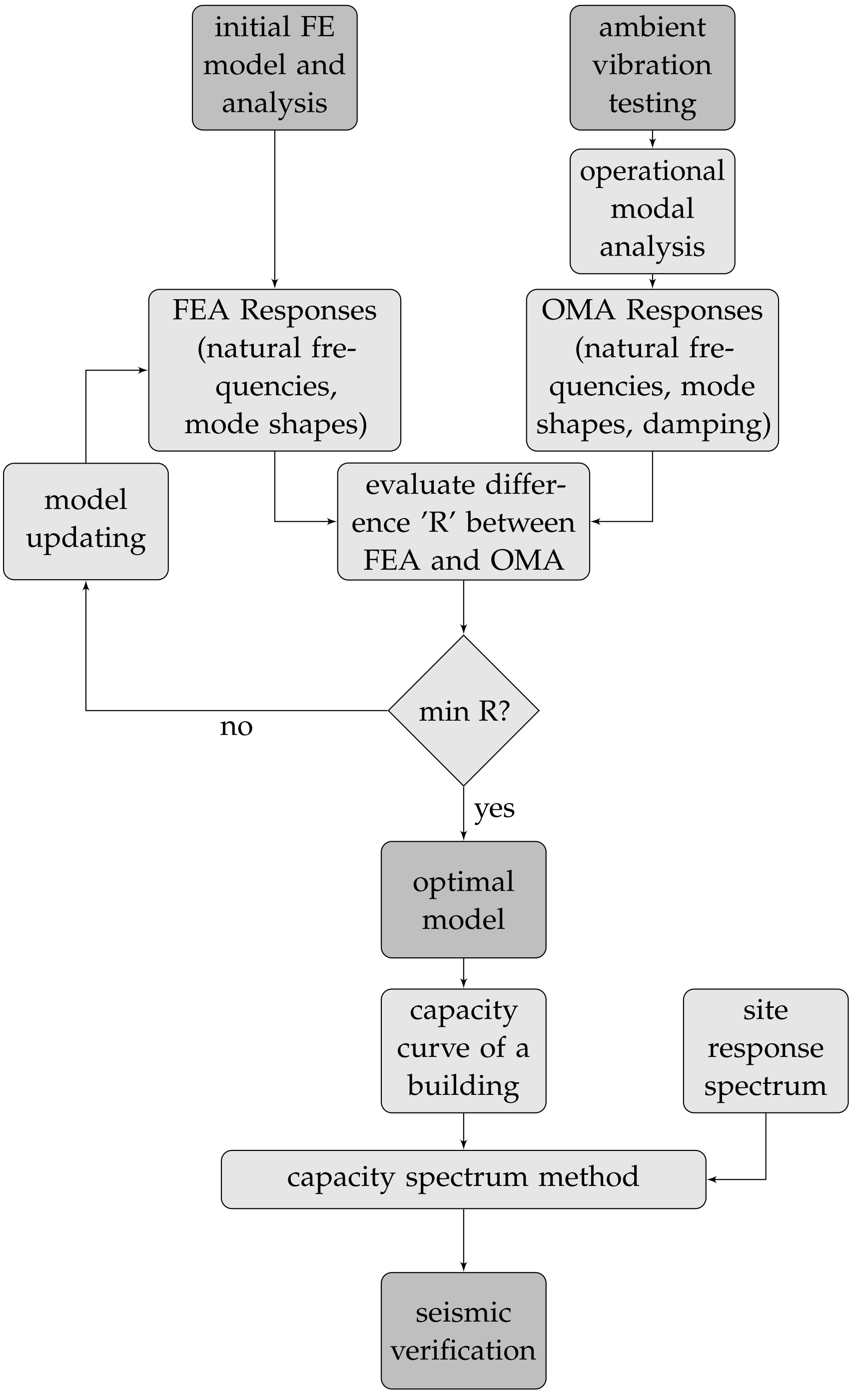

Figure 123: Methodology for dynamic-based assessment applied to an existing building

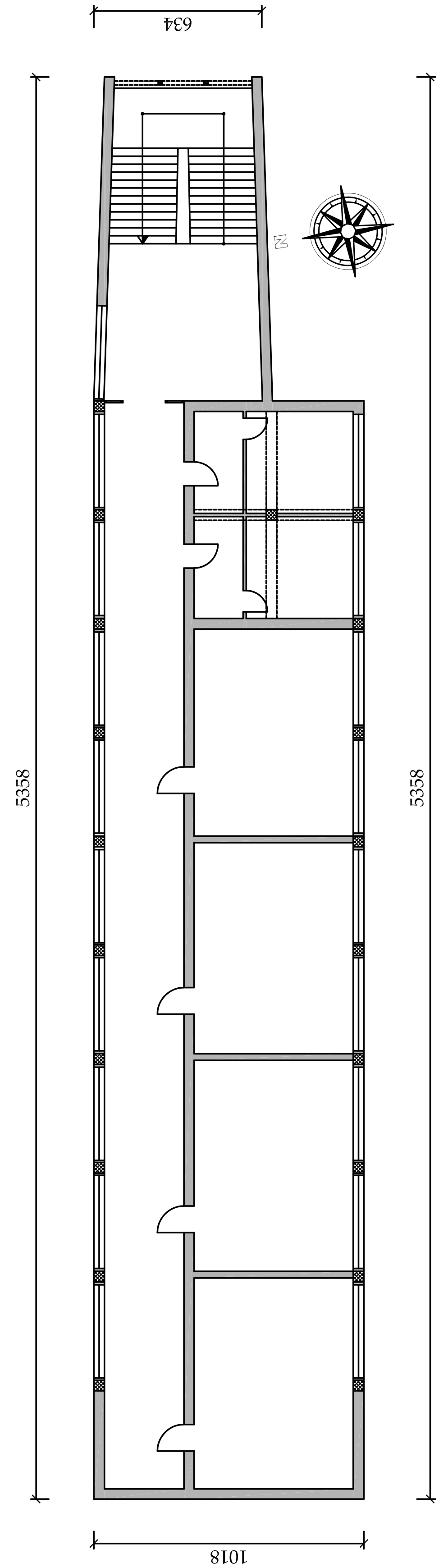

Figure 124: Typical building floor plan

(a) North-West view

(b) West-East view

(c) Hallway view

Figure 125: Characteristic views of the building

was discovered that the building was constructed in 1952; it consists of ground floor and 2 upper floors with rectangular shape in layout and dimensions 53.58 x 10.18 m, see Figure 124. From the available documentation it was found out that the structural system is confined masonry. It is composed from solid brick units and mortar with unknown properties and regularly spaced RC columns made from concrete class MB16 and certain number of RC beams. The concrete beams of class MB22 were used to connect few columns, while the other beams were located over the openings. The floors were designed and constructed as ribbed slabs from concrete class MB22. The building was designed by taking into account vertical gravitational loads only as seen in the design documentation. Typical views on the building are given in Figure 125.

With the purpose to determine the real geometry, detailed on-site measurements were performed which confirmed many design parameters, but also notified some significant differences of the actual building configuration from the original documentation. The survey of the documentation and the current state of the building verified presence of RC columns which function as a confinement of the ma-

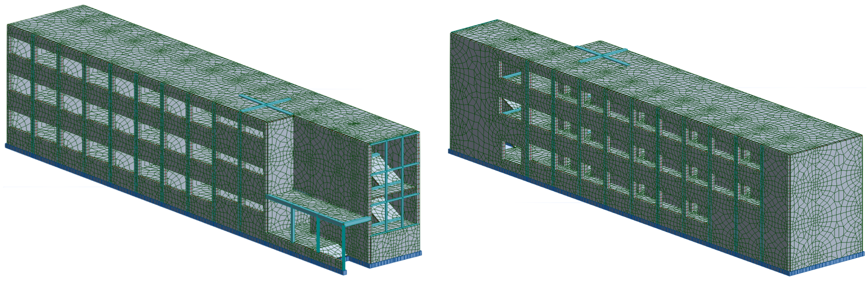

(a) South-East view (b) North-West view

Figure 126: 3D mathematical finite element model

sonry. The floors were assessed to have sufficient in-plane rigidity and can be treated as rigid diaphragm in the analysis.

Complete information about the properties of the construction material was missing, except very few parameters given in the original documentation. Because it was impossible to perform destructive tests and extract test samples from the building, the only possible method to discover the material properties was to conduct non-destructive tests and to use ambient vibration measurements. Therefore, series of ambient vibration measurements were carried out and these results were used to update the FE model of the building.

6.5.2 *FE modelling and identification of the dynamic properties*

Initial 3D calculation FE model of the building based on the geometry survey was developed prior performing the ambient vibration tests, see Figure 126.

The masonry walls and the floor slabs were modelled with 4-node shell FE, while the RC beams and columns with frame elements. To obtain proper mass distribution in the model and to correctly represent the openings in the masonry walls, relatively large number of FE was used. Several assumptions were followed during development of the model. It was assumed that the model is fully fixed at the supports. Masonry was assumed to have constant unit weight of 19.6 $\mathrm{kN/m^3}$and Poisson's ratio of 0.15, while the Young's modulus was taken as 2800 $\mathrm{N/mm^2}$. The RC elements were modelled with material properties according to their design class. The floor slabs were modelled as absolute rigid in their plane.

In order to determine the dynamic properties of the structure, modal analysis was performed. Beside the mass from the self-weight of the structural elements, additional mass from the dead load calculated according the design project specification was applied. Calculated natural frequencies and periods for the first 6 mode shapes of the initial calculation model are given in Table 61.

The building responds with translation oscillation in the north-south direction in the first mode and small rotation which originates

Mode	Frequency (f) (Hz)	Period (T) (sec)
1	5.33	0.19
2	6.58	0.15
3	7.80	0.13
4	8.78	0.11
5	12.34	0.08
6	12.98	0.08

Table 61: Natural frequencies and periods of the initial calculation model

from the stiffness difference of the structure in the part where the classrooms and the stairways are located. In the second mode the structure oscillates with torsion, while translation in the east-west direction is dominated in the third mode. The first 3 identified mode shapes are shown in Figure 133.

6.5.3 *Ambient vibration tests and analysis methods*

Three series of ambient vibration tests were conducted on August 18, 2011. Each series contains results from acceleration sensors located on each floor. Nine roving accelerometers and one fixed reference sensor (T1) located on the top floor were used. Calibration of the sensors was applied prior each measurement. It consists of positioning the sensors on a flat surface next to each other. All sensors are invoked to record the accelerations in the same direction. The acceleration response spectrum of all sensors are compared. If a sensor reports acceleration time history which deviates from the time histories acquired with the remaining sensors, then a calibration of the input parameters of that sensor is performed. This procedure is necessary to provide consistent measurement and reliable results. The total recording time in each recording session was 212 sec, while the sampling frequency was fixed to 200 Hz.

6.5.3.1 *Test equipment*

To measure and store the ambient vibration effects on the building, Digitexx PDAQ Premium portable system with physical dimensions 457 x 330 x 170 mm as shown in Figure 127a was used. This system supports data acquisition and analysis from distance.

Main characteristics of the system are: 16 channels, 24 bits, local and remote real time data analysis, FFT, transfer functions, inter-storey drift based on FEMA 351 [2000] and FEMA 274 [1997] seismic safety standards, hysteresis curve for the inter-storey drift, computation of

(a) Digitexx PDAQ Premium (b) Digitexx D110-T triaxial sensor

Figure 127: Hardware equipment for ambient vibration tests

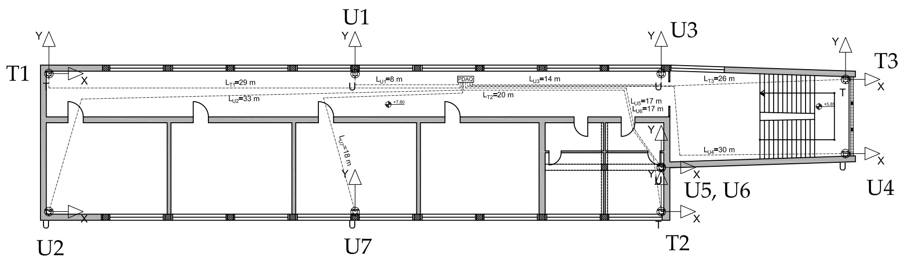

Figure 128: Sensor location and connecting cables in the second floor

acceleration, velocity and displacement. This system is best option for permanent structural health monitoring for a period up to 6 months. The main characteristics of the acceleration sensors are: uni- and triaxial micro electro-mechanical capacity sensors with wide dynamic range +/- 3 g, perfect band and ultra low noise, which make them ideal for structural health monitoring, Figure 127b.

6.5.3.2 *Arrangement of the test equipment and measurement*

Ambient vibration (AV) tests were accomplished with uniaxial (U) and triaxial (T) acceleration sensors and measurements in 9 points on each floor. Figure 128 schematically presents the plan view of the building and the arrangement of the sensors on the second floor, cable disposition and measurement direction of the sensors. The arrangement of the test equipment on the other floors was identical, while the roof floor was not measured due to its inaccessibility. PDAQ device was moved to each floor prior the measurements. All sensors were placed carefully and levelled on the hard 'terazzo' flooring, except the sensors U2 and U7 which were placed over hard wood flooring. A view of the PDAQ and one sensor location in the school hallway is presented in Figure 129.

While the measurements were on their way, there were no other people present in the building, apart from the test operators who

Figure 129: PDAQ and U1 sensor location

stayed still during the recording. There were no active heating and cooling devices turned on, and the running water in the building was stopped. This procedure was not necessary due to the ability of the applied experimental method to isolate the actual structural response, but was found suitable to exclude any contribution in the noise signal originating from undesired sources. The recording was carried out between 10 am and 2 pm. The outside temperature was in the range $26 - 33\,^{\circ}\mathrm{C}$. The total number of measurement points from all three series where accelerations were recorded was 27. The recorded analog signals were digitized and saved in ASCII format on the hard disk of the computer used for data acquisition.

6.5.3.3 *Methods for analysis of the measured data and results*

For analysis of the complex non-stationary nature of the measured excitations it is necessary to use techniques for identification of the dynamic properties based on Output-Only experimental data, like: Frequency Domain Decomposition (FDD), Enhanced Frequency Domain Decomposition (EFDD) and Stochastic Subspace Identification (SSI) methods [El-Borgi et al., 2005]. These methods were successfully applied to buildings and bridges and are implemented in ARTeMIS software [Structural Vibration Solutions, Inc., 2011].

The essence of the FDD technique is to perform an approximate decomposition of the measured system response into a set of responses of independent single degree of freedom (SDOF) systems, one for each mode. The decomposition is performed by a Singular Value Decomposition (SVD) of each of the spectral density matrices obtained from the measurements. The results of the decomposition are a set of singular values and associated singular vectors. The singular values are estimates of the auto spectral density of the component SDOF systems, and the singular vectors are estimates of the mode shapes. A further refinement of the FDD, the Enhanced Frequency Domain

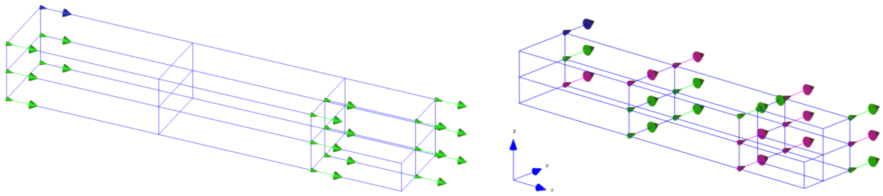

(a) X direction (b) Y direction

Figure 130: Disposition of the measurement points in the ARTeMIS software

Decomposition method in ARTeMIS, uses the modal estimates from the FDD technique to identify the bell-shaped spectral functions of the SDOFs. From these functions, it estimates additional modal parameters such as modal damping [El-Borgi et al., 2005].

The time domain estimation is based on Stochastic Subspace Identification technique. In the SSI techniques a parametric model is fitted directly to the raw time series data obtained from the accelerometers. The parametric models are characterized by the assumption of a mathematical model constructed from a set of parameters, where the mathematical model is a linear and time-invariant system of differential equations. The task of the SSI technique is to adjust the parameters in order to change the way the model fits to the data. In general, the objective is to estimate a set of parameters that will minimize the deviation between the predicted system response (predicted transducer signal) of the model and the measured system response (transducer signal) [Ibsen and Liingaard, 2006]. This method has great advantage over the frequency domain methods because the modal density can became very high due to occurrence of close mode shapes with high damping values. Further details about these analysis methods can be found in the cited references.

The analysis of the measured data was performed with ARTeMIS software for each direction independently. Two calculation models were established, each of them with sensors pointing in the respective direction X or Y, see Figure 130. This simplification was made after performing analysis with the combined action of the sensors. Within this analysis it was not possible reliably identify the vibration modes of the building.

The measured ambient vibration response of the building was analysed with FDD and EFDD methods. Figure 131 and Figure 132illustrates the average of the normalized singular values of spectral density matrices (ANPSD) for all test set-ups estimated with FDD and EFDD method, together with identified peaks. The singular values of the peaks in this figure correspond to the identified frequencies. The analysis with both analysis methods was performed to identify the natural frequencies in the frequency range of 0-20 Hz.

By comparing the results for the identified modes from both methods with respect to the orthogonal directions, similar results for natural

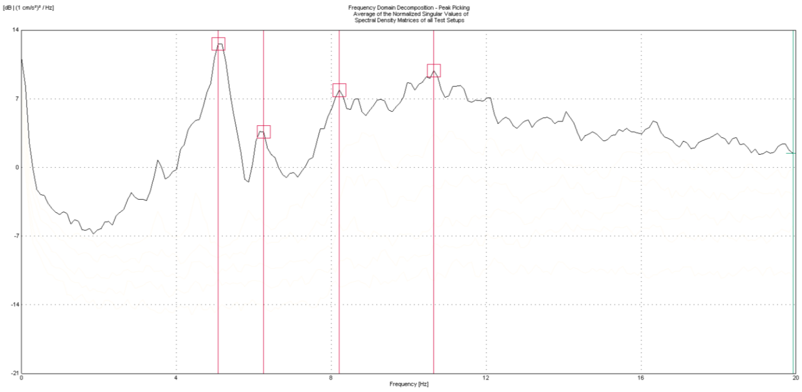

(a) FDD - peak picking for X direction

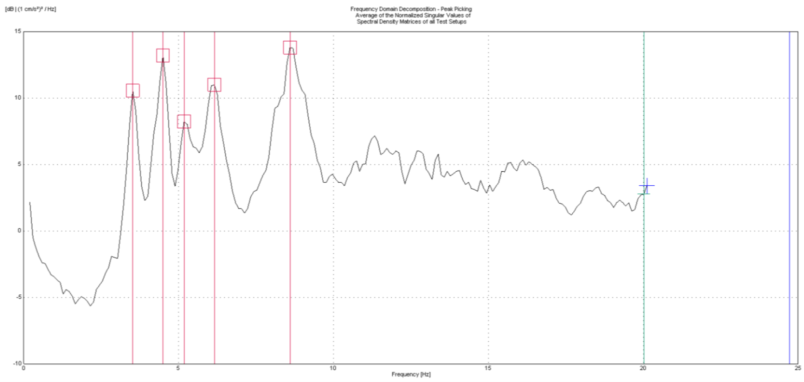

(b) FDD - peak picking for Y direction

Figure 131: ANPSD for FDD method

frequencies were obtained. However, a notable difference for the estimated fourth and fifth vibration mode was obtained. The damping identified with EFDD method range between $1.19 - 4.32\,\%$ for X direction and $1.36 - 3.06\,\%$ for Y direction. The average damping was estimated to $2.6\,\%$. Table 62 presents the results from the performed analysis. The slanted values in the table denote the identified dominant vibration modes in the respective directions obtained with analysis of the mode shapes animated within the software. The first modes in X direction was estimated to $5.08\,Hz$and in Y direction $4.49\,Hz$.

Figure 133 shows a comparison of the first mode shapes of the building in directions X and Y calculated by the initial FE model and identified with the analysis methods in ARTeMIS. Good agreement of mode shapes was achieved.

6.5.4 *FE model updating*

The basic principle of FE model updating technique consists of changing certain critical parameters in the model until the calculated dynamic properties do not match the experimental results. The updated FE model assures better analytical representation of the dynamic

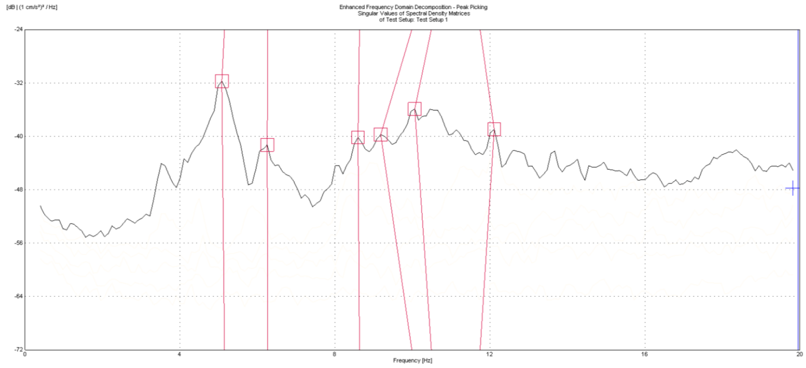

(a) EFDD - peak picking for X direction

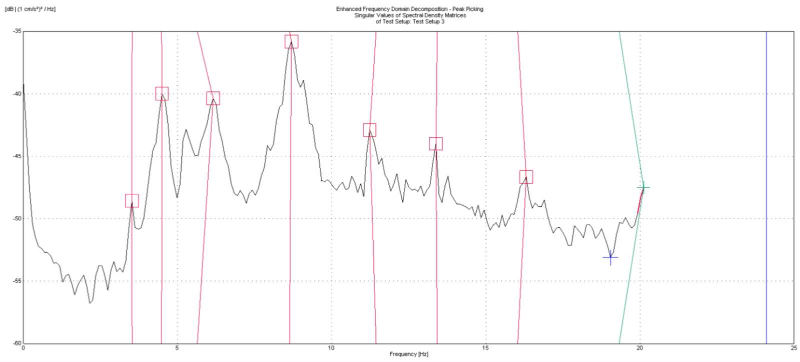

(b) EFDD - peak picking for Y direction

Figure 132: PSD for EFDD method

response of the structure and serves as a calibration tool for prediction of the seismic response [Lord et al., 2004]. The main goal of the updated model is to achieve acceptable correlation between the calculated dynamic properties and those measured experimentally. This operation comprehends sensitivity analysis of the stiffness matrix of the model in correlation with changing values of certain predefined parameters [Ventura et al., 2005].

To improve the correlation of the experimental and calculated results, a correlation analysis of the selected response parameters was executed. Usually, it is fulfilled by iterative change of the selected parameters until the correlation coefficients do not satisfy the convergence criteria. FE model updating can be achieved by manual or automatic modification of the parameters. Automatic updating has advantage over the manual in the iterative modification of several parameters at a time, while the comparison of the frequencies is made by controlling the relative error of the calculated and the measured frequencies. The relation of the calculated and the measured mode shapes is estimated by MAC criterion [Allemang and Brown, 1982].

This study uses manual FE model updating. The first step of the FE model updating was to change the absolute rigid diaphragm behaviour of the floor slabs to a flexible behaviour by using real material

Mode	X direction			Y direction		
	FDD (Hz)	EFDD (Hz)	Damping (%)	FDD (Hz)	EFDD (Hz)	Damping (%)
1	*5.08*	5.15	4.32	3.52	3.52	2.72
2	6.25	6.27	2.27	*4.49*	4.48	3.06
3	8.20	8.63	1.19	5.17	5.64	2.87
4	10.64	9.98	2.79	6.15	8.63	1.36
5	19.92	10.49	3.03	8.59	11.44	2.16

Table 62: Estimated values for natural frequencies and damping coefficients

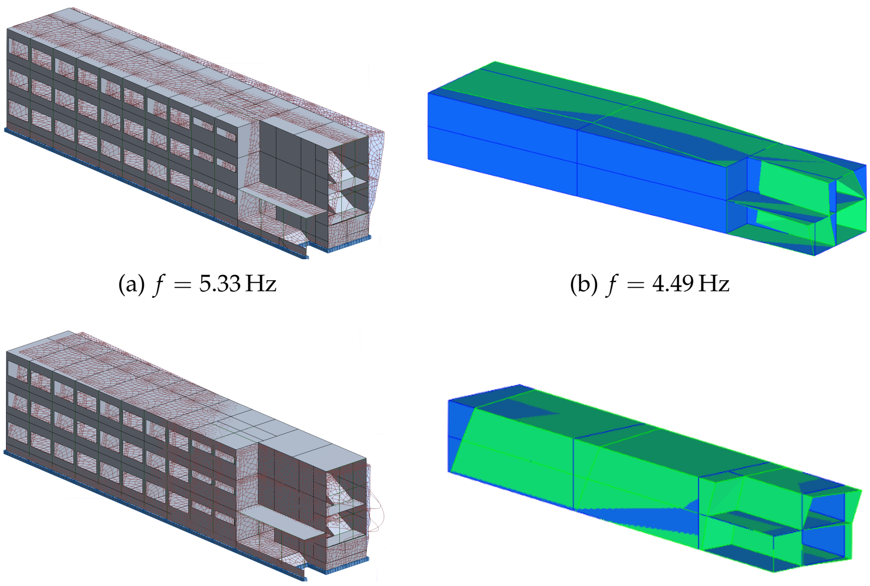

(a) $f = 5.33\,\mathrm{Hz}$ (b) $f = 4.49\,\mathrm{Hz}$

(c) $f = 7.80\,\mathrm{Hz}$ (d) $f = 5.08\,\mathrm{Hz}$

Figure 133: The dominant mode shapes calculated with the initial FE model (left) and identified with FDD method (right)

Mode	Initial FE model-stiff (Hz)	Estimated with tests-FDD (Hz)	Initial FE model-flexible (Hz)	Updated FE model-flexible (Hz)	Relative error (%)
1	5.33	4.49	4.38	4.17	7.7
2	7.80	5.08	7.26	6.78	1.5

Table 63: Comparison of the first three natural frequencies before and after FE model updating

Element	Type	Unit	Initial value	Actual value	Difference (%)
Wall	E	(N/mm^2)	2800	2850	1.8
Wall	γ	(kg/m^3)	19.6	18.7	4.6

Table 64: Comparison of the initial and actual values of the selected updating parameters

parameters. In absence of reliable data for the mechanical and strength properties of masonry, in the second step it was decided to modify the Young's modulus and unit weight of the masonry. Several manual iterations were performed. Table 63 shows the values for the natural frequencies of the first three mode shapes calculated with the initial calculation model, the estimated frequencies based on AV tests and the calculated frequencies with the updated FE model.

The modification of the floor structural type from absolute rigid to flexible had significant impact on the values of the natural frequencies. They differ from the estimated frequencies about $3 - 5\,\%$ which on one side is a result from the good engineering assessment for masonry material properties in the initial model. FE model updating of the selected parameters further improves the determined parameters and thus an optimal model of the building was achieved. Table 64 summarizes the values for the masonry Young's modulus and the unit weight before and after FE model updating. These parameters, together with the identified natural frequencies, were used as input values for the masonry materials in the numerical model used for seismic verification analysis.

6.5.5 *Displacement-based seismic verification*

The condition of the existing building was assessed by using the displacement-based seismic verification concept described previously. The capacity curves of the individual walls were computed by means

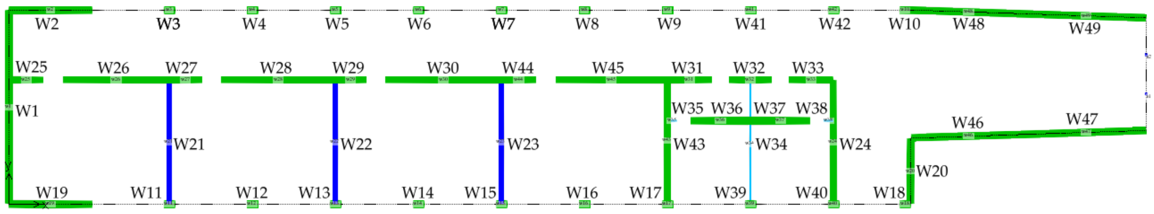

Figure 134: Wall numbering in the ground floor

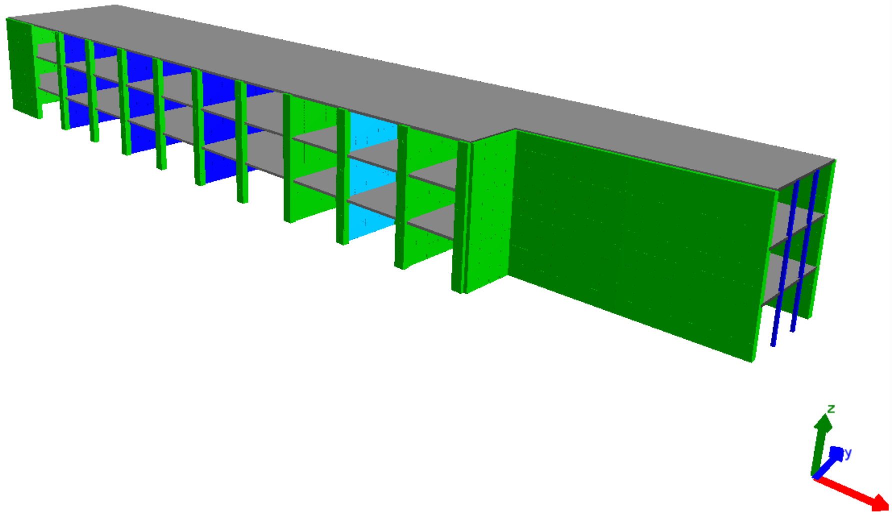

Figure 135: 3D numerical model for deformation based seismic verification

of the proposed idealisation according to DIN Eurocode 6/NA [2011]. The vertical load levels of the walls were calculated using the load distribution areas. Idealised bilinear (elastic-plastic) capacity curves for each masonry wall included in the model were calculated within the software.

6.5.5.1 *Input values for non-linear analysis of the building*

All walls present in the building have been inserted in the numerical model, see Figure 134. The window and door openings, as well as the the spandrel walls were excluded from the analysis. Only continuous walls with rectangular shape were included for calculation of the building capacity curves, see Figure 135. The wall height of the three stories was 3900 mm. As discovered from the original design project, three different thickness of the walls were modelled, namely 120 mm, 250 mm and 400 mm.

All walls were modelled from unreinforced masonry and were considered fully fixed on both edges ($\alpha = 0.5$). Additionally, two rectangular columns ($150x150\,mm$) from reinforced concrete were added to the model where the openings for the windows at the stairs are located. Moreover, due to the unknown properties of the RC columns for confinement at window piers, as well as their connection with the

Material	Compressive strength (N/mm^2)	Char. initial shear (N/mm^2)	Modulus of elasticity (N/mm^2)	Density (kg/m^3)	Poisson's ratio
URM	2.83	0.08	3107.99	1870.00	0.1
RC	20.50	/	31500.00	2500.00	0.2

Table 65: Material data for analysis of the existing state of the building

masonry, those elements were treated as unreinforced masonry piers. Following the basic assumptions of the software, the floor structure was taken as RC rigid diaphragm. The slab thickness was 150 mm. The roof structure was modelled as rigid RC slab with thickness of 120 mm. The material data for the analysis is provided in Table 65.

The strengthened masonry included in the analysis consists of reinforcement meshes with diameter $\emptyset\,8$ mm at a mutual distance on vertical and horizontal direction of 100 mm. In total, the area of the reinforcement mesh was 503 mm^2. The yield strength of the reinforcement mesh was 600 N/mm^2.

In addition to the self-weight, live load with intensity of 1.50 kN/m^2 was applied in vertical direction on all slabs. Load combination factors for office building $\psi_0 = 0.7$ and $\psi_2 = 0.3$ were applied. The roof was loaded with additional load of 1.00 kN/m^2.

The idealized capacity curves for each wall were calculated within the software with the analytical model provided in Section 6.4. First, ultimate resistance of each wall was calculate for the case of shear and flexural failure mode, by using the respective formulas. The wall failure mode was determined with respect to the smaller value between both. Next, initial stiffness, elastic displacement and ultimate displacement were calculated.

The seismic load was defined according to Eurocode 8 [2004] for assumed ground type B and estimated site elastic ground acceleration of $a_g = 2.94\,m/\text{s}^2$ (~ 0.3 g). The demand curves were represented by earthquake response spectra for various levels of damping. Three damped response spectra curves were used, 3 %, 5 % and 10 %. The 3 percent damping was defined according to the results from the ambient vibration test. The 5 percent response spectrum is generally used to represent the demand when the structure is responding linearly-elastic. Higher damped response spectra are used to represent inelastic response spectra to account for hysteretic non-linear response of the building [Freeman, 1998]. The applied design spectra are shown in Figure 136.

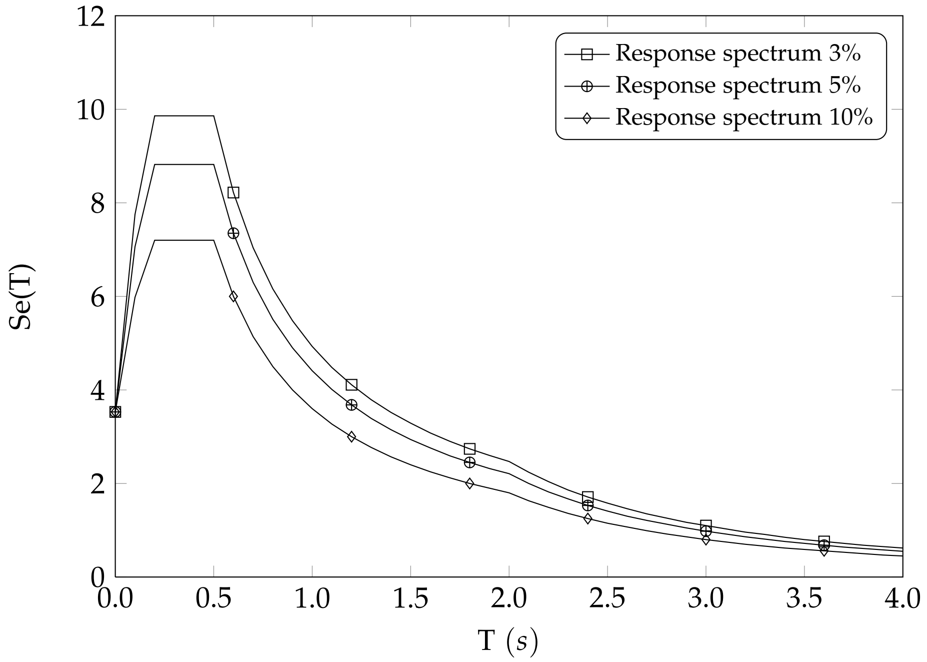

Figure 136: Elastic response spectra for different damping coefficients

6.5.6 *Assessment of the existing building*

The main results for the unreinforced masonry walls are given in Table 66. The results from the analysed unreinforced masonry building showed that all walls oriented in Y direction of the global coordinate system will fail in shear, because their shear resistance was smaller that their flexural resistance. Also, most of the walls positioned in the global X direction will fail in flexure, 71 %, while only 29 % of the walls will fail in shear. Very interesting finding was that all walls that were assessed to fail in shear have height to length (h/L) ratio smaller than 1.7, while the flexural failure mode would occur at walls with $h/L > 1.7$. The normal stress level achieved in the walls was in the range $\sigma_0 = 0.18 - 0.75\,N/\text{mm}^2$. The total resultant floor masses are: floors 1,2 $=$ 594.46 t and floor 3$=$ 408.45 t. The graphical presentation of the input capacity curves of the walls participating to the stiffness of the building in both orthogonal directions, X and Y, are presented in Figure 137.

The calculated capacity curves for the unreinforced masonry building in both orthogonal directions (X and Y) are shown in Figure 138. As can seen from the figure, the capacity of the building in Y direction is about 2 times less than the capacity in X direction. This means that the building is more vulnerable in Y direction and the first failures of the walls are expected to happen in the walls oriented with their plane in Y direction. The building has greater ductility in X direction. The assessed capacity was expected, considering the orientation of the walls in the floor plan layout.

Wall	Dir.	Length $L\,(mm)$	Thickness $t\,(mm)$	Ratio h/L	Normal force $N\,(kN/m')$	Normal stress $\sigma_0\,(N/mm^2)$	Flexural resistance $H_{uf}\,(kN)$	Shear resistance $H_{us}\,(kN)$	Displacements Elastic $d_e\,(mm)$	Displacements Ultimate $d_u\,(mm)$	Initial stiffness $K_e\,(kN/m')$	Failure mode
W1	Y	10000	400	0.39	73.94	0.18	1346.11	422.81	3.30	15.60	127969.18	shear
W2	X	4300	400	0.91	83.35	0.21	277.60	187.91	2.57	15.60	73038.07	shear
W3	X	600	400	6.50	203.23	0.51	11.38	35.31	13.31	101.40	854.64	flexure
W4	X	600	400	6.50	204.29	0.51	11.42	35.38	13.36	101.40	854.64	flexure
W5	X	600	400	6.50	203.36	0.51	11.38	35.32	13.32	101.40	854.64	flexure
W6	X	600	400	6.50	203.36	0.51	11.38	35.32	13.32	101.40	854.64	flexure
W7	X	600	400	6.50	203.95	0.51	11.41	35.36	13.35	101.40	854.64	flexure
W8	X	600	400	6.50	203.52	0.51	11.39	35.33	13.33	101.40	854.64	flexure
W9	X	600	400	6.50	202.52	0.51	11.35	35.26	13.28	101.40	854.64	flexure
W10	X	600	400	6.50	181.26	0.45	10.44	33.83	12.22	101.40	854.64	flexure
W11	X	600	400	6.50	117.63	0.29	7.33	29.11	8.58	101.40	854.64	flexure
W12	X	600	400	6.50	300.71	0.75	14.67	41.25	17.16	101.40	854.64	flexure
W13	X	600	400	6.50	117.54	0.29	7.32	29.10	8.57	101.40	854.64	flexure
W14	X	600	400	6.50	300.04	0.75	14.65	41.21	17.14	101.40	854.64	flexure
W15	X	600	400	6.50	118.21	0.30	7.36	29.16	8.61	101.40	854.64	flexure
W16	X	600	400	6.50	300.10	0.75	14.65	41.22	17.14	101.40	854.64	flexure
W17	X	600	400	6.50	117.70	0.29	7.33	29.12	8.58	101.40	854.64	flexure
W18	X	600	400	6.50	95.85	0.24	6.13	27.31	7.17	101.40	854.64	flexure
W19	X	4300	400	0.91	96.53	0.24	316.68	196.13	2.69	15.60	73038.07	shear
W20	Y	3400	400	1.15	77.92	0.19	163.25	145.81	2.75	15.60	53062.08	shear
W21	Y	6400	250	0.61	80.54	0.32	563.38	199.98	2.54	15.60	78608.43	shear
W22	Y	6400	250	0.61	80.41	0.32	562.60	199.87	2.54	15.60	78608.43	shear
W23	Y	6400	250	0.61	80.56	0.32	563.52	200.00	2.54	15.60	78608.43	shear
W24	Y	6400	400	0.61	100.24	0.25	725.33	295.27	2.77	15.60	106654.81	shear
W25	X	1800	400	2.17	92.95	0.23	53.65	81.18	3.40	33.80	15785.11	flexure
W26	X	5500	400	0.71	113.80	0.28	598.56	264.02	2.79	15.60	94574.96	shear
W27	X	1700	400	2.29	105.77	0.26	53.66	79.74	3.88	35.79	13841.25	flexure
W28	X	5900	400	0.66	114.59	0.29	692.92	283.85	2.83	15.60	100360.24	shear
W29	X	1600	400	2.44	105.55	0.26	47.44	75.00	3.95	38.03	11999.21	flexure
W30	X	6000	400	0.65	114.57	0.29	716.48	288.64	2.84	15.60	101700.86	shear
W31	X	2300	400	1.70	95.27	0.24	89.55	104.50	3.36	26.45	26667.98	flexure
W32	X	2200	400	1.77	102.10	0.26	87.11	102.07	3.57	27.65	24370.14	flexure
W33	X	2300	400	1.70	107.52	0.27	99.63	108.44	3.74	26.45	26667.98	flexure
W34	Y	6200	120	0.63	43.45	0.36	279.77	96.76	2.43	15.60	39842.24	shear
W35	X	500	120	7.80	34.27	0.29	1.49	7.21	9.86	121.68	150.98	flexure
W36	X	3100	400	1.26	86.51	0.22	149.21	136.91	2.98	15.60	45891.26	shear
W37	X	3100	400	1.26	86.51	0.22	149.21	136.91	2.98	15.60	45891.26	shear
W38	X	500	120	7.80	35.07	0.29	1.52	7.26	10.06	121.68	150.98	flexure
W39	X	600	400	6.50	118.21	0.30	7.36	29.16	8.61	101.40	854.64	flexure
W40	X	600	400	6.50	111.08	0.28	6.98	28.58	8.16	101.40	854.64	flexure
W41	X	600	400	6.50	204.51	0.51	11.43	35.39	13.37	101.40	854.64	flexure
W42	X	600	400	6.50	200.94	0.50	11.28	35.16	13.20	101.40	854.64	flexure
W43	Y	6400	400	0.61	95.06	0.24	692.01	290.58	2.72	15.60	106654.81	shear
W44	X	1800	400	2.17	106.71	0.27	60.62	84.66	3.84	33.80	15785.11	flexure
W45	X	5800	400	0.67	113.12	0.28	662.20	277.89	2.81	15.60	98977.77	shear
W46	X	6002	400	0.65	106.46	0.27	672.71	282.13	2.77	15.60	101732.62	shear
W47	X	6203	400	0.63	87.31	0.22	602.41	274.69	2.63	15.60	104298.39	shear
W48	X	6003	400	0.65	96.73	0.24	618.35	273.99	2.69	15.60	101744.82	shear
W49	X	6203	400	0.63	87.23	0.22	601.94	274.63	2.63	15.60	104298.39	shear

Table 66: Results for the case of unreinforced masonry walls

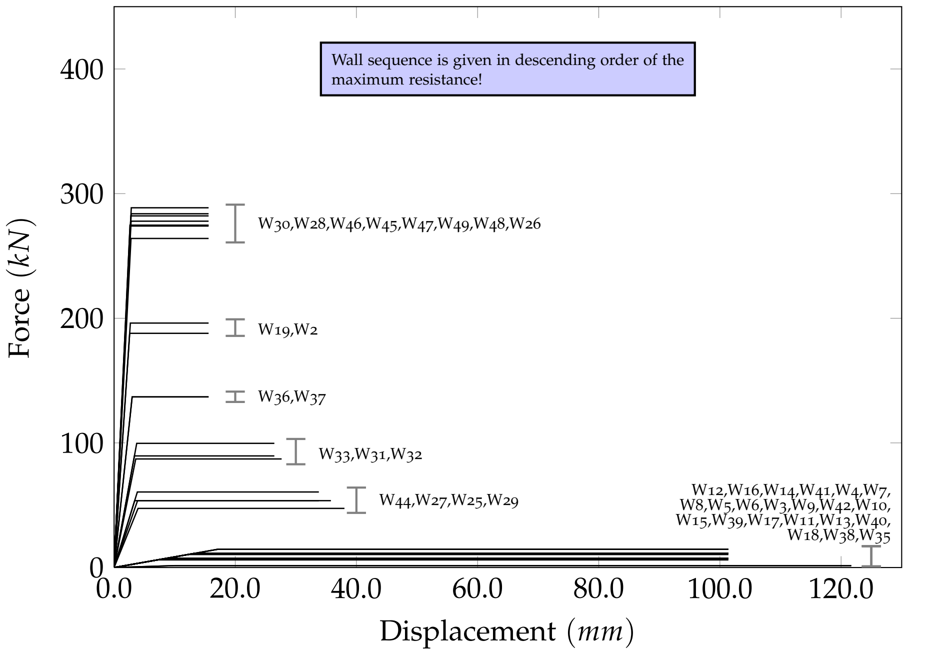

(a) X direction

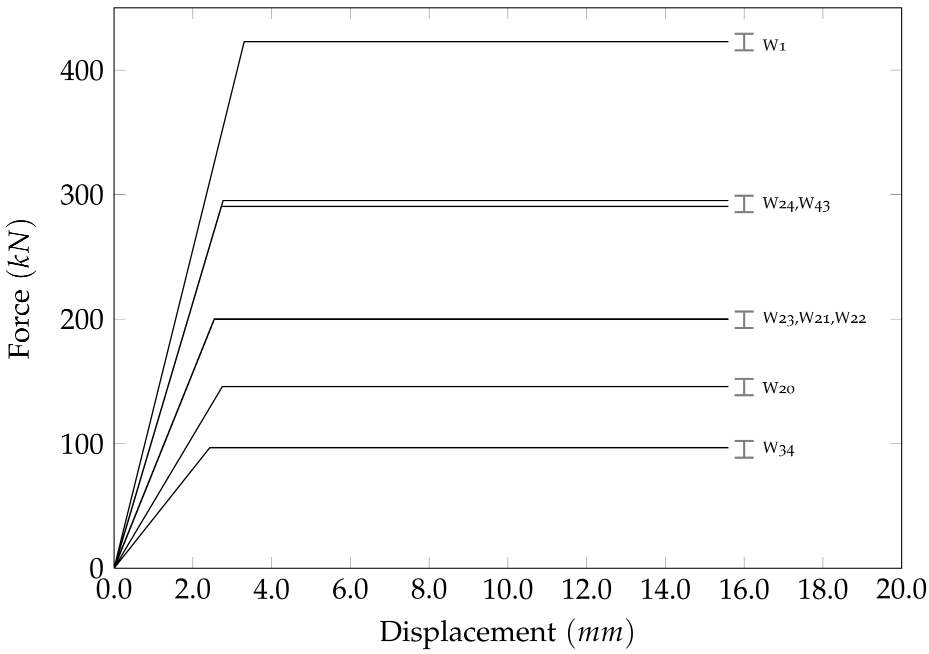

(b) Y direction

Figure 137: Capacity curves of the unreinforced masonry walls

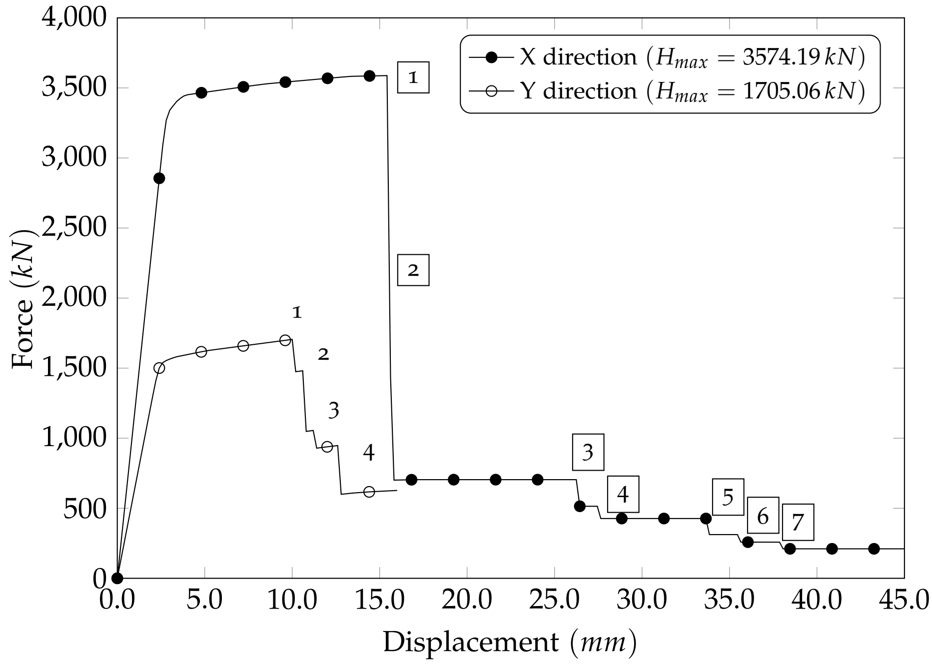

Figure 138: Capacity curves of the URM building in the orthogonal directions

The non-linear displacement-based method was applied in both directions of the building. The building's capacity curve was converted into a spectral acceleration-spectral displacement diagram by using the dynamic characteristics of the fundamental mode to represent the structure as a single-degree-of-freedom structure. Thus, a capacity spectrum was obtained.

Both the capacity spectrum and the demand response spectrum were defined with the same set of coordinates and plotted together as shown in Figure 139. The intersection point in the diagram represents the "Performance Point", i.e. the inelastic response of the building. If the capacity curve intersects the demand curve, then the building should survive the earthquake. In the case of unreinforced masonry building no performance point could be established for either 3, 5 or 10 % damping. This indicates critical situation and possible failure of the building in the ground floor.

No performance point in the existing building!

Figure 140 and Figure 141 illustrate the sequence of the wall failure in the ground floor for the unreinforced masonry building in both orthogonal directions. The sequence of failure of the walls in X direction is denoted with numbers in squares, while the sequence of wall failures in Y direction is marked with numbers only. Some of the identified wall failures are presented beside the capacity curves in the corresponding loading directions in Figure 138.

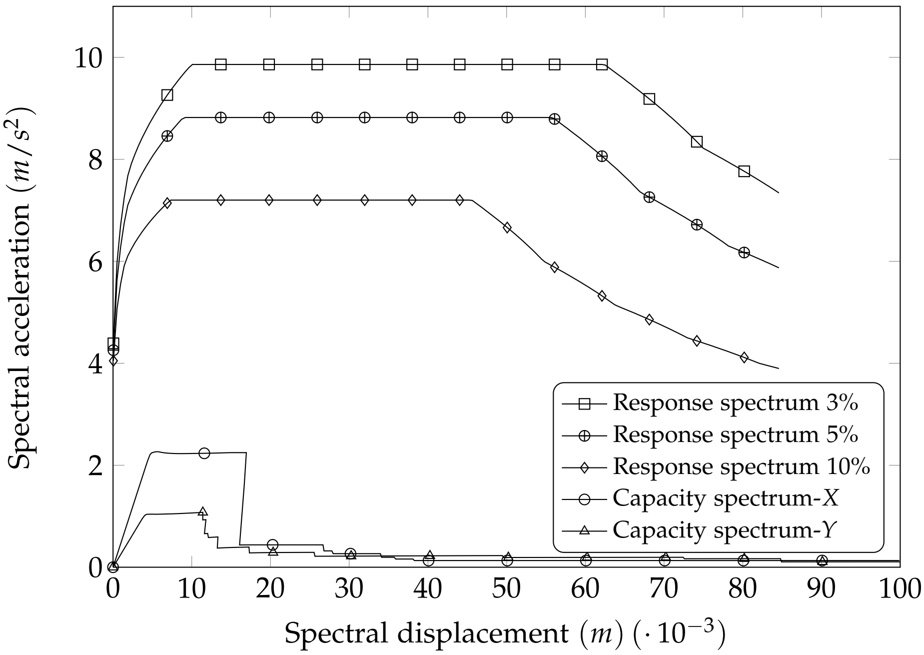

Figure 139: Determination of the "Performance Point" for the unreinforced masonry building

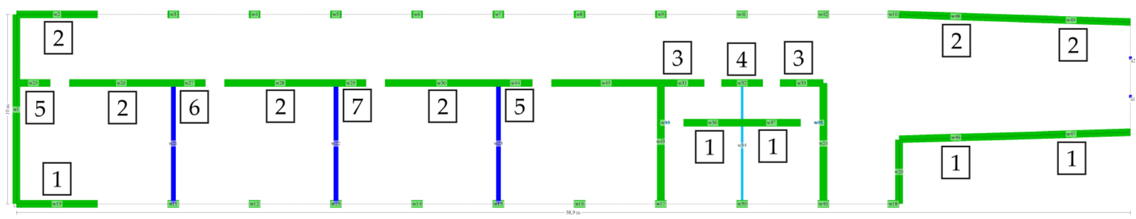

Figure 140: Wall failure sequence of URM building in X direction

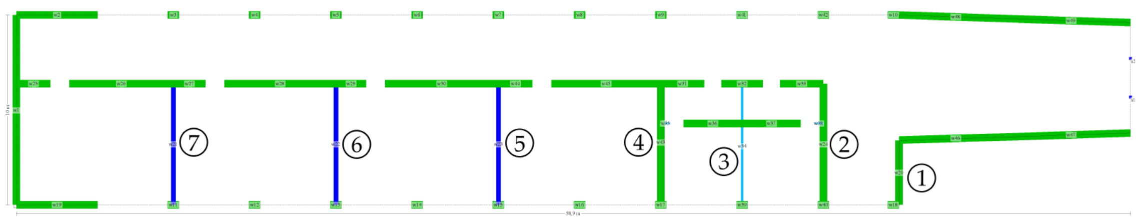

Figure 141: Wall failure sequence of URM building in Y direction

Wall	Dir.	Length $L\,(mm)$	Thickness $t\,(mm)$	Ratio h/L	Normal force $N\,(^{kN}/_{m'})$	Normal stress $\sigma_0\,(^{N}/_{mm^2})$	Flexural resistance $H_{uf}\,(kN)$	Shear resistance $H_{us}\,(kN)$	Displacements Elastic $d_e\,(mm)$	Displacements Ultimate $d_u\,(mm)$	Initial stiffness $K_e\,(^{kN}/_{m'})$	Failure mode
W2	X	4300	400	0.91	83.35	0.21	360.88	1909.53	0.99	15.71	365190.37	flexure
W19	X	4300	400	0.91	96.53	0.24	411.68	1926.83	1.13	15.20	365190.37	flexure
W20	Y	3400	400	1.15	77.92	0.19	212.22	1484.27	0.80	20.15	265310.38	flexure
W21	Y	6400	250	0.61	80.54	0.32	732.39	2546.57	1.86	13.10	393042.17	flexure
W22	Y	6400	250	0.61	80.41	0.32	731.39	2546.33	1.86	13.10	393042.17	flexure
W23	Y	6400	250	0.61	80.56	0.32	732.58	2546.61	1.86	13.10	393042.17	flexure
W24	Y	6400	400	0.61	100.24	0.25	942.92	2874.95	1.77	13.10	533274.03	flexure
W26	X	5500	400	0.71	113.80	0.28	778.13	2492.66	1.65	14.00	472874.82	flexure
W28	X	5900	400	0.66	114.59	0.29	900.80	2675.30	1.80	13.60	501801.20	flexure
W30	X	6000	400	0.65	114.57	0.29	931.43	2720.60	1.83	13.50	508504.28	flexure
W34	Y	6200	120	0.63	43.45	0.36	363.70	2160.08	1.83	13.30	199211.22	flexure
W36	X	3100	400	1.26	86.51	0.22	193.97	1323.22	0.85	18.80	229456.30	flexure
W37	X	3100	400	1.26	86.51	0.22	193.97	1323.21	0.85	18.80	229456.30	flexure
W43	Y	6400	400	0.61	95.06	0.24	899.62	2865.00	1.69	13.10	533274.03	flexure
W46	X	6002	400	0.65	106.46	0.27	874.53	2707.44	1.72	13.50	508663.12	flexure
W47	X	6203	400	0.63	87.31	0.22	783.14	2762.27	1.50	13.30	521491.93	flexure
W48	X	6003	400	0.65	96.73	0.24	803.86	2690.44	1.58	13.50	508724.08	flexure
W49	X	6203	400	0.63	87.23	0.22	782.53	2762.12	1.50	13.30	521491.93	flexure

Table 67: Results for the case of RC jacketed masonry walls

6.5.7 *Assessment of the strengthened building*

The effectiveness of strengthening method which uses RC jackets has been illustrated with this application example. RC jacketing has been applied to modify the original structural material, i.e. unreinforced masonry. Therefore, it was assumed that the steel reinforcing meshes have bar diameter of Ø 8 mm distributed on equal distances in both directions of 100 mm. The total reinforcement area was 503 $^{mm^2}/_{m^2}$. However, with respect to the test results on the jacketed masonry walls without anchorage of the vertical reinforcement in the floor beams, in this example, the participation of the vertical reinforcement to the seismic resistance of the walls was neglected.

The main analysis results of the building with strengthened masonry walls (SM) are presented in Table 67. Only results for the jacketed walls are presented. In X direction, the jacketing has been applied only to the walls that failed in the sequences 1 and 2 during the analysis of unreinforced building, see Figure 140. In Y direction, the strengthening has been applied to all walls. The rest of the walls remain in unreinforced masonry, and therefore the same results shown in Table 66 are valid for this case, as well. The strengthened masonry walls showed that each of them would fail with flexure failure mode. The flexural and shear capacity of the jacketed walls was increased in comparison with the unreinforced walls. The flexural resistance was increased for 30 %, while the shear resistance was increased in a range of $843 - 2132$ %, or in average for about 1010 %. The increased resistance was due to the contribution of the horizontal reinforcement.

The appropriate capacity curves for the strengthened individual walls have been developed according to the previously suggested analytical concepts, see Figure 142.

The capacity curves for the strengthened building in both horizontal orthogonal directions of the building was plotted on the same diagram with the capacity curves for the unreinforced building, see Figure 143. As can be seen, higher capacity of the strengthened building was obtained in each direction in comparison with the unreinforced building. The seismic capacity of the strengthened building in direction X was about 7 times higher, while in direction Y it was approximately 10 times higher than the capacity of the unreinforced building. Also, the ductility of the building with respect to the ultimate displacements has been increased for about 30 %. The results indicate that the applied strengthening method improved the seismic resistance of the building.

The capacity spectrum method has been applied to the strengthened building to verify the seismic capacity, see Figure 144. The performance points have been identified in the intersection of the capacity and the demand spectra for both directions. In both cases, the performance point lies in the ascending range of the capacity spectrum. For example, for 5 % damped response spectrum, the performance point in Y direction was detected at a spectral acceleration of 7.123 m/s^2 and a spectral displacement of 0.00178 m, giving a period of $T = 0.099$ s. From all the results shown above, it can be concluded that the the jacketed masonry applied to the selected walls increased the seismic resistance and global stability of the building, for the given seismic intensity.

6.6 SUMMARY AND CONCLUSIONS

In this chapter, application of a displacement-based analysis and seismic verification of masonry buildings was presented. The capacity spectrum method has been applied on a numerical model of a school building. The material and dynamic characteristics of the building have been estimated by updating selected parameters based on the results from ambient vibration tests. The CSM was applied for the two cases: existing building (unreinforced masonry) and strengthened building (RC jacketed masonry). Two essential findings from this comparison are summarized in the following paragraphs.

A. The assessment of the existing building in its present state was performed by using the seismic verification approach and the

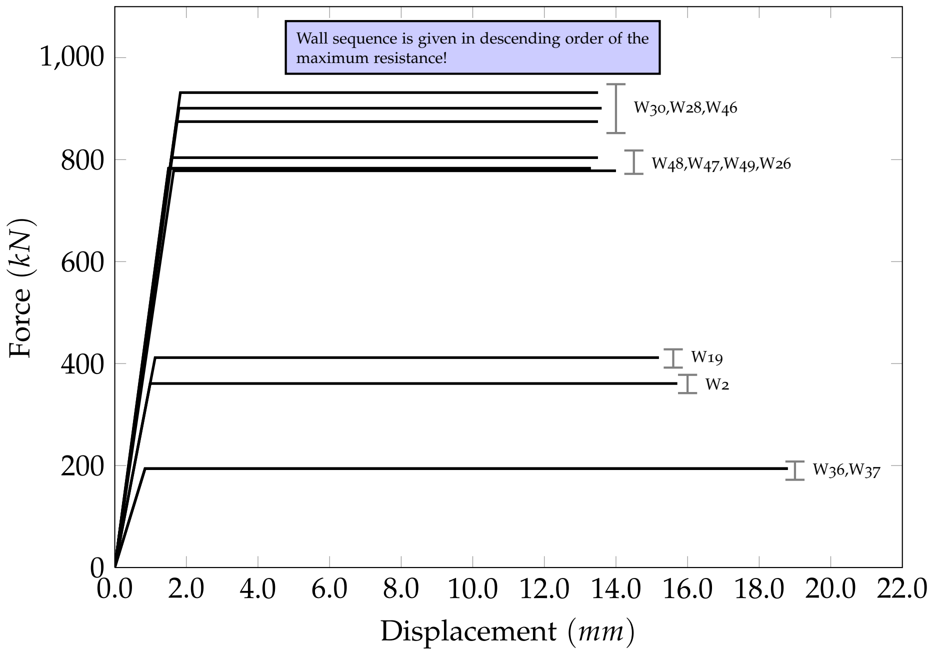

(a) X direction

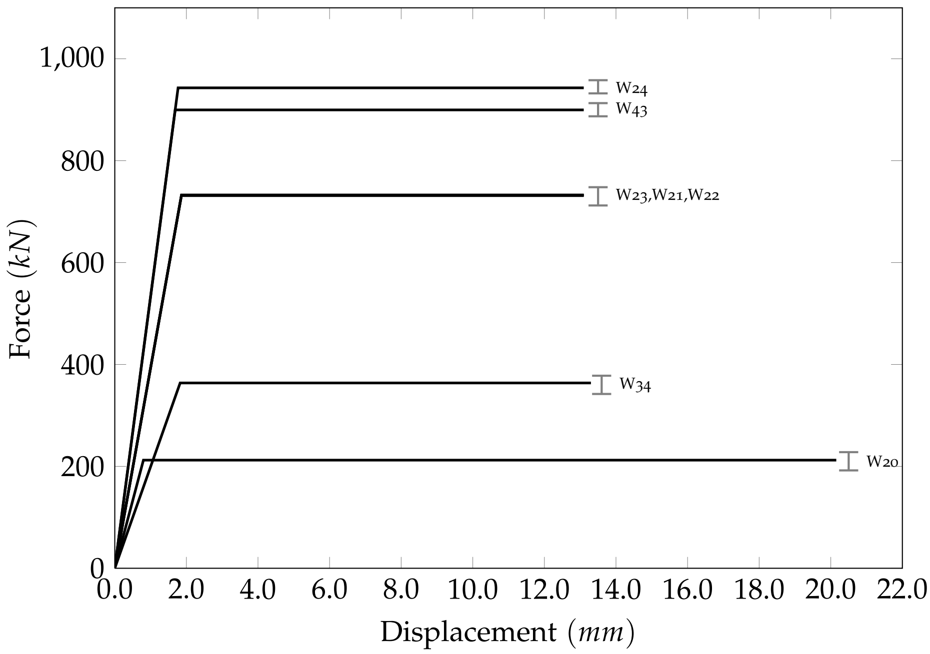

(b) Y direction

Figure 142: Capacity curves of the jacketed masonry walls

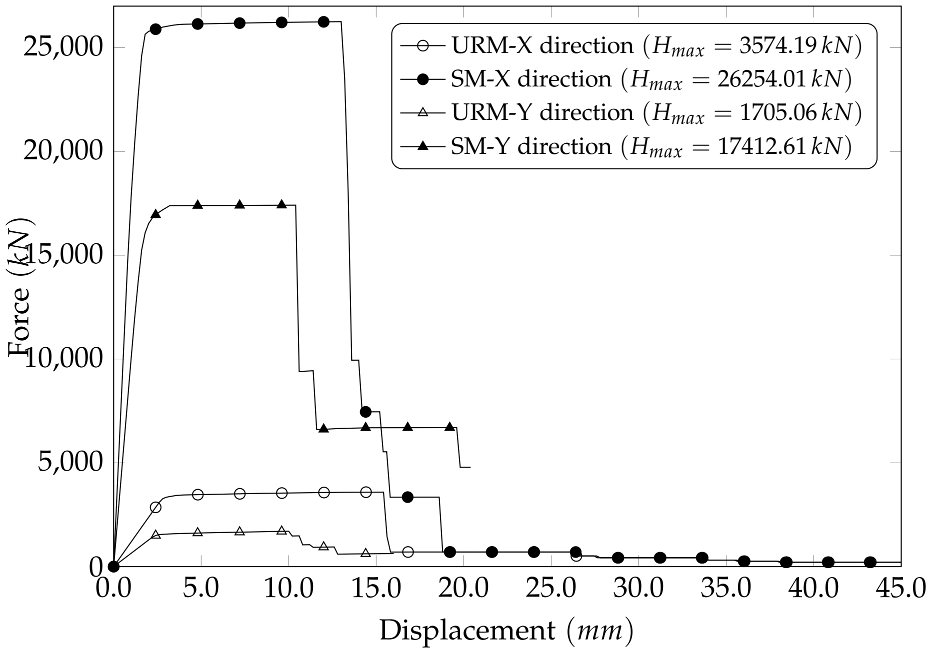

Figure 143: Comparison of the capacity curves of the unreinforced and strengthened building

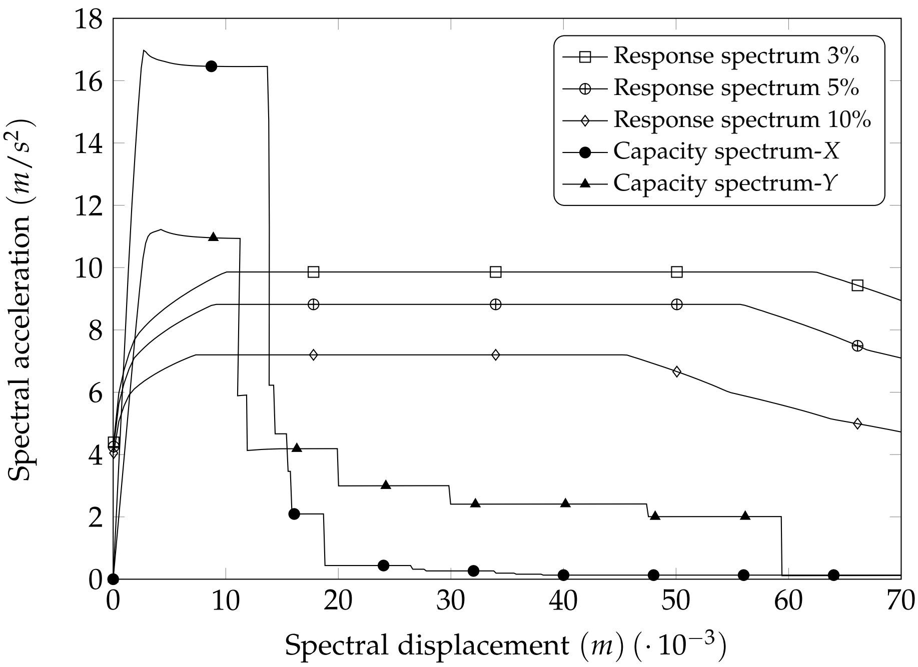

Figure 144: Determination of the "Performance Point" for the strengthened masonry building

capacity spectrum method. There was no performance point identified during this analysis. This important finding suggests that the building does not posses enough capacity to resist the loads from the applied seismic action. To improve the capacity of the building, a strengthening method with application of RC jackets was applied. The contribution of the vertical reinforcement to the overall seismic resistance was ignored.

B. The strengthening method was applied on selected walls in both orthogonal directions. The decision which walls should be strengthen was based on the detected wall failure sequence from the analysis of the unreinforced building. In X direction only walls that failed first were selected, while in Y direction all walls were strengthened. This was made since the Y direction was twice 'weaker' than the X direction in terms of maximum seismic resistance. It was proved that the strengthened, RC jacketed, masonry improved the seismic capacity of the building in both directions and performance points have been identified in both directions. With the applied strengthening material the seismic safety of the building was increased.

Part IV

CONCLUSIONS

A summary of the content of the current research is presented in the following pages. The main aims of the work are briefly stated, together with the major findings in the study and the possible implications. The significance of the work was highlighted, but also some limitations of the current study have been pointed out. In the end, recommendations for further work were emphasized with implications and recommendations for practice.

7 CONCLUSIONS AND FINAL REMARKS

7.1 CONCLUSIONS

The complex behaviour of masonry under in-plane loading was elaborated in the present work. The main aim of this work was to contribute to the understanding of the strengthened masonry walls with RC jackets subjected to cyclic lateral loading. This work contributed for a better insight on the in-plane behaviour of masonry walls considering the influence of the geometry conditions and the precompression levels. The work was divided in three parts: (i) experimental analysis, characterisation of the physical and the mechanical properties of masonry components and masonry walls, (ii) analytical evaluation of models for predicting the maximum resistance of unreinforced and reinforced masonry walls, and (iii) application of the selected analytical model to an existing building through a displacement-based non-linear analysis. The purpose of the current research was to compare the main results from the experimental program with the analytical models for reinforced masonry. Due to similarity of the behaviour to reinforced masonry walls, evaluation relations for seismic design and verification of jacketed masonry walls were proposed.

RC jacketing is considered one of the conventional methods for strengthening and retrofitting of masonry structures. But, due to the lack of experimental and analytical investigations on the behaviour of jacketed masonry walls, the design of such element is usually based on empirical relations which might lead to over- or under-design details. In this thesis, appropriate analytical design relations for different failure modes were compared to the experimentally obtained capacity of the jacketed walls. Based on the results, a method for design and seismic evaluation of jacketed walls was proposed. However, this method is not a general solution for calculation of the capacities for RC jacketed walls. The proposed relations should be verified more extensively by performing additional experimental tests.

The main conclusions of the work are synthesized in the following three sub-chapters.

7.1.1 *Tests on masonry materials*

The material properties of the masonry components play an important role in the analysis of the experimental results of masonry walls. The results obtained from the tests conducted on the masonry materials and materials used for strengthening are fundamental for the experimental analysis of the walls and later for numerical analysis of masonry buildings. This findings enhance the understanding of the behaviour of masonry under the applied loads. The following conclusions can be formulated regarding the properties of the masonry materials:

A. The compressive strength obtained on the selected clay bricks shows large scatter of the results, as experienced by numerous previous studies. The specimen size has significant influence on the results for this essential brick property. The tensile flexural strength of the bricks showed large dispersion, also.

B. The mortar types tested represent the common mortars used in the existing masonry buildings. The big difference obtained in the mechanical properties of the lime and cement-lime mortar indicates serious influence of the mortar strength on the mechanical properties of the masonry.

C. The equation proposed in Eurocode 6 [2005] for determination of the compressive strength of masonry as a function the compressive strength of the units and the mortar presented acceptable correlation with the experimental results. Good agreement for the estimated modulus of elasticity suggested in the code and assessed from the tests was obtained. Also, the compressive stress-strain diagram was well described with a stress-strain model for confined reinforced concrete.

7.1.2 *Experimental analysis of masonry walls*

The experimental analysis of the masonry walls was carried out on two different structural materials, unreinforced masonry and strengthened masonry with RC jackets. In these tests, the influence of the geometry and the precompression level was considered as variation parameters. From the limited experimental programme and the obtained test results, the following conclusions can be made:

A. The failure modes of the tested unreinforced masonry walls were found to be governed by diagonal shear. The obtained failure mode of the unreinforced masonry walls was previously designated as target mode, within the purposes of this research. Nevertheless, other failure modes may occur in the unreinforced masonry walls. These failure modes are bending behaviour (flexural), shear sliding and compressive behaviour.

B. Strengthened masonry walls with RC jackets tested within this investigation failed with mixed failure mode, bending and separation of the jacket from the masonry. Bending failure is considered ductile behaviour that can dissipate a lot of seismic energy. That is one of the reasons why it is desired failure mode in seismic loading situations. The strengthened walls presented higher capacities in comparison with the tested unreinforced masonry walls, and thus the proposed strengthening method was successfully verified.

c. The level of the precompression load influences the behaviour of the walls. Higher values of the vertical stresses are related to higher values of the lateral capacity. Also, the obtained results indicate increase of the shear capacity of the strengthened walls, in the range of 2–3 times, if compared to the unreinforced masonry walls.

d. The geometry ratio affects the lateral capacity of the walls. The squat walls tested in the experimental part demonstrated higher lateral capacity than the tall walls.

e. The ultimate displacements obtained in the unreinforced walls could not be associated to the geometry configuration and the precompression levels. The strengthened walls presented a relation between the ultimate displacements and the precompression levels. Higher ultimate displacements were obtained for the walls loaded with lower vertical stresses.

f. The effectiveness of the strengthening method appears to be related with the geometry of the walls and the vertical stress levels. The strengthening improved the lateral capacity of the walls, but it was demonstrated that the deformation capacity was increased only for the cases of wall loaded with low vertical stresses.

7.1.3 *Analytical models for strengthened masonry walls*

The current study considers several available analytical models for determination of the shear capacity of unreinforced and reinforced masonry. The models for reinforced masonry walls were used due to the similarity in the applied materials and behaviour of the strengthened walls and moreover because no reliable analytical model for RC jacketed walls exists. The examined analytical models assume the shear capacity of the strengthened wall as a sum of the capacities of the masonry wall and the capacity of the reinforcing meshes. The contribution of the concrete layer was neglected.
The analysed analytical models calculate the contribution of the masonry with two approaches. The first one uses the shear sliding failure mode along the bed joints as a governing mode, while the second approach considers diagonal tensile failure as referential mode. Following this two approaches, in the first case a corresponding design relation were developed describing the shear strength of masonry

with the analogy to the friction theory and in the second case, diagonal tensile strength was assumed as mechanisms for controlling the masonry resistance.

Based on the examined analytical models compared to the test results, the following list summarizes the major findings from the analytical analysis:

A. All analytical models for unreinforced masonry walls can predict successfully the maximum shear capacity of the walls. This was verified for the failure mode obtained with the tests and the associated analytical model. The comparison of the behaviour was made considering fully fixed boundary conditions on the top and bottom edges of the walls.

B. The proposed model by Tomaževič [1999] for reinforced masonry walls was found the best model to correlate the test results for the RC jacketed walls. Fully fixed boundary conditions of the walls were considered. The tests were performed without anchorage of the vertical reinforcement in the top and bottom beams. This approach was used in order to study the behaviour of the 'new' (strengthening) structural material, rather than to investigate the behaviour of the strengthened structural element - a wall. By anchoring the reinforcing bars to the floor levels, this strengthening method effectively increases the overall capacity of the structure. The behaviour of the jacketed walls is most likely to the reinforced masonry walls with considering the contribution of the masonry and the horizontal reinforcement. The contribution of the vertical reinforcement was neglected, because no anchorage with the top and bottom beams was established during the tests.

C. Due to the best overall correlation with the test results, the models suggested in DIN Eurocode 6/NA [2011] and Tomaževič [1999] were selected to be implemented in a new analysis module for displacement-based analysis of masonry buildings within the software package MINEA [2011].

D. The performed analysis of the design provisions are limited to the obtained test results and consider only diagonal tensile failure mode. Other failure modes have to be tested experimentally and the design relation should be verified on order to provide general solution for calculation of the capacities for RC jacketed walls.

7.2 ADVANTAGES OF THE CURRENT RESEARCH

The current research offers several positive reflections in the understanding of the behaviour of RC jacketed masonry walls, with respect

to experimental and analytical methods.
First of all, for the first time in the country, a test set-up for experimental determination of the lateral capacity of masonry walls in real (normal) position was designed and developed. It uses controlled boundary conditions and also ensures uniform distribution of the normal stresses to the whole cross-section of the walls.
Secondly, laboratory experimental tests on RC jacketed masonry walls in real scale were performed for the first time in the country by quasi-static loading. The data acquisition was automatic and displacements were measured at different points and directions during the testing.
Thirdly, normal stress levels and wall dimensions were considered as governing parameters for wall behaviour and two levels of precompression load and two wall geometries were tested.
Finally, the lateral capacity of the strengthened walls with respect to the diagonal tensile failure mode were computed with the proposed relations in this study and were compared with the observed capacities obtained with the tests. As it was shown, the strength predictions have good agreement with the test results and accurately predicted failure mode.

7.3 LIMITATIONS OF THE CURRENT RESEARCH

A number of important limitations of the current research need to be considered. Firstly, the experimental research was limited on a small number of test specimens mainly due to the limited budget for testing and due to the limiting testing equipment. Therefore, the current research was specifically designed to consider these limiting factors. The current study has only examined the influence of the strengthening method on the in-plane behaviour of masonry walls by considering the geometry and precompression levels as variable parameters. Due to the aforementioned reasons, only two sets of variable data were used.
Secondly, the small number of test specimens restrained the overall understanding for the behaviour of the strengthened walls. Therefore, it was not possible to develop any analytical or numerical model based on such small amount of variable test results. Thus, the main intention was to propose analytical model which can predict the masonry behaviour with acceptable accuracy.
Thirdly, influence of the brick units and mortar types on the in-plane behaviour of the walls was not considered. The current investigation was limited to clay bricks and lime mortar, only. The influence of masonry materials, bond pattern, geometry and vertical load levels of the walls, concrete thickness, amount reinforcement, number and position of anchor bars have to be studied in more details.

7.4 FURTHER WORK

In the scope of identification of the mechanical properties of masonry, the following aspects require attention and further work:

A. Assessment of the influence of the brick units and mortar types on the compressive strength of masonry, the tensile strength of masonry established through diagonal tensile tests and in tensile and shear strength of the unit-mortar interface;

B. Evaluation of the influence of the strengthening method in determination of the compressive and shear strength of the masonry walls, as well as the modulus of elasticity;

C. Assessment of the bond strength of the anchor bars used to connect the jackets in case of double-sided jacketing and assessment of the bond strength of reinforcement cages in case of single-sided jacketing.

In the scope of experimental research for in-plane behaviour of the strengthened masonry walls, the following aspects are highlighted:

A. Study of strengthened walls with anchorage of the vertical reinforcement in the top and bottom beams;

B. Investigation of the behaviour of the strengthened walls with respect to the boundary conditions;

C. Study of the influence of the geometry and the vertical load levels on the behaviour of the strengthened walls;

D. Detailed study on the influence of the number and position of the anchor bars in the behaviour of the strengthened walls;

E. Study of the influence of the bond strength between the concrete for strengthening and the masonry walls;

F. Investigation of the effectiveness of the strengthening method applied to the masonry walls with different brick units and mortar types;

G. Improvement of the test set-up to account for automatically controlled vertical load levels and automatically applied horizontal loads.

S. M. Alcocer, J. Ruiz, and J. A. Pineda nd J. A. Zepeda. Retrofitting of confined masonry walls with welded wire mesh. In *11^{th} World Conference on Earthquake Engineering*, Acapulco, Mexico, June 23-28 1996. ISBN 0-08-042822-3. Paper No. 1471. (Cited on page 37.)

R.J. Allemang and D.L. Brown. A correlation coefficient for modal vector analysis. In *Proceedings of the 1^{st} International Modal Analysis Conference (IMAC)*, Orlando, Florida, USA, 1982. (Cited on page 224.)

N. Ambraseys. 1963 Skopje Earthquake. CD, March 1967. (Cited on page 29.)

M. Angelillo and R. S. Olivito. Experimental analysis of masonry walls loaded horizontally in plane. *Masonry International*, 8(3):91–100, 1995. (Cited on pages xv, 19, 24, and 25.)

R.P. Apostolska, G.S. Necevska-Cvetanovska, and V.I. Sendova. Methodology for renovation and seismic strengthening of St. Clement's church, St. Panteleymon-Plaoshnik-Ohrid. In Mazzolani, editor, *Protection of Historical Buildings, PROHITECH 09*, volume 1, pages 101–106. Taylor & Francis Group, London, 2009. (Cited on page 61.)

F. Aras, L. Krstevska, G. Altay, and Lj. Tashkov. Experimental and numerical modal analyses of a historical masonry palace. *Construction and Building Materials*, 25:81–91, January 2011. (Cited on page 205.)

A. S. Arya, T. Boen, and Y. Ishiyama. *Guidelines for earthquake resistant non-engineered construction*. International Association for Earthquake Engineering (IAEE), United Nations Educational, Scientific and Cultural Organization (UNESCO) and International Institute of Seismology and Earthquake Engineering (IISEE), draft for revision edition, July 2010. (Cited on page 13.)

AS 3700. Masonry Structures. Standards Australia Committee BD-004 Fourth edition, Standards Australia Limited, 14 October 2011. (Cited on page 109.)

H. Bachmann. *Seismic Conceptual Design of Buildings-Basic principles for engineers, architects, building owners, and authorities*. BWG Biel, 2002. (Cited on page 13.)

D. Beg. Repair of damaged masonry wall with reinforced-cement coating. Technical Report FP6-2002-INCO-MPC-1, Doc.No. 09.01.03.01, Final report of PROHITECH WP1-Overview of existing techniques, 2005. (Cited on pages 34 and 45.)

V. Bosiljkov, A. W. Page, V. Bokan-Bosiljkov, and R. Žarnić. Performance based studies of in-plane loaded unreinforced masonry walls. *Masonry International*, 16(2):39–50, 2003. (Cited on page 146.)

V. Bosiljkov, A.W. Page, V. Bokan-Bosiljkov, and R. Žarnić. Evaluation of the seismic performance of brick masonry walls. *Structural Control and Health Monitoring*, 17(1):100–118, 2010. ISSN 1545-2263. doi: 10.1002/stc.299. (Cited on pages 21 and 138.)

Z. Bozinovski, B. Stojanovski, and R. Petrusevska. Repair, strengthening and stability analysis of the structural system of the school building "Goce Delcev", building 3, Bitola. IZIIS Report 95-32, Institute of earthquake engineering and engineering seismology (IZIIS), 1995. (Cited on page 62.)

Z. Bozinovski, E. Gjorgjievska, and S. Radončić. Strengthening of basic and upgraded building structure of the regional court in Shtip. IZIIS Report 2006-34, Institute of earthquake engineering and engineering seismology (IZIIS), 2006. (Cited on page 63.)

A. Brignola, S. Frumento, S. Lagomarsino, and S. Podestà. Identification of shear parameters of masonry panels through the in-situ diagonal compression test. *International Journal of Architectural Heritage*, 3(1):52–73, 2009. (Cited on page 23.)

C. Butenweg, C. Gellert, L. Reindl, and K. Meskouris. A nonlinear method for the seismic safety verification of masonry buildings. In M. Papadrakakis, N.D. Lagaros, and M. Fragiadakis, editors, *Compdyn 2009 - ECCOMAS Thematic Conference on Computational Methods in Structural Dynamics and Earthquake Engineering*, Rhodes, Greece, June, 22-24, 2009. (Cited on page 206.)

A. K. Chopra. *Dynamics of Structures - Theory and Applications to Earthquake Engineering*. Paerson Prentice Hall, 2007. (Cited on pages 139 and 143.)

A. Costa. Experimental testing of lateral capacity of masonry piers. An application to seismic assessment of AAC masonry buildings. Master's thesis, Rose school, January 2007. (Cited on pages xv, 22, and 146.)

G. Croci. *The Conservation and Structural Restoration of Architectural Heritage*. WIT Press, illustrated edition, 1988. ISBN 978-1853124822. (Cited on page 9.)

CSA S304.1-04. Design of masonry structures. Canadian Standards Association, December 2004. (Cited on pages xi, xiii, xix, xxii, xxiii, 51, 53, 54, 109, 179, 184, 185, 186, 193, 194, 195, 196, 197, and 199.)

DIN 4149-04. Bauten in deutschen Erdbebengebieten-Lastannahmen, Bemessung und Ausführung üblicher Hochbauten. Berlin, Deutsches Institut für Normung (DIN), April 2005. (Cited on page 213.)

DIN Eurocode 6/NA. National Annex - Eurocode 6: Design of masonry structures - Part 1-1: General rules for reinforced and unreinforced masonry structures. Berlin, DIN EN 1996-1-1/NA, DIN Deutsches Institut für Normung, April 2011. (Cited on pages xiii, xix, xxii, xxiii, 181, 182, 183, 184, 185, 190, 191, 192, 193, 197, 199, 202, 207, 209, 210, 211, 212, 227, and 244.)

R.G. Drysdale, A.A. Hamid, and L.R. Baker. *Masonry structures: behavior and design*. The Masonry Society, 1999. ISBN 9781929081011. (Cited on page 9.)

E. Dumova-Jovanoska and S. Churilov. Calibration of a numerical model for masonry with application to experimental results. In Mazzolani, editor, *Protection of Historical Buildings, PROHITECH 09*, volume 2, pages 1139–1145. Taylor & Francis Group, London, 2009. (Cited on page 66.)

E. Dumova-Jovanoska, Ž. Božinovski, and K. Gramatikov. Traditional concept for repair and strengthening of masonry and concrete structures. Technical Report FP6-2002-INCO-MPC-1, Doc.No.03.01.02.01, Final report of PROHITECH WP1-Overview of existing techniques, 2005. (Cited on pages 29, 31, and 36.)

E. Dumova-Jovanoska, G. Markovski, and S. Churilov. FEM updating of existing structures based on ambient vibration measurements. In *International conference - Innovation as a Function of Engineering Development*, volume 1, Nis, Serbia, November 25-26 2011. (Cited on page 214.)

S. El-Borgi, S. Choura, C. Ventura, M. Baccouch, and F. Cherif. Modal Identification and Model Updating of a Reinforced Concrete Bridge. *International Journal of Smart Structures and Systems*, 1(1):83–101, 2005. (Cited on pages 221 and 222.)

M. ElGawady, P. Lestuzzi, and M. Badoux. A review of conventional seismic retrofitting techniques for URM. In *13^{th} International Brick and Block Masonry Conference*, Amsterdam, The Nederlands, July 4-7 2004. (Cited on page 37.)

M. ElGawady, P. Lestuzzi, and M. Badoux. Retrofitting of masonry walls using shotcrete. In *Remembering Napier 1931-Building on 75 Years of Earthquake Engineering in New Zealand, Conference*. New Zealand Society for Earthquake Engineering, 2006. (Cited on page 33.)

EN 1015-11. Methods of test for mortar for masonry - Part 11: Determination of flexural and compressive strength of hardened mortar. Brussels, CEN, August 1999. (Cited on pages 86, 90, and 92.)

EN 1052-1. Methods of test for masonry - Part 1: Determination of compressive strength. Brussels, CEN, September, 1998 1999. (Cited on pages 104, 105, and 107.)

EN 1052-3. Methods of test for masonry - Part 3: Determination of initial shear strength. Brussels, CEN, August 2002. (Cited on pages 46, 109, 110, 112, and 115.)

EN 1052-4. Methods of test for masonry. Determination of shear strength including damp proof course. Brussels, CEN, 15 September 2000. (Cited on pages 46 and 109.)

EN 197-1. Cement - Part 1: Composition, specifications and conformity criteria for common cements. Brussels, CEN, June, 2000. (Cited on page 86.)

EN 1998-3. Design of structures for earthquake resistance - Part 1: Assessment and retrofitting of buildings. Brussels EN 1998-3:2005, CEN, June 2005. (Cited on pages 211 and 212.)

EN 772-1. Methods of test for masonry units - Part 1: Determination of compressive strength. Brussels, CEN, May, 2011. (Cited on page 79.)

Eurocode 6. Design of masonry structures - Part 1-1: General rules for reinforced and unreinforced masonry structures. EN 1996-1-1:2005, 2005. (Cited on pages xi, xiii, xxiii, 22, 42, 46, 47, 48, 49, 50, 104, 107, 108, 109, 115, 151, 174, 179, 181, 182, 190, 191, 192, 197, 210, 211, and 242.)

Eurocode 8. Design of structures for earthquake resistance - Part 1: General rules, seismic actions and rules for buildings. Brussels EN 1998-1:2004, CEN, December 2004. (Cited on pages 79, 84, and 228.)

C. Faella, E. Martinelli, E. Nigro, and Sergio Paciello. Shear capacity of masonry walls externally strengthened by a cement-based composite material: An experimental campaign. *Construction and Building Materials*, 24:84–93, 2010. (Cited on page 32.)

FEDRA. *Masonry Buildings according to Eurocode 6, User Manual*. Runet software & expert systems, Norway, 2/03 edition, 2003. (Cited on pages xi, xiii, xxiii, 49, 179, 195, 197, and 199.)

FEMA 273. NEHRP Guidelines for the seismic rehabilitation of buildings. Washington, D.C. FEMA, Federal Emergency Management Agency, October 1997. (Cited on pages 211 and 212.)

FEMA 274. NEHRP Commentary on the Guidlines for the Seismic Rehabilitation of Buildings. Washington, D.C. FEMA, Federal Emergency Management Agency, October 1997. (Cited on page 219.)

FEMA 351. Recommended Seismic Evaluation and Upgrade Criteria for Existing Welded Steel Moment-Frame Buildings. SAC Joint Venture FEMA, Federal Emergency Management Agency, June 2000. (Cited on page 219.)

S. A. Freeman. The capacity spectrum method as a tool for seismic design. In *Proceedings of the 11^{t}h European Conference on Earthquake Engineering*, Paris, September 6-11 1998. A.A.Balkema. (Cited on page 228.)

S. A. Freeman, J.P. Nicoletti, and J.V. Tyrell. Evaluations of existing buildings for seismic risk. In *Proceedings of 1st U.S. National Conference on Earthquake Engineering*, volume 113-22, Berkeley, USA, 1975. EERI. (Cited on page 206.)

A. Galasco, G. Magenes, A. Penna, and M. Da Paré. In-plane cyclic shear tests of undressed double leaf stone masonry panels. In *14th European Conference on Earthquake Engineering*, Ohrid, Macedonia, 2010. (Cited on page 20.)

P. Gavrilović and Z. Bozinovski. Repair and strengthening of the principal structural system and analysis of the stability of the structure of the students' dormitory - Unit a, Bitola. IZIIS Report 94-59, Institute of earthquake engineering and engineering seismology (IZIIS), 1994. (Cited on page 62.)

P. Gavrilović, W. S. Ginell, V. Sendova, and L. Šumanov. *Conservation and Seismic Strengthening of Byzantine Churches in Macedonia*. Number ISBN: 0-89236-777-6. Getty Conservation Institute, 2004. (Cited on page 60.)

C. Gellert. *Nonlinear analysis of unreinforced masonry structures under earthquake actions*. PhD thesis, RWTH Aachen, LBB, December 2010. (in German). (Cited on pages 47, 146, 151, and 211.)

C. Gellert, H. Norda, and C. Butenweg. Nonlinear behavior of masonry under cyclic loading. In *7th European Conference on Structural Dynamics - Eurodyn 2008*, number E39, Southampton, UK, July, 7-9, 2008. (Cited on page 206.)

B. Ghiassi, M. Soltani, and A. A. Tasnimi. In-plane lateral response of brick masonry walls retrofitted with reinforced concrete layer. In *The 14th World Conference on Earthquake Engineering*, Beijing, China, October 12-17 2008. (Cited on page 38.)

J. P. Gouveia and P. B. Lourenço. Masonry shear walls subjected to cyclic loading: Influence of confinement and horizontal reinforcement. In *10th North American Masonry Conference, June 3-5*, pages 838–848, 2007. (Cited on pages xv, 25, and 26.)

V. G. Haach. *Development of a design method for reinforced masonry subjected to in-plane loading based on experimental and numerical analysis*. PhD thesis, Universidade do Minho, Escola de Engenharia, 2009. (Cited on pages xv, 26, 28, 84, 133, and 146.)

A.W. Hendry and F.M. Khalaf. *Masonry wall construction*. Spon Press, 2000. ISBN 978-0415232821. (Cited on page 11.)

D. L. Hutchinson, P. M. F. Yong, and G. H. F McKenzie. Laboratory testing of a variety of strengthening solutions for brick masonry wall panels. In *8th World Conference on Earthquake Engineering*, volume 1, pages 575–582, San Francisco, California, 1984. (Cited on page 33.)

L.B. Ibsen and M. Liingaard. Experimental modal analysis. DCE Technical Report No. 10, Aalborg University, 2006. (Cited on page 222.)

J. M. Ingham and M. C. Griffith. The performance of unreinforced masonry buildings in the 2010/2011 Canterbury earthquake swarm. Technical report, Report to the Royal Commission of Inquiry, August 2011. (Cited on page 29.)

Md. T. Islam, A. Melnik, and V. Bindiganavile. Textile reinforced mortar (TRM) for external strengthening of stone masonry units under impact. In *11th North American Masonry Conference*, Minneapolis, USA, June 5-8 2011. (Cited on page 32.)

ISO 6892-1. Metallic materials - Tensile testing - Part 1: Method of test at room temperature. First edition: 2009-08-15, International Organization for Standardization (ISO), August 2009. (Cited on page 100.)

S.S. Ivanović, M.D. Trifunac, E.I. Novikova, A.A. Gladkov, and M.I. Todorovska. Ambient vibration tests of a seven-story reinforced concrete building in van nuys, california, damaged by the 1994 northridge earthquake. *Soil Dynamics and Earthquake Engineering*, 19:391–411, 2000. (Cited on page 203.)

M. Jovanovski and J. Josifovski. PROHITECH WP7: Laboratory testing on the intact parts of stone used in construction of large scale model for "Mustapha Pasha mosque" in Skopje. Testing Report FP6-2002-INCO-MPC-1, Doc.No. 09.01.03.01, University "Ss. Cyril and Methodius", Skopje, Rep. of Macedonia, Faculty of Civil Engineering, Department for Geotechnics, 2006. (Cited on page 78.)

D. Jurukovski, L. Krstevska, R. Alessi, P.P. Diotallevi, M. Merli, and F. Zarri. Shaking table tests of three four-storey brick masonry models: Original and strengthened by RC core and by RC jackets. In *10th World Conference on Earthquake Engineering*, volume V, pages 2795–2800, Madrid, Spain, 19-24 July, 1992. Balkema. (Cited on page 58.)

JUS U.M2.010. Mortar for masonry. No. 15-01-237/22 (05.02.1992), Official Gazette of (former) SFRY, 1992. (Cited on page 84.)

L. F. Kahn. Shotcrete retrofit for unreinforced brick mas. In *8th World Conference on Earthquake Engineering*, volume 1, pages 583–590, San Francisco, California, 1984. (Cited on page 33.)

L. W. King. *The code of Hammurabi*. Paulo J. S. Pereira, 2011. (Cited on page vii.)

G. Kokalanov, Lj. Tashkov, L. Krstevska, and M. Aleksovska. Analytical and experimental investigations of Byzantine church. In Mazzolani, editor, *Protection of Historical Buildings, PROHITECH 09*, volume 1, pages 149–154. Taylor & Francis Group, London, 2009. (Cited on pages 66 and 67.)

L. Krstevska. *Development and application of non-linear micro models for evaluation of seismic behaviour of RC frames infilled with plain and reinforced masonry*. PhD thesis, Institute of Earthquake Engineering and Engineering Seismology (IZIIS), University "Ss. Cyril and Methodius", Skopje, 2002. (Cited on pages xv, xvi, 28, 61, and 62.)

L. Krstevska and Lj. Tashkov. Experimental testing of buildings in Skopje after the catastrophic earthquake - IZIIS experience. In *10th International symposium of MASE*, volume 2, pages 531–536, Ohrid, Macedonia, 25-27 September, 2003. Macedonian Association of Structural Engineers. (Cited on page 204.)

L. Krstevska and Lj. Tashkov. Experimental In-situ testing of dynamic characteristics of structures - recent experience. In *13th International symposium of MASE*, volume 2, pages 635–640, Ohrid, Macedonia, 14-17 October, 2009. Macedonian Association of Structural Engineers. (Cited on page 205.)

L. Krstevska, Lj. Tashkov, K. Gramatikov, F.M. Mazzolani, and R. Landolfo. Shaking table test of mustafa pasha mosque model in reduced scale. In Mazzolani, editor, *Protection of Historical Buildings, PROHITECH 09*, volume 2, pages 1633–1639. Taylor & Francis Group, London, 2009a. (Cited on page 65.)

L. Krstevska, Lj. Tashkov, and M. Kustura. Ambient vibration testing of old bridge in Mostar. In Mazzolani, editor, *Protection of Historical Buildings, PROHITECH 09*, volume 1, pages 217–221. Taylor & Francis Group, London, 2009b. (Cited on page 205.)

L. Krstevska, Lj. Tashkov, V. Gocevski, and M. Garevski. Experimental and analytical investigation of seismic stability of masonry walls at beauharnois powerhouse. *Bulletin of Earthquake Engineering*, 8(2): 421–450, 2010. (Cited on page 204.)

M. Lafuente, E. Castilla, and C. Genatios. Experimental and analytical evaluation of the seismic resistant behavior of masonry walls. *Masonry International*, 11(3):80–88, 1998. (Cited on page 20.)

R. Landolfo, O. Mammana, F. Portioli, and F.M. Mazzolani. Numerical analysis of the large scale model of Mustafa Pasha Mosque in Skopje strengthened with FRP. In Mazzolani, editor, *Protection of Historical Buildings, PROHITECH 09*, volume 1, pages 617–622. Taylor & Francis Group, London, 2009. (Cited on page 66.)

L. Lazarov and K. Todorov. Numerical vs. experimental analyses of Mustafa Pasha Mosque model. In Mazzolani, editor, *Protection of Historical Buildings, PROHITECH 09*, volume 2, pages 1165–1170. Taylor & Francis Group, London, 2009a. (Cited on pages 66 and 67.)

L. Lazarov and K. Todorov. New strengthening approach of Mustafa Pasha Mosque to seismic loads. In Mazzolani, editor, *Protection of Historical Buildings, PROHITECH 09*, volume 2, pages 1747–1752. Taylor & Francis Group, London, 2009b. (Cited on page 66.)

T. Li, N. Galati, J. G. Tumialan, and A. Nanni. FRP strengthening of URM walls with openings - numerical analysis and design. *TMS Journal*, 23(1):9–22, 2005. (Cited on page 32.)

J.F. Lord, C.E. Ventura, and E. Dascotte. Automated model updating using ambient vibration data from a 48-storey building in vancouver. In *Proceedings of the 22nd International Modal Analysis Conference*, Dearborn, Michigan, USA, 2004. (Cited on page 224.)

P. B. Lourenço. *Computational strategies for masonry structures*. PhD thesis, Delft University of Technology, 1996. (Cited on page 10.)

G. Magenes. *Seismic behaviour of brick masonry: strength and failure mechanism of shear-walls*. PhD thesis, Dipartimento di Meccanica Struturale dell'Universita di Pavia, 1992. (Cited on page 22.)

G. Magenes. Masonry building design in seismic areas: Recent experiences and prospects from a European standpoint. In *First European Conference on Earthquake Engineering and Seismology*, Geneva, Switzerland, September, 3-8 2006. 13th ECEE & 30th General Assembly of the ESC. Keynote address K9. (Cited on page 146.)

H. Mahmood, A. P. Russell, and J. M. Ingham. Laboratory testing of unreinforced masonry walls retrofitted with glass FRP sheets. In *14th International Brick and Block Masonry Conference, Sydney, Australia, 17-20 February*, 2008. (Cited on pages xv, 26, and 27.)

J. B. Mander, M. J. N. Priestly, and R. Park. Theoretical stress-strain model for confined concrete. *Journal of Stru*, 114(8):1804–1826, August 1988. (Cited on page 108.)

F.M. Mazzolani. Tehe output of the PROHITECH research project. In Mazzolani, editor, *Protection of Historical Buildings, PROHITECH 09*, volume 1, pages 63–74. Taylor & Francis Group, London, 2009. (Cited on page 64.)

R. Meli. Behaviour of masonry walls under lateral loads. In *Proceedings of 5th World Conference on Earthquake Engineering, Rome, Italy, 25-29 June*, 1973. (Cited on pages 19 and 29.)

R. Meli, S. Brzev, M. Astroza, T. Boen, F. Crisafulli, J. Dai, M. Farsi, T. Hart, A. Mebarki, A.S. Moghadam, D. Quiun, M. Tomaževič, and L. Yamin. *Seismic Design Guide for Confined Masonry Buildings*. World Housing Encyclopedia, EERI & IAEE, draft edition, April 2010. (Cited on page 13.)

MINEA. *Design & analysis of masonry buildings*. SDA-engineering GmbH, Research version v2.3.54 edition, November, 2011. (Cited on pages xxiii, 202, 211, 212, and 244.)

MKS B.C8.022. Bending and compressive strength of hydraulic cement mortars. No. 17-10701/1 (22.2.1975), Official Gazette of (former) SFRY, No. 1, December 1976. (Cited on pages 90 and 92.)

MKS B.C8.042. Building lime. Methods of physical and mechanical testing. No. 31-14586/1 (17.12.1980), Official Gazette of (former) SFRY, No. 31, June 1981. (Cited on pages 86, 90, and 92.)

MKS B.D1.011. Massive clay bricks. Technical requirements. No. 07-4713/1 (25.11.1986), Official Gazette of (former) SFRY, No. 4, January 1987. (Cited on pages 73 and 77.)

MKS B.D8.011. Testing methods of clay bricks, blocks and slabs. No. 07-4713/1 (25.11.1986), Official Gazette of (former) SFRY, No. 4, January 1987. (Cited on pages 77 and 78.)

MKS C.A4.002. Mechanical testing of metals. Testing tensile strength. (30.1.1985), Official Gazette of (former) SFRY, January, 1985. (Cited on page 100.)

MKS U.M8.002. Mortars for masonry and plastering. testing methods. No. 18-9612/1 (22.12.1967), Official Gazette of (former) SFRY, No. 1, December 1968. (Cited on page 86.)

T. Morton. *Earth Masonry, Design and construction guidelines*. IHS BRE Press, 2008. ISBN 978-1-86081-978-0. (Cited on page 13.)

D. V. Oliveira. *Experimental and numerical analysis of blocky masonry structures under cyclic loading*. PhD thesis, Department of Civil Engineering, University of Minho, 2003. (Cited on page 11.)

OPCM 3274. Norme tecniche per il progetto, la valutazione e l'adeguamento sismico degli edifici. testo integrato dell'allegato 2-edifici-all'ordinanza 3274 come modificato dall'opcm 3431 del 3/5/05. Roma n. 3274, Ordinanza del Presidente del Consiglio dei Ministri, 2005. (Cited on pages 211 and 212.)

C. G. Papanicolaou, T. C. Triantafillou, M. Papathanasiou, and K. Karlos. Textile reinforced mortar (TRM) versus FRP as strengthening material of urm walls: out-of-plane cyclic loading. *Materials*, 41: 143–157, 2008. (Cited on page 32.)

D. Penazzi, M.R. Valluzzi, A. Saisi, L. Binda, and C. Modena. Repair and strengthening of historic masonry buildings in seismic areas. In *International Millenium Congress "More than Two Thousand Years in the History of Architecture Safeguarding the Structure of our Architectural Heritage"*, volume 2 of *V 11*, Bethlehem (Palestine), September 10-12 2001. (Cited on page 37.)

PIOVSP. Code of technical regulations for the design and construction of buildings in seismic regions. No. 50-3547/1 (25.2.1981), Official Gazette of (former) SFRY, No. 31, June 1981. (Cited on pages 39, 40, 71, 84, 179, 204, and 214.)

PROHITECH. Earthquake protection of historical buildings by reversible mixed technologies, 2007. Project coordinator: Prof. Federico M. Mazzolani. Sixth Framework Programme Priority FP6-2002-INCO-MPC-1. (Cited on page 15.)

PSZRV. Code for technical regulations for repair, strengthening and reconstruction of buildings damaged in earthquakes and for reconstruction and revitalization of buildings. Technical Report 52, Offizial Gazette of (former) SFRY, No. 52, October 1985. (Cited on page 40.)

PZZ. Code of technical regulations for masonry walls. No. 87/91 (29.11.1991), Official Gazette of (former) SFRY, 1991. (Cited on pages 79, 84, 109, and 137.)

V. Shendova, Z. Bozinovski, and E. Gjorgjievska. Strengthening of basic and upgraded building structure of typical city house-Cilimanovi-Skopje. IZIIS Report 2005-22, Institute of earthquake engineering and engineering seismology (IZIIS), 2005. (Cited on page 62.)

P. Sheppard and S. Terčelj. The effect of repair and strengthening methods for masonry walls. In 7^{th} *World Conference on Earthquake Engineering*, volume 6, pages 255–262, 1980. (Cited on pages 35, 36, and 152.)

P. B. Shing, J. L. Noland, E. Klamerus, and H. Spaeh. Inelastic behavior of concrete masonry shear walls. *Journal of Structural Engineering*, 115(9):2204–2225, 1989. ISSN 07339445. (Cited on pages xv, 19, and 24.)

V. Stoian, T. Nagy-Gyórgy, D. Dan, and J. Gergely. Retrofitting the shear capacity of the masonry walls using cfrp composite overlays. In *International Conference on Earthquake Engineering to Mark 40 Years from the Catastrophic 1963 Skopje Earthquake and Successful City construction, Skopje Earthquake -40 Years Of European Earthquake Engineering (SE 40EEE)*. Institute of Earthquake Engineering and Engineering Seismology (IZIIS), University "Ss. Cyril and Methodius", Skopje, August 2003. (Cited on pages xv, 25, 27, and 32.)

Structural Vibration Solutions, Inc. *ARTeMIS Testor 5.2, ARTeMIS Extractor 5.3*. Aalborg, Denmark, 2011. www.svibs.com. (Cited on page 221.)

Lj. Tashkov and L. Krstevska. Ambient vibration measurements of a R/C silo for grain storage in Skopje. In A. Pecker P. Bisch, P. Labbe, editor, *11th European Conference on Earthquake Engineering*, number CD-ROM, page 434, Paris, France, 6-11 September 1998. Taylor & Francis. (Cited on page 205.)

Lj. Tashkov, L. Krstevska, M. Garevski, and V. Gocevski. Experimental investigation of seismic stability on masonry walls at Beauharnois powerhouse. In *12th International symposium of MASE*, pages 75–86, Struga, Macedonia, 27-29 September, 2007. Macedonian Association of Structural Engineers. (Cited on page 204.)

Lj. Tashkov, L. Krstevska, K. Gramatikov, and F.M. Mazzolani. Shake-table test of the model of St. Nicholas church in reduced scale 1/3.5. In Mazzolani, editor, *Protection of Historical Buildings, PROHITECH 09*, volume 2, pages 1691–1697. Taylor & Francis Group, London, 2009a. (Cited on page 65.)

Lj. Tashkov, L. Krstevska, G. De Matteis, K. Gramatikov, and F.M. Mazzolani. Shake-table test of a model of Fossanova church in reduced scale. In Mazzolani, editor, *Protection of Historical Buildings, PROHITECH 09*, volume 2, pages 1683–1689. Taylor & Francis Group, London, 2009b. (Cited on page 65.)

D. Tirelli, F. Bono, and V. Renda. Characterisation of shape memory alloys - application to the retrofitting of brick masonry walls by the pseudo-dynamic method and numerical models. In A.W. Heemink, L. Dekker, H. de Swaan Arons, I. Smit, and Th.L. van Stijn, editors, *4th International EUROSIM Congress*, Delft, The Netherlands, June 26 - 29 2001. (Cited on page 32.)

M. Tomaževič. *Earthquake-resistant design of masonry buildings*, volume 1 of *Series on Innovation in Structures and Construction*. Imperial College Press, 1999. (Cited on pages xi, xiii, xix, xxii, xxiii, 23, 29, 30, 34, 36, 41, 42, 43, 45, 47, 140, 146, 148, 149, 152, 179, 180, 181, 187, 188, 189, 190, 197, 199, 202, 207, 210, and 244.)

M. Tomaževič. Earthquake rehabilitation and design: the case study of masonry structures. Online Presentation slides, 2007. Faculty of Civil Engineering and Geodesy, University of Ljubljana. (Cited on pages xv and 24.)

M. Tomaževič. *Potresno odporne zidane stavbe*. Tehnis, 2009a. (Cited on pages 108, 167, and 175.)

M. Tomaževič. Shear resistance of masonry walls and eurocode 6: shear versus tensile strength of masonry. *Materials and structures*, 42: 889–907, 2009b. (Cited on pages 41, 42, 115, 117, 138, 146, and 151.)

M. Tomaževič and P. Weiss. Robustness as a criterion for use of hollow clay masonry units in seismic zones: an attempt to propose the measure. *Materials and Structures*, 1:1–19, 2011. ISSN 1359-5997. URL `http://dx.doi.org/10.1617/s11527-011-9781-2`. 10.1617/s11527-011-9781-2. (Cited on pages 23 and 133.)

D. Trpeski. *Virtual models of dwellings from Macedonian traditional construction*. University "Ss. Cyril and Methodius", Faculty of Natual Sciences and Mathematics, Institute of Ethnology and Anthropology, 2006. (in Macedonian). (Cited on page 13.)

V. Turnšek and F. Čačovič. Some experimental results on the strength of brick masonry walls. In *Proceedings of the 2nd international brick-masonry conference*, pages 149–156. British Ceramic Society, Stoke-on-Trent, 1971. (Cited on pages 41, 109, and 180.)

G. Vasconcelos. *Experimental investigations on the mechanics of stone masonry: Characterization of granites and behavior of ancient masonry shear walls*. PhD thesis, Universidade do Minho, Escola de Engenharia, 2005. (Cited on pages 133 and 146.)

Miodrag Velkov. *Duktilizacija zidarije kod aseizmičkih zidanih konstrukcija*. PhD thesis, Univerzitet u Beogradu, Gradjevinski fakultet, 1970. (Cited on pages xv, 55, 56, and 57.)

C.E. Ventura, J.F. Lord, M. Turek, R. Brincker, P. Andersen, and E. Dascotte. FEM updating of tall buildings using ambient vibration data. In *Proceedings of Eurodyn Conference*, 2005. (Cited on page 224.)

K. C. Voon. *In-plane Seismic Design of Concrete Masonry Structures*. PhD thesis, University of Auckland, March 2007. (Cited on page 18.)